Proceedings of the International Conference "Micro- and Nanoelectronics – 2016"

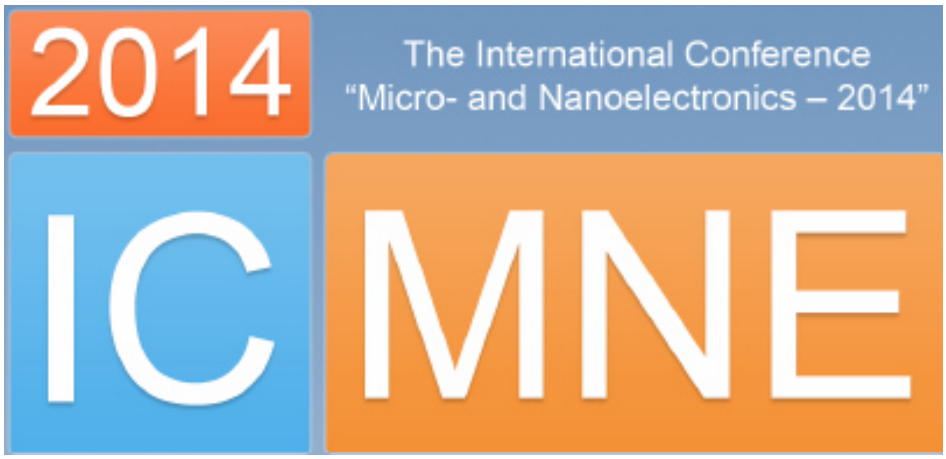

with the Extended Session

Book of
ABSTRACTS

October 3 – 7, 2016
Moscow – Zvenigorod, Russia

RUSSIAN ACADEMY OF SCIENCES
FEDERAL AGENCY OF SCIENTIFIC ORGANISATIONS
INSTITUTE OF PHYSICS AND TECHNOLOGY

Proceedings of the International Conference «Micro- and Nanoelectronics – 2016» ICMNE – 2016

Book of Abstracts

October 3–7, 2016
Moscow – Zvenigorod, Russia

MAKS PRESS

MOSCOW – 2016

УДК 621
ББК 32.85
М59

Издание осуществлено при поддержке
Российского фонда фундаментальных исследований по проекту 16-07-20515

Под редакцией:
чл.-корр. РАН *В.Ф. Лукичева*;
д.ф.-м.н. *К.В. Руденко*

Составитель к.ф.-м.н. *В.П. Кудря*

Микро- и наноэлектроника – 2016: Труды международной конференции (3–7 октября, 2016, г. Звенигород, РФ): Сборник тезисов / Под ред. В.Ф. Лукичева, К.В. Руденко. Составитель В.П. Кудря. – М.: МАКС Пресс, 2016. – 234 с.

М59

ISBN 978-5-317-05369-7

Сборник содержит тезисы докладов, представленных на Международной конференции «Микро- и наноэлектроника – 2016» (ICMNE-2016), включающая расширенную сессию «Квантовая информатика» (QI-2016). Тематика конференции охватываетбольшинство областей физики микро- и наноразмерных приборов, а также микро- и наноэлектронных технологий, и концентрируется на освещении последних достижений в этой сфере. Она продолжает серию всероссийских (с 1994 года) и международных конференций (с 2003 года).

Ключевые слова: нанотранзисторы, затворные стеки, квантовые компьютеры, МЭМС, магнитные материалы, оптоэлектроника.

УДК 621
ББК 32.85

Publishing was supported
by Russian Foundation for Fundamental Research, project 16-07-20515

Micro- and Nanoelectronics – 2016: Proceedings of the International Conference (October 3–7, 2016, Zvenigorod, Russia): Book of Abstracts / Ed. by V.F. Lukichev and K.V. Rudenko. Compiler V.P. Kudrya. – M.: MAKS Press, 2016. – 234 p.

The Book of Abstracts contains the abstracts of the papers presented at the biannual International Conference “Micro- and Nanoelectronics – 2016” (ICMNE-2016) including the extended Session “Quantum Informatics” (QI-2016). The Conference topics cover the most of the areas dedicated to the physics of integrated micro- and nanoelectronic devices and related micro- and nanotechnologies. The Conference is focused on recent progress in those areas. It continues the series of the AllRussian Conferences (since 1994) and the International Conferences (since 2003).

Keywords: nanoscale transistors, gate stacks, quantum computers, MEMS, magnetic materials, optoelectronics.

ISBN 978-5-317-05369-7

OXFORD INSTRUMENTS

Oxford Instruments Plasma Technology

Лидер по производству систем плазмохимического осаждения/травления для научно-исследовательских целей и мелкосерийного производства

ALE
Атомно-слоевое травление

ALD
Атомно-слоевое осаждение

CNT

CVD
Плазмо-химическое осаждение

ICP CVD

Bosch

RIE
Реактивное ионное травление

IBE
Ионно-лучевое травление

PVD
Магнетронное напыление

PECVD

IBD

Crestec Corporation CRESTEC

Передовые технологии в электронно-лучевой литографии и уникальные решения

CABL-9000 / CABL-UH

Системы нанолитографии высокого разрешения

- ускоряющее напряжение до **130 кВ**
- минимальная ширина линии **5 нм**
- диаметр пятна до **1,6 нм**
- диаметр пластин до **200 мм**
- **полевой катод (ZrO/W)**
- ручная загрузка
- размер поля 30мкм,60мкм,120мкм, 300мкм, 600мкм, 1200мкм,2400мкм)
- векторное сканирование (x,y)
- векторное сканирование (R,f)
- растровое сканирование
- компактные размеры системы
- термостатированный кожух
- минимальные затраты на подготовку помещения

Ваш надежный партнер в мире нанотехнологий

Ion Beam Services

Самое современное оборудование для ионной имплантации, разработка технологий на заказ, сервис

ibs Innovative Ion Implant

IMC-200/ IMC-400

Ионно-лучевая имплантация

- диаметр пластин до **150 мм**
- энергии **2 - 400 кэВ**
- токи до **3000 мкА**
- дозы до **10E18**
- температура **-150... 600 С**
- автоматическая, либо ручная загрузка

PULSION

Плазменная иммерсионная ионная имплантация

- диаметр пластин до **460 мм**
- энергии **1 - 30 кэВ**
- токи до **300 мА**
- дозы до **10E18**
- температура **-150... 600 С**
- автоматическая, либо ручная загрузка

- разработаны рецепты имплантации для более **60 примесей**

www.technoinfo.ru / sales@technoinfo.ru / +7(499) 243-66-26

НИКС
КОМПЬЮТЕРНАЯ КОМПАНИЯ

БИЗНЕС, ОСНОВАННЫЙ НА НАУЧНОМ ПОДХОДЕ

Спонсор конференций ICMNE2003, Qi2004, ICMNE2005, 2007, 2009, 2012, 2014, 2016

Год основания: **1991**

Профиль: **компьютеры,**
- комплектующие,
- программное обеспечение,
- бизнес-анализ

Учредители: **выпускники МФТИ**

Сотрудники: **600 человек,**
- из них 20% выпускников МФТИ и других физико-математических вузов России

Годовой оборот: **$80млн**

Сайт: www.nix.ru
- **150 тыс. уникальных посетителей в день**

Компьютерный супермаркет НИКС в рамках собственного проекта NANOSOFT® занимается всесторонней поддержкой российской науки и образования, исследований в области квантовой информатики. На гранты нашей компании многие талантливые студенты, преподаватели и российские учёные смогли успешно развивать свою научную деятельность.

NANOSOFT.RU

ваш шанс на прорыв в будущее

Nanosoft® - собственная программа Компьютерного супермаркета НИКС по поддержке российских ученых, занимающихся теоретическими и экспериментальными исследованиями квантовых приборов и нанотехнологий.

http://www.nanosoft.ru, science@nix.ru

TABLE OF CONTENTS

How to search for necessary abstract?

Every Abstract has its own identification number (for instance, L1-04, O1-07, P2-28, and so on), which is printed at the page bottom. This number corresponds to the one in the *Conference Programme*. If you do not know the number of the paper, but know at least one of the authors it is possible to find the Abstract using the *Author Index* located in the end of the *Book of Abstracts*.

Как отыскать интересующие Вас тезисы доклада?

Каждый доклад имеет собственный идентификационный номер (например, L1-04, O1-07, P2-28 и т.д.), который указан внизу страницы. Этот номер совпадает с номером, присвоенным докладу в *Программе конференции*. Если Вы не знаете номера доклада, но Вам известен хотя бы один из авторов, вы можете воспользоваться *Авторским указателем*, расположенным в конце *Сборника тезисов.*

III-Nitride Advanced Technologies and Equipment for Microelectronics

A.N. Alexeev[1], S.I. Petrov[1], V.V. Mamaev[1,3], D.M. Krasovitsky[2], V.P. Chaly[2]
1. SemiTEq, JSC, 27 Engels ave., Saint Petersburg, Russia
2. Svetlana-Rost, JSC, 27 Engels ave., Saint Petersburg, Russia
3. State Polytechnical University, 29 Polytechnicheskaya st., Saint Petersburg, Russia
Presenter's e-mail address: alex@semiteq.ru

The complete set of technologies including molecular beam epitaxy and submicron planar processing are developed to realize novel electron devices based on III-nitride multilayer heterostructures using SemiTEq equipment.

Wide conditions range available on growth equipment used as well as flexible heterostructure designs allows controlling of device oriented material properties. For microwave applications, thick AlN "templates" grown at extremely high (up to 1150 °C) substrate temperature in conjunction with multilayer transition region design both provide low dislocation density in the order of 10^8 cm^{-2} and DEG mobility up to 2000 $cm^2/V \cdot s$. The strong carrier confinement in two-dimensional electron gas for collapse-free transistor's operation is provided by placing GaN channel between AlGaN barriers of various Al content, keeping low sheet resistance of 240-270 Ohm/□.

3 inch SiC DHFET processes are developed, including active elements with gates of 0.5 μm for S- to C- band, 0.25 μm for X-band applications, TFR and MDM-based passive elements. Multilevel metallization, including field plates, via-holes provides all necessary elements for design of high power transistors and MMICs. Both processes are designed for maximum rating of 28 V drain bias, but due to typical breakdown voltages >100 V could be used up to 48 V. The technologies demonstrate prospective device level performance. Up to 50% PAE and delivered power density of 5.5 W/mm at 4 GHz and small signal gain up to 11 dB at 10 GHz are achieved. Recently developed Process Design Kit (PDK) including layout cell libraries, design manuals, active and passive device models now are under verification.

For various types of bulk acoustic elements (resonators, filters etc.), stress-controlling technology of AlN/GaN layers up to several microns on Si substrates is also developed. Precise thickness control for all layers is shown to be very critical. Experimental FBARs based on SiO_2/Mo Bragg reflectors were processed to provide resonant frequencies in 4-12 GHz range depending on thicknesses of AlN layer and electrode metallization as well as design of Bragg layers stack.

New generation of Oxford Instruments Plasma Technology equipment for the micro- and nano- engineering of materials for semiconductors, optoelectronics, MEMS and other applications

A. Krynin
Technoinfo Limited, Moscow, kryninalex@technoinfo.ru

Oxford Instruments Plasma Technology (OIPT) provides a range of high performance, flexible tools to semiconductor and electronic processing customers in both R&D and production. Today the company offers equipment and technology for Plasma Etch and Deposition, Atomic Layer Deposition, Ion Beam Etch and Deposition, Nanoscale Growth and Hydride Vapour Phase Epitaxy. With a 30-year history of high performance tools production and process development, OIPT has great experience in this area and good worldwide reputation. More than 2.500 systems were installed around the world.

Oxford Instruments has a process library of over 6,000 recipes developed in our process laboratories. Our processes are backed by process guarantees for key parameters and repeatability such as rate and uniformity to ensure rapid start-up during installation. Oxford Instruments' process tools offer a powerful range of stand-alone and clusterable process modules to enable the widest range of applications: Plasma Etch (ICP, RIE, RIE/PE, DRIE), Plasma Deposition (PECVD and ICP CVD, ALD (PE & thermal), DLC, PVD).

ALD systems have next features: Plasma and thermal ALD in one tool, possibility to be clustered to other modules using hex handler with robot and 25 wafer cassette for 4", 6", or 8" wafers, 100% conformal coatings of up to 200mm wafers handling and pieces on carrier plate.

Nanoscale features can be formed by growth techniques ('bottom up') and etching ('top down'). The NanofabTM Systems are aimed to satisfy the nanotechnology market. Nanoscale growth processes encompass: Nanotubes/nanowires, Nanoscale thin films. Nanofab700 and Nanofab800Agile: can accommodate variable sample sizes up to 200 mm wafer with excellent temperature uniformity, can provide growth of nanotubes and nanowires with a flexible temperature range up to 700 °C and 800 °C respectively.

Oxford Instruments' Ion Beam technology offers unique abilities in etch and deposition. OIPT Ion Beam tools have next benefits: Etch and Deposition tools, Versatile tool for a wide range of applications, Flexible system configuration to match specific process applications, easy optimisation for repeatable process results. Next processes can be started: Ion Beam Etch (IBE), Reactive Ion Beam Etch (RIBE), Chemical Assisted Ion Beam Etch (CAIBE), Ion Beam Deposition (IBD), Reactive Ion Beam Deposition (RIBD).

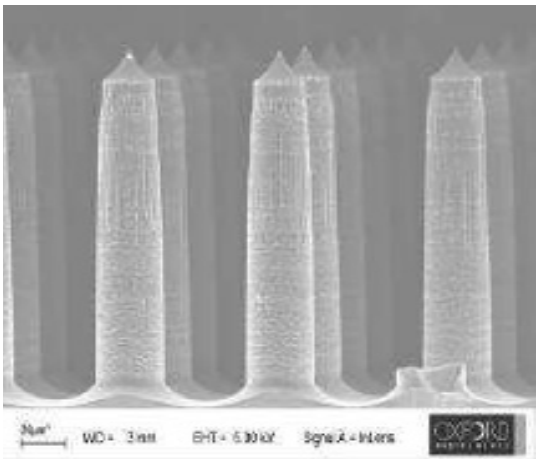

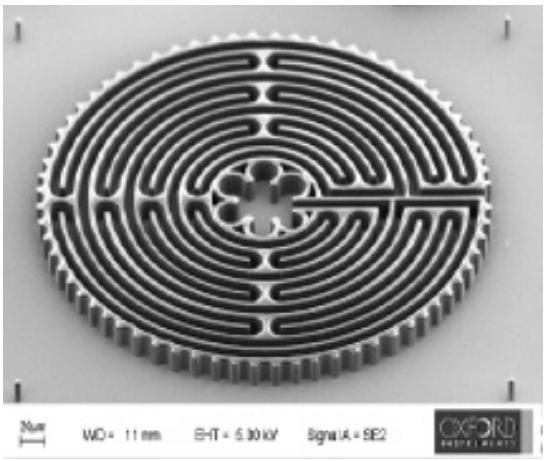

Left Image: Microneedles (Bosch-process) for Bio-medical application.
Right Image: Micro-mould (Cryo etching) for Micromachines / Actuators

New opportunities of scanning probe microscopy and spectroscopy for micro and nanoelectronic structures investigations

Victor A. Bykov[1,2], Arseny Kalinin[2], Artem Shelaev[2]
1. Research Institute of Physical Problems & NT-MDT Companies Group
www.ntmdt.com, spm@ntmdt.ru
2. Moscow Institute of Physics and Technology & NT-MDT Spectral Instruments Companies Group

During last years the development of SPM technology was transformed to the side of specialization. The application field was increased very wide – from one side micro- and nanoelectronics with extra high-level the metrology requirements and up to material science, biology, ecology with requirements to the side of simplification in operation procedures, possibility of the materials and molecules recognitions.

Scanning Probe Microscopy gives an opportunity to carry out studies of spatial, physical and chemical properties of objects with the typical dimensions of less than a few nanometers. Owing to its multifunctionality, availability and simplicity, Atomic-Force Microscope (AFM) has become one of the most prevailing “tools for nanotechnology” nowadays. NTEGRA platform has been designed as the special base for the constantly developing options of Scanning Probe Microscopy that combines them with various other modern research methods. Integration of SPM and confocal microscopy / luminescence / Raman scattering spectroscopy/Infrared Apertureless Nearfield Spectroscopy and Microscopy. Owing to the effect of giant amplification of Raman scattering (TERS – Tip Enhances Raman Scattering) it allows carrying out spectroscopy studies and obtaining images with 10 nm resolution. For micro-&nanoelectronics new SPM created – VEGA-SPM. This SPM based on special controller included the powerful digital feedback control of a number of measured dates as in usual SPM modes and in a number of modes of SPM spectroscopies. The maximum weather size is 200 mm.

New generation of AFM control electronics now allows a real-time cantilever deflection tracking and analyzing. Based on a fast force-distance measurement we developed a new group of non-resonant atomic force microscopy methods of scanning probe spectroscopy - called Hybrid mode. Hybrid mode is the most proposal AFM mode since it summarizes all advantages of amplitude modulation and contact modes allowing simultaneously: free of share force topography measurement with direct tip-sample interaction control, real-time quantitative nanomechanical measurements, conductivity, piezoresponse and electrostatic imaging, all with conventional scanning speed. Hybrid mode is also very helpful for liquid measurements because it utilizes the issue with cantilever eigenfrequency detection. Progress in micromechanics manufacturing resulted in significant increase of the cantilever yield rate (to practically 100%) with repeatability of resonant characteristics at 10% level, thus preconditioning implementation of the concept of multi-probe cartridges for AFM.

A cartridge of this type is a multi-probe contour-type sensor with 38 cantilevers. The cantilevers can be either of the same type or "colored" with predefined coverings and rigidities. Depending on AFM system type the cartridge rotation to select working cantilever can be manual or software-controlled and takes only a few seconds.

A whole cartridge can be exchanged manually through a simple procedure without the risk to damage cantilevers. The cartridges operate in dedicated measuring heads, which are designed for integration in the latest instruments by the Company (VEGA-SPM, Titanium, NEXT, SOLVER-NANO, NANOEDUCATOR-II).

New opportunities in semiconductor manufacturing by maskless multiple e-beam lithography

H. Kersting[1], M. van Kervinck[1], D. Shamiryan[2]
1. Mapper Lithogrpahy BV, Delft, the Netherlands, hans.kersting@mapperlithography.com
2. Mapper LLC, Moscow, Russia, denis.shamiryan@mapperlithography.com

In recent years, development of semiconductor manufacturing technology was following so-called Moore's law, which states that number of transistors in an integrated circuit doubles approximately every two years. One of the consequences of this law is continuous shrinkage of critical dimensions (CD) of transistors. The smallest CD is determined by capabilities of photolithography that is used for pattern transfer on a semiconductor wafer. Until now, the development of photolithography was targeted at reducing CD, which was achieved mostly by shortening the wavelength of the light used for exposure.
However, in recent years following Moore's law started to become more and more difficult. First, continuous shrinking of device dimensions lead to physical limitations of the materials. This limitation was overcome by using new materials and architectures, so the progress could continue. Second, continuous shrinking of wavelength in photolithography led to significant increase in costs: both litho tools and masks become more and more expensive with each technology node. In order to make semiconductor manufacturing economically feasible, costs must be spread over huge amount of chips, with mask cost becomes prohibitive for small series of most advanced products. How to continue progress in lithography in ways other than just shrinking CD?
One of the options is multiple e-beam lithography. Conventional e-beam lithography is known for decades. The biggest advantage of it is the ability of direct pattern generation without any mask. Another advantage of the e-beam lithography is high resolution as electron wavelength is very small. The biggest disadvantage of e-beam is its speed: classical e-beam pattern generator would need about a month to expose a 300 mm wafer, so its use in wafer production is out of the question. Multiple e-beam lithography keeps the advantages of direct patterning and high resolution, but removes the low-speed obstacle by using thousands of e-beams in parallel. Using 13 000 e-beam simultaneously, one can pattern ten 300 mm wafers per hour (wph), which is acceptable for low volume manufacturing.
What can be done with a litho tool that can directly generate pattern on a wafer with a resolution compatible with sub-90 nm node and with throughput of 10 wph? Competition with conventional litho tools in high-volume manufacturing (about 100 wph with a mature technology) seems to be unlikely. However, multiple e-beam lithography could be used for number of applications, where conventional lithography is to expensive to be used or cannot be used at all.
Just at a first glance, we can propose the following applications: development of new products, making small series of advanced products, making unique chips and making ultra-large image sensors. Since multiple e-beam litho does not require a mask, one can easily prototype many designs on one wafer, select the best one and order a mask with the best design for high-volume manufacturing using conventional litho. Alternatively, small series of advanced products can be manufactured without incurring huge mask costs, which makes such production economically feasible. Interesting application that opens new markets is making unique chips. Since no repetitive printing from a mask is used, every chip on a wafer can be made different, which might be used for security or product traceability applications. Since e-beam operates in continuous scanning mode, its field of view is not limited, unlike the conventional lithography. As a result, multiple e-beam lithography can print ultra-large chips (as big as 300 mm wafer) which could be used, for example, for ultimate quality image sensors.
Thus, newly developed by Mapper Lithography multiple e-beam lithography tool could provide alternative ways for technology development in modern semiconductor manufacturing.

NanoCMOS and Tunnel FET for high performance and ultra low power applications

F. Balestra
IMEP-LAHC, Grenoble INP-Minatec, Grenoble, France

We are facing many challenges for future nanoelectronic devices in the next two decades dealing with scaling, power consumption and performance.

This paper presents the most promising solutions for the end of the roadmap in the More Moore and Beyond-CMOS fields, including innovative nanomaterials such as ultra-thin Si-Ge-III-V/OI, 2D layers (graphene, phosphorene, transition-metal dichalcogenides), 1D semimetals, Heterostructures using strained materials, Ge, III-V (InAs, GaSb, AlGaSb, graded layers, quantum wells, …).

These innovatise boosters can be combined with advanced nanodevice architectures, especially ultimate multigate nanoCMOS and Nanowire FETs, Small Slope Switches like Tunnel FETs, and combinations of these nanoscale transistors such as FeTFET or TMOSFET [1-4].

1. F. Balestra, *Beyond CMOS Nanodevices 1*, Book (tomes 1 & 2) edited by Francis Balestra, ISTE-Wiley, 2014.
2. F. Balestra, E. Sangiorgi, M. Östling, P.E. Hellström, Nanowires for very low power ICs and new functionalities, Chapter, in "*CRC Concise Encyclopedia of Nanotechnology*", CRC Press, 2014
3. F. Balestra, Silicon-On-Insulator Devices, Chapter in the "*Wiley Encyclopedia of Electrical and Electronics Engineering*", 2014.
4. F. Balestra, Challenges to ultra-low-power operation, Chapter in "*Future Trends in Microelectronics, Journey into the Unknown*", S. Luryi et al Eds, Wiley, 2015.

Carbon nanotubes – a new material for vacuum electronics

Yu.V. Gulyaev
Kotel'nikov Institute of Radio Engineering and Electronics, Moscow, Russia.

High frequency carbon nanotube FETs for mobile communications

S.E. Schulz[1,2,3], S. Hermann[1,2,3], M. Hartmann[2,3], J. Tittmann-Otto[2,3], M. Claus[3,4], M. Schroeter[3,4,5]
1. Fraunhofer Institute for Electronic Nano Systems (Fraunhofer ENAS), Chemnitz, Germany
2. Technische Universität Chemnitz, Center for Microtechnologies, Chemnitz, Germany
3. Center for Advancing Electronics Dresden (cfaed), Germany
4. TU Dresden, Chair of Electron Devices and Integrated Circuits, D-01062 Dresden, Germany
5. UC San Diego, ECE Department, California, USA
E-Mail: Stefan.Schulz@enas.fraunhofer.de

While numerous fundamental studies have demonstrated the potential of Carbon Nanotubes (CNT) for various applications, making use of the intrinsic properties with industrial compatible integration technologies remains extremely challenging and delays applications such as CNT-based high-frequency transceivers [1, 2]. Contributions to this open topic are addressed by the development of a modeling and technology platform enabling the use of high-frequency CNT field-effect transistors (CNTFETs) for wireless communication. CNTFETs are of particular interest for those applications since they promise linear amplification leading to lower signal distortion, lower power consumption and a simpler design of high frequency circuitry. Therefore, we combine the extensive and complementary multi-disciplinary CNTFET competences covering materials science, multi-scale device modeling, device fabrication, RF circuit design, and wireless communication. An overview about our platform and recent achievements will be presented.
For guiding the technology development and for enabling circuit design studies, an experimentally verified multiscale simulation framework for CNTFETs covering all levels from atomistic simulations over TCAD simulation up to compact models has been established [3-5]. Besides contact studies, the multiscale simulation framework allows the study of defects and different transport phenomena at different channel length scales from a few nanometers up to several micrometers. We show a theoretical guideline to approach linearity in Schottky barrier FETs [4]. Moreover, we discuss issues and challenges on the electrical characterization of FET devices [6]. On the technology site, we show our holistic wafer-level approach enabling the fabrication of FET arrays (3000 FETs/mm^2) with structured local bottom gates used for statistical studies on process steps. This platform is used to fabricate high-frequency FETs in multi-tube configuration. We present recent achievements on channel engineering covering the integration of length-separated CNTs as well as a novel in-situ post-polymerization procedure enabling significant transistor performance enhancements. Based on statistical studies on large FET arrays we demonstrate a comparative study on different post-treatments of FETs in order to tackle contact and hysteresis issues [7, 8]. Moreover, the progress on understanding and controlling of CNT assembly at wafer-level is presented addressing issues such as metallic impurities in CNTFETs. Finally, we demonstrate TCAD optimized high-frequency CNTFETs fabricated at wafer scale.

This work was partly financed by the German Research Foundation (DFG) within the cluster of excellence “Center for Advancing Electronics Dresden” (cfaed, EXC1056) and by the Volkswagen Foundation.

1. C. Rutherglen, D. Jain, and P. Burke “Nanotube electronics for radiofrequency applications,” Nature Nanotechnology, 2009, **4**, pp. 811–819.
2. M. Schroter et al., "Carbon nanotube FET technology for radio-frequency electronics: state-of-the-art overview," IEEE Journal of the Electron Devices Society, 2013, **1** (1), pp. 9-20.
3. A. Fediai, et al., “Towards an optimal contact metal for CNTFETs”, ACSNano/Nanoscale, 2016, DOI: 10.1039/C6NR01012A.
4. S. Mothes, M. Claus, and M. Schroter, “Toward linearity in schottky barrier CNTFETs,” IEEE Transactions on Nanotechnology, 2015, **14** (2), pp. 372-378.
5. M. Schroter et al., “A semi-physical large-signal compact carbon nanotube FET model for analog RF applications”, IEEE Trans. Electron Dev., 2015, **62** (1), pp. 52-60.
6. M. Haferlach et al., “Electrical characterization of emerging transistor technologies: issues and challenges,” IEEE Transactions on Nanotechnology, 2016, **15** (4).
7. J. Tittmann-Otto et al., "Effect of cleaning procedures on the electrical properties of carbon nanotube transistors—A statistical study", Journal of Applied Physics, 2016, **119** (12), 124509.
8. M. Toader et al., "Competitive Impact of Nanotube Assembly and Contact Electrodes on the Performance of CNT-based FETs", Journal of Physical Chemistry C, 2016, **120** (18), pp. 10020-10026.

Barrier/liner stacks for next generation Cu interconnect

Xin-Ping Qu
State key Lab of ASIC and Systems, School of Microelectronics, Fudan University, shanghai, China,
xpqu@fudan.edu.cn

An ultrathin adhesion/barrier layer for copper metallization with good thermal stability and adhesion with Cu/low k becomes more and more important in the next generation interconnect technology. The current Ta/TaN bilayer scheme is difficult to fulfill the requirement. Aspects from diffusion barrier properties, electrical stability, adhesion with low k, CMP properties, electroplating fill properties, oxgen barrier properties of the ultrathin barrier are all need to be considered. Co, Ru have been heavily researched as liner together with ALD TaN layer as barrier. Many novel single layer alloy films have been proposed, such as RuTa, RuTiN, CoW, and self-formed barrier.

In this work, we propose a novel CoMo alloy as barrier layer to Cu according to density functional theory calculation. We have studied the adhesion properties of CoMo with Cu and with ultra low k. The thermal stability, electrical stability, oxygen barrier properties were also studied. Then the direct electroplating of Cu on CoMo is studied as well as the CMP properties.These results show that, by optimizing the composition of the CoMo alloy, a good single alloy layer with good thermal stability, good adhesion, direct copper electroplating capability and reasonable CMP properties can be achieved.

The author would also like to acknowledge the support by NSFC (61574047) and “Shu Guang” project supported by Shanghai Municipal Education Commission and Shanghai Education Development Foundation.

Experimental and theoretical investigations of quantum state transfer and decoherence processes in quasi-one-dimensional systems in multiple-quantum NMR experiments

G.A.Bochkin, S.I. Doronin, S.G.Vasil'ev, A.V.Fedorova, E.B.Fel'dman
Institute of Problems of Chemical Physics of Russian Academy of Sciences, Chernogolovka, 142432, Moscow Region, Russia

Multiple quantum[1] (MQ) NMR is an important method for the investigation of various problems of quantum information processing such as transmission of quantum information and decoherence processes. MQ NMR not only creates multi-qubit coherent states but also allows the investigation of their relaxation under the action of the correlated spin reservoir.

MQ NMR dynamics is described by the two-spin/two-quantum Hamiltonian[1] which is the XY-Hamiltonian for one-dimensional spin chains in the approximation of the nearest neighbor interactions. A simple unitary transformation connects[2] the XY Hamiltonian with the flip-flop one. As a result, it is possible to organize quantum state transfer along a linear spin chain. However, this is possible only if the accuracy of the XY-Hamiltonian is sufficiently high. We improve this accuracy by an order of magnitude owing to the use of ultrashort radio-frequency pulses[3]. The fidelity of the quantum state transfer of over 0.95 can be achieved.

To perform multiple quantum NMR experiments, we used quasi-one-dimensional chains of ^{19}F in calcium fluorapatites $Ca_5(PO_4)_3F$. Experiments were performed on a Bruker Avance III spectrometer with the static magnetic field B_0 = 9.4 T (the corresponding frequency on ^{19}F nuclei is 376.6 MHz). The experiment consists of four main periods: preparation, free evolution, mixing, and detection. These periods are repeated many times with the phase increment of the radio-frequency pulses irradiating the spin system in the preparation period at each repetition.

Relaxation of the MQ NMR coherences can be studied[4] on the evolution period of the MQ NMR experiments. This relaxation can be considered as the simplest model of decoherence processes. We developed a theory of the dipolar relaxation of the MQ NMR coherences in one-dimensional systems. The theory is based on the approximation of the ZZ-Hamiltonian (ZZ-model) when only the ZZ-part of the dipole-dipole interactions (DDI) is taken into account. We showed that the MQ NMR coherence of the zeroth order is not subject to the dipolar relaxation in the ZZ-model. At the same time, the experimental data demonstrate the relaxation decay of that coherence. However, the MQ NMR coherence of the zeroth order does not decay completely in the relaxation processes. The point is that the initial density matrix in the beginning of the evolution period contains a part which commutes with the secular part of the DDI. This part of the density matrix does not decay on the evolution period of the MQ NMR experiment. We obtained[4] a formula for the stationary intensity of the MQ NMR coherence of the zeroth order. This formula is in a good agreement with the experimental data obtained at different values of the preparation period of the MQ NMR experiment.

We have found that the MQ NMR coherence of the second order goes to zero with the rate, exceeding the relaxation rate of the MQ NMR coherence of the zeroth order which does not decay completely.

The work is supported by the Russian Foundation for Basic Research (Grants 16-03-00056 and 16-33-00867) and the Program of RAS "Element base of quantum computers" (Grant No. 0089-2015-0220).

1. Baum J., Munowitz M., Garroway A. N. et. al. "Multiple-quantum dynamics in solid state NMR". J. Chem. Phys.**83**, 2015 (1985).
2. S.I. Doronin, I.I. Maksimov, E.B. Fel'dman. "Multiple quantum dynamics of one-dimensional nuclear spin systems in solids". JETP **91**, 597 (2000)
3. S.I. Doronin, G.S. Vasil'ev, A.A. Samoilenko, E.B. Fel'dman, and B.A. Shumm. "Dynamics and relaxation of multiple quantum NMR coherences in a quasi-one-dimensional chain of nuclear spins ^{19}F in calcium fluorapatite". JETP Letters **101**, 613 (2015).
4.G.A. Bochkin, E.B. Fel'dman, S.G. Vasil'ev. Zeitschrift für Physikalische Chemie (in press).

Post-selection free spatial Bell state generation

E.V. Kovlakov, I.B. Bobrov, S.S. Straupe, and S.P. Kulik
Faculty of Physics, M.V. Lomonosov Moscow State University, Russia

We report first experiment results on measuring correlations between arbitrary superpositions of orbital angular momentum (OAM) states generated by spontaneous parametric down-conversion. Our technique allows one to access fully a two-dimensional OAM subspace described by a Bloch sphere, within the higher-dimensional OAM Hilbert space. We quantify the entanglement through violations of a Bell-type inequality for pairs of modal superpositions that lie on equatorial, polar, and arbitrary great circles of the Bloch sphere. Finally we demonstrate that this approach can be used to measure arbitrary spatial states with a fidelity sufficient for appropriate quantum information processing systems

Broadband quantum memory in a nanofiber-coupled ring-cavity array

S.A. Moiseev[1], E.S. Moiseev[1], and A.M. Zheltikov[2,3,4]

1. Kazan Quantum Center, Kazan Scientific Research Technical University, 10, K. Marx, Kazan, 420111, Russia
2. Department of Physics and Astronomy, Texas University, College Station TX, 77843-4242 USA,
3. Physics Department, International Laser Center, M.V. Lomonosov Moscow State University, Moscow 119992, Russia
4. Russian Quantum Center, ul. Novaya 100, Skolkovo, Moscow Region, 143025 Russia

Optical quantum memory based on an array of ring cavities coupled to a common nanofiber is proposed. Herein, the cavities create a periodic structure of narrow lines characterized by high finesse that provides a broadband spectral range for quantum storage. We have shown that such a optical system can provide highly efficient storage of quantum light fields at room temperature on the milliseconds timescale. The proposed scheme can be implemented by using cutting-edge nano- and micro-optical technologies, suggesting a practical solution for optical quantum memory.

Quantum Cryptographic Hashing

Farid Ablayev[1], Marat Ablayev[2]
1. Department of Theoretical Cybernetics, Kazan Federal University, Kazan, Russia. Email: fablayev@gmail.com,
2. Laboratory of Quantum Informatics, Kazan Federal University, Kazan, Russia

Hashing is an important tool and has a various applications in Computer Science. A hash functions are designed to take a long string as input and produce a short string (hash value). A cryptographic hash function has the following main properties: 1) it is easy to compute the hash value for any given message, 2) it is infeasible to generate a message from its hash value except by trying all possible messages (the one-way property), 3) it is infeasible to find two different messages with the same hash value (the collision resistant property). Cryptographic hash functions have many information-security applications, notably in digital signatures, message authentication codes, and other forms of authentication. Note that for now days there are no one-way functions that are known to be provably more difficult to invert than to compute, the security of modern classical cryptographic hash functions is "computationally conditional": the mathematical proof of one-way property for a particular function will follow the proof of P not equal NP problem.

A quantum hash function [1, 2, 3] is a function ψ that maps words w of length k to a quantum states $|\psi(w)\rangle$ of s-qubits and has the following properties: (i) Function ψ must be one-way resistant. In quantum case this means that $k > s$. (ii) Function ψ must be collision resistant. In quantum case this means that for different words w, v states $|\psi(w)\rangle$, $|\psi(v)\rangle$ must be “almost orthogonal” [2]. Such a function ψ satisfy all of the properties that a "classical" hash function should satisfy. Unconditional one-way property follows from Holevo’s theorem (we can not extract from s-qubit more than s bits of information). Collision resistance follows, because all input states are mapped to states that are almost orthogonal. Note that quantum functions with the property (ii) are also important for constructing quantum bounded-error computational models. $k > s$ property is the basis for building quantum computational models of low complexity. Such functions were invented by different authors: first for quantum finite automata [4] and later for quantum communication computations [6]. In [6] authors called such function a quantum fingerprinting.

We present examples and discussion that supports the idea of quantum hashing from [1, 2, 3]. Our examples demonstrate that in the quantum setting the one-way resistance property and collision resistance property can correlate: the "more" a quantum function is one-way resistant the "less" it is collision resistant and vice versa. Such correlation leads to the notion of balanced quantum hash function. We present methods that allow effectively construct different balanced quantum hash functions. The methods are based on small-biased sets [7] and Cayley expanders graphs [8]. The construction of quantum hash functions, which is based on composition of classical universal hash family of functions with a given generator of quantum hash function, allows us to build a large family of balanced quantum hash functions [1].

Note, that a realization of such quantum functions as the balanced quantum hash function requires the high degree of entanglement between the qubits makes such a state difficult to create with current technology. Applying the "phase transformation" presentation of quantum hash states and using the mapping balanced quantum hash states to a coherent states [5] we can use a quantum optic technology for developing quantum signature schemes based on balanced quantum hash functions [3].

1. F. Ablayev and M. Ablayev, *ArXiv*:1404.1503v2 [quant-ph] (2015).
2. F. Ablayev and A. Vasiliev, *Laser Phys. Lett*. **11** (2), 025202 (2013).
3. F. Ablayev and M. Ablayev, *Laser Phys. Lett.* **12**, 125204 (2015).
4. A. Ambainis and R. Freivalds, *ArXiv:quant-ph*/9802062v3 (1998).
5. R. Amiri and E. Andersson, *Entropy*, **17**, pp. 5635-5659 (2015).
6. H. Buhrman, R. Cleve, J. Watrous, and R. de Wolf, *Phys. Rev. Lett*. **87**, 167902 (2001).
7. A. Vasiliev, *arXiv:*1603.02209 [quant.ph] (2016).
8. M. Ziatdinov, *arXiv*:1606.00256 [quant-ph] (2016).

Characterization of InSb nanocrystals ion-beam synthesized in SiO_2 films

I.E. Tyschenko[1], V.A. Volodin[1,2], A.G. Cherkov[1,2], M. Stoffel[3], H. Rinnert[3], M. Vergnat[3]
1. A.V. Rzhanov Institute of Semiconductor Physics, Novosibirsk, Russia, tys@isp.nsc.ru
2. Novosibirsk State University, Novosibirsk, Russia, volodin@isp.nsc.ru
3. Université de Lorraine, Institut Jean Lamour UMR CNRS 7198, B.P. 70239, 54506 Vandœuvre-lès-Nancy Cedex, France.

InSb is an A_3B_3 semiconductor with one of the smallest band gap (0.17 eV) and the highest room-temperature carrier mobility (electron mobility is about 80 000 cm^2/Vs). These properties are arguments for its application in the infrared detectors, magnetic sensors, cooling devices, high-speed field-effect transistors and low-power devises production. The very small electron and hole effective masses ($0.015m_0$ and $0.39m_0$ respectively) and the high dielectric permittivity (~17.9) provide the largest exciton Boron radius (about 65 nm) in InSb. As a result, InSb nanocrystals show good quantum confinement. However, InSb nanoparticles have not been quite sufficiently investigated up to now. In this study, we present the characterization of the InSb nanocrystals ion-beam synthesized in the thermally-grown SiO_2 layers.

In^+ and Sb^+ ions at an energy of 200 keV to dose 8×10^{15} cm^{-2} were embedded into the 300 nm thick SiO_2 films thermally-grown on (100)-oriented Si wafers. The ion implantation parameters produced Gauss-like In and Sb atom distributions with the respective peak concentration 1.2×10^{21} cm^{-3} at a depth of about 110 nm below the top SiO_2 surface. Following the implantation, in order to prevent the out-diffusion of In atoms during subsequent high-temperature annealing, the 600 nm thick silicon layer was transferred on the ion-implanted silicon dioxide. The produced wafer was cut in small pieces which were heat treated at temperature 600–1100 °C for 0.5 hour in an N_2 ambient. Raman spectroscopy, photoluminescence (PL), high-resolution electron microscopy (HREM) and energy-dispersive X-ray spectroscopy (EDS) were employed to study the produced layer properties.

The Raman measurements showed no In-Sb optical phonon mode from the samples heat-treated at the temperature below 800 °C. As the annealing temperature reached 800 °C, the broad Raman scattering band at about 180-200 cm^{-1} was seen. As annealing temperature grown to 900-1100 °C, two overlapping Raman peaks at 187 and 194 cm^{-1} were good pronounced, and the Raman scattering intensity was increased. The obtained peak positions are high-frequency shifted by 8 and 3.7 cm^{-1} to the respective frequencies corresponded to TO (179.7 cm^{-1}) and LO (190.7 cm^{-1}) phonon modes in the bulk crystalline InSb. The observed high-frequency shifts indicate the compressive stresses within the synthesized InSb phase. These stresses are not uniform. HREM analysis of the prepared structures showed the formation of the InSb nanocrystals with the mean diameters varied from 5 to 20 nm depending on their occurrence depth. The majority of nanocrystals observed after high temperatures had the interplanar spacing 0.374 nm corresponding to the (111) orientation in the InSb lattice. However, the interplanar spacing in the lattice being 0.392-0.295 nm was seen too. In order to estimate the effect of quantum confinement and stresses on the Raman peak shift, the optical phonon mode frequency as a function of the nanocrystal size was calculated in frame of the phonon localization model. The optical phonon mode shift ≤1 cm^{-1} was obtained for the experimentally observed nanocrystal size. The stress magnitudes 13.8 kbar and 7.4 kbar were also estimated from the TO and LO phonon mode shifts respectively. An origin of these stresses is discussed.

The samples annealed at the temperature ≥800 °C exhibited the room-temperature ultraviolet PL band peaked at about 360 nm. The PL intensity correlated with the Raman peak intensity. The nature of the observed PL band is discussed.

HfO_2/Pr_2O_3 gate dielectric stacks

F. Sidorov[1, 2], A. Molchanova[1, 2], A. Rogozhin[1, 2]
1. Institute of Physics and Technology of RAS, Moscow, Russia
2. Moscow Institute of Physics and Technology, Moscow, Russia

High leakage currents through SiO_2 dielectric layers in MOS capacitors have resulted in substitution SiO_2 with Hf-based high-k dielectric. Low-k interfacial layer typically exists in the gate stacks with high-k dielectric layer. Formation of high-k interfacial layer is a possible solution of the problem.
In this work high-k interfacial layers of Pr_2O_3 for HfO_2-based gate structures of MOSFETs are used. According to Osten *at al* [1] praseodimium oxide provides high dielectric constant and epitaxial growth on silicon. HfO_2/Pr_2O_3 dielectric stacks and back contact were formed by electron beam evaporation and gate contact was formed by W magnetron sputtering. In order to obtain parameters of HfO_2/Pr_2O_3 dielectric stacks and Pr_2O_3/Si interface using methods, based on MOS structure admittance measurements, HfO_2/Pr_2O_3 layers were relatively thick (10 nm). Leakage current values were also measured.
Leakage current density accounted $2\cdot10^{-7}$ A/cm^2 at 1 V gate voltage. Effective dielectric constant of HfO_2/Pr_2O_3 stacks comprised 11. Interface traps level density was obtained using single-frequency conductance method, Terman method and conductance method, which gave $3\cdot10^{12}$, 10^{13}, and $7\cdot10^{11}$ eV^{-1}cm^{-3} values respectively (fig. 1).

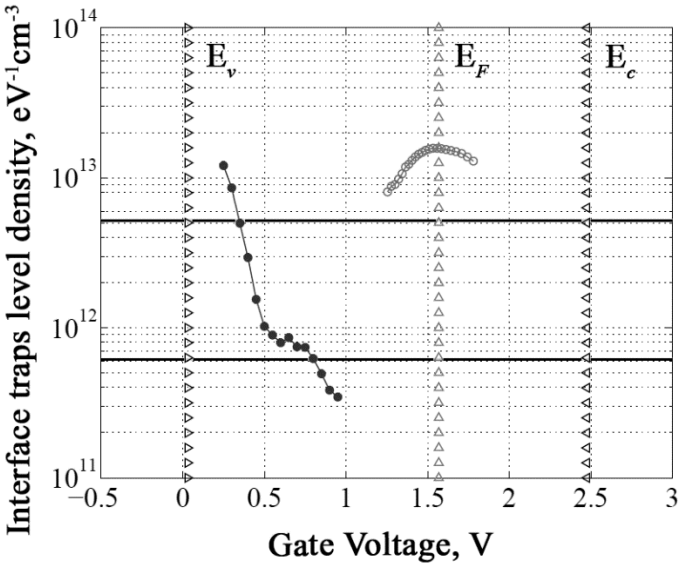

Fig. 1. Interface traps level density values obtained for structure with HfO_2/Pr_2O_3 dielectric stacks by single-frequency conductance method at 1 MHz (lower solid line) and 10 kHz (upper solid line) frequencies, Therman method (open dots) and conductance method (close dots). E_v, E_c and E_F correspond to valence band and conductance band edges and Fermi level respectively.

1. H.J. Osten, E. Bugiel, and A. Fissel. “Epitaxial praseodimium oxide: a new high-k dielectric”. Sol. St. Electron., **47**, pp. 2161-2165, 2003.

Quantum-mechanical relaxation model for characterization of fine particles magnetic dynamics in an external magnetic field

I. Mischenko, M. Chuev
Institute of Physics and Technology, Russian Academy of Science, Moscow, Russia, mishchenko@ftian.ru

Principal difference of magnetic nanoparticles from the bulk matter which cannot be ignored when constructing upon them combined metamaterials and modern devices is the essential influence on their behavior thermal fluctuations of the environment. These disturbances lead to specific distributions of the particles characteristics and to stochastic reorientations of their magnetic moments.

On the basis of quantum-mechanical representation of the particle with the total spin S, possessing intrinsic magnetic anisotropy with the energy density K [1] and being placed onto the external magnetic field with the normalized strength $h = H/H_c$ (H_c is the complete reversal field) we developed general approach to describe equilibrium magnetization curves and relaxation Mössbauer spectra of magnetic nanoparticles [2] (see Fig. 1) for diagnostics of magnetic nanomaterials in the whole temperature or external field ranges. This approach has universal character and may be applied not only to the systems under thermal equilibrium, but may in principle describe macroscopic dynamical phenomena such as magnetization reversal.

Authors thanks Russian Scientific Foundation for financial support, Grant № 14-15-01096.

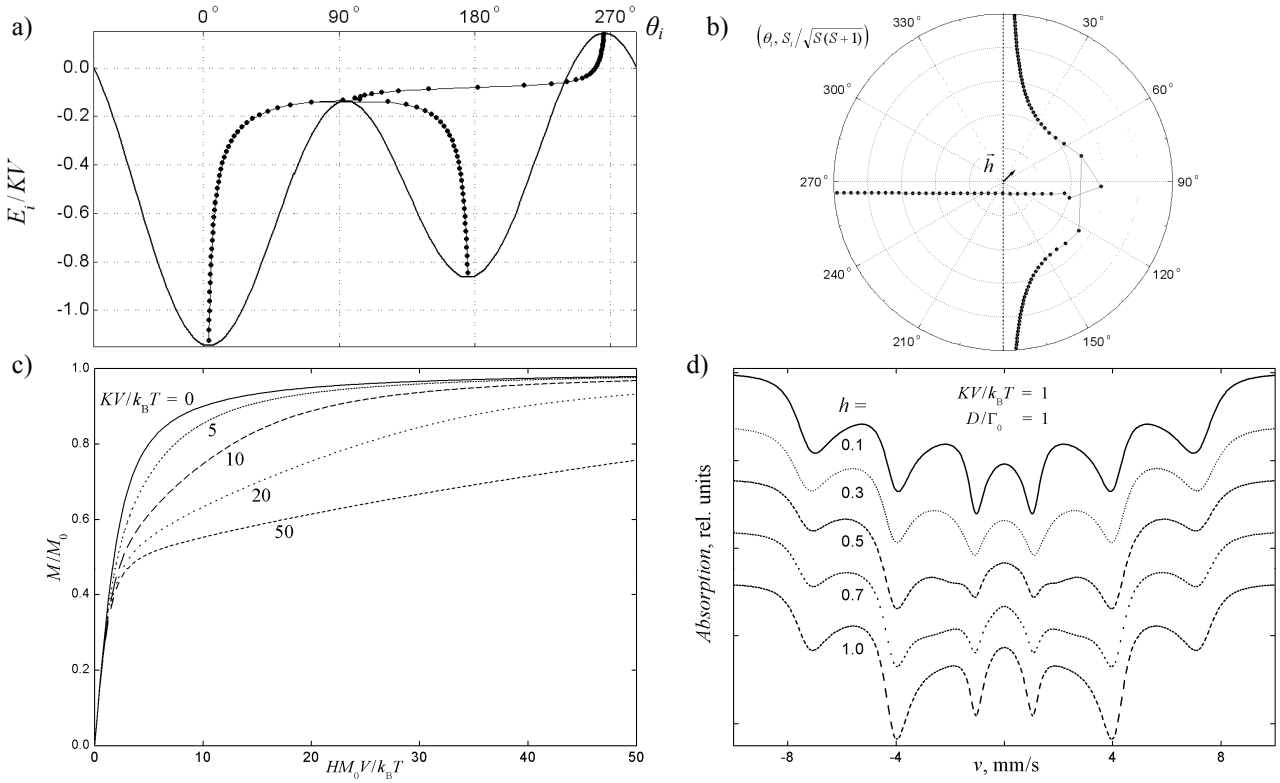

Fig. 1. a) Macroscopic energy profile of a ferromagnetic particle in an external magnetic field with normalized strength $h = 0.1$ turning away from the easy axis on $\Theta = 45°$ together with the set of quantum-mechanical energy levels of the particle at $S = 50$. b) Corresponding stationary states of the particle in the plane of the easy axis and the external field. c) Equilibrium magnetization curves of an ensemble of nanoparticles depending on the energy of their magnetic anisotropy. d) Relaxation Mössbauer absorption spectra of an ensemble of particles in the transversal magnetic field of various intensity.

1. D.H. Jones and K.K.P. Srivastava. “Many-state relaxation model for the Mössbauer spectra of superparamagnets”. Phys. Rev. B, **34**, pp. 7542–7548, 1986.

2. M.A. Chuev, "Multilevel relaxation model for describing the Mössbauer spectra of nanoparticles in a magnetic field", JETP, **114**, 609-630, 2012.

Modulation of magnetic interaction in Bismuth ferrite through strain and spin cycloid engineering

Rama Shanker Yadav[1*], Hilal Ahmad Reshi[1], Shreeja Pillai[1] D. S. Rana[2] and Vilas Shelke[1]

1. Novel Materials Research Laboratory, Department of Physics, Barkatullah University, Bhopal INDIA-462026 Email: ramaphysics09@gmail.com*

2. Department of Physics, Indian Institute of Science Education and Research, Indore By-pass road, Bhauri, Bhopal INDIA-462030 Email: dsrana@iiserb.ac.in

Bismuth ferrite, a widely studied room temperature multiferroic, provides new horizons of multifunctional behavior in phase transited bulk and thin film forms. Bismuth ferrite thin films were deposited on lattice mismatched $LaAlO_3$ substrate using pulsed laser deposition technique. X-ray diffraction confirmed nearly tetragonal (T-type) phase of thin film involving role of substrate induced strain. The film thickness of 56 nm was determined by X-ray reflectivity measurement. The perfect coherence and epitaxial nature of T-type film was observed through reciprocal space mapping. The room temperature Raman measurement of T-type bismuth ferrite thin film also verified phase transition with appearance of only few modes. In parallel, concomitant La and Al substituted $Bi_{1-x}La_xFe_{0.95}Al_{0.05}O_3$ (x = 0.1, 0.2, 0.3) bulk samples were synthesized using solid state reaction method. A structural phase transition into orthorhombic (Pnma) phase at x = 0.3 was observed. The structural distortion at x = 0.1, 0.2 and phase transition at x = 0.3 substituted samples were also confirmed by changes in Raman active modes. The remnant magnetization moment of 0.199 emu/gm and 0.28 emu/gm were observed for x = 0.2 and 0.3 bulk sample respectively. The T-type bismuth ferrite thin film also showed high remnant magnetization of around 20emu/cc. The parallelism in magnetic behavior between T-type thin film and concomitant La and Al substituted bulk samples is indication of modulation, frustration and break in continuity of spiral spin cycloid.

Optical coefficients of nanometer chromium films in 0.25–1.1 THz frequency range

V.G. Andreev[1], A.A. Angeluts[1], V.F. Lukichev[2], A.P. Shkurinov[1], V.A. Vdovin[3]
1. Moscow State University, Moscow, 119991 Russia, andreev@acs366.phys.msu.ru.
2. Institute of Physics and Technology of RAS (IPT RAS), Moscow, 117218 Russia,
3. Kotel'nikov Institute of Radio Engineering and Electronics of RAS, Moscow, 125009 Russia.

Terahertz (THz) radiation is widely used for the screening of objects that are nontransparent in the visible spectral range and for the purposes of medical diagnostics, which makes the creation of high sensitivity detectors of this radiation a topical task. We have shown recently that THz pulses can be measured effectively by the thermoacoustic detector (TAD) [1]. The key element of the TAD is the 10-nm thickness chromium film sputtered on the silica substrate, which absorbs up to 60% of electromagnetic radiation. The present work is aimed at a measurement of the optical characteristics of thin chromium films on silica substrates and quantitative estimation of the sensitivity and working frequency range of the TAD, which utilizes the nanometer chromium films.

Thin chromium films with thicknesses ranging from 1.5 to 40 nm were prepared by magnetron sputtering in a Z-550 vacuum deposition setup (Leybold AG) on 2-mm thick silica substrates with a diameter of 20 mm. The optical characteristics (reflection, transmission, and absorption coefficients) of thin films were measured on a setup described in detail in [2]. The probing THz radiation beam was generated on the surface of indium arsenide (InAs) pumped by femtosecond titanium sapphire laser, collimated by a quartz crystal lens and directed on the surface of the film. Radiation transmitted through (or reflected from) the film was focused by lens on photoconductive receiving antenna – Auston switch. The response photocurrent proportional to the electric field of THz radiation was amplified by a lock-in amplifier, digitized, and fed into a computer for processing and storage. The spectra of pulse amplitude were calculated using the Fourier transform. The normalization of spectrum measured in the presence of the films to reference spectrum of radiation not interacting with the object yields the true spectrum of transmission or reflection.

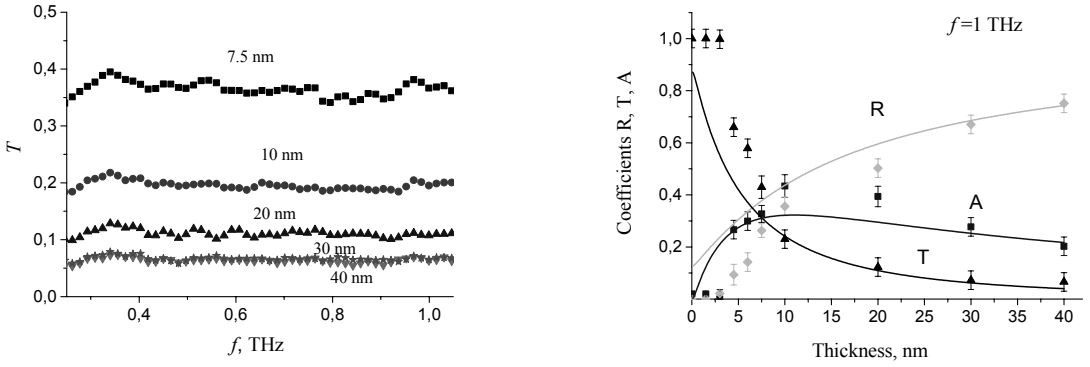

Fig. 1. (a) Measured transmission spectra of chromium films with thicknesses of 7.5, 10, 20, 30, and 40 nm and (b) comparison of the measured (symbols) and calculated (lines) dependences of coefficients *R*, *T*, and *A* on the film thickness (at a fixed frequency of 1 THz).

The maximum absorption coefficient (43%) was observed at a film thickness of 10 nm. Theoretical calculations of optical coefficients were performed with the expressions that took into account a phenomenological dependence of electrical conductivity on film thickness. It is demonstrated that the conductivity of thick chromium films (20 – 40 nm) is less than the conductivity of bulk metal by an order of magnitude. This work was supported by RFBR grant 16-07-01246.

1. V.G. Andreev, V.A. Vdovin, and Yu.K. Kalynov. "Recording of terahertz pulses of microsecond duration using the thermoacoustic effect". Radiophys. Quant. Electron., **56** (8–9), pp. 566-573, 2014.
2. M.M. Nazarov, A.P. Shkurinov, E.A. Kuleshov, and V.V. Tuchin. "Terahertz time-domain spectroscopy of biological tissues". Quant. Electron., **38** (7), pp. 647-654, 2008.

Quantum capacitance in thick 2G SOI transistors

V.P. Popov[1], M.A. Ilnitskii[1], V.N. Mordkovich[2], and A.V. Leonov[2]
1. Institute of Semiconductor Physics, SB RAS, Novosibirsk, Russia
2. Institute of Microelectronics Technology and High-Purity Materials RAS, Moscow, Russia

The classic description of the effect of charge coupling between the threshold voltage V_{th} of two gates is fully clear for field effect transistor (2G FET) on nanometer thick silicon-on-insulator (SOI) in the model proposed by Lim and Fossum (LF) [1]. Their model determines the interval of the upper gate voltage V_{top}, where the threshold voltage of the lower gate threshold voltage ($V_{th,sub}$) is a linear function of top gate voltage V_{top} or $V_{th,sub} = A'V_{top}$. This effect was used to control the subthreshold regime for 2G nanowire transistors, providing the sensitivity to proteins in biological liquids at the level as low as near femtomole/l. The thinner the silicon layer, the higher the sensitivity of the sensor, due to growth of the ratio of atoms on surface and in volume. However, it is known, that the thickness of the Si layer $h_{Si} < 10$ nm leads to quantum mechanical (QM) dimensional effect, which limits the current in the channel of FET devices. They should be taken into account to correctly predict the interval of LF effect for the charge coupling. It is particularly important to take into account an additional effect, reinforced by high electrostatic (ES) field between the two gates for 2G transistors in asymmetric mode (AM) of operation, which limits the region of current flow. This additional effect was observable for relatively thick films of silicon (h_{Si} ~ 20-30 nm), where threshold voltage, as generally considered, does not depend on the effects of dimensional quantization.

In our work we investigated the expression of ES LF effect even in much thicker Si films up to $h_{Si} = 200$ nm, taking into account the charge state on both Si/SiO_2 interface as in real experiments in biological liquids. Two types of devices ($h_{Si} = 40$ and 200 nm) were tested in the model experiments. The threshold voltage of the gates were determined using experimental and calculated I_{Ds} - V_{top} curves and differentiation dG_M/dV_{top}, where $G_M = dI_{Ds}/dV_{top}$, is the conductance of the channel. Calculations of threshold voltage (V_{th}), sub(V_{top}) was carried out without / with charged states at interfaces entered to match the calculations with the measurements. Si film thickness was experimentally determined by X-SEM measurements and comparison with simulation of LF effect region in classical approach of calculation similar to LF model. The last one showed an overestimation of Si film thickness. The numerical calculations by TCAD Synopsys with classical and quantum models showed, that the difference between classical and quantum threshold voltage $\Delta V_{th} = V_{QMth,sub}(V_{top}) - V_{Clth,sub}(V_{top})$ is reduced from 140 to 50 mV with the introduction of rechargeable states on the upper boundary with Si/SiO_2 in contrast to the results obtained for lower thicknesses $h_{Si} = 20–40$ nm in work [2]. Calculated and experimental curves for thick 200 nm Si film 2G FETs show that I_{ds} - V_{sub} and dg_m/dV_{subp} dependences have got the features due to the formation of at least two ways for current flows near each gates and even more at the edges of real 3D structures in the experiment. A comparative analysis of the data with the corresponding values of the properties of charge carriers in Si layers and their traps at the both interfaces shows a similarity between experiments and calculations. For last one it was shown using QM and classic approach that even for microscopic thickness of Si layer $h_{Si} = 0.2$ μm the difference in saturation threshold voltages in asymmetric mode is still measurable $\Delta V_{th} = 0.05$ V. Quantum dimensional effect in strong transversal electrostatic field leads to narrow triangle well for charge carriers in the cannels with comparative width to quantum depletion width d_{Qua} at the Si/SiO_2 interfaces decreasing the full capacity as $C = S\varepsilon_0\varepsilon_{Si}/[h_{Si}(1 + d_{Qua}/h_{Si})] = S\varepsilon_0\Delta V_{th}\varepsilon_{Si}(1 - d_{Qua}/h_{Si})/h_{Si}$, where S is the gate area. Then ΔV_{th} is equal to $\Delta V_{th} = q\Delta C = -qS\varepsilon_0\varepsilon_{Si}d_{Qua}/h_{Si}^2$. These results show that the ES in LF effect should be considered even for 200 nm 2G FETs in the AM regime defining the region of linear dependence of LF effect of the charge coupling. This dependence is clearly observed not only for tens but even for hundreds nanometers. SEM measurements also confirm overestimation of Si film thickness by calculating of LF effect on $2d_{Qua}$ ~ 3 nm in accordance with numerical QM simulation.

1. H.K. Lim, J.G. Fossum. "Threshold voltage of thin-film silicon-on-insulator (SOI) MOSFETs", IEEE TED, **30**, pp.1244-1251, 1983.
2. V.P. Popov *et al.,* "Quantum corrections to the threshold voltage for fully depleted SOI transistors with two independent gates". Semicond., **48**, pp.1348-1353, 2014.

Simple models of Tristate transistors

S. Krivelevich
Institute of Physics and Technology (Yaroslavl Branch), RAS, Yaroslavl, Russia, s.kivelevich@mail.ru

Development of micro-nanoelectronics was associated with an increase in the number of transistors on a single processor for many years. This happened in the second half of the sixties of the last century to the present time probably. The dependence of the number of transistors in a single processor of the time period is described by an exponential function. This empirical relationship became known as Moore's Law after its author. The increasing number of transistors has been associated with a decrease in the size of individual transistors and increasing packing density.
At present, quite clearly, that attempts to further reduce linear single valve sizes lead to insoluble contradictions. These contradictions are caused by technological limitations and the fundamental laws of nature. On the other hand, transition from a silicon-based technology for processing other semiconductor materials also is not very promising. But it is possible to create a number of valves with stable logic states greater than two. One of the options for establishing such valves offered in this paper. We also consider simple mathematical and physical models describing the functioning of these tristate devices.
The proposed class of valves is based on bipolar - field devices that can be used as transistors. Each transistor must comprise two pairs of electrodes. Two electrodes are used to modulate the conductivity of the active region of the transistor. These electrodes can be called "emitter" and "collector". The other two electrodes are designed to "measure" of the active region of the transistor ("source" and "drain"), the layer conductivity. Each transistor should also contain injecting (extracting) p-n junction.
Described transistors have the following set of operating modes and conditions. When a large value of the voltage biases p-n transition in the forward direction, the transistor enters to the saturation mode with lower layers of the active region of the resistance. Resistance layers of the active region increases with a decrease in the value of the forward bias voltage. The transistor falls to a low level of injection mode. If you change the polarity of the voltage on the p-n transition begins depletion of the active region of the moving charge carriers. Sheet resistance begins to grow. Mode, in which the offset voltage is much less than the contact potential difference can be called active. The transistor in this case can be used as an amplifier. The transistor becomes quasi-stable depletion mode with a further increase in the absolute value of the reverse bias. In this mode, the sheet resistance of the active slowly increases with the absolute value of the reverse voltage. Further increase in the absolute value of the reverse bias leads to a sharp increase of layer resistance of the active region. The transistor switches in the full depletion mode. The full depletion mode sheet resistance hardly varies with increasing absolute value of the reverse bias. Further increase in the absolute value of the reverse bias leads to avalanche breakdown of p-n junction.
All these modes and states simply modeled using the classical equations of transfer of mobile charge carriers. These equations are widely used in micro- and nanoelectronics.
Technology of creation considered tristate gates is a classic "silicon" technology. It includes the creation of local processes and doped buried insulating regions, these processes are standard process.

Abrupt current switching in graphene bilayer tunnel transistors enabled by van Hove singularities

G. Alymov[1,2], V. Vyurkov[1,2], V. Ryzhii[3], D. Svintsov[1]
1. Moscow Institute of Physics and technology, 141700 Dolgoprudny, Russia.
2. Institute of Physics and Technology RAS, 117218, Moscow, Russia
3. Research Institute of Electrical Communication, Tohoku University, Sendai, Japan
alymow@yandex.ru

Graphene bilayer (GBL) is a unique material demonstrating a "Mexican-hat" electron-hole dispersion and possessing a van Hove singularity in the density of states (DOS) near the band edges. This singularity can manifest itself in an enhanced optical absorption [1] and conduction step in GBL field-effect transistors (FETs) [2]. In this report, we theoretically study the interband tunneling in gated GBL. We show that a singular DOS leads to a linear dependence of tunnel current J_{tun} on the conduction-valence band overlap, inherent to one-dimensional tunnel junctions. This dependence is much steeper than that in 2d semiconductors with parabolic bands, where $J_{tun} \propto \Delta_{cv}^{3/2}$. Motivated by this result, we propose and simulate a graphene bilayer tunnel FET with an electrically induced tunnel junction [Fig. 1 A] demonstrating a record steepness of the gate characteristics [3]. We show the accessibility of 3.5×10^4 ON/OFF current ratio with 150 mV gate voltage swing, and a maximum subthreshold slope of (20 μV/dec)$^{-1}$ (Fig. 2). High ON-state current of ~ 1 mA/μm is enabled by a narrow (<0.4 eV) extrinsic band gap, while the weak leakage current is due to the blocking of thermally injected minority carriers by the electric field of auxiliary gates at source and drain (Fig. 1 B). The proposed structure employs electrical doping instead of chemical one. This allows to avoid the band-tail and trap-assisted tunneling which masked the density-of-states features in the characteristics of GBL tunnel junctions reported previously [4].

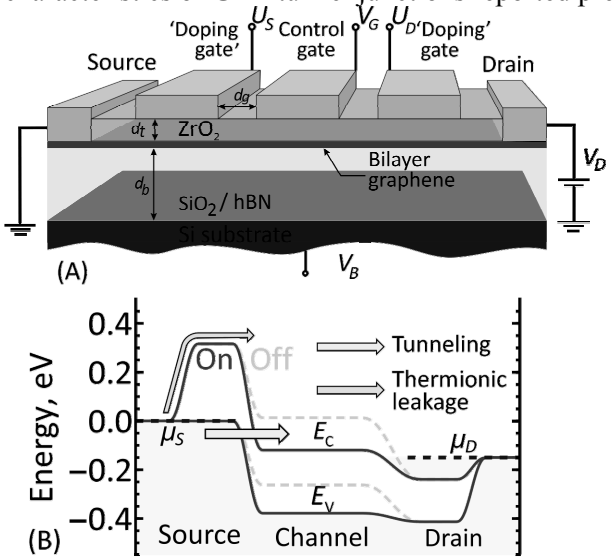

Fig. 1. (A) Layout of the proposed GBL tunnel FET with electrically defined tunnel junction (B) Band diagram for the optimal biasing conditions: $V_B > 0$, $U_S < 0$, $U_D > 0$. Red line corresponds to the ON-state, blue dashed line corresponds to the OFF-state.

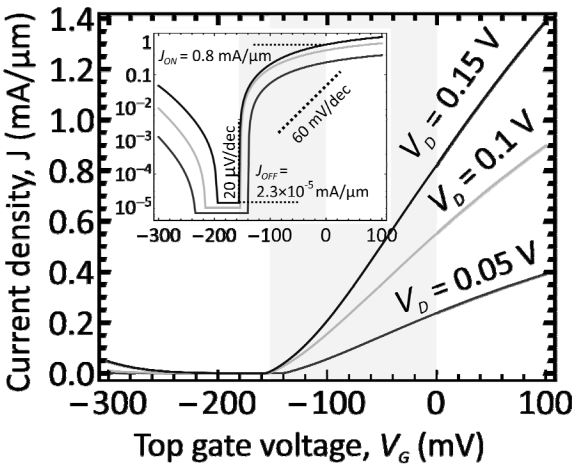

Fig. 2. Calculated gate characteristics of GBL tunnel FET at different drain bias and fixed voltages at auxiliary gates: V_B = 3.3 V, U_S= -0.6 V, U_D = 0.25 V. Top gate dielectric is 2 nm ZrO_2, κ = 25, back gate dielectric is 10 nm SiO_2. Inset: gate characteristics in the log scale. The optimal drive voltage range of 150 mV is highlighted.

1. A.B. Kuzmenko *et. al.* "Infrared spectroscopy of electronic bands in bilayer graphene" Phys. Rev. B **79**, 115441 (2009).
2. D. Svintsov *et.al.* "Effect of Mexican hat on graphene bilayer field-effect transistor characteristics" Jpn. J. Appl. Phys. **50**, 070112 (2011).
3. G. Alymov *et.al."*Abrupt current switching in graphene bilayer tunnel transistors enabled by van Hove singularities*"* Sci. Rep. **6** 24654 (2016).
4. H. Miyazaki *et. al.*"Observation of Tunneling Current in Semiconducting Graphene p-n Junctions" J. Phys. Soc. Jap. **81**, 014708 (2012).

Photoresponse in graphene field effect transistors under ultra-short pulsed laser irradiation

A.V. Emelianov[1], D.M. Kireev[2], I.I. Bobrinetskiy[3], N. Otero[3], P. Romero[3]
1. National Research University of Electronic Technology, Moscow, Russia, emmsowton@gmail.com.
2. Forschungszentrum Juelich GmbH, Juelich, Germany, d.kireev@fz-juelich.de.
3. Laser Applications Centre, AIMEN, Porriño, Spain, ivan.bobrinetskiy@aimen.es

Graphene is one of the most promising materials for advanced electronic applications, due to its extraordinary chemical and physical properties [1]. Particularly the interaction between graphene lattice and light irradiation opens the ways for development of new optoelectronics and photovoltaic devices and tuning their properties by chemical and physical patterning of graphene.

We have developed the ultra-short pulsed laser processing methods for patterning of graphene field effect transistors in topological and chemical way. The ultrafast laser pulses (pico- and femtoseconds) can provide not only photophysical but photochemical processes [2]. In laser ablation, with making use of fast galvoscanner (with scanning speed up to 2 m/s) and high numerical aperture lenses it is possible pattern graphene with resolution down to 1 μm at the scale up to 1×1 cm^2. The same processing parameters can be achieved for laser induced oxidation of graphene because of high intensity laser pulses providing nonlinear effect in graphene like multiphoton absorption and hot carries generation [3].

The process of laser induced local oxidation was investigated on single layer graphene field effect transistors (GFETs). GFETs were produced by wet transfer of CVD grown graphene on copper foil (graphene was provided by prof. X. Xie, SIMIT, China) onto the Si/SiO_2 substrate. The graphene was patterned in 20×20 μm^2 channels with drain and source Au/Ti contacts evaporated on top. The 280 fs laser with 515 nm wavelength applied to graphene with varied pulse energy to modify graphene electrical and optical properties. We observed that with increased laser fluence, the ON/OFF ratio of the GFET increases, the Dirac point shifts to the right side and the overall resistance of the channel increases. Moreover, the light induced response is larger for narrower graphene channels. This effect can be explained by different impact of resistance from contacts (R_C) and graphene channel (R_{Ch}): for narrow graphene the contact resistance can be negligible compare to the body resistance.

We investigated in details the photoresponse in graphene FETs before and after laser-induced modification for laser fluence below threshold energy. We observed two different mechanisms of the photoresponse under ultra-short pulses (280 fs). The photocurrent, observed for both pristine and laser processed graphene is raised because the laser induced charge is transferred from graphene to trapped levels in SiO_2 surface resulting in electrostatic Dirac point shift, thus local p-n junction organization. For laser oxidized areas we observed more pronounced photocurrent because of heterojunction formation in laser-processed area. While for electrostatic effect the relaxation time estimated as 50 seconds, the heterojunction relaxation is observed for less than 3 ms.

We discuss the possible mechanisms of laser induced modification of graphene and effects of ultra-short laser pulses in development of laser microprocessing technology of photovoltaic devices based on new principles.

1. A.C. Ferrari, F. Bonaccorso, V. Falko, K.S. Novoselov, S. Roche, P. Bøggild, and B.J. Van Wees. “Science and technology roadmap for graphene, related two-dimensional crystals, and hybrid systems”. Nanoscale, 7, pp. 4598-4810, 2015.
2. K.J. Tielrooij, L. Piatkowski, M. Massicotte, A. Woessner, Q. Ma, Y. Lee, ... & F.H. Koppens. “Generation of photovoltage in graphene on a femtosecond timescale through efficient carrier heating”. Nat. Nanotech, 10, 437-443, 2015.
3. I.I. Bobrinetskiy, A.V. Emelianov, N. Otero, P.M. Romero. “Patterned graphene ablation and two-photon functionalization by picosecond laser pulses in ambient conditions”. Appl. Phys. Lett., 107, p. 043104, 2015.

Field effect transistor with two-dimensional gate and channel with carriers in different valleys

V.G. Popov
Institute of Microelectronics Technology of RAS, Chernogolovka, Russia, popov@iptm.ru.

Application of resonant tunneling of carriers is considered in modern transistors. It is shown that the resonant character of the tunneling allows us to reduce a tunnel leakage current, which is one of the main causes of the crisis in the development of transistors today. The problem of the tunnel leakage current arose from extremely decrease of an oxide layer thickness in a metal-oxide-semiconductor field effect transistor (MOSFET) that accompanying by increase of the MOSFET cut-off frequency. The same tendency cases shrinkage of the MOSFET channel width provided size-quantization in a carrier spectrum. Thus the tunnel effect and two-dimensional systems of carriers (2DSC) are inherent to modern MOSFET. In particular when an operation-region size of MOSFET reduces down to 65 nm the tunnel current between gate and channel consists of more than 90% of whole leakage in the MOSFET [1].

In this paper a new type of field-effect transistor (FET) is proposed with a gate and a channel on the basis of 2DSC. The key point of the device is that the 2DSCs are different. In particular they are formed in different valleys of the carriers spectrum. Due to this difference the carrier tunneling requires additional excitations with significant momentum and energy. This decreases the tunneling rate significantly. For example the intervalley tunneling rate is less than intravalley that in 9 orders of magnitude in GaAs/AlAs heterostructures [2]. The two-dimensional character is also can decrease the tunnel probability in a wide voltage range [3].

Application of the FET with different valley 2DSCs in the gate and channel can significantly decrease the tunnel leakage and allow further cut-off frequency increase. Moreover in the case of low intervalley carriers scattering the dielectric layer can be removed that increases the transconductance of the FET. Some realization of the FET can be found in Figure 1. In the insert (a) the conduction-band-bottom diagram is shown of an $Al_{0.45}Ga_{0.55}As$ (layer 1)/AlAs(layer 2)/GaAs (layer 3) heterostructure. The heterostructure is modulation-doped by Si donors (see + in the insert (a)). The AlAs is indirect semiconductor where X-valley has lower energy than Γ-one. Hence in the layer 2 a quantum well (XQW) is formed in the X-valley that is shown by long-dashed line in the insert (a). The XQW can be used as a FET gate. A GaAs quantum well is formed in Γ-valley (ΓQW) and can be used as a FET channel. A topology of the FET is shown in Fig. 1. There are three ohmic contacts made to both QWs. Two of them are contacted to the ΓQW and third is contacted to the XQW (see arrow 3 in Fig. 1). To organize these separate contacts additional gates are used. In particular the gates 2 deplete the low ΓQW while gate 1 depletes XQW. Prospects of further transistor miniaturization are also discussed

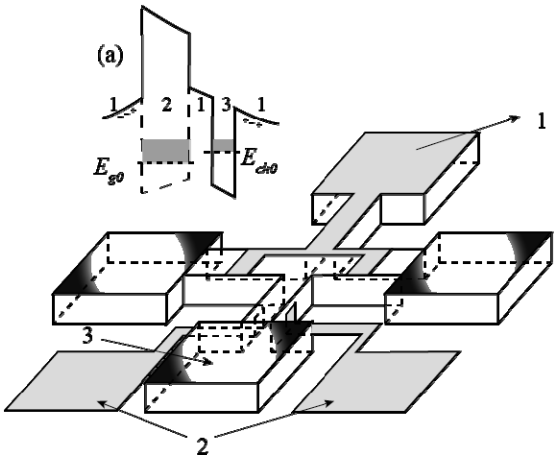

Fig. 1. Topology of the field-effect transistor with 2DCS in the gate and channel. In the insert (a) the conduction band bottom profile is shown for Γ-valley as solid line and for the X-valley in AlAs layer as long-dashed line.

1. E.N. Shauly. “CMOS Leakage and Power Reduction in Transistors and Circuits: Process and Layout Considerations”. J. Low Power Electron. Appl., **2**, pp. 1-29 (2012).
2. E.E. Mendez, E. Calleja, C.E.T. Goncalves da Silva, L.L. Chang, and W.I. Wang. “Observation by resonant tunneling of high-energy states in GaAs-$Ga_{1-X}Al_XAs$ quantum wells”. Phys. Rev. B, **33**, p. 7368 (1986).
3. V.G. Popov. “Field effect transistor with two-dimensional gate and channel”. Semiconductors, **50**, p. 235 (2016).

Problems and prospects of maskless (B)EUV lithography

N.I. Chkhalo, N.N. Salashchenko, M.N. Toropov
Institute for Physics of Microstructures of RAS, Nizhny Novgorod, Russia, chkhalo@ipmras.ru

Maskless lithography (MLL) in (B)EUV range can be an alternative to conventional electron beam lithography, combining high performance lithographic process characteristic of the projection optical lithography [1], and the absence of expensive masks as in electron beam lithography. If implemented in full, all advantages of this technology, it can be expected that (B)EUV MLL may take a certain niche and actually present a window of opportunity for domestic microelectronics industry in terms of small-scale production of chips with nanometer scale topology.

As the masks the MLL uses a computer-controlled microelectromechanical system (MEMS), the surface of which is covered with an interference coating, reflecting the (B)EUV radiation. So the MEMS provides an electronic coding mask. Similar schemes have been used successfully in the ultraviolet range, a resolution of about 100 nm was demonstrated [2]. However, until now, there are no significant results in (B)EUV range.

The objective of this work is the most common, a preliminary review of MLL's problems in (B)EUV region. The following issues are discussed.

1. Feasibility study MLL in this range. To do this on the basis of published technical and cost characteristics of commercially available electron beam lithographers to formulate the basic requirements for the MLL:
   - the minimum performance (wafers per hour) of the lithographic process;
   - the maximum cost of MLL installation.
2. Selection of the optical circuit (or class) for MLL system, optimized for (B)EUV range, and based on experimental data of the radiation sources efficiency, the reflection coefficients of mirrors and the photoresist sensitivity in (B)EUV region:
   - selection of the most promising wavelengths;
   - assessment of achievable at present and in the long term performance;
   - designation of the key issues that must be addressed to create an installation – an demonstrator of MLL technology.
3. A brief analysis of the state of affairs and scientific groundwork existing in Russia in the field of selected critical technologies for the MLL.

In the report we will focus on the following problems.

1. Optimization of the optical circuit of the MLL lithographer. Specificity of the problem as compared to conventional EUV lithography is that the required reduction is of x100 and above.
2. MEMS for coding images in (B)EUV range.
3. Diffraction quality optics for wavelengths beyond 13.5 nm with a numerical aperture NA > 0.4.
4. Sources of (B)EUV radiation. Specificity of the problem as compared with "traditional" sources for EUV-lithography is that the source to be required should be with a smaller size and higher pulse repetition frequency (in the limit a CD source).
5. XY scanning system.

This work was supported by RFBR, grants ## 16-07-00247 and 16-07-00306.

1. R. Menon, A. Patel, and H.I. Smith. "Maskless lithography". Materials Today, **8**, pp. 26-33, 2005.
2. D. Gil, et al. J. Vac. Sci. Technol. B, **21**, p. 2810, 2003.

Modeling the distribution of energy deposited by FIB in ion beam lithography

Ya. Shabelnikova, S. Zaitsev
Institute of Microelectronic Technology Problems and High Purity Materials, Chernogolovka, Russia, janeshabeln@yandex.ru

For various reasons, at present ion beam lithography is insignificant in comparison to the position of the electron-beam lithography. On the other hand ion beam lithography is very similar to electron beam lithography, but uses much heavier charged particles, ions. In addition to that ions move in straighter paths than electrons, secondary particles (mainly atoms) have very short ranges because of a lower speed of the ions [1]. This suggests that ion-beam lithography can overcome the fundamental physical resolution limit of electron beam lithography of ~10nm.

To verify this assumption, the authors had modeled the distribution of energy deposited by a focused ion beam (FIB) and estimated the size of deposited energy area for several ions (He, Ne, Ar, Ga, Kr, Xe and Rn) that can be used in ion lithography and two types of the most commonly used resists (PMMA and HSQ). The size of area where the main part of energy was deposited was investigated depending on the ion beam energy, ions mass and time of exposure. It was shown that in the case of heavy ions the transverse size of the deposited energy area (and, hence, the characteristic size of structure parts manufactured during the lithographic process) may be less than ten nanometers.

An analytical description was proposed for the function of deposited energy spatial distribution. The description is the product of two Gaussian functions. One of them describes the radial energy distribution; the other represents the dependence on depth. The widths and the centers of these Gaussian functions are determined by the range, transport length and atomic number of ions in the resist. The proposed description of the deposited energy distribution can allow the assessment of the resist modified area size for all types of ions with energies of tens keV and for light resists. Therefore it can be used for a priori estimates of the resolution and efficiency, as well as for selection of ion-resist pairs and ion beam energies.

1. Watt F., Bettiol A.A., Van Kan J.A., Teo E.J., and Breese M.B.H. " Ion Beam Lithography and Nanofabrication: a Review". International Journal of Nanoscience, **4**, pp. 269-286, 2005.

Experimental investigation of the distribution of energy deposited by FIB in ion-beam lithography

N. Gusseinov[1], M. Gabdullin[1], Ya.L. Shabelnikova[2], S.I. Zaitsev[2]
1. Al-Farabi Kazakh National University, Almaty, Kazakhstan
2. Institute of microelectronic technology problems and high purity materials RAS, Chernogolovka, Russia.
zaitsev@iptm.ru

Ion beam lithography is very similar to electron beam lithography, but uses much heavier charged particles, ions. For various reasons, at present ion beam lithography is insignificant in comparison to the position of the electron-beam lithography. In addition to that ions move in straighter paths than electrons, secondary particles (mainly atoms) have very short ranges because of a lower speed of the ions. This suggests that ion-beam lithography can overcome the fundamental physical resolution limit of electron beam lithography of ~10nm. But for various reasons, at present ion beam lithography is insignificant in comparison to the position of the electron-beam lithography.

In a report at the beginning the undoubted advantages of ion-beam lithography is listed and as consiquence a task of the study of basic laws of ion impact on modern resists is formulated. Two important results will be reported. First rigorous comparison of sensitivity of the resist (PMMA) to irradiation by electron and ion beams was conducted. It is shown that as in the case of an electron exposure the resist demonstrates both a positive (at low doses) and negative (at higher doses) behavior. It turned the sensitivity of the resist is approximately a thousand times higher in positive and in the negative regions. The second series of the experimental study concerned investigation of etching depth of the (thick) resist depending on the radiation dose. It is found that, in contrast to electron resist, the distribution of energy deposited is strongly inhomogeneous in depth, which results to strongly inhomogeneous etching rate as function of the depth and the radiation dose.

These data served as the basis for attempts to restore quantitatively the spatial distribution of the energy losses of fast ions in matter.

Resistless lithography: Selective etching of silicon with gallium doping regions

D. Abdullaev[1,2], R. Milovanov[1], D. Zubov [1]
1. Institute of Nanotechnology of Microelectronics, Russian Academy of Science, Russia, 119991 Moscow, Leninsky Prospekt, 32A, milovanov_r@inbox.ru
2. Moscow Technological University (MIREA), 119454 Moscow, Vernadsky Prospekt, 78, abdullaev@mirea.ru.

Usually during prototyping and manufacturing of different micro- and nanoscale structures we use different methods which includes sample surface covering with resist and further processing (lithography, development, etching, resist aching etc.). Recently resistless lithography methods explosive developing. One of the most dynamic methods based on focused ion beams (FIB). Commonly such FIB methods assume local surface modification by sputtering or etching. In this case ions from FIB implants to sample and changing some initial properties of material. Structures sensitive to such ion contamination can be made with a method which include local ion (Ga^+) implantation and further wet or dry etching [1 - 4].
In our work we research possibility of micro- and nanoscale silicon structures making with available equipment. Local ion implantation was done by the FIB system Quanta 200 3D FEI with source of gallium ions, for etching we used dry etching system PlasmaLab 100 OIPT. As a mask for local implantation we used the array of circles with different exposure time.
Our experimental research shows ability of use this resistless lithography method for formation micro- and nanoscale structures (fig.1). The form of the received structures considerably depends on an ion-implantation dosage, implantation strategy, plasma chemistry etc.

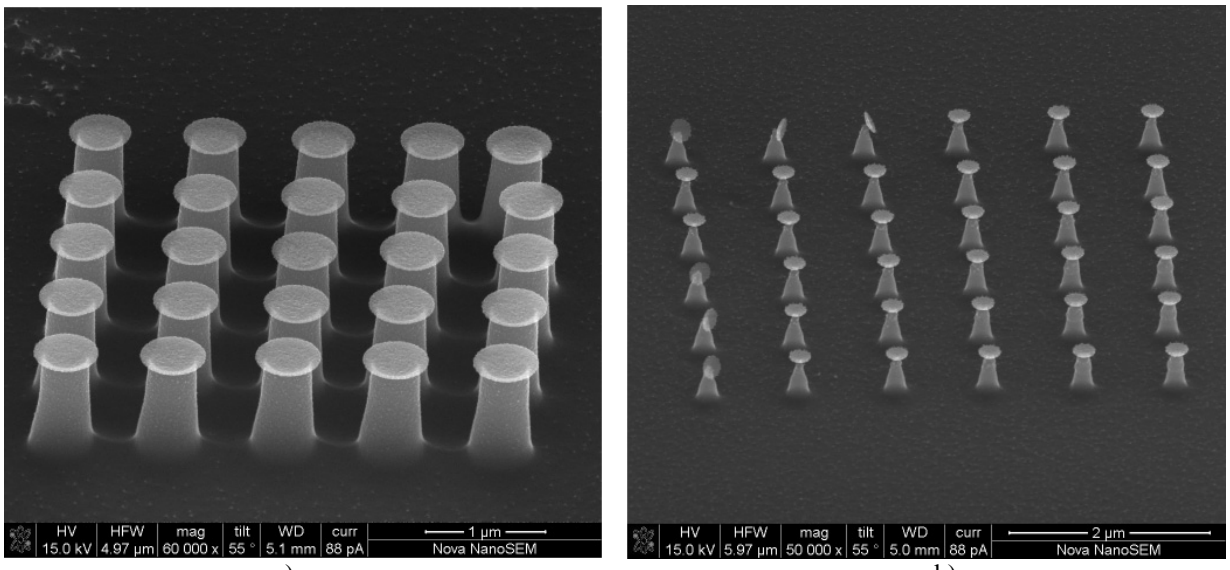

a) b)

Fig.1. Silicon surface after local ion (Ga^+) implantation and further dry etching.

1. Chekurov N., Grigoras K., Peltonen A., Franssila S., Tittonen I. "The fabrication of silicon nanostructures by local gallium implantation and cryogenic deep reactive ion etching". Nanotechnology **20**, 065307 (5), 2009.
2. Sievilä P., Chekurov N., Tittonen I. "The fabrication of silicon nanostructures by focused-ion-beam implantation and TMAH wet etching". Nanotechnology **21**, 145301 (6), 2010.
3. Schmidt B., Oswald S., Bischoff L. "Etch Rate Retardation of Ga^+-Ion Beam-Irradiated Silicon". J. Electrochem. Soc. **152**, pp. 875-879, 2005.
4. Fischer A.C., Gylfason K.B., Belova L.M., Malm B.G., Radamson H.H., Kolahdouz M., Rikers Y.G.M., Stemme G., Niklaus F. "Layer-by-layer 3D printing of Si micro- and nanostructures by Si deposition, ion implantation and selective Si etching". Proceedings of the 12th IEEE Conference on Nanotechnology (IEEE-NANO), 2012.

Features of local probe oxidation process

S.V. Lemeshko[1], A.N. Belov[2], Yu.A. Chaplygin[2], I.V. Sagunova[2], V.I. Shevyakov[2]
1. Nanotechnology Instruments Europe B.V, Netherlands, Lemeshko@spectrum-instr.com
2. National Research University of Electronic Technology, Russia, Sagunova@list.ru

The investigation of local probe oxidation process of solid bulk materials and thin conducting films started a long time ago. In contrast to the present-day projection-type photolithography where extreme ultraviolet is currently used for structure formation, the probe nanolithography based on local anodic oxidation is much more cost-effective and available for research laboratories. This method can be efficiently used both for local modification of different hard materials' properties and for the study of various active and passive components in nanoelectronics. The theoretical underpinnings of the procedure are being constantly advanced [1, 2].

While developing the local anodic oxidation model presented in [1] we did not take into account the device current limitations ($I_{\max}$) and obtained an expression for oxide thickness in the potentiostatic mode:

$$h_{ox}(t) = \frac{U - U_0}{E}\left(1 - \exp\left(-\frac{E\chi}{R_c S}t\right)\right), \quad (1)$$

where U is the bias voltage, and U_0 is the threshold voltage of anodic oxide formation, E is the electric field intensity in the dielectric material, R_c is the resistance of the 'conducting cantilever surface – conductive substrate' system, S is the oxidized area, $\chi = A_{ox}/(\rho_{ox} zF)$ is the electrochemical constant of the oxidation process, A_{ox} is the molar mass of the new material, ρ_{ox} is its specific density, z is the number of electrons required for oxidation reaction, F is the Faraday constant.

In this case, $R_c = (U - U_0)/I$, where $I < I_{\max}$ is the greatest possible magnitude of the current flowing through the system. In other words, $R_c > R_{bv}$, where R_{bv} is the intrinsic resistance of the bias voltage source in the AFM. The potentiostatic mode of anodization is effective here. In this work we show that at $R_c = (U - U_0)/I_{\max}$ and lower resistance values in the conductive cantilever-conductive surface system the constant current has an $I_{\max}$ limitation, and the galvanostatic mode of anodization takes effect. From 0 until t_1 the oxide growth takes place at the galvanostatic mode, wherein the oxide thickness, in accordance with (1), grows linearly:

$$h_{ox}(t) = \frac{\eta\chi}{S} I_{\max} t\,, \quad (2)$$

where η is the current yield. The galvanostatic mode lasts until t_1 when the thickness reaches the $(U - U_0)/E$ value. Later, the process switches to the potentiostatic mode and in a very short period the current value drops to zero. Thereby, if $R_c < R_{bv}$, the oxide thickness can be expressed by the following formula:

$$h_{ox}(t) = \frac{\eta\chi}{S} I_{\max} t, t \le t_1 \text{ and } h_{ox}(t) = \frac{U - U_0}{E}, t > t_1 \quad (3)$$

Thuswise, this mode allows to control the thickness of growing oxide carefully due to constant of velocity.

Earlier, there were theoretical attempts to make the process of height modulated oxide film formation multifunctional [3]. The work also demonstrates the possibility of creating a height-modulated oxide by applying the method of local anodic oxidation based on any greyscale modulated mask when the impulse duration and its magnitude is varied proportionally to the grayscale intensity.

This work was supported by both the Russian Scientific Foundation (Grant No. 15-19-00138) and Russian Foundation for Basic Research (Grant No. 16-38-00070).

1. A.N. Belov, S.A. Gavrilov, I.V. Sagunova, V.I. Shevyakov. "Kinetic of local oxidation of ultrathin metal films of V, Nb, Ta, Ti, TiN, W". J. Semiconductors, **44**, pp. 1709–1713, 2010.
2. Jen Fin Lin, Chih Kuang Tai, Shuan Li Lin. "Theoretical and experimental studies for nano-oxidation of silicon wafer by ac atomic force microscopy". J. Appl. Phys. Lett., **99**, pp. 1-11, 2006.
3. S. Lemeshko, V. Bykov, S. Saunin, V. Roschin, S. Gavrilov. "The factors influence investigation on a tip-induced oxidation process and its applications for nanoscale image creation". 12th International Conference on Scanning tunneling microscopy. Netherlands, pp. 83, 2003.

Automatic optimization of resistive switching parameters in HfO_2-based 1T1R devices

E. Kondratyuk, Y. Matveyev, I. Kiseleva, R. Kirtaev, D. Negrov, and A. Zenkevich
Moscow Institute of Physics and Technology, Dolgoprudny, Moscow Region, Russia,
E-mail address: ekaterina.v.kondratyuk@phystech.edu

Among the variety of alternative non-volatile memory concepts, the one based on the reversible resistance switching (RS) effect in a few-nm-thick dielectric layer (sandwiched between two electrodes) is one of the most promising [1]. It has a simple two-terminal architecture and can provide non-volatile storage with long retention times, high cycling endurance, low write and readout energy consumption. One of the key shortcomings hindering this type of memory from commercialization is the non-uniformity of cell characteristics during switching cycles, which is multiplied in big arrays by a number of cells.

The search for the optimal biasing parameters to switch the device is one of the serious issues, since the reliability of the device critically depends on the so-called "voltage overshooting". When dealing with tens of individual devices in the lab, this problem can be solved manually by the operator. However, it becomes unsolvable when it comes to large arrays of devices. In this work, we propose a fully automatic algorithm for the determination of RS effect parameters in 1 transistor-1 resistor (1T1R) devices. The developed methodology allows the optimization of all RS stages, from the initial forming up to the reliability testing. The input parameters are the transistor type, the approximate level of resistance (or just required R_{On}/R_{Off} ratio), and the required switching speed (e.g., switching pulse length). As a result, it provides all required information for further analysis of RS devices: the forming voltage, the switching voltage in DC and pulse regimes as well as resistance levels.

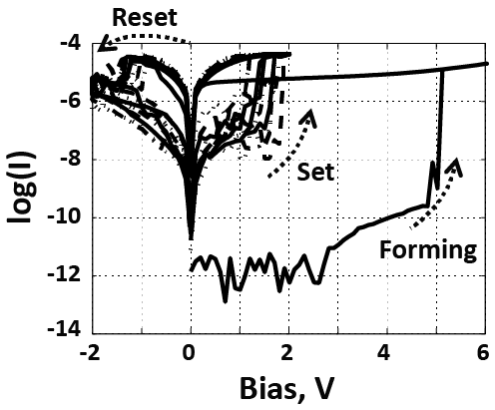

Figure 1. DC I-V curves

The proposed algorithm was tested on HfO_2-based 1T1R devices. The switching elements were made as a back end of line process on the silicon wafer with the 10×10 matrix of transistors pre-fabricated in the fab at *Mikron JSC*. More specifically, RS devices were formed on top of a second metallization layer and consist of a 20-nm-thick e-beam evaporated Pt bottom electrode, 6-nm-thick atomic layer deposited HfO_2 functional layer capped with a 50-nm-thick magnetron sputtered TiN layer used as the upper electrode. All deposited layers were patterned by maskless laser lithography in order to get 3×3 μm^2 devices.

Thus prepared 1T1R devices were tested by the proposed algorithm. It was found that as grown devices require forming at $U_{formig} = 3.4 \div 4.5$ V with the compliance current set to $I_{cc} = 6 \cdot 10^{-7} \div 1.4 \cdot 10^{-6}$ A (see Fig. 1 for example) defined by the transistor, working in saturation mode with $U_{gate} = 0.7 \div 1$ V. The set and reset voltages for DC regime were determined as $U_{set} = 1 \div 3.1$ V, $U_{reset} = -2 \div -3.5$ V (Fig. 1) and $U_{gate} = 0.7 \div 1.9$ V, providing $R_{Off}/R_{On} > 10$. For the pulses $\tau_{FWHM} = 5$ μs the operating voltages rises up to the following values: $U_{set} = 2 \div 5$ V, $U_{reset} = -2 \div -3.5$ V and $U_{gate} = 0.7 \div 1.9$ V (Fig. 2). In this regime, the devices exhibit the endurance more than $1 \cdot 10^5$ cycles. All these parameters were determined automatically, without any involvement of the operator. The obtained results show the workability of the proposed algorithm and strongly indicate that HfO_2-based 1T1R devices are the promising candidate for the next generation of non-volatile memory.

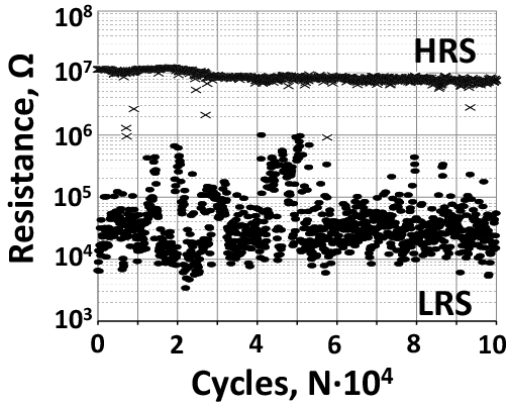

Figure 2. The results of endurance testing

1. R. Waser, "Redox-Based Resistive Switching Memories", J. Nanosc. and Nanotech., **12**, pp. 7628–7640, 2012.

Memristive devices for analog memory applications

S. Zimmermann[1,2,*], N. Köhler[1], A. Shah[1], P. Matthes[2], R. Reich[2]
1. Technische Universität Chemnitz, , Center for Microtechnologies, D-09107 Chemnitz, Germany
2. Fraunhofer ENAS, Department Back-end of Line, D-09126 Chemnitz, Germany
** Corresponding author: Phone: (+49) 371 531 33671, eMail: sven.zimmermann@zfm.tu-chemnitz.de*

With the evidence of the memristive effect by Strukov et.al. in the year 2008 [1] a lot of research activities concerning the fabrication of devices with memristive components took place. The efforts are mainly concentrated on the implementation of filament type resistive switches with a strong focus on resistive switching random access memory ReRAM. Aside from filament growth, titanium oxide based memristive systems offer an interface type switching mechanism based on the movement of bridging oxygen vacancies. The growth of parasitic filaments will be typical suppressed by using thicker titanium oxide layers. The corresponding small-signal behavior and the time dependent nonvolatile change in flowing current offer the possibility of beyond CMOS-devices, e.g. neuromorphic architectures, and special applications, e.g. hardware based data encryption [2] and self-sustaining sensor systems.

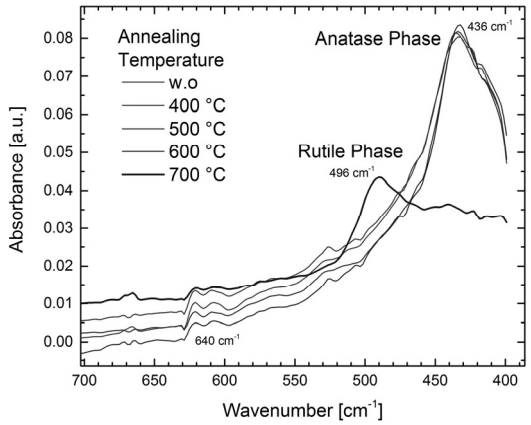

Fig. 1. Transition between anatase and rutile phase of TiO_x during annealing (dep. temperature: 550 °C)

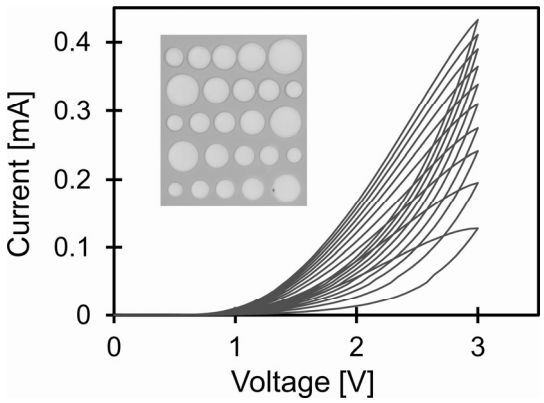

Fig. 2. Forward characteristics of TiO_x based memristive device (11 sweeps between 0 and 3 V)

The study deals with titanium oxide based memristive devices, which are mainly designated for the storage of voltage signals cumulatively over a defined time. Such devices are necessary to fabricate piezoelectric self-sustaining sensor systems with a combined voltage generation and storage functionality for long time vibration or shock monitoring. The requirements for such memristor applications differ from the specifications of filament type switches in the linearity, the threshold voltage for ballistic transport and the characteristic of the hysteresis. The analyzed film stacks consist of a titanium oxide double layer, in which one of the films is slightly doped with nitrogen during deposition, and two platinum electrodes. For interface type switching the rutile phase of TiO_x is necessary, which can be produced by a defined regime of high temperature deposition and annealing, see FTIR spectra in Fig. 1. Undoped TiO_x films form a stoichiometric TiO_2 after annealing whereas nitrogen doped TiO_x films show a transition to a substoichiometric conductive Magnéli phase with $Ti_xO_{(2x-1)}$ composition. This phase is the source for moveable oxygen vacancies, which are responsible for the hysteresis in the electrical behavior. With the changeover of oxygen vacancies from the Magnéli to the TiO_2 phase a nonvolatile drop in the resistivity of the films stack is reachable, see Fig. 2. This effect is reversible by applying the corresponding negative voltage. In this study the influence of film thickness and nitrogen concentration of doped and undoped TiO_x, geometrical dimensions of the electrodes and film compositions after annealing on the electrical device behavior was analyzed continuatively.

1 D. Strukov, G.S. Snyder, D.R. Stewart, R.S. Williams, "The missing memristor found", Nature **453**, p. 80, 2008.
2 N. Du, N. Manjunath, Y. Shuai, D. Bürger, I. Skorupa, R. Schüffny, C. Mayr, D.N. Basov, M. Di Ventra, O.G. Schmidt, H. Schmidt, "Novel implementation of memristive systems for data encryption and obfuscation", J. Appl. Phys. **115**, p. 124501, 2014.

Multiple Cell Upsets in Nanoscale Memories: Characterization and Modeling

G.I. Zebrev, A.M. Galimov, K.S. Zemtsov, I.V. Elushov
National Research Nuclear University MEPHI, Moscow, Russia, gizebrev@mephi.ru

The memory of the spaceborne semiconductor electronics is inevitably in contact with the space radiation environment. There is no reliable way to physically protect the integrated circuits from the penetrating action of the cosmic ray ions with typical energies ~ hundreds MeV/nucleon. The problem of the single event effects in memory cells has been arisen and realized in the eighties, and it is currently one of the most important challenges to ensure reliable operation of modern electronics at least in space environment [1, 2].The downscaling of the memory cell sizes into the sub-100 nm region has lead to an absolutely novel situation when a single ion track size turns out to be much larger than the cell size. Unlike the old low-scaled circuits, in which not everyone heavy ion hit leads to the single bit errors, the multiple cell upset (MCU) from a single particle normally cover a few (up to tens) neighboring memory cells. Thus, MCUs are typical for the highly scaled memories. If the upset cells belong to the same logical word they are named multiple-bit upsets (MBUs) which are uncorrectable by simple error correction codes. Therefore, the rise of the multiple cell upsets has led to new challenges for efforts to calculate the soft error rate (SER) and ensuring of reliable functioning in the space. This report is devoted to some new challenges and ideas in concerning the MCU physics, characterization, soft error rate (SER) computation, and error correction [3-5].

1. E.L. Petersen et al. “Single Event Revolution,” IEEE Trans. Nucl. Sci. Vol. 60, No. 3, pp. 1824-1825, 2013.
2. G.C. Messenger, G.C.M. Ash, *Single Event Phenomena* / Springer-Science. Chapman & Hall, 1997.
3. G.I. Zebrev et al., “Statistics and methodology of multiple cell upset characterization under heavy ion irradiation,” Nuclear Instruments and Methods in Physics Research Sec. A, Vol. 775, pp. 41-45, March 2015.
4. G.I. Zebrev et al., “Multiple Cell Upset Cross-Section Uncertainty in Nanoscale Memories: Microdosimetric Approach,” RADECS -2015 Proceed., pp. 1-5, 2015.
5. G.I. Zebrev, K.S. Zemtsov et al., “Multiple cell upset cross-section modeling: A possible interpretation for the role of the ion energy-loss straggling and Auger recombination,” Nuclear Instruments and Methods in Physics Research Sec. A, Vol. 827, pp. 1-7, August 2016.

Crossbar Nanoscale HfO_2-Based Electronic Synapses

Y. Matveyev, R. Kirtaev, A. Fetisova, S. Zakharchenko, D. Negrov, and A. Zenkevich
Moscow Institute of Physics and Technology, Dolgoprudny, Moscow region, Russia,
E-mail address: matveyev.ya@mipt.ru

Modern computers based on the von-Neumann architecture cannot compete with their biological counterparts in solving some problems of the real world. The challenge is to build brain-inspired, "neuromorphic" computational systems, which mimic the ability of the brain to perform energy-efficient and fault-tolerant computation as well as to combine memory and computation in single elements. Until recently, one of the more serious "bottlenecks" of the latter approach has been the lack of a compact device emulating the functionality of biological synapses.

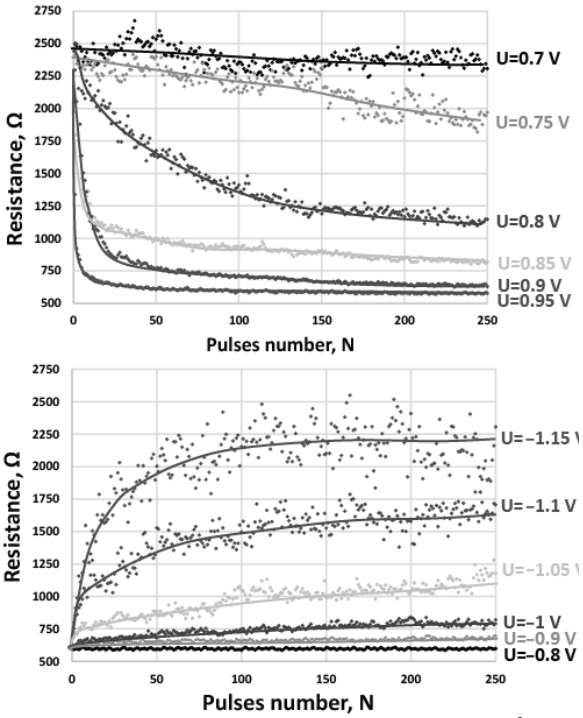

Figure 1. The resistance of 40 × 40 nm² 4 nm-thick HfO_2 device vs. biasing pulse number: a) SET and b) RESET transition, emulating long term potentiation and depression in biological synapses, respectively

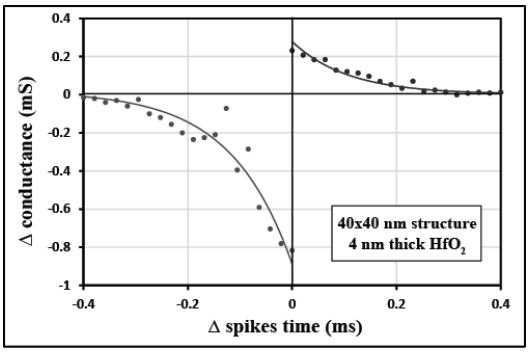

Figure 2. Asymmetric STDP function emulated in 40 × 40 nm², 4 nm-thick HfO_2 memristors

The gradual, analog-like transition between the resistance states observed in memristors emulates the plasticity of biological synapses. Other properties of memristors, such as scaling to tens nm lateral size, low energy consumption per switching event and the possibility for 3D integration in crossbar geometry with the current CMOS technology, make them attractive candidates for synaptic devices.

The purpose of this work is to integrate HfO_2-based memristors in crossbar geometry down to 40×40 nm² in size and to demonstrate their synaptic functionality.

The matrices of Pt/HfO_2/TiN devices were produced, utilizing the developed BEOL-compatible process, combing e-beam and optical lithography. The 4 series of samples, comprising 3, 4, 5, and 6 nm-thick HfO_2 functional layer were studied.

Upon electroforming with current compliance I_{cc} = 1 mA, the devices exhibit resistance switching to low/high resistance state at U_{SET} ~ +0.8÷1 V / U_{RESET} ~ -0.8÷1 V. For "fresh" devices R_{off}/R_{on} is ~15, while the endurance is ~$2 \cdot 10^5$ switching cycles.

Figure 1 displays memristive (gradual) switching of 4 nm-thick Pt/HfO_2/TiN devices, following the series of τ = 2 μs long identical bias pulses. The observed behavior emulates the so-called "long term plasticity" process in biological synapses. Moreover, the devices exhibit the so-called pair-pulse fluctuation behavior of biological synapses, where the relative change of resistance depends not only on the amplitude, but also on the delay time between voltage pulses (not shown).

Emulation of another learning mechanism – spike-timing-dependent plasticity – was performed with the help of previously developed methodology, utilizing the electric signals ("spikes") with the shape, reproducing shape of real biological spikes. The resulting relative change of the conductance ΔG as a function of the spikes' delay time Δt obtained for 4-nm-thick HfO_2 40×40 nm² device is shown in Fig. 2.

The emulated synaptic functionalities indicate the suitability of the developed nanoscale TiN/HfO_2/Pt memristor devices for hardware implementation of hybrid CMOS/memristor neural networks (CMHNN).

Electronic and phonon properties of molecular switch based on Y-splitter of trans-polyacetylene molecules

M.N. Zhuravlev[1], A.A. Gorbatsevich[1, 2], T.S. Kataeva[1]
1. National Research University of Electronic Technology, Moscow, Russia, aagor137@mail.ru
2. P.N. Lebedev Physical Institute of the Russian Academy of Sciences, Moscow, Russia

Quantum design of molecular structures is a new interdisciplinary approach to design of logical gates. It allows to decrease in size of functional elements to single molecule scale. In present this direction develops on the way of production of high-ordered technological polymer materials with possibility to modify of magnetic, electronic and optical properties [1]. The most accepted method for modification of structure and properties of the basic polymer chain is copolymerization of monomers in the chain with monomers which contain additional functional groups. Such polymers become nonlinear and their properties – depending on topology and interaction between chains. Polymers with conjugated π-bonds are in great interest for electronics.

The simplest structure of a molecular switch is Y-splitter formed by combination of three polyacetylene molecules. It is shown that there are several stable configurations of Y-splitter with a different symmetry. The real geometry of the molecular structure and the Coulomb interchain interaction can be properly taken into account in *ab initio* simulations in the framework of the density functional theory. Transitions between different configurations are realized by means of rotation of the splitter's branches.

Two levels appear in the energy gap of Y-splitter at branching of long trans-polyacetylene molecules corresponding to topological localized states near the branching point [2]. Unlike bound state on impurity atom, the bound states of this type exist both one for electron and one for hole. So local narrow of the energy gap occurs. Presence of additional charge carries changes locally the electrostatic potential and the molecule's reaction properties what assists, in particular, connection of new functional groups. Formation of splitter leads to asymmetry of the HOMO-orbilal's electron density distribution between different branches and localization near the branching point. However, the phase permanence keeps in the boarder of the unity cell. Localization take place at minimal length of attached chain without essential changes in the energy spectrum.

Raman spectrums of polyacetylene molecules have well-defined structure with two strong lines corresponding to ν_1 and ν_3 normal modes. These lines associate with Ag phonon. Chemical defects like a branching point and conformational transformations associated with rotation of splitter's branches change overlap of π-electrons between nearest carbon atoms and lead to partial coherence breakdown of main vibrational modes. This effect affects in structure of the vibrational spectrum. Four intensity lines appear in Raman spectrum of the Y-splitter in frequency range 1450–1650 cm^{-1} instead single ν_1 mode. Three of these lines with frequencies 1491, 1527, and 1570 cm^{-1} are localized in contrast to delocalized ν_1 and ν_3 normal modes. Localization is confirmed presence of maximums in potential energy distribution. Vibrational amplitudes decay at moving off the branching point. Separated lines can combine in one wide band at certain conditions. Splitting is explained by mechanical interaction and changes in the shape of normal vibrations. Strong influence of molecule extend on intensities in Raman spectrums is explained presence of strong interference at superposition of the coherent vibrations in branches of molecule.

Injection of electric charge in the splitter creates stable polaronic-like state in the one branch near the branching point. This state creates additional levels in the early forbidden energy range. As a result, the energy of HOMO orbital increases depending on splitter branch length. HOMO-LUMO gap in splitter of $C_{20}H_{22}$ molecules equals 1.43 eV for the original neutral polymer and 0.41 eV to for configuration with injected charge. Group of carbon atoms near the branch point becomes more tenuous. The length of the chemical bond increases from 1.39 Å to 1.43 Å. This bond becomes single-one. The shape of branches of the splitter changes as well.

1. D.M. Bassani, L. Jonusauskaite, A. Lavie-Cambot et al "Harnessing supramolecular interactions in organic solid-state devices: Current status and future potential". Coord. Chem. Rev., **254,** pp. 2429–2445, 2010.
2. A.A. Gorbatsevich, M.N. Zhuravlev. "Localized Electronic States in Branching Polyacetylene Molecules". JETP Letters, **100**, pp. 576–580, 2014.

Magnus paradox for entanglement in multi-pulse spin locking

E.B. Fel'dman[1], D.E. Feldman[2], E.I. Kuznetsova[1]
1. Institute of Problems of Chemical Physics of Russian Academy of Sciences, Chernogolovka, 142432, Moscow Region, Russia.
2. Department of Physics, Brown University, Providence, Rhode Island 02912, USA

We consider a two-spin system coupled by the dipole-dipole interaction (DDI) in a multi-pulse spin locking NMR experiment[1] where the system in a strong external magnetic field is irradiated by a periodical sequence of resonance rf-pulses. We use an effective time-independent Hamiltonian[2] (the Floquet Hamiltonian) for the investigation of entanglement in the system. The standard approach for the calculation of the Floquet Hamiltonain is the Magnus expansion. Within that approach, entanglement never emerges at any parameters of the pulse sequence. This conflicts with our exact results. There are no entangled states, indeed, in the multi-pulse spin locking NMR experiment with $\pi/2$ pulses. However, entanglement emerges in the multi-pulse spin locking with $\pi/4$ pulses.

We clarify the reasons of the conflict of the two approaches for $\pi/4$-pulses and their agreement for $\pi/2$-pulses. The difficulties of the Magnus expansion are related to the multi-valueness of the Floquet Hamiltonian and the divergence of the Magnus expansion[3]. This means that the choice of the proper branch of the Floquet Hamiltonian is very important. The effect of the branch choice is demonstrated on the model of the continuous spin locking NMR experiment[4].

Our analysis extends beyond NMR to many problems in periodically driven interacting lattice systems which have recently attracted much interest[5,6].

This work was partially supported by the Russian Foundation for Basic Research, Grant No. 16-03-00056 and by the Program of RAS "Element base of quantum computers" (Grant No. 0089-2015-0220).

1. A. Abragam, M. Goldman. *Nuclear magnetism: order and disorder*. Clarendon Press. Oxford. 1982.
2. E.I. Kuznetsova, E.B. Fel'dman, D.E. Feldman. "Magnus expansion paradoxes in the study of equilibrium magnetization and entanglement in multiple spin locking". Physics-Uspekhi **59**, issue 6 (2016).
3. E.B. Fel'dman. "On the convergence of the Magnus expansion for spin systems in periodic magnetic fields". Physics Letters A **104**, 479 (1984).
4. M. Goldman. *Spin temperature and nuclear magnetic resonance in solids*. Oxford. Clarendon Press. 1961.
5. L.D. Alessio and M. Rigol. "Long time behavior of isolated periodically driven interacting lattice systems". Physical Review X **4**, 041048 (2014).
6. T. Micami, S. Kitamura, K. Yasuda, N. Tsuji, T. Oka, H. Aoki. "Brillouin-Wigner theory for high-frequency expansion in periodically driven systems: Application to Floquet topological insulators". Physical Review B **93**, 144307 (2016).

MQ NMR dynamics and quantum correlations in dimers in the multiple-quantum NMR experiment

S.A. Gerasev[1,2], E.I. Kuznetsova[2]

1. M.V. Lomonosov Moscow State University, Faculty of Fundamental Physical-Chemical Engineering, 119991, Moscow GSP-1, Russia.

2. Institute of Problems of Chemical Physics of Russian Academy of Sciences, Chernogolovka, 142432, Moscow Region, Russia

Quantum correlations in multiple-quantum (MQ) NMR experiments[1] are investigated in two-spin systems. Crystalline hydrates are examples of such systems. In the initial moment of time one spin is in a pure quantum polarized state and the other spin is in the thermodynamic equilibrium state defined by the temperature of the sample. This state can be written as

$$\rho_0 = \frac{(\alpha \mid 0> + \beta \mid 1>)(\alpha^* < 0 \mid + \beta^* < 1 \mid) \otimes exp\left(\frac{\hbar \omega_0}{kT} I_{2z}\right)}{Z}, \qquad (1)$$

where Z is the partition function ($Z = \mathrm{Tr}\{\rho_0\}$), α and β are complex numbers($|\alpha|^2 + |\beta|^2 = 1$), and I_{2z} is the z-projection of the spin angular momentum of spin 2. MQ NMR dynamics on the preparation period of the MQ NMR experiment can be described by the two-spin Hamiltonian[1,2]

$$H_{MQ} = d(I_1^+ I_2^+ + I_1^- I_2^-), \qquad (2)$$

where $d = \frac{\gamma^2 \hbar (1 - 3\cos^2 \theta_{12})}{2 r_{12}^3}$ is the dipole-dipole coupling constant of spins 1 and 2, $I_{1,2}^{\pm}$ are raising and lowering operators. It is shown that only the MQ NMR coherences of the zeroth and +/- second orders emerge in this model. The intensities of those coherences are

$$G_0(\tau) = \frac{(e^b |\alpha|^2 - |\beta|^2)\cos^2(2d\tau)}{e^b + 1}, \qquad G_{\pm 2}(\tau) = \frac{(e^b |\alpha|^2 - |\beta|^2)\sin^2(2d\tau)}{2(e^b + 1)}, \qquad (3)$$

where $b = \frac{\hbar \omega_0}{kT}$ is a dimensionless parameter. It is shown that entanglement emerges at arbitrary temperatures for the considered model. We have found a relation between the concurrence and the intensities $G_{\pm 2}$ of the MQ NMR coherences of the +/- second order.

$$C = \frac{\left|\left(e^b |\alpha|^2 - |\beta|^2\right)\sin 2d\tau\right|}{e^b + 1} = \sqrt{\frac{\left(e^b |\alpha|^2 - |\beta|^2\right)\left(G_2(t) + G_{-2}(t)\right)}{e^b + 1}}. \qquad (4)$$

The quantum discord[3] is obtained in the high temperature approximation. The optimization of the quantum conditional entropy was performed with the computer resource “Mathematica”. The quantum discord exists even when the concurrence equals zero.

This work was supported by the Russian Foundation for Basic Research (Grant 16-03-00056) and Program of the Presidium of RAS 1.26 Electron Spin Resonance, Spin-Dependent Electron Effects and Spin Technologies (grant 0089-2015-0191)

1. Baum J., Munowitz M., Garroway A.N. et. al. "Multiple-quantum dynamics in solid state NMR". J. Chem. Phys., **83**. pp. 2015-2025, 1985.

2. Fel’dman E.B. and Pyrkov A.N.. “Evolution of Spin Entanglement and an Entanglement Witness in Multiple-Quantum NMR Experiments”. JETP Letters, **88**, pp. 398–401, 2008.

3. Ollivier H., Zurek W.H. “Quantum discord: a measure of the quantumness of correlations”. Phys. Rev. Lett., **88**, 017901, 2001.

Entanglement of the sender and receiver at the quantum state transfer in a spin chain with the XY Hamiltonian

I.D. Lazarev[1,2], E.I. Kuznetsova[2]

1. M.V. Lomonosov Moscow State University, Faculty of Fundamental Physical-Chemical Engineering, 119991, Moscow GSP-1, Russia.

2. Institute of Problems of Chemical Physics of Russian Academy of Sciences, Chernogolovka, 142432, Moscow Region, Russia.

Transfer of a pure quantum state from the first node of a one-dimensional spin chain to an arbitrary node is considered. The state transfer[1] is controlled by the XY interactions of the nearest neighbor spins. In the initial moment of time all spins besides the first one are in the thermodynamic equilibrium state. A transfer of the pure quantum state of the first polarized spin is investigated. The Fidelity[2] is used to estimate the accuracy of the quantum state transfer. The Fidelity[2] is

$$F = \langle \psi | \rho_m | \psi \rangle, \tag{1}$$

where $|\psi\rangle = a|0\rangle + b|1\rangle$ is the transmitted quantum state (a, b are complex numbers, $|a|^2 + |b|^2 = 1$), ρ_m is the density matrix of the system when spin m is the receiver. We have obtained an exact formula

$$\begin{aligned} F = & \frac{e^{\beta} - e^{\beta}|b|^2 + |b|^2 + |f|^2 (2e^{\beta}|b|^4 + 2|b|^4 - e^{\beta}|b|^2 - 3|b|^2 + 1)}{e^{\beta} + 1} \\ & + 2|ab|^2 \operatorname{Re} f \cdot \left(- \tanh\left(\frac{\beta}{2} \right) \right)^{N-1}, \end{aligned} \tag{2}$$

where the transmission function f is

$$f = \frac{2}{N+1} \sum_{n=1}^{N} \exp(i \cos(k)\tau) \sin(k) \sin(mk), \tag{3}$$

where $k = \frac{\pi n}{N+1}$, $n = 1,2...N$ and τ is the transfer time. In order to study entanglement between the sender and the receiver we have obtained the density matrix, reduced over all spins except the sender and receiver. The conccurrence[3] is used for the calculation of entanglement. We have found that entanglement emerges in the course of the pure quantum state transfer. The dependence of entanglement on the chain length and the temperature is also investigated. When the chain length increases the transfer time increases too and the fidelity and entanglement get less. The critical temperature of the emergence of entanglement is found. Our investigations demonstrate that a one-dimensional spin chain with the XY interactions can be considered as a quantum register for problems of quantum communication.

This work was partially supported by the Russian Foundation for Basic Research, Grant No. 15-07-07928 and by the Program of RAS “Element base of quantum computers” (grant No. 0089-2015-0220).

1. S. Bose. “Quantum Communication through an Unmodulated Spin Chain”, Phys. Rev. Lett., **91**, 207901, 2003.
2. R. Jozsa. “Fidelity for Mixed Quantum States”. Journal of Modern Optics, **41**, pp. 2315-2323, 1994.
3. S. Hill and W.K. Wootters. “Entanglement of a Pair of Quantum Bits”. Phys. Rev. Lett., **78**, p. 5022, 1997.
4. E.B. Fel’dman, E.I. Kuznetsova, and A.I. Zenchuk. “Temperature-dependent remote control of polarization and coherence intensity with sender's pure initial state”. Quantum Information Processing, **15**, pp. 2521-2552, 2016.

Permanent characteristics of spin-communication line and robustness of remote two-qubit state creation

J. Stolze[1], A.I. Zenchuk[2]
1. Technische Universität Dortmund, Fakultät Physik, D-44221 Dortmund, German, E-mail address joachim.stolze@tu-dortmund.de
2. Institute of Problems of Chemical Physics, RAS, Chernogolovka, Moscow reg., Russia, E-mail address zenchuk@itp.ac.ru

We consider the problem of remote state creation of the two-qubit receiver using the two-qubit excitation pure initial state of the four-qubit sender [1]. This is a prolongation of the problem of the one-qubit state creation considered in our recent works [2, 3], which, in turn, are the consequent development of the well known problem of pure state transfer first formulated by Bose [4] and then developed in series of papers [5-7].

The communication line of our interest is based on the optimized boundary controlled chain with the two pairs of properly adjusted coupling constants whose dynamics is governed by the nearest-neighbor XY-Hamiltonian. We show that the communication line can be characterized by a set of parameters P independent of the initial state of the sender. These parameters are permanent attributes of a communication line and can be either calculated theoretically or measured in experiment. Their number is defined by the dimensionality of the both sender and receiver and does not depend on the length of the communication line. These are parameters responsible for the size and position of the creatable region of the receiver's state space. The creation of a particular state within the creatable region is achieved by a proper choice of the independent parameters of the sender's initial state (control parameters) and reduces to the solvability of a certain system of algebraic equations. The creation of the two-qubit Werner state is considered as an example. We also show the robustness of the state-creation with respect to the chain imperfections which are the deviations of the coupling constants from their required values. These imperfections change the above mentioned parameters P. To show the robustness, we introduce the mean values of these parameters and their standard deviations from theoretically prescribed values and show that these deviations are ~5 % for small imperfections ~5 %.

This work is partially supported by the program of RAS "Element base of quantum computers" (No. 0089-2015-0220) and by the Russian Foundation for Basic Research, grant No.15-07-07928.

1. J.Stolze and A.I. Zenchuk, "Remote two-qubit state creation and its robustness", Quant. Inf. Proc., **15**, pp. 3347-3366, 2016.
2. A.I. Zenchuk, "Remote creation of a one-qubit mixed state through a short homogeneous spin-1/2 chain", Phys. Rev. A, **90**, 052302(13), 2014.
3. G.A. Bochkin and A.I. Zenchuk, "Remote one-qubit-state control using the pure initial state of a two-qubit sender. Selective-region and eigenvalue creation", Phys. Rev. A **91**, 062326(11), 2015.
4. S. Bose, "Quantum Communication through an Unmodulated Spin Chain", Phys. Rev. Lett., **91**, 207901(4), 2003.
5. M. Christandl, N. Datta, A. Ekert, and A.J. Landahl, "Perfect State Transfer in Quantum Spin Networks", Phys. Rev. Lett. **92**, 187902(4), 2004.
6. P. Karbach and J. Stolze, "Spin chains as perfect quantum state mirrors", Phys. Rev. A, **72**, 030301(4)(R), 2005.
7. G. Gualdi, V. Kostak, I. Marzoli, and P. Tombesi, "Perfect state transfer in long-range interacting spin chains", Phys. Rev. A, **78**, 022325(5), 2008.

Remote creation of one-qubit mixed state and its optimization via local unitary transformations

G.A. Bochkin, A.I. Zenchuk
Institute of Problems of Chemical Physics of RAS, Chernogolovka, Moscow region, Russia, bochkin.g@yandex.ru.

The pure state transfer problem in a system of spin-1/2 particles was first considered by Bose [1] for a homogeneous chain. Then, to provide perfect (or high probability) state transfer in long chains, the fully engineered (with properly adjusted coupling constants) and the boundary-controlled spin chains (with adjusted boundary coupling constants) were considered [2, 3].

Now we extend the problem of pure state transfer and consider the remote state creation problem [4, 5]. Here we study the problem of remote creation of a mixed state of the 1-qubit receiver using the variable parameters of the initial state of the 2-qubit sender. A chain of spin-1/2 particles with XY interaction is used as a transmission line. We show that the parameters of the receiver's created state can be expressed in terms of the parameters of the sender's initial state and set of transition amplitudes. The properties of the map (sender parameters) → (receiver parameters) are studied in detail. It is shown that the entire receiver's state space is creatable only in chains engineered for perfect end-to-end state transfer.

In general, only a subregion of the receiver's state space is creatable. Therefore, as a characteristic of the communication line, we propose the interval of creatable eigenvalues of the receiver's state (there is only one independent eigenvalue of a one-qubit receiver). We found that, in the case of homogeneous chain with the nearest-neighbor interactions, any eigenvalue can be created in communication lines of up to $N_c = 34$ nodes. However, this length can be significantly increased in the model with all dipole-dipole interactions involving an additional local unitary transformation at the receiver side [6]. In this case, we obtain $N_c = 109$. The same transformation allows us to increase the high-probability (i.e. > 0.9) pure-state transfer in homogeneous chains from $N = 4$ to $N = 17$ nodes.

This work is supported by the program of RAS "Element base of quantum computers" (No. 0089-2015-0220) and by the Russian Foundation for Basic Research, grant No.15-07-07928.

1. S. Bose, "Quantum Communication through an Unmodulated Spin Chain". Phys. Rev. Lett. **91**, 207901 (2003).
2. M. Christandl, N. Datta, A. Ekert, and A.J. Landahl, "Perfect State Transfer in Quantum Spin Networks". Phys. Rev. Lett. **92**, 187902 (2004).
3. G. Gualdi, V. Kostak, I. Marzoli, and P. Tombesi, "Perfect state transfer in long-range interacting spin chains". Phys. Rev. A **78**, 022325 (2008).
4. A.I. Zenchuk, "Remote creation of a one-qubit mixed state through a short homogeneous spin-1/2 chain". Phys. Rev. A **90**, 052302 (2014).
5. G.A. Bochkin and A.I. Zenchuk, "Remote one-qubit-state control using the pure initial state of a two-qubit sender: Selective-region and eigenvalue creation". Phys. Rev. A **91**, 062326 (2015).
6. G.A. Bochkin and A.I. Zenchuk, "Extension of the remotely creatable region via the local unitary transformation on the receiver side". Submitted to Quant. Inf. Comp., arXiv:1511.03507 [quant-ph].

Multifunctional quantum node based on a double quantum dot in laser and cavity fields

A.V. Tsukanov[1,2]
1. Institute of Physics and Technology, Russian Academy of Science, Moscow, Russia
2. Moscow Institute of Physics and Technology, Dolgoprudny, Russia, tsukanov@ftian.ru

The concept of multifunctional device (a quantum node) composed of a semiconductor single-electron four-level double-quantum dot coupled to an optical microcavity resonator is developed, see fig.1. The terahertz laser field and voltage biases provide an external control. The structure enables flexible driving via appropriate variations of field amplitudes and switching between resonant and off-resonant modes. As shown this hybrid electron-photon system can be used as a) the charge qubit with flying-to-stationary qubit conversion or b) the single-photon transistor or c) the frequency shifter and several others. Each of listed devices works in the specific regime of system evolution. For example, the qubit is robust when the optical resonator and laser Rabi frequencies dominate the dissipation rates – the so-called strong coupling regime. From another hand, in order to attain the steady-state one has to work in the so-called weak coupling regime when the dissipation rates are comparable to or greater than the Rabi frequencies. Further, the single-photon driving is required for spectroscopic applications of this system. We numerically investigate the population dynamics to reveal the parameter choice corresponding to each device. The model is based on Lindblad formalism where all incoherent processes are considered as the Markovian ones. The time dependencies of populations and spectrograms for different pairs of parameters are obtained. The specific features concerned with working characteristics of the quantum node in different modes are discussed.

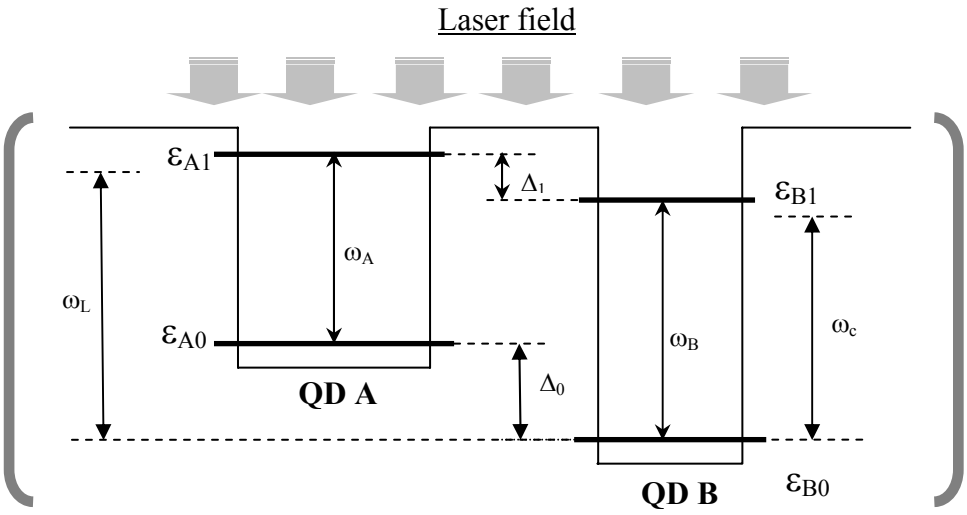

Figure 1. The scheme of energy levels of the double-quantum dot composed of tunnel-coupled single quantum dots A and B embedded in the optical resonator with the frequency ω_c. The dot k (k = A, B) is modeled as two-level one with the energies $\varepsilon_{k,0}$ and $\varepsilon_{k,1}$ of ground and excited levels, respectively. The detunings of the ground and excited levels in different dots are Δ_0 and Δ_1. The electron remains localized in the ground states and can tunnel between excited states. Laser with the frequency ω_L acts as the external control field populating the systems with up to one photon. The non-trivial dynamics is expected when the laser and resonator frequencies are close to the transition frequencies ω_A and ω_B in the double-dot structure.

Diamond chip under single-photon driving as a high-spatial resolution quantum magnetometer and electrometer

A.V. Tsukanov[1,2], I.Yu. Kateev[1,2]
1. Institute of Physics and Technology, Russian Academy of Science, Moscow, Russia
2. Moscow Institute of Physics and Technology, Dolgoprudny, Russia, ikateyev@mail.ru

The problem of practical realization of a universal compact sensing device with high-spatial resolution is addressed. The principle of external field measuring uses analysis of transmission or reflection spectra from diamond microstructure composed of three-microdisk optical resonators (fig. 1). Due to Zeeman and Stark shifts of energy levels of NV-centers formed in edge microdisk the hybrid electron-photon spectrum changes depending on the strength and direction of magnetic and electric fields, respectively. Probe laser with tunable wavelength excites the structure in single-photon regime and its response enables one to detect the fields via spectral behavior. The model of sensor dynamics accounts for both coherent driving and incoherent processes (center relaxation and dephasing and photon leakage) in terms of Lindblad formalism. With use of finite-difference time-domain numerical method three-disk spectrum is calculated and TM eigen-modes close to NV-center zero-phonon line are found. Electromagnetic field shows whispering-gallery behavior, so NV-center is coupled to a common three-disk mode antinode. As we show in steady-state regime our approach gives the possibility of measuring the external fields in large strength range with high sensitivity.

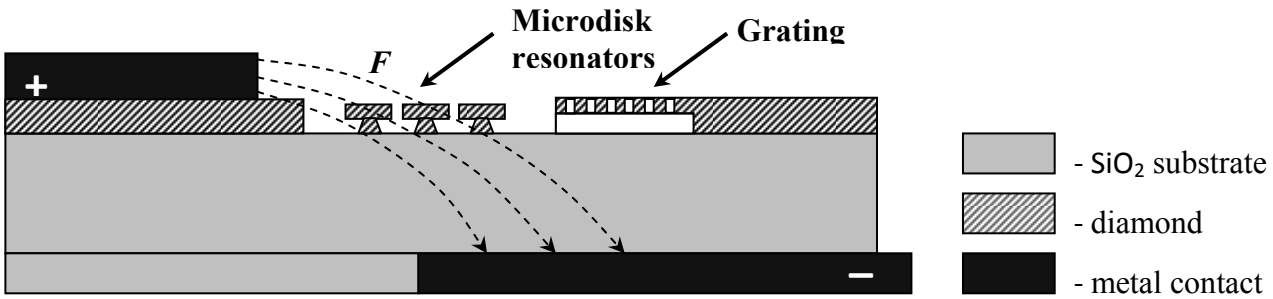

Figure 1. A three-disk diamond NV-sensor scheme. *F* – external electric or magnetic field.

Single-electron solitons in magnetic field

M. Rudenko[1], D. Svintsov[1,2], S. Filippov[1,2], V. Vyurkov[1,2]
1. Institute of Physics and Technology RAS, Moscow, Russia
2. Moscow Institute of Physics and Technology (State University), Moscow, Russia
vyurkov@ftian.ru

Single-electron solitons (SES) can originate near metal surface owing to interaction with image charges [1-3]. Image charges (really, surface charges) appear in response to 'instant' electron density $|\psi|^2$. Therefore, to calculate a SES wave function $\psi(\vec{r},t)$ the self-consistent solution of 2D Schrödinger and Poisson equations modified for a *single electron* should be fulfilled. It allows for the field of surface charges on metal but excludes the action of the own electron field on itself [3]. Evidently, the SES very much reminds a polaron originating in dielectrics. Polarons in ionic dielectrics have fairly high binding energy, but almost cannot move because of very low polarization rate of those dielectrics (10^5 s^{-1}). Polarons in electronic dielectrics can move due to sufficiently high polarization rate (10^{15} s^{-1}) but, at the same time, they possess very low binding energy. Solitons (polarons) near metal surface may have rather high binding energy of the order of 10 meV and can move with a velocity 10^8 cm/s due to very small Maxwellian relaxation time in metals (10^{-15} s).
Solitons may exist in a usual field-effect transistor and affect its characteristics. However, all peculiarities could be attributed to many other phenomena. A crucial experiment thus seems challenging. Here we propose an experiment with SES in magnetic field. It is well known, that conventional Landau levels are degenerated with respect to the number $m+n$, where n is a radial quantum number and m is an angular quantum number. When a polarization of environment is taken into account the degeneracy is lifted [4]. Here we argue that in the case of metal gates an equidistant splitting of Landau levels occurs (Fig. 1). That splitting could be detected via Integer Quantum Hall Effect, where intermediate plateaus appear resembling that in Fractional Quantum Hall Effect. Spectroscopy could also reveal the split Landau level.

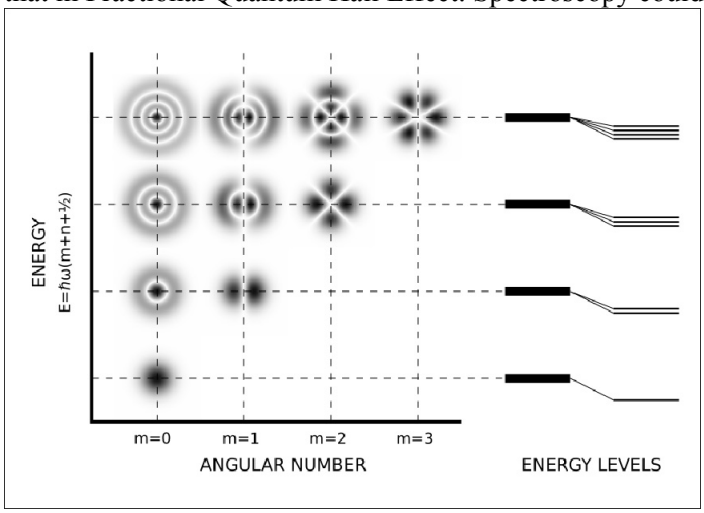

Fig. 1. Degeneracy (n+m) of Landau levels is removed by interaction with metallic gates.

Polarization of environment has a strong influence on a charge qubit functioning [3]. Namely, the evolution of qubit phase cannot be compensated as the amplitude of qubit state during quantum calculations is unknown. On one hand, such a qubit does not function properly, on the other hand, that opens prospects to non-linear qubits which could be used to widen the class of problems to be efficiently solved on quantum computers.

1. K. Yano and D.K. Ferry. "Single-electron solitons". Superlatt. and Microstr., **17**, pp. 61-64, 1992.
2. S. Bednarek, B. Szafran, and K. Lis. "Electron soliton in semiconductor nanostructures". Phys. Rev. B **72**, 075319, 2005.
3. V. Vyurkov and D. Svintsov. "Quantum single electron solitons near metal surface". *http://arxiv.org/abs/1308.3460*, 2013.
4. V. Cheianov, A.P. Dmitriev, and V.Yu. Kachorovskii. "Splitting of Landau levels of a two-dimensional electron due to electron-phonon interactions". Phys. Rev., **58**. pp. 776-781, 1998.

Two-particle fermionic quantum walks

A. Melnikov[1], L. Fedichkin[1,2,3]
1. Institute of Physics and Technology, Russian Academy of Sciences, Moscow, Russia.
2. Moscow Institute of Physics and Technology, Dolgoprudny, Russia, leonid@phystech.edu.
3. NIX, Moscow, Russia, leonid@nix.ru.

We study quantum walks of identical particles from the perspective of quantum information processing. It is known that entanglement creation process plays a pivotal role in most of the subfields of quantum information. Here we introduce a method for generating a two-qudit (two d-level systems) entangled state by means of continuous-time quantum walk on a cycle graph. This method allows to observe diverse structures of entangled subsystems of high dimensions. For the purposes of physical implementation of the proposed model, it is important to consider physically realizable models of quantum walks. The physical system under our consideration is an array of tunnel-coupled semiconductor quantum dots as shown in Fig. 1. Quantum dots in semiconductors can be used as building blocks for a construction of a quantum computer, where each quantum dot represents a spatial degree of freedom of a quantum state. It was shown that a spatial location of an electron in one of two semiconductor quantum dots can serve for encoding a qubit and errors that occur because of the interaction with acoustic phonons can in principle be corrected. Here we study quantum dots arranged in a circle, where each quantum dot can be populated by no more than one electron. By placing two identical electrons in this system, one can define higher dimensional quantum states, qudits. Depending on the distance between the quantum dots, electrons can exhibit an additional Coulomb interaction. First, we analyzed dynamics of non-interacting particles, then we proceeded to study of interacting electrons.

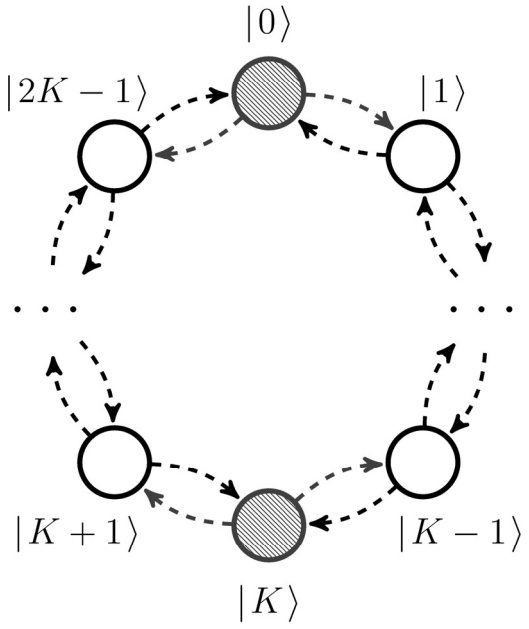

Figure 1. Two fermions in graph formed of ring of coupled quantum dots.

The dynamics of fermionic entanglement was obtained for both cases. We showed that fermionic entanglement can be used to prepare quantum states for quantum information processing. These highly entangled states of qudits can be obtained by only using the free quantum evolution of identical particles, without relying on any additional manipulations with electrons. In addition, we supplemented our protocol of obtaining entangled states with analytical solutions for certain sizes of a graph and proved a general aperiodic nature of the continuous-time quantum walk of identical particles on a cycle graph.

Quantum-classical transition in quantum walks mixing

L. Fedichkin[1,2,3], F. Meshchaninov[1,2]
1. Institute of Physics and Technology, Russian Academy of Sciences, Moscow, Russia.
2. Moscow Institute of Physics and Technology, Dolgoprudny, Russia, leonid@phystech.edu.
3. NIX, Moscow, Russia, leonid@nix.ru.

Quantum walks of single particle in the presence of decoherence are studied. All nodes of the cycle graph are set to be physically equivalent. At the beginning of quantum walks process the particle is placed at one specific node then its quantum evolution starts. Each node of the graph subjected to dephasing which can be natural decoherence process or can be achieved by monitoring artificially each node by independent identical weak observers. Important parameter characterizing speed-up of quantum information processing in quantum walks architecture is mixing time which is the first moment when probability to find particle at all nodes reaches uniform distribution with given accuracy. We obtained the dependence of mixing time versus decoherence rate. It exhibits global minimum and sharp transition from quantum to classical behaviour at some intermediate decoherence. The behaviour of mixing time in tiny vicinity of transition is shown in Fig. 1.

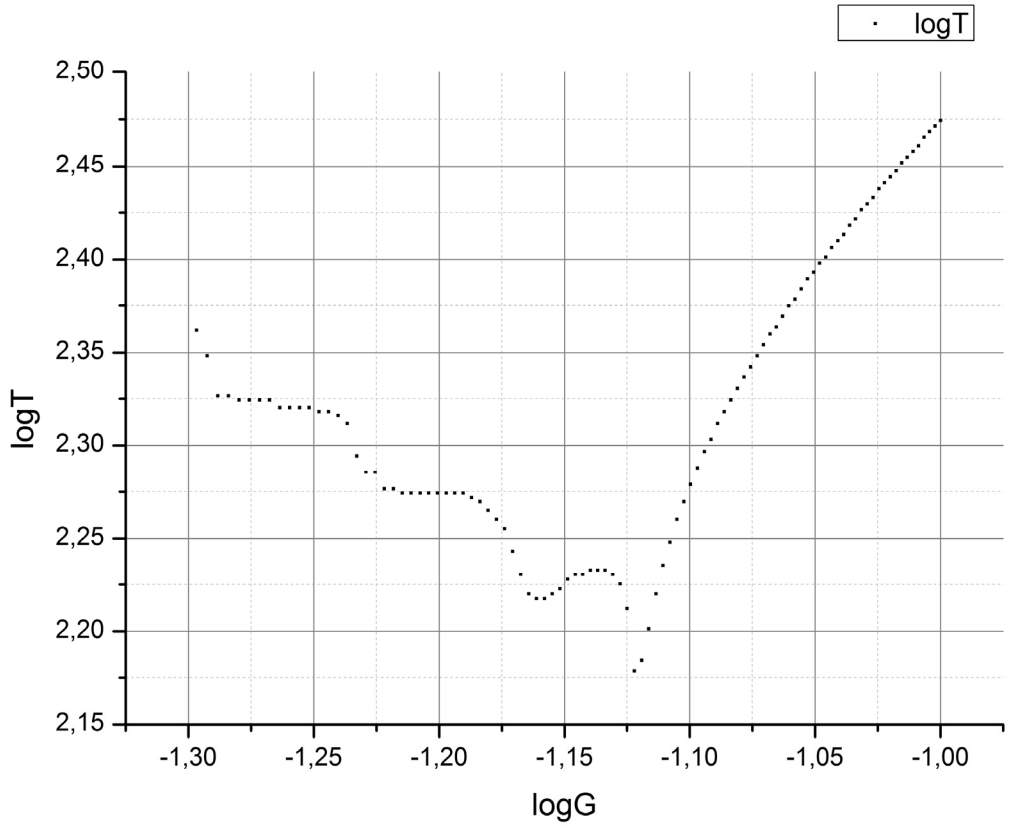

Figure 1. Mixing time *T* versus decoherence rate *G* for the cycle of 40 vertices with required accuracy of mixing 1/40000 plotted in double-log scale.

Current injection terahertz lasing in graphene-channel field-effect transistors under population inversion

T. Watanabe[1], G. Tamamushi[1], A.A. Dubinov[2], A. Satou[1], M. Ryzhii[3], V. Ryzhii[1,4], and T. Otsuji[1]
1. Research Institute of Electrical Communication, Tohoku University, Sendai 980-8577, Japan
2. Institute for Physics of Microstructures, RAS, Lobachevsky State University of Nizhny Novgorod, Nizhny Novgorod 603950, Russia
3. Department of Computer Science and Engineering, University of Aizu, Aizu-Wakamatsu 965-8580, Japan
4. Institute of Ultra-High-Frequency Semiconductor Electronics, Moscow 111005, Russia
E-mail address: watanabe@riec.tohoku.ac.jp

Introduction: Graphene, a monolayer carbon-atomic honeycomb lattice crystal, has attracted attention due to its superior carrier transport properties owing to the massless and gapless energy spectrum [1]. Optical and/or injection pumping of graphene can exhibit negative-dynamic conductivity in the terahertz (THz) spectral range, which may lead to new types of THz lasers [2]. In the graphene structures with p-i-n junction, the injected electrons and holes have relatively low energies compared with those in optical pumping, so that the effect of carrier cooling can be rather pronounced, providing a significant advantage of the injection pumping in realization of graphene THz lasers [3, 4].

Device Fabrication: Graphene was synthesized by the thermal decomposition of a C-face 4H-SiC substrate [5]. The Raman spectrum (no peak at the D, and sharp mono-peaks at the G and G' bands) confirmed a high-quality, a few layer non-Bernal stacked graphene (Fig. 1(a)). The GFET was fabricated by using a standard photolithography and the gate stack with a SiN dielectric layer, providing an excellent intrinsic field-effect mobility exceeding 100,000 cm^2/Vs at 300K at the maximal transconductance [6]. A pair of teeth-brash-shaped gate electrode was patterned to form a DFB cavity with the principal mode of 5.0 THz [7] (Fig. 1(b)).

Results and Discussion: The emission spectra from the device were measured at 300K and 100K using a Fourier-transform spectrometer with a 4.2K-cooled Si bolometer. A rather sharp single mode emission at 5.2 THz was observed at 100K when a certain drain bias was applied for symmetric electron and hole injection (Figs. 2(a, b)) while no distinctive emissions were observed at 300K. The single mode emission exhibits a non-monotonic threshold behavior (Fig. 2(b)) with its maximum intensity of ~10 μW.

Conclusion: A forward-biased graphene structure with lateral p-i-n junctions was implemented in a DFB-DG-GFET and exhibited a single mode emission at 5.2 THz at 100K. The observed emission is still preliminary level but it could be interpreted as THz lasing in population-inverted graphene by carrier-injection.

References: [1] A.K. Geim, and K.S. Novoselov, "The rise of graphene," *Nature Mater.* **6**, 183 (2007). [2] T. Otsuji et al., "Terahertz-wave generation using graphene -toward new types of terahertz lasers," *IEEE J. Sel. Top. Quantum Electron.* **19**, 8400209 (2013). [3] M. Ryzhii, and V. Ryzhii, "Injection and population inversion in electrically induced p-n junction in graphene with split gates," *Jpn. J. Appl. Phys.* **46**, L151 (2007). [4] V. Ryzhii, M. Ryzhii, V. Mitin, and T. Otsuji, "Toward the creation of terahertz graphene injection laser," *J. Appl. Phys.* **110**, 094503 (2011). [5] H. Fukidome et al., "Precise control of epitaxy of graphene by microfabricating SiC substrate," *Appl. Phys. Lett.* **101**, 041605 (2012). [6] G. Tamamushi et al., "High carrier mobility graphene-channel FET using SiN gate stack," *Int. Symp. Compound Semicond. Dig.*, Tu1AD2.4, 2015. [7] B.S. Williams et al., "Distributed-feedback terahertz quantum-cascade lasers with laterally corrugated metal wavuguides," *Opt. Lett.* **30**, 2909-11 (2005). [8] B.W. Hakki and T.L. Paoli, "Gain spectra in GaAs double-heterostructure injection lasers," *J. Appl. Phys.* **46**, 1299-1306 (1975).

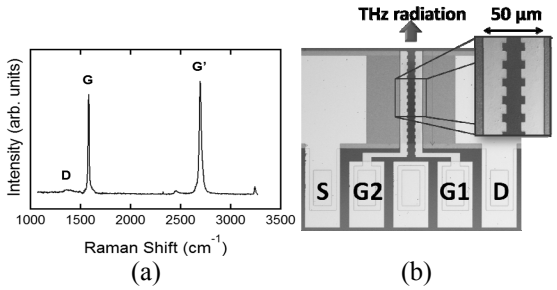

(a) (b)

Fig. 1. (a) Raman spectrum of the synthesized graphene on C-face 4H-SiC. (b) Photo images for the fabricated DFB-DG-GFET.

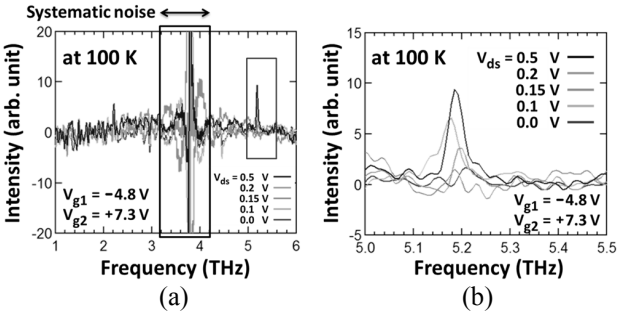

(a) (b)

Fig. 2. Observed emission spectra at 100K in (a) broad range and (b) magnified range at around the single mode emission at 5.2 THz.

Emission and Detection of Terahertz Radiation in Graphene/hBN Heterostructures

S. Boubanga Tombet[1], D. Yadav[1], T. Watanabe[1], V. Ryzhii[1, 2], and T. Otsuji[1]
1. Research Institute of Electrical Communication, Tohoku University, Sendai 980-8577, Japan
2. Institute of Ultra-High-Frequency Semiconductor Electronics, RAS, Moscow 111005, Russia

This communication reviews recent advances in terahertz (THz) emission and detection in graphene based heterostructures. The first part will focus on double-graphene-layered van der Waals (vdW) heterostructure. We report on the first experimental observation of THz emission and detection in those structures and demonstrate that the photon-assisted inter-graphene-layer resonant tunneling (RT) radiative transitions enable their applications for THz/IR lasers [1] and photodetectors (PDs) [2]. Our fabricated devices consist of two independently contacted graphene layers (GLs) separated by the thin transparent hexagonal Boron Nitride (h-BN) tunnel-barrier layer. The bias voltage applied between the GL's contacts induces the electron and hole gases in the opposing GLs. The band-offset energy ('Δ') between the Dirac points of the GLs determines the energies of the photons emitted or absorbed by the structure in the RT inter-GL transitions. The inter-GL population inversion and photon assisted RT transitions are explored for new types of THz devices. We conducted THz emission experiments using a Fourier-transform far-infrared (FTIR) spectrometer to observe the spontaneous emissions associated with the photon assisted RT transitions. For the band offset (Δ) conditions where the energy of the final state is lower than the initial state, the tunneling is associated with emission of the electromagnetic photon. Our experimental results show THz emission exclusively in this case. When the energy of the final state is higher, the tunneling is preceded by absorption of photons. Room temperature detection results at 1 THz was observed in this case. Those results give important insights of carrier dynamics in graphene-based vdW heterostructures and pave the way towards new THz graphene based devices. The second part will focus on plasmonic structures based on hBN/graphene/h-BN heterostructure featuring an interdigitated dual-grating-gate (DGG). We explore current driven plasmon generation and instabilities in those graphene plasmonic structures. The results show that terahertz absorption spectra in the graphene DGG devices exhibit gate tunable pronounced peak associated with excitation of the plasmons. We also show that direct current flow along the graphene channel induces red shift of the plasmonic resonance with a significant reduction of THz absorption up to a transparency regime. Above this regime, the current induces amplification of the incoming THz radiation and a blue shift of the resonances. The absorption completely vanishes, meaning that our structure becomes totally transparent to the incoming THz beam from a threshold region where the energy transfer from the electromagnetic wave to the plasmonic system stops as the current induced wave growth takes over their decay and the plasmon radiative damping becomes zero. For values of drain current above this threshold, the energy transfer goes from the plasmonic system to the electromagnetic wave as the incoming THz beam is being amplified. The additional energy supply is likely coming from the current flow via the applied drain-to-source voltage, which is first transferred to the plasma wave through different processes such as reflection at asymmetric boundaries [3], an electron transit time based mechanism [4], and/or lowering plasmonic velocity in the adjacent cavity [5]. This energy transfer drives the plasma waves in an instability regime when the instability increment takes over the decrement related to the plasmon damping [6]. The energy stored in the plasmon field is then released and transferred to the electromagnetic radiation with the help of the grating. This finding opens pathways to use graphene for THz emitters and amplifiers. This work was supported by JSPS KAKENHI (# 16H06361), Japan.

1. V. Ryzhii, A.A. Dubinov, T. Otsuji, V.Ya. Aleshkin, M. Ryzhii, and M. Shur, *Opt. Exp.* **21**, pp. 31569-31579 (2013).
2. V. Ryzhii, T. Otsuji, V.Ya. Aleshkin, A.A. Dubinov, M. Ryzhii, V. Mitin, and M.S. Shur, *Appl. Phys. Lett.* **104**, 163505 (2014).
3. M. Dyakonov and M. Shur, *Phys. Rev. Lett.* **71**, pp. 2465-2468 (1993).
4. V. Ryzhii, A. Satou, and M.S. Shur, *IEICE Trans. Electron.* **E89-C**, pp. 1012-1019 (2006).
5. V.Y. Kachorovskii and M.S. Shur, *Appl. Phys. Lett.* **100**, 232108 (2012).
6. M.V. Krasheninnikov and A.V. Chaplik, *Zh. Eksp. Teor. Fiz.* **79**, p. 555 (1980) [*Sov. Phys. JETP* **52**, p. 279 (1980)].

Detectors of Infrared and Terahertz Radiation based on Graphene-van der Waals Heterostructures

Victor Ryzhii[1,2,3], Maxim Ryzhii[4], Vladimir Leiman[5], Dmitry Svintsov[5], Vladimir Mitin[1,6], Michael S. Shur[7], and Taiichi Otsuji[1]

1. Research Institute of Electrical Communication, Tohoku University, Japan
2. Institute of Ultra High Frequency Semiconductor Electronics, RAS, Russia
3. Center for Photonics and Infrared Engineering, Bauman Moscow State Technical University, Russia
4. Department of Computer Science and Engineering, University of Aizu, Japan
5. Laboratory of Optoelectronics of 2D Materials, Moscow Institute Physics and Technology, Russia
6. Department of Electrical Engineering, University at Buffalo, USA
7. Department of Electrical, Computer, and Systems Engineering, Rensselaer Polytechnic Institute, USA

We propose the concept of the detectors of infrared and terahertz radiation based on van der Waals (vdW) heterostructures in which graphene layers (GLs) serve as radiation absorbing elements. The operation of the GL-vdW detectors is associated with the electron photoexcitation from the GL valence band to the continuum states above the inter-GL barriers (either via tunneling of the photoexcited electrons or via the direct their transitions to the continuum states). Using the developed device model, we evaluate the performance of these detectors In particular, we find the spectral and voltage dependences of the detector responsivity and detectivity as functions of the heterostructure parameters. We show that due to relatively large probability of the electron photoexcitation and low capture probability of the electrons propagating over the barriers, the GL-vdW detectors can exhibit elevated performance. The GL-vdW characteristics are compared with the characteristics of lateral multiple-GL p-i-n photodiodes, quantum-well inter-subband infrared photodetectors, and uni-travel carrier photodiondes.

This research is supported by the Japan Society for Promotion of Science, Grant #23-000008 and by the Russian Scientific Foundation, Grant # 14-29-00277. The work by V.L and D.S was supported by the Russian Scientific Foundation, Grant #16-19-10557.

Low-dimensional transit-time diodes for terahertz generation

R. Khabutdinov[1,2], I. Semenikhin[1], F. Davydov[1], V. Vyurkov[1,2],
L. Fedichkin[1,2], K. Rudenko[1,2], A.V. Borzdov[3], V.M. Borzdov[3]
1. Institute of Physics and Technology RAS, Moscow, Russia, vyurkov@ftian.ru
2. Moscow Institute of Physics and Technology (State University) Moscow, Russia
3. Belarusian State University, Minsk, Belarus, borzdov@bsu.by

The breakthrough to the exponential dip in output power existing in the range of 0.1-10 THz is nowadays undertaken from both sides, that is, from optic devices and from electronic devices. 3D electronic devices cannot fill up that gap because of very large output capacitance. For example, a resonant tunnel diode (RTD) induces an antenna (or a waveguide) by the field penetrating from side walls of the structure [1]. The power is too small as, in fact, the interior part of the diode is useless for generation. Therefore, a transition to lateral (low-dimensional) structures seems feasible. One of the proposals of terahertz generation with the help of low-dimensional structures (namely, ballistic quantum wires) was put forward in 1994 [2]. It turned out that ballistic regime is sufficient for the negative conductivity at THz frequencies. Up to date facilities in silicon technology allow fabrication of thin layers (2D) and arrays of nanowires (1D). The oscillating current could be put out through the suspended electrodes (gates) over the lateral structure (whatever it is). Then that current should be transmitted to a wave-guide (or antenna) (Fig. 1) [3].
However, in real structures the negative conductivity has a threshold with respect to scattering rate like a similar threshold of generation in optical devices. Fortunately, there are effects which are favorable to negative conductivity even in case of rather strong scattering. They are the impact ionization in IMPATT diodes [4] and the operation on barrier injection in BARITT diodes [5]. In present communication we discuss a joint action of scattering and BARITT effect in silicon nanostructutes and demonstrate a possibility of negative conductivity at THz frequencies (Fig. 2). As for the IMPATT effect, it results in lower efficiency and strong noise, nevertheless, that effect should be also kept in mind for future investigations.

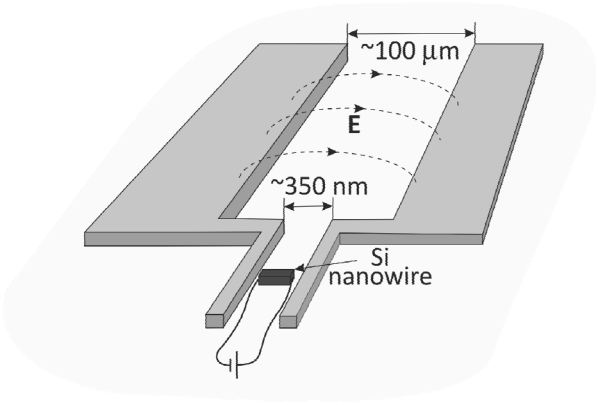

Fig. 1. Schematic view of a THz-generator based on lateral (low-dimensional) structures.

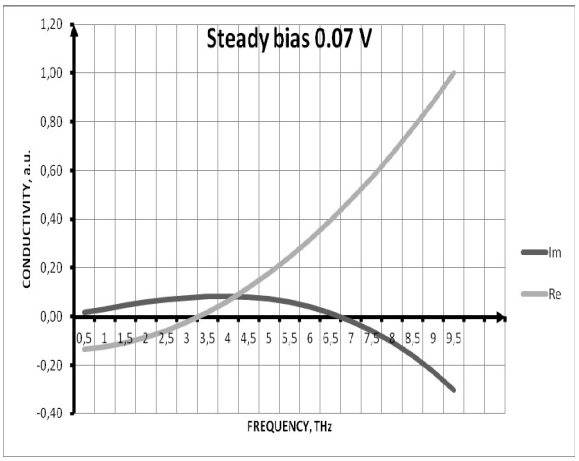

Fig. 2. Real and imaginary parts of conductivity vs. frequency for steady bias 0.07 V, silicon channel length 100nm and room temperature.

1. M. Asada, S. Suzuki, N. Kishimoto. “Resonant Tunneling Diodes for Sub-Terahertz and Terahertz Oscillators”. Jap. J. Appl. Phys., **47**, pp. 4375–4384, 2008.
2. L. Fedichkin and V.V’yurkov, “Quantum ballistic channel as an ultrahigh frequency generator,” Appl. Phys. Lett., **64**, pp. 2535-2536, 1994.
3. V. Vyurkov, D. Svintsov, A. Pilgun, and A. Orlikovsky. “Nanowire transit-time diodes for terahertz generation”. Proc. 4th Russia-Japan-USA Symposium on Fundamental & Applied Problems of Terahertz Devices & Technologies (RJUS TeraTech-2015), June 9-12, 2015, Chernogolovka, Russia, pp. 58-59.
4. A.S. Tager. Sov. Phys. Usp., **9**, p. 892 (1967).
5. D.J. Coleman, Jr. “Transit-Time Oscillations in BARITT Diodes”. J. Appl. Phys., **43**, pp.1812-1818, 1972.

SOI and SOS heterostructures produced by only silicon layer transfer after plasma activation bonding

V.P. Popov
Institute of Semiconductor Physics, SB RAS, Novosibirsk, Russia

Silicon based heterostructures open the door for post-Moore law electronics in order to incorporate new semiconductor materials in silicon based CMOS micro- and nanoelectronics. Unfortunately, heterointegration of other semiconductors with silicon by epitaxy is difficult due to their lattice constant (a) mismatch $\varepsilon = (a - a_{Si})/a_{Si}$, where a_{Si} is the silicon lattice constant, and the difference in their linear thermal expansion coefficient $\delta = (\alpha - \alpha_{Si})/\alpha_{Si}$ with thermal expansion coefficient of silicon α_{Si}. These obstacles limit the thickness of layers in heterostructures and thermal interval for heteroepitaxial growth. Even for zero mismatch in ε for GaP and zb-ZnSe their epitaxy on silcon is limited by δ, which is equal to 75 and 165% respectively. Well matched with each other Ge and GaAs semiconductors have the values of δ = 130% at relatively small lattice mismatch ε = 4.6% that leads to the problems of their heterointegration with silicon. To avoid these obstacles direct bonding (DB) technique is developed [1].Using this method allow to set and keep by Fraunhover ISE and SOITEC the world record for multijunction solar cell efficiency as high as 46% in 2014 [2].

The well known problems of heterointegration of mismatched materials in silicon-on-insulator (SOI) and silicon-on-sapphire (SOS) were also solved successfully by hydrogen induced transfer of thin SiO_2Si heterofilm on Si substrate [3] or by direct bonding of SOI wafer with sapphire wafer and followed etching of sacrificial silicon substrate from SOI wafer [4]. Earlier we have suggested using for mass SOI production more simple hydrogen induced transfer of only Si layers from hydrogen irradiated silicon wafer without the additional SiO_2 layer. Such approach allows avoiding at hydrogen irradiation the mobile positive charge and scattering centers in the future buried oxide (BOX), which degrade charge carrier mobilities in the upper Si layer on BOX [4]. In order to reach these properties we modified hydrophilic DB method using bonding in vacuum at elevated temperatures. We used also surface plasma activation (SPA) in different plasma sources to avoid of gas blistering at the bonding interface in the case of ultra thin BOX layer. The source of the gas is the different reaction between atoms in adsorption layer for hydrophilic surfaces. Such approach was useful also in the case of hydrogen induced Si layer transfer during hot bonding of silicon and sapphire wafers [5]. Si films with thickness 0.1-2.0 μm were successfully created in SOS structures with electronic properties quit similar the same in SOI wafers. According to Raman measurements Si stress after high-temperature annealing at 1000-1100 °C were in the range of 4-8 kbar decreasing with increase in bonding temperature. Suggested transfer of monocrystalline layer of silicon on oxidized silicon substrate or sapphire wafers treated by O_2 plasma provides the full integrity at the interfaces. The technology of one layer transfer to CTE inconsistent and lattice constant mismatched sapphire substrate can be used for other semiconductor heterointegration. Necessary conditions are to carry out the splicing and shearing of thin enough layers when the bonding temperature is closed to the exfoliation temperature (ΔT < 200 K) and moderately high temperatures for the final formation of heterostructures with mismatched lattices are used. The types and regimes of plasma surface treatments of materials for direct bonding should be chosen without the participation of the hydroxyl groups, which form gas bubbles on the bonding interface or by interface layer with recovery and binding reactions of bonding by-products to eliminate gas bubbles at the interface.

1. Q.-Y. Tong, U. Gösele. *Semiconductor wafer bonding.* Jon Wiley and Sons, Inc. 1999.
2. "New world record for solar cell efficiency at 46% French-German cooperation confirms competitive advantage of European photovoltaic industry". Fraunhofer ISE. Retrieved 2016-03-24.
3. V.P. Popov, I.V. Antonova, V.F. Stas, et al. “Properties of extremely thin silicon layer in silicon-on-insulator structure formed by smart-cut technology”, J. Mater. Sci. Eng. B, **73**, pp.82–86, 2000.
4. G. Gaudin, A. Vaufredaz, F. Guittard. “Method of producing a silicon-on-sapphire type heterostructure” Patent US 20110195560 A1, 2011.
5. E.D. Zhanaev, N.V. Dudchenko, V.A. Antonov, A.I. Popov, V.P. Popov. “Method of manufacture of silicon-on-sapphire”. Patent № RU 2538352. The priority of 11.06.2013, Bull. Invent. no. 1. 2015 (in Russian).

GeSi nanocrystals formed by high temperature annealing of GeO/SiO_2 multilayers: structure and optical properties

V.A. Volodin[1,2], A.G. Cherkov[1,2], V.I. Vdovin[1,2], M. Stoffel[3], H. Rinnert[3], M. Vergnat[3]

1. A.V. Rzhanov Institute of Semiconductor Physics, Russian Academy of Sciences, Lavrent'eva ave., 13, 630090, Novosibirsk, Russia, E-mail address: volodin@isp.nsc.ru; 2. Novosibirsk State University, Pirogova street, 2, 630090, Novosibirsk, Russia; 3. Université de Lorraine, Institut Jean Lamour UMR CNRS 7198, B.P. 70239, 54506 Vandœuvre-lès-Nancy Cedex, France.

The development of Si and Ge-based optoelectronic devices is a challenging issue [1]. Silicon and germanium nanocrystals (NCs) embedded in dielectric matrices are potential candidates for applications in nano- and optoelectronic devices. Exciton confinement effects in NCs become brightly apparent at room temperature, a single Si NC reveals delta-function-like energy spectra [2], indicating that the NCs can be considered as quantum dots. The properties of $Ge_xSi_{(1-x)}$ NCs depend on the stoichiometry parameter x and on the NC size. In the literature, several approaches have been proposed to form $Ge_xSi_{(1-x)}$ NCs. They can be formed either by Ge and Si implantation in SiO_2 films or by co-evaporation of Ge, Si and SiO_2 [3].

In our case, Ge and GeSi NCs were formed using high temperature annealings of $GeO(5nm)/SiO_2(5nm)$ multilayers. The multilayers were obtained by alternating evaporations of GeO_2 and SiO_2 powders in high vacuum conditions (10^{-8} Torr) onto Si(001) substrates heated up to 100 °C. The deposition rate (~0.1 nm/s) was controlled by a quartz microbalance. The samples that contain 20 periods of $GeO(5nm)/SiO_2(5nm)$ layers were capped by a 40 nm thick SiO_2 layer. The samples were annealed ex-situ in a quartz tube under high vacuum at 700, 800, and 900 ^oC for 30 minutes. The heating rate was 10 $^oC\ min^{-1}$, after 30 minutes at the setpoint temperature the oven was removed and the films cooled down naturally. The stoichiometry of the $Si_yGe_{(1-y)}O_2$ matrix was determined using Fourier transform infrared (FTIR) absorption spectroscopy, the spectrometer having a spectral resolution of about 2 cm^{-1}. Raman spectra were recorded in the back-scattering geometry and the 514.5 nm Ar^+ laser line was used as excitation source. The optical properties of the as-deposited and annealed samples were investigated by photoluminescence (PL) spectroscopy. The structural properties of the samples were investigated by electron microscope (JEM-2200FS, 200 kV accelerating voltage) using the cross-sectional high resolution transmission electron microscopy (HRTEM) and the energy dispersive spectroscopy (EDS) modes. Cross-sectional specimens were conventionally prepared by mechanical polishing with the use of Leica EM TXP, followed by ion milling. The growth and measurement procedures are described in more details elsewhere [4, 5].

According to electron microscopy data, the size distribution and stoichiometry of the NCs depend on the annealing temperature (700, 800, or 900 ^oC). Spatial redistribution of Ge with the formation of large faceted NCs located near the Si substrate and GeSi intermixing at the substrate/film interface were observed. In the case of the 900 ^oC annealed sample, we note that some NCs have a pyramid-like shape. FTIR absorption spectroscopy demonstrates that intermixing takes place between the GeO and SiO_2 layers leading to the formation of $SiGeO_2$ glass. Raman spectroscopy confirms the formation of Ge NCs after annealing at 700 °C and GeSi NCs after annealing at 800 and 900 °C. For all annealed samples, we have observed infrared PL at low temperatures (10K-100K) in the spectral range 1300-2000 nm. Such long-wavelength PL (up to 2000 nm) has been observed in the films containing GeSi NCs for the first time. Presumably, this PL is due to defect-induced radiative transitions in the NCs.

Russian Fund for Basic Researches has supported this work – project 15-07-02298. V.A.V. is thankful to administration of Université de Lorraine for visit grant.

1. Y. Guo, Q. Wang, Y. Kawazoe, P. Jena. Scientific Reports, **5**, 14342, 2015.
2. I. Sychugov, R. Juhasz, J. Valenta, J. Linnros. Phys. Rev. Lett., **94**, 087405, 2005.
3. S. Takeoka, K. Toshikiyo, M. Fujii, S. Hayashi, K. Yamamoto. Phys.Rev., **B61**, 15988, 2000.
4. V.A. Volodin, D.V. Marin, H. Rinnert, M. Vergnat, J. Phys. D: Appl. Phys., **46**, 275305, 2013.
5. V.A. Volodin, M.P. Gambaryan, A.G. Cherkov, V.I. Vdovin, M. Stoffel, H. Rinnert, M. Vergnat. Journal of Experimental and Theoretical Physics, **121**, p. 1076, 2015.

Epitaxy of Gallium Nitride Nanowires on Graphene

V. Kumaresan*,[1], L. Largeau[1], A. Madouri[1], F. Glas[1], H. Zhang[2], F. Oehler[1], A. Cavanna[1], A. Babichev[2,3], N. Gogneau[1], M. Tchernycheva[2], J-C. Harmand[1]

1. Laboratoire de Photonique et de Nanostructures (LPN), CNRS, Université Paris-Saclay, Route de Nozay, F-91460 Marcoussis, France.

2. Institut d'Electronique Fondamentale, UMR 8622 CNRS, University Paris Sud, University Paris-Saclay, 91405 Orsay cedex, France.

3. ITMO University, St. Petersburg 197101, Russia, E-mail address: andre.babichev@gmail.com.

The use of graphene as a substrate to grow III-V semiconductor nanowires (NWs) has been of increased interest recently [1]. There have been several attempts to grow vertical Gallium nitride (GaN) NWs on graphitic surfaces by metal organic chemical vapor deposition. However, the NWs grew along several directions [2, 3] unless a buffer layer is used [4] or unless graphene is placed on a crystalline substrate [5]. To our knowledge, to date there is only one report of GaN NW growth by plasma-assisted molecular beam epitaxy (PAMBE) on graphite layers [6] and no results of PAMBE growth of GaN on single layer graphene have been reported. In the present work, we use the PAMBE technique to assess graphene transferred onto SiO_2 as an alternative substrate for GaN NW growth. We have produced dense arrays of vertical NWs on pristine graphene with a very good selectivity: NW growth is almost completely inhibited on the SiO_2 surface. GaN NWs grow vertically (fig. 1a) along their c axis and are in-plane oriented over several μm^2 (fig. 1b), an area comparable to the graphene grain size of the polycrystalline mono-layered graphene patch (fig. 1b). Via SEM and TEM analysis, we have determined the relative orientation of the two lattices using monocrystalline graphene domains as substrate. Given this relationship, we propose an epitaxial relationship that induces -3.1% misfit. Strikingly, the number of graphene layers has a strong impact on GaN nucleation: the NW density and height decrease rapidly when this number increases. We propose a model that explains quantitatively this variation of the NW density. Finally, we analyze the structural and optical quality of the NWs using TEM and PL analysis. The PL of GaN NWs grown on graphene shows a near band edge emission dominated by the D_0X_A transition. The optical quality is comparable to that of GaN NWs grown on crystalline Si substrate. This successful epitaxial growth of GaN NWs on graphene seems particularly promising for the development of flexible devices. Our study indicates that many inexpensive amorphous substrates could be usable to grow high quality vertical GaN NWs.

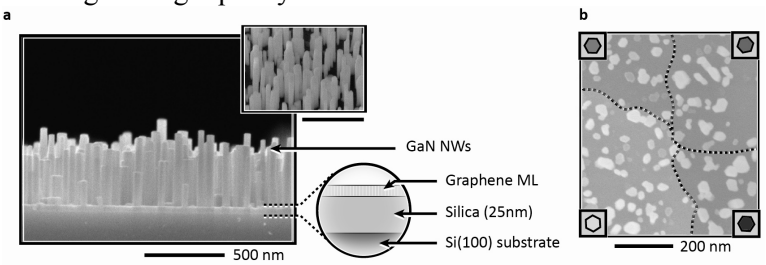

Fig. 1. a) Cross-section SEM image of GaN NWs grown on a 1 cm^2 patch of a graphene monolayer. Inset is a 45°-titled view. b) Top view SEM image showing 4 domains (marked with different background colors) with different NW in-plane orientations. Within each domain, all the NWs have the same sidewall facet orientation, as shown in the insets.

1. A.M. Munshi, et al. "Vertically aligned GaAs nanowires on graphite and few-layer graphene: generic model and epitaxial growth". Nano Lett., **12**, pp. 4570-4576, 2012.
2. F. Yuan, et al. "Synthesis, microstructure, and cathodoluminescence of [0001]-oriented GaN nanorods Grown on conductive graphite substrate", ACS Appl. Mater. Interfaces, **5**, pp. 12066-12072, 2013.
3. J.B. Park, et al. "Metal catalyst-assisted growth of GaN nanowires on graphene films for flexible photocatalyst applications". Curr. Appl. Phys., **14**, pp. 1437-1442, 2014.
4. K. Chung, et al. "Growth and characterizations of GaN micro-rods on graphene films for flexible light emitting diodes". APL Mater., **2**, 092512, 2014.
5. M. Heilmann, et al. "Growth of GaN Micro-and Nanorods on Graphene-Covered Sapphire: Enabling Conductivity to Semiconductor Nanostructures on Insulating Substrates". Cryst. Growth Des., **15**, pp. 2079-2086, 2015.
6. S. Nakagawa, et al. "GaN nanowires grown on a graphite substrate by radio frequency molecular beam epitaxy". Jpn. J. Appl. Phys., **52**, 08JE07, 2013.

Low-threshold field emission in planar cathodes with nanocarbon materials

V. Zhigalov[1], V. Petukhov[1], A. Emelianov[1], V. Timoshenkov[1], Yu. Chaplygin[1], A. Pavlov[2], A. Shamanaev[3]

1. National Research University of Electronic Technology, Moscow, Russia, zhigalov@gmail.com
2. Institute of Nanotechnologies of Microelectronics, Russian Academy of Sciences, Moscow, Russia
3. Technology Center Research and Production Complex, Moscow Institute of Electronic Engineering, Moscow, Russia

The nanocarbon materials are studied as field emitters more than 20 years. Carbon nanotubes (CNT) are known as promising material for the field emission cathodes due to their intrinsic geometric properties. But difficulties of using CNT as field emitters are considerable: emission current is not stable and has limitation, field emitters have short work period. There are also technological issues of optimal arrangement of CNT on the substrate. In this work we measure field emission properties of field emitting cathodes with different arrangement of carbon nanomaterials on the substrate surface.

Four types of samples were studied: 1) CNT deposited from solution on conducting substrate; 2) nonaligned CNT grown from gas phase on stainless steel substrate; 3) aligned CNT grown from gas phase on Al substrate; 4) graphene material derived from graphite cold destruction. The current-voltage curve of samples was measured in vacuum 10^{-6} Torr. The electron work function of samples was measured using method of static capacitor with ionized gap (SCIG) [1].

The current-voltage curves of samples 1-4 are given in Fig. 1. Low-threshold field emission is observed for all samples (threshold 5…20 V/μm).

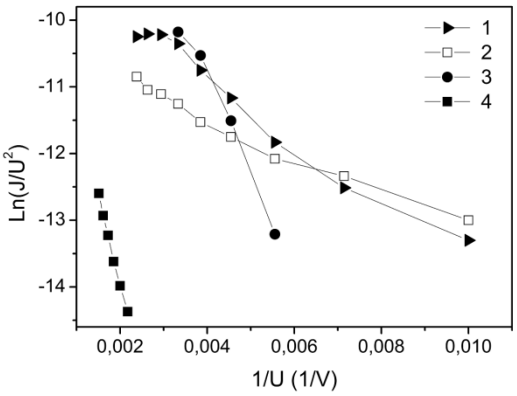

Fig. 1. The current-voltage curves of samples 1-4 in Fowler-Nordheim coordinates.

The slope of the current-voltage curve allows to calculate the work function if the geometric coefficient β is known. We can only estimate the order of β due to difficulties of its modeling in the real samples. We estimate β as 10 for the samples 1 and 4, and as 100 for the samples 2 and 3. Calculating from Fowler-Nordheim theory gives very low values (0.18, 0.50, 1.53, 0.48 eV for the samples 1…4 respectively). Work function measured by SCIG method has values 4.1…4.4 eV. Such a great difference between the values given from current-voltage curve and the direct measured values can indicate the non-applicability of Fowler-Nordheim theory for the nanocarbon materials, what was shown also in [2]. Very actual is the question about the cause of the low-threshold field emission. Ones traditionally consider that geometrical field amplification of the nanocarbon structures is the main reason. But in our samples only weak field amplification can be obtained (order of 10…100). We conclude that the low threshold of field emission is provided not by the geometrical factors, but is intrinsic to the whole class of nanocarbon materials besides of geometric factors. This allows making effective field emission cathodes with arbitrary arrangement of CNT.

1. Novikov S.N., Timoshenkov S.P., "Using static ionizing capacitor method for the electron work function measurement", Izv. Vuzov. Electronica 5, 81-88 (2002) (in Russian).
2. Fursey G.N. et al. "Extremely low threshold of field emission from graphene nanoclusters", Vacuum Nanoelectronics Conference (IVNC), 2012 25th International IEEE, 1-2 (2012).

Chemical surface treatment of $Ge_2Sb_2Te_5$ for phase memory devices

S. Nemtseva[1], M. Mikhailova[1], P. Lazarenko[1], A. Sherchenkov[1], S. Kozukhin[2], A. Shulyat'ev[1], V. Glukhenkaia[1], S. Timoshenkov[1]

1. National Research University of Electronic Technology (MIET), nemtseva1@mail.ru

2. Kurnakov Institute of General and Inorganic Chemistry of the Russian Academy of Sciences (IGIC RAS)

Non-volatile phase memory (PCM) based on the material $Ge_2Sb_2Te_5$ (GST225) is one of the main candidate for the memory of new generation. The choice of material is connected with the unique properties allowing to apply thin films based on it as functional layers of the phase memory. However, optimization of PCM technology for formation of nanodimensional programmable areas of cells is necessary, so the purpose of this work is researching of etching process of thin films GST225 for the formation of cells of the phase memory.

The thin films of $Ge_2Sb_2Te_5$ has been investigated by chemical reagents in this work. Sedimentation of amorphous thin films was carried out by vacuum-thermal evaporation of the synthesized material on SiO_2 substrates with an average roughness ~0.2 nm. Concentration of solutions was selected according to conditions and requirements to the carried-out process. The morphology of a surface of the samples was investigated by optical microscope (Carl-ZeissAxiovert 40 MAT) and by AFM (NT-MDTIntegra (ImageAnalysis)). The level of wettability of a surface of the studied solutions was determined using the goniometer CAM KSV 101 at the room temperature.

Processing in DMFA does not influence on morphology of a surface of an initial film of GST225, and the average roughness after etching corresponds to initial structure ~ 0.2 nm.

Processing of thin films by solution 30 vol. % H_2O_2 was carried out at temperatures from 25 to 70 °C and showed that the higher the temperature and the dwell time in the solution, the greater the amount of bleed layer.

Thin films of $Ge_2Sb_2Te_5$ interact with 20 vol. % HNO_3, and in 20 vol. % solutions H_2SO_4, H_3PO_4, HCl only with addition H_2O_2. With growth of concentration of an etchant process of etching goes more actively. As the result of the conducted researches the best etchant film of $Ge_2Sb_2Te_5$ – solution 20 vol. % HCl + 30 vol. % H_2O_2, because the speed of bleed layer thin films in this solution is higher concerning other reactants.

Selective solution for the formation of conductive paths from Al is solution based on $CuCl_2$ + $HCl_{(c)}$. This reagent at short endurance in the concentrated solution and at longer influence of smaller concentration slightly influences on $Ge_2Sb_2Te_5$ layer.

The work is made with the support of the project RFMEFI57514X0096.

1. S. Kozyukhin, A. Sherchenkov, V. Novotortsev, S. Timoshenkov. Materials phase memory based on a complex chalcogenides and their application in devices memory. Nanotechnologies in Russia **6**, p. 227 (2011).
2. H.-Y. Cheng, C.-A. Jong, C.-M. Lee, and T.-S. Chin. "Wet-Etching Characteristics of $Ge_2Sb_2Te_5$ Thin Films for Phase-Change Memory". IEEE Trans. Mag., **41** (2), pp.1031-1033 (2005).
3. S. Nemtseva, M. Mikhailova, P. Lazarenko, A. Sherchenkov, S. Kosyukhin, S. Timoshenkov. "Investigation of wet etching of $Ge_2Sb_2Te_5$ thin films for non-volatile phase change memory application". NanoIsrael 2016, 5th International Nanotechnology Conference & Exhibition. Israel, Tel-Aviv (2016).

Analytical derivation of Low-Tc DC SQUID response

I. Soloviev[1-3], N. Klenov[1-6], A. Shchegolev[4,5], S. Bakurskiy[1,3], M. Kupriyanov[1,3,7]
1. Lomonosov Moscow State University Skobeltsyn Institute of Nuclear Physics, Moscow, Russia
2. Lukin Scientific Research Institute of Physical Problems, Zelenograd, Moscow, Russia
3. Moscow Institute of Physics and Technology, State University, Dolgoprudniy, Moscow region, Russia
4. Physics Department, Moscow State University, Moscow, Russia
5. Moscow Technical University of Communications and Informatics (MTUCI), Moscow, Russia;
6. N. L. Dukhov All-Russia Research Institute of Automatics, Moscow, Russia
7. Solid State Physics Department, Kazan Federal University, Kazan, Russia

The superconducting quantum interference device (SQUID) is a basic component of superconductor electronics having numerous applications. The DC SQUID, being basically a magnetic flux-to-voltage transformer is used e.g. in highly sensitive magnetometers, amplifiers, readout circuits and antennas. These devices are routinely designed for fabrication process utilizing low temperature superconductors (LTS) and tunnel Josephson junctions, which have become a workhorse of modern superconducting electronics.

Qualitative understanding of SQUID or SQUID-based structure response can be based on an analytical approach, assuming zero SQUID inductance. However, for quantitative estimation of designed LTS circuit characteristics, accounting for a certain real value of the inductance is inevitable.

Despite the fact that half a century is gone since the year of the first demonstration of quantum interference between two Josephson junctions connected in parallel by superconducting inductance [1], a shape of DC SQUID response still was not found analytically for practical parameters of the device at low temperature ($T \sim 4.2$ K). This statement is confirmed by the fact that practical circuit optimization is always performed in the context of numerical analysis, which slows down the design process.

We consider [2] voltage and current response formation in low-Tc DC superconducting quantum interference device (SQUID) with overdamped Josephson junctions in resistive and superconducting state in the context of a resistively shunted junction (RSJ) model. For simplicity we neglect the junction capacitance and the noise effect. Explicit expressions for the responses in resistive state were obtained for a SQUID which is symmetrical with respect to bias current injection point. Normalized SQUID inductance $l = 4\pi e I_c L/h$ (where I_c is the critical current of Josephson junction, L is the SQUID inductance, e is the electron charge and h is the Planck constant) was assumed to be within the range $l < 1$, subsequently expanded up to $l \sim 7$ using two fitting parameters. SQUID current response in the superconducting state was considered for arbitrary value of the inductance. The impact of small technological spread of parameters relevant to low-temperature superconductor (LTS) technology was studied, using a generalization of the developed analytical approach, for the case of a small difference of critical currents and shunt resistances of the Josephson junctions, and inequality of SQUID inductive shoulders for both resistive and superconducting states. Comparison with numerical calculation results shows that developed analytical expressions can be used in practical LTS SQUIDs and SQUID-based circuits design, e.g. large serial SQIF, drastically decreasing the time of simulation.

This work was supported by RFBR grants no. 15-32-20362-mol_a_ved, 16-29-09515-ofi_m, Ministry of Education and Science of the Russian Federation, grant no. 14Y26.31.0007, Russian President grant MK-5813.2016.2, Dynasty Foundation and Program of Competitive Growth at Kazan Federal University.

1. R.C. Jaklevic, J. Lambe, A.H. Silver, and J.E. Mercereau. “Quantum Interference Effects in Josephson Tunneling”. Phys. Rev. Lett., **12**, pp. 159, 1964.
2. I.I. Soloviev, N.V. Klenov, A.E. Schegolev, S.V. Bakurskiy, and M.Yu. Kupriyanov. “Analytical derivation of DC SQUID response”. Supercond. Sci. Technol. **29**, 094005, 2016.

Sub-micron inorganic masks for fabrication of nanostructures with Josephson junctions

S.B. Izyurov[1,2], V.L. Gurtovoi[1,2], I.N. Khrapach[1,3], A.A. Galiullin[1], O.V. Astafiev[1,4]
1. Moscow Institute of Physics and Technology, Dolgoprudny, Russia
2. Institute of Microelectronics Technology RAS, 142432 Chernogolovka, Russia, gurtovoi@iptm.ru
3. Russian Quantum Center, Skolkovo, Moscow, Russia, ik@rqc.ru
4. Royal Holloway University of London, Egham, Surrey TW20 0EX, UK, Oleg.Astafiev@rhul.ac.uk

For fabrication of superconducting nanostructures with Josephson junctions (SQUIDs, qubits, parametric amplifiers, metamaterials etc), standard technology of shadow evaporation is used, which is typically consists of two angle aluminum evaporation through double layer resistive mask and surface oxidation of the first aluminum layer for AlO_x tunneling dielectric formation. This technology have essential disadvantages due to organic material residues on the surface of substrate [1] and extraction of volatile organic gases in process of both metal deposition and aluminum oxidation, which results in two level systems (TLS) formation with distributed energy spectrum. TLSs are typically the main source of extra noise in different detectors and quantum devices, moreover they result in decoherence of superconducting qubits [2].

The technological disadvantages could be eliminated by the usage of inorganic masks [3], which allow improvement of the substrate surface purity and ability to heat substrate to about 500 °C with the aim of single crystal qubit material growth to get higher coherence time. We use germanium and niobium as materials of inorganic mask. Electron beam lithography is used to pattern the niobium (upper mask layer) by plasma etching using PMMA resist mask. Then, PMMA mask is removed and germanium layer is etched in aqueous solution of H_2O_2 through the openings in niobium layer to form suspended inorganic mask (Fig. 1). Shadow evaporation of aluminum is used to fabricate single Josephson junctions and SQUID structures with the junction area of 200×500 nm^2 (Fig. 2). At the final stage, lift-off of germanium layer is done in H_2O_2 solution. For inorganic mask technology working out, we have used Si substrates and Al deposition at room substrate temperature. Current-voltage curves of a typical SQUID structure at T=20 mK are shown in Fig. 3.

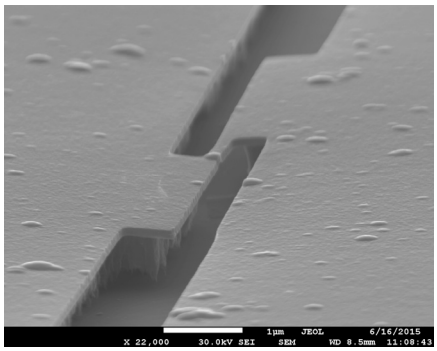

Fig. 1. Suspended niobium mask over sacrificial germanium layer.

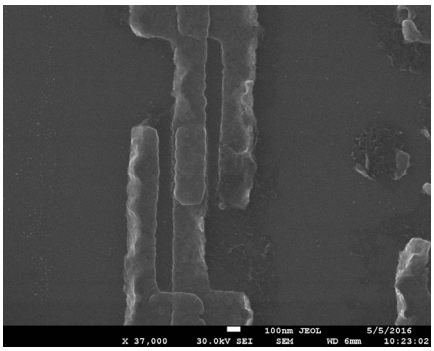

Fig. 2. SQUID structure Josephson junction with the area of 200×500 nm^2.

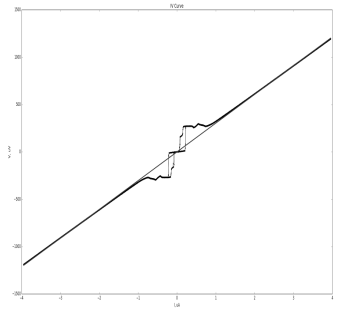

Fig. 3. Typical current-voltage curves of a SQUID at T = 20 mK.

This technology has potential of high coherence time superconducting qubit fabrication. Different cuts of sapphire substrates and substrate heating are planned to use in fabrication of fully single crystalline Al-Al_2O_3-Al or partially crystalline Nb-AlO_x-Nb structures.

1. I.M. Pop, T. Fournier, T. Crozes, F. Lecocq, I. Matei, B. Pannetier, O. Buisson, and W. Guichard. "Fabrication of stable and reproducible submicron tunnel junctions". J. Vac. Sci. Technol. B, **30**, pp. 010607-010611, 2012.
2. J.M. Martinis, et al. "Decoherence in Josephson qubits from dielectric loss". Phys. Rev. Lett., **95**, 210503, 2005.
3. P.B. Welander, V. Bolkhovsky, T.J. Weir, M.A. Gouker, W.D. Oliver. "Shadow evaporation of epitaxial Al/Al_2O_3/Al tunnel junctions on sapphire utilizing an inorganic bilayer mask". arXiv:1203.6007v1.

Down-conversion phenomenon in quantum circuits coupled with an embedded rf-SQUID

C.S. Kim[1], V.O. Munyaev[2], A.M. Satanin[2]
1. Department of Physics, Chonnam National University, S. Korea, E-mail: cskim@jnu.ac.kr
2. Lobachevsky State University of Nizhny Novgorod, Nizhny Novgorod, Russia, E-mail: sarkady@mail.ru

Over the last few years novel methods for the generation, manipulation and detecting of strongly correlated photons have been developed in area of quantum circuit electrodynamics [1-3]. As a main mechanism for generation of strong correlated photons – bi-photons or multiphotons – is usually used the down-conversion processes which have already been considered from phenomenological point of view in nonlinear optics [2]. Parametric down-conversion dynamics in quantum superconducting networks with incorporated Josephson junctions is considered as a promising phenomenon for generating entangled microwave photons. Such kind of photons is a key ingredient for quantum information processing and metrological applications.

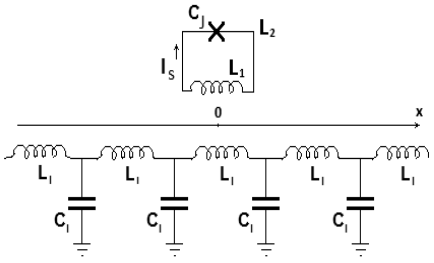

Fig.1. Discrete element model of transmission line coupled inductive with the loop containing a Josephson junction (JJ).

We investigate in the preset work the down-conversion in superconducting coplanar waveguide with an embedded superconducting loop, interrupted by a single Josephson junction. The model considered in this study is illustrated in figure 1.

The quantized Hamiltonian of the system has a form

$$\hat{H}=\sum_k \hbar\omega_k \hat{b}_k^{\dagger}\hat{b}_k+\hbar\omega_J \hat{a}^{\dagger}\hat{a}-\frac{1}{3}\hbar\chi\left(\hat{a}+\hat{a}^{\dagger}\right)^3+i\hbar g\left(\hat{a}-\hat{a}^{\dagger}\right)\hat{Q}_{\mu}+\frac{1}{2C_J}\hat{Q}_{\mu}^2+\frac{c^2}{2L_{\mu}}\hat{\Phi}_{\mu}^2, \quad (1)$$

where the first term describes microwave photons in co-planar line, the second and the third terms are responsible for the Josephson junction, the fourth term is the interaction between them, and the last terms are some constrictions. Both of the constants g (coupling) and χ (nonlinearity) are defined by parameters of the system.

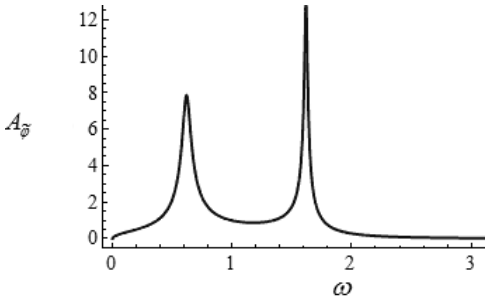

Fig. 2. The two-picks amplitude of Josephson oscillator as a function of frequency of external pulse (in arbitrary units).

The equations for bosonic field operators $\hat{b}_k$ are linear and may be solved exactly. The nonlinear equation motion for the JJ operator is more complex. By using of resonant perturbation theory we can find the Heisenberg equations for slow operators $\tilde{\hat{a}}(t)$. The nonlinear equation $\tilde{\hat{a}}(t)$ shows that there is a region of system parameters when the down-conversion can be realized (see Fig. 2).

In summary, we have investigated a realistic model of nonlinear element coupled with microwave photons in co-planar superconducting wave guide. Our results demonstrate that in the system under the consideration takes place down-conversion processes for incoming photons. We shall note that in this system is very easy to manipulate of effective potential of Josephson oscillator, effective nonlinearity and coupling constant by applying an external flux penetrating the superconducting loop.

1. A. Houck, *et al*.," Generating single microwave photons in a circuit", Nature, **449**, p. 328 (2007).
2. M. Hofheinz, *et al.*, "Synthesizing arbitrary quantum states in a superconducting resonator", Nature, **459**, p. 546 (2009).
3. C. Eichler, *et al.*, "Observation of entanglement between itinerant microwave photons and a superconducting qubit", Phys. Rev. Lett. **109**, 240501 (2012).
4. D.N. Klyshko, " Scattering of light in a medium with monlinear polarizability", Sov. Phys. JETP **28**, p. 522 (1969).

Voltage plateaus on *V*(*I*) curves of a long quasi-onedimensional superconducting aluminum wire

V.I. Kuznetsov

Institute of Microelectronics Technology and High Purity Materials, Russian Academy of Sciences, Chernogolovka, Moscow Region, Russia, E-mail address: kvi@iptm.ru

Bistable voltage plateaus at voltages close to $V_0 \sim 0.43\Delta(0)$ observed [1] in current-voltage characteristics (CVCs) of short (with the length L satisfying the condition $\xi(T) << L << \lambda_Q(T)$ where $\xi(T)$ is the superconducting coherence length, $\lambda_Q(T)$ is the length of quasi-particle imbalance) quasi-onedimensional (with the diameter less than $2\xi(T)$) wires measured in magnetic fields B at various temperatures T. Here $\Delta(0)=1.764kT_c$ is an equilibrium value of a superconducting gap and T_c is the critical temperature. This effect is a result of coexistence of superconductivity and dissipation caused by the formation of a phase slip center.
This work reports a study of another case of coexistence of superconductivity and dissipation in a long ($L = (6\div10)\lambda_Q(T)$) quasi-onedimensional aluminum wire at temperatures $T < T_c$ in magnetic field B normal to the substrate surface. In this work CVCs of the wire (the sketch of the wire is given in the inset of the Fig. 1) were measured as a function of magnetic field at T slightly below T_c. The wire was prepared by the thermal sputtering of an aluminum film 32 nm thick onto a silicon substrate, using the lift-off process of electron beam lithography. The wire was 70 μm long and w_I = 0.46 μm wide along all the length. The voltage was measured in the central wire part 8 μm long between the probes V_1 и V_2. The width and thickness of the wire in experimental temperature range were less than $2\xi(T)$. Voltage wires with the total length 70 μm were also w_V = 0.46 μm wide. The direct current through the I_1 и I_2 probes was passed along all the 70 μm long wire.
It was observed that CVC is of hysteresis depending on the direction of current sweep (Fig. 1).

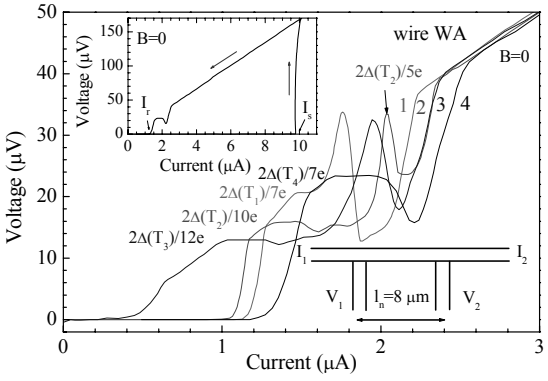

Fig.1. *V*(*I*) curves of the wire measured at a decreasing current in $B = 0$ at T: T_1=1.347 K – curve 1, T_2=1.344 K - 2, T_3=1.341 K - 3, T_4=1.340 K - 4. T_c=1.407 K. Voltages $V_{pl} = 2\Delta(T)/ne$ (n=7, 10, 12, 7 for curves 1-4, respectively) corresponding to the voltage plateaus showed near the plateaus. The left inset: *V*(*I*) curve recorded at both an increasing and a decreasing currents in B=0 at T=1.34 K. The right inset: the sketch of the wire.

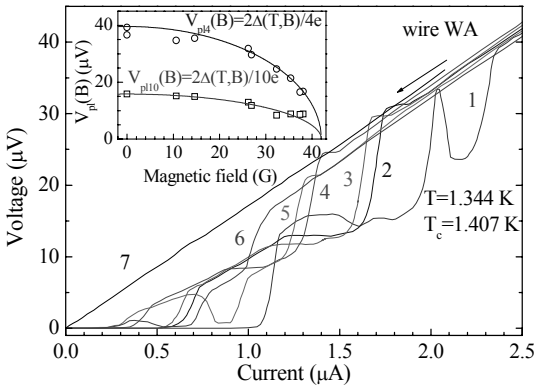

Fig.2. *V*(*I*) curves recorded at a decreasing current at T = 1.344 K in fields B: 0 G – curve 1, 26.2 G - 2, 26.9 G - 3, 32.3 G - 4, 35.4 G - 5, 37.4 G - 6, 49.4 G –7. The inset: $V_{pl}(B)$ dependences of heights of the voltage plateaus on B. Measured data (circles and squares) approximated by the theoretical curves $V_{pl}(B) = (2\Delta(T)/ne)[1 - (B/B_m)^2]^{1/2}$ (where n are 4 and 10 for circles and squares, respectively, and B_m is the fitting parameter for the maximum critical field close to the calculated value B_{mth} = 38 G).

CVCs recorded at a decreasing current in B=0 exhibit the plateaus at voltages $V_{pl}=2\Delta(T)/ne$ where $\Delta(T)$ is the temperature-dependent superconducting gap in B=0 (Fig.1). In the magnetic field, a set of voltage plateaus were found at voltages $V_{pl}=(2\Delta(T)/ne)[1-(B/B_m)^2]^{1/2}$ (Fig.2). These results radically differ from those in work [1]. The *V*(*I*) curves were of hysteresis shape unlike those in [1]. Subharmonic features of the superconducting gap, appearing as stable voltage plateaus in the CVCs can be due to multiple Andreev reflection and a quasi-particle overheating caused by the formation of the phase slip center in the wire.

1. Y. Chen, Y.-H. Lin, S. Snyder, et al., Nature Physics **10**, pp. 567-571 (2014).

A new type of Superconducting Quantum Interference Device

V.L. Gurtovoi[1,2], V.N. Antonov[2,3], A.V. Nikulov[1], R. Shaikhaidarov[3], and V.A. Tulin[1]
1. Institute of Microelectronics Technology, Russian Academy of Sciences, 142432 Chernogolovka, Moscow Region, Russia. E-mail: nikulov@iptm.ru
2. Moscow Institute of Physics and Technology, 29 Institutskiy per., 141700 Dolgoprudny, Moscow Region, Russia.
3. Physics Department, Royal Holloway University of London, Egham, SurreyTW20 0EX, UK

Superconducting Quantum Interference Device (SQUID) is the most sensitive detectors of magnetic field [1]. The classical dc SQUID consists of two Josephson junctions mounted in a superconducting loop with an area S. The critical current $I_c = 2I_{cj}|\cos\pi\Phi/\Phi_0|$ of the two junctions oscillates as a function of the external magnetic flux threading the loop $\Phi = BS$, with the period equal the flux quantum $\Phi_0 = \pi\hbar/e \approx 2.07\ 10^{-15}$ T m^2 [1]. The SQUID sensitivity is determined by the maximum value of $(\partial V/\partial\Phi)_I$ [1]. This value depends on the interval of magnetic flux $\Delta\Phi$ in which the voltage V measured a given value of the bias current I_B changes from minimal to maximal value [1]. This interval equals $\Delta\Phi = \Phi_0/2$ for the classical SQUID. We present experimental results demonstrating the opportunity of SQUID of a new type, the voltage of which changes in a more narrow interval of magnetic flux.

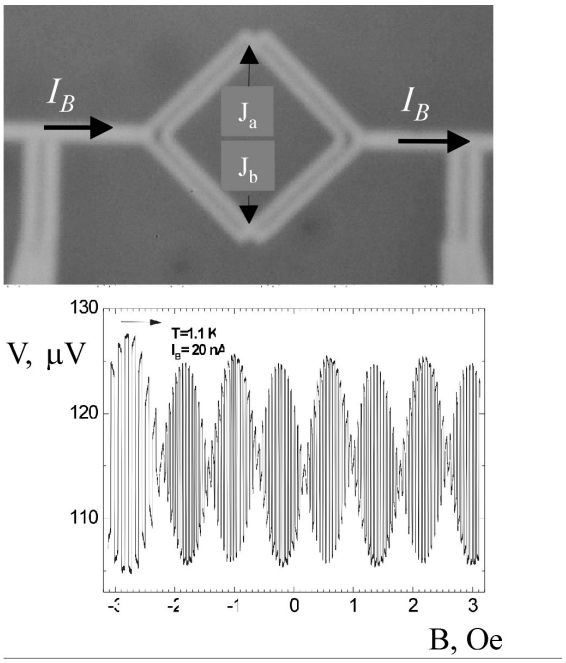

Fig.1. The voltage V, measured on the DDCI, shown at the top of figures, at the temperature $T \approx 1.1$ K and the bias current $I_B = 20$ nA changes by jump when the sum $n_u + n_d$ of the quantum numbers changes on $\Delta n = 1$. Modulated oscillations are observed with period $B_0 = \Phi_0/S \approx 0.052$ Oe corresponding to the area $S = a^2$ of the loops with the square side $a \approx 20$ μm. Periodic amplitude modulation with the period ~0.8 Oe is observed because of the shift of the upper loop relatively the lower loop

This dc SQUID consists of two superconducting loops connected in two points by two Josephson junctions J_a and J_b, Fig. 1. The superconducting current through such superconducting differential double contour interferometer (DDCI) equals

$$I_s = I_a \sin\varphi_a + I_b \sin(\varphi_a + \pi(n_u + n_d)) \qquad (1)$$

in the ideal case [2], when the upper loop is placed exactly above the lower loop. The critical current of this ideal DDCI has only two values at $I_a = I_b = I_{cj}$: $I_c = 2I_{cj}$ when $n_u + n_d$ is an even number and $I_c = 0$ when $n_u + n_d$ is an odd number. Here I_a and I_b are the critical currents of the Josephson junctions; $\sin\varphi_a$ and $\varphi_a + \pi(n_u + n_d)$ are the phase differences between the up and down boundaries of J_a and J_b Josephson junctions; n_u and n_d are the quantum numbers describing the phase φ change of the wave function $\Psi = |\Psi|e^{i\varphi} = |\Psi|e^{i(\varphi+2\pi n)}$ at a complete turn along the upper and lower loops. We used no quite ideal DDCI aluminium structure in order to demonstrate the jump of the critical current with n_u and n_d change on $\Delta n = 1$, Fig. 1. This experimental result confirms the opportunity to use the superconducting differential double contour interferometer as a new type of the dc SQUID with a higher value of $(\partial V/\partial\Phi)_I$ due to a very narrow interval $\Delta\Phi << \Phi_0/2$ in which the quantum number n corresponding to the equilibrium state of real superconducting loops is changed [2].

1. B.B. Schwartz and S. Foner, Superconductor Applications: SQUIDs and Machines. Plenum Press, New York, 1977.
2. A.V. Nikulov, Discrete spectrum of measured parameters of a superconductor nanostructure. In Proceedings of 18th International Symposium "NANOSTRUCTURES: Physics and Technology" St Petersburg: Ioffe Institute, p. 367 (2010); arXiv: 1006.5332 (2010).

About the mechanism determining the spin-injection radiation frequencies in ferromagnetic junctions

Yu.V. Gulyaev[1], E.A. Vilkov[1], G.M. Mikhailov[2], A.N. Maksimov[1], A.I. Panas[1], S.G. Chigarev[1], A.V. Chernikh[2]

1. Kotel'nikov V.A. Institute of Radio-engineering and Electronics RAS (div.), Vedenskiy sq, 1, 141190, Fryazino, RF

2. Institute of Microelectronics Technology and High Purity Materials RAS, Academician Osypian str., 6, 142432, Chernogolovka, RF, E-mail address: mikhailo@iptm.ru

Previously, the theoretical [1-3] and experimental [4] investigations revealed ability to emit terahertz (THz) radiation in ferromagnetic-ferromagnetic (F-F) and ferromagnetic-antiferromagnetic junctions supplied by the current. However, it was noted that theoretically predicted radiation frequencies differ in some extent those found experimentally. This demands more intensive theoretical analysis of the mechanism that determines spin-injection radiation frequencies in magnetic junctions.

In the presented report, this mechanism is considered for a contact-type junction, formed by ferromagnetic electrodes with different magnetization. It is also regarded how to tune radiation frequencies. Final equation for radiation frequency range defined by direct and indirect electron transitions was obtained after consideration of imbalanced spin transport at the interface in F-F junctions supplied by the current. The range of frequencies depends on difference between quasi Fermi levels of spin sub-bands when a current flows through a magnetic junction. It was found that at some values of the current exceeding the threshold current the radiation frequency belongs to THz frequency range. In general it depends on a current density j, misorientation angle φ between magnetizations of contacted ferromagnetic electrodes (fig. 1), and electrode spin polarizations in equilibrium P_i.

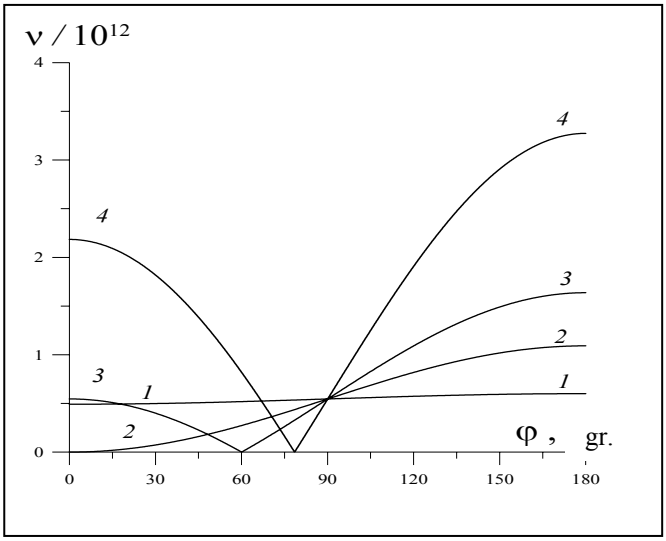

Fig. 1. Dependence of maximum radiation frequency ν at j/j_D =0.01 against misorientation angle φ between magnetizations of ferromagnetic electrodes for their particular spin polarizations P_1/P_2 = 0.1 (*1*), 1 (*2*), 2 (*3*), 5 (*4*).

At $j << j_D$, where $j_D = enD/l_s \sim 10^{13}$-$10^{15}$A/m^2 is a spin diffusion current, e and n are the charge and the bulk density of electrons, D is diffusion coefficient and $l_s \sim$ 30-50 nm is a spin diffusion length, the maximum value of radiation frequency is directly proportional to the current. For $j >> j_D$, it is not sensitive to the current, supplied to the F-F junction and becomes to plateau at large current. This is the result of spin saturation in the irradiation area when maximum possible imbalanced spin density is reached. By change the current density and misorientation angle the spin-injection radiation may tune in its radiation frequency in a wide range and may belong to THz and far infrared frequency ranges at appropriate ratio of electrode spin polarizations.

1. Yu.V. Gulyaev, P.E. Zil'berman, E.M. Epshtein, R.J. Elliott, "Current-induced spin injection and surface torque in ferromagnetic metallic junctions", JETP **100**, pp. 1005-1017, 2005.

2. Kadigrobov A., Shekhter R.I., Jonson M. "Novel laser based on magnetic tunneling" Low Temp. Phys. **31**, pp. 352-359, 2005.

3. Yu.V. Gulyaev, E.A. Vilkov, P.E. Zil'berman, G.M. Mikhailov, S.G. Chigarev "*sd*-Exchange Emission in Ferromagnetic Junctions" J. Comm. Tech. and Electron., **58**, pp. 1137-1141, 2013.

4. Yu.V. Gulyaev, P.E. Zil'berman, I.V. Malikov, G.M. Mikhailov, A.I. Panas, S.G. Chigarev, E.M. Epshtein, "Spin-injection terahertz radiation in magnetic junctions" JETP Lett., **93**: pp. 259-261, 2011.

Numerical simulation of thin-film microthermocouple for the research of dissipation in tunneling contact

V. Kravchenko, V.A. Petukhov
Moscow Institute of Electronic Technology, Zelenograd, vov4ick@mail.ru

The aim of this work is the calculation of the heat distribution in a planar microthermocouple with different designs and obtaining heat flux caused by the tunneling current based on the average temperature of the junction from of the input.

Use of scanning tunneling microscope for the research of thermal phenomena in tunnel contact at the initial stage is most appropriate way. STM is a good method to eliminate the complicated technological operations for the manufacture of tunnel contacts with the necessary parameters. It is also easier to change the materials of the electrodes and the tunneling gap during experiments.

Transmission capacity research of the tunnel contact with small area requires a small dimensions temperature sensors, termoresistors (RTD's) can't be used in this case because RTD is made by thin-film technologies have a larger area and, consequently, low sensitivity due to the strong heat radiation to the substrate. The thermocouple, manufactured by thin-film technology doesn't have the disadvantages of RTDs because it can be manufactured in a small area as in Fig. 1a. Thin-film thermocouples have long applied to measure temperature because of their small size, good thermal contact with the substrate and a small time constant [1]. However, when used to measure the heat flow the opposite problem of converting the measured temperature difference in the desired heat flux must be solved.

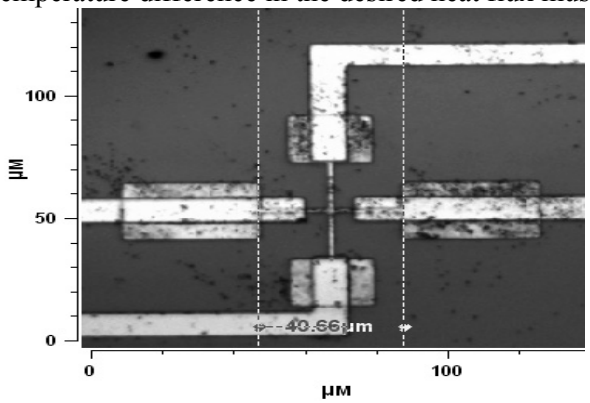

Fig. 1a

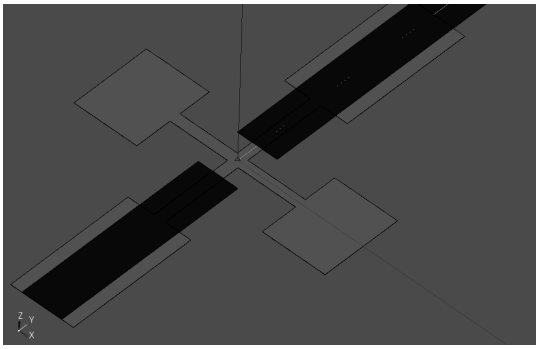

Fig. 1b

In order to solve the problem, authors conducted numerical calculations of heat distribution. For the research we used the thermocouple, previously manufactured by thin-film technology on silicon substrates with thermally grown isolation oxide. The materials we used for the electrodes of thermocouple are chromel (НХ 9,5) and copel (МНМц43-0,5) alloys due to its high thermoelectric-EMF. We used software package Salome for the numerical calculations. We contracted structure of thermocouple by the Geometry module (Fig. 1b). We used Code_Aster package for calculations based on constructed grid. Task files were formed by program Eficas. The results of the calculation were the temperature distribution in the sample, specifically the junction temperature and the conversion capacity ratio of the tunnel contact at the "hot" junction temperature.

Series of experiments, which concluded about the optimal design of microthermocouple, were performed on the basis of assumptions about the heat transfer in tunnel junctions. The simulation results determined the magnitude of the transmitted power required for observation of the effect.

1. L.C. Martin, R. Holanda, «Applications of Thin Film Thermocouples for Surface Temperature Measurement», National Aeronautics and Space Administration Lewis Research Center Cleveland, Ohio 44135. Conference on Spin-Off Technologies and Scientific Instrumentation, San Diego, California, July 24-29, 1994.

Superconducting Spin Valves Based on Noncollinear Antiferromagnets

N. Pugach[1], M. Safonchik[2]
1. Skobelsyn Institute of Nuclear Physics Lomonosov Moscow State University, Moscow, Russia, pugach@magn.ru
2. Ioffe Institute, St. Petersburg, Russia, miksaf@gmail.com

The proximity effect between superconductor (S) and ferromagnet (F) leads to spatial oscillations of the superconducting order parameter with the fast decay into the F layer due to suppression by the exchange magnetic field [1-3]. If the magnetization of the F part is inhomogeneous, the long-range triplet correlations (LRTC) between particles with equal-spin projections also appear [4]. They are not affected by depairing influence of the exchange field. LRTC penetrates into a magnetic material for a rather large distance, like in normal metal, and do not oscillate [3]. The experimental evidence of such triplet correlations was revealed by the recent observation of the long-range Josephson effect [1, 2, 5, 6], which was an important breakthrough in this domain. Recently also spiral (or conical, like Ho) ferromagnets have been used as elements of complex multilayered magnetic structures [5, 7, 10], and the corresponding proximity effect was calculated for some configurations [8-10]. All these LRTC magnetic structures [1, 2, 4-6] contained from 4 to 9 layers of different magnetic and nonmagnetic materials. Such structures demand high requirements to technology and magnetic configuration controlling.

We propose, instead, to use only one magnetic layer with Dzyaloshinsky-Moriya type interaction and intrinsic non-collinear magnetization to create superconducting LRTC spin valves of new type. These junctions are promising for application as elements of magnetic memory for low-temperature electronics, which has become recently a very quickly developing direction of research [11, 12] related to the urgent need for energy-efficient logic for supercomputers. Non-collinear magnetic ordering is necessary to convert singlet superconducting correlations into long-range triplet correlations (LRTC) [1-3]. The magnetically controlled appearance of such correlation may be used to change the state of low-temperature spintronics devices. The novel of this proposition is that the spin-valve effect may be realized on only one spiral-magnetic layer. It may be easier fabricated and controlled at contemporary technology.

The calculations are based on Green's functions method within the framework of quasiclassical theory of superconductivity in the “dirty” limit using the Usadel equations. Suitable materials for the realization of the proposed structures may be Nb or Al as a superconductor and MnSi like compounds as magnetic material. The existence of different magnetic orientations separated by a potential well may help to solve the problem of half-select for the magnetic memory, developed for superconducting electronics [12].

The work was supported by RFBR, grant N15-52-10045 and the Royal Society, UK.

1. M. Eschrig. Physics Today **64**, p. 43, 2011.
2. J. Linder and J.W.A. Robinson. Nature Physics **11**, p. 307, 2015.
3. F.S. Bergeret, A.F. Volkov, and K.B. Efetov, Rev. Mod. Phys. **77**, p. 1321, 2005.
4. A.I. Buzdin, Rev. Mod. Phys. **77**, p. 935, 2005.
5. J.W.A. Robinson, J.D.S. Witt, and M.G. Blamire, Science **329**, p. 59, 2010.
6. T.S. Khaire, W.P. Pratt, Jr., and N.O. Birge, Phys. Rev. Lett. **104**, 137002, 2010.
7. I. Sosnin, H. Cho, V. Petrashov, Phys. Rev. Lett. **96**, 157002, 2006.
8. T. Champel, M. Eschrig. Phys. Rev. B **72**, 054523, 2005.
9. C. Wu, O. Valls, K. Halterman. Phys. Rev. B **86**, 184517, 2012.
10. G. Halasz, J. Robinson, M. Blamire, et. al., Phys. Rev. B **79**, 224505, 2009; ibid. **84**, 024517, 2011.
11. B. Baek, et al. Nat. Commun. **5,** p. 3888, 2014.
12. T. Larkin, V. Bol'ginov, V. Ryazanov, et. al. Appl. Phys. Lett. **100**, 222601, 2012.

Elastically driven magnetic excitations for acoustic spin pumping in ZnO–GGG –YIG–Pt - bulk acoustic wave resonator

S. Alekseev, I. Pyataikin, N. Polzikova, I. Kotelyanskii, V. Luzanov, A. Raevskiy, L. Galchenkov
Kotel'nikov Institute of Radio Engineering and Electronics of Russian Academy of Sciences, Moscow, Russia, alekseev@cplire.ru

Non-magnetic ways of exciting magnetic oscillations, in particular due to strain mediated coupling between the electric field in a piezoelectric film and magnetization in a magnetostrictive ferromagnetic layer, are quite topical today because of possible applications in strain-tunable spintronic devices, magnetoelectric spin wave logic circuits, and sensors.

Acoustic spin pumping (ASP), the generation of spin currents from a magnetization precession excited by a microwave phonons, has attracted much attention recently. The possibility for pure spin current generation based on acoustic driving magnetic dynamics both under magnetoelastic resonance (MER) [1] and the off-resonance conditions [2] has been demonstrated. In [3, 4] we showed theoretically and observed experimentally that excitation of non-uniform ferromagnetic resonance (FMR) occurs in a Al-ZnO-Al-GGG-YIG high overtone bulk acoustic wave resonator (HBAR) at frequencies close to the ones of MER. Magnetic oscillations in YIG arise because of spatially inhomogeneous strain and manifest themselves as HBAR resonance frequency shift $\Delta f_n(H)$ at magnetic fields H corresponding to MER, when HBAR resonance frequency $f_n(H)$ is close to FMR frequency. The generation of pure spin current in such HBAR has been demonstrated recently in [5]. Magnetic dynamics excited acoustically in the YIG film induces spin current from it into a thin layer of platinum deposited on the YIG. This spin-polarized current is transformed to electrical current by means of the inverse spin Hall effect (ISHE).

Here, we report some important features of generation of pure spin current in such a system caused by crystal and magnetoelastic anisotropy. Namely, the effect of the mutual orientation of the transverse acoustic wave polarization (established by the projection of ZnO texture axis on a plane (111) of epitaxial YIG films), the bias magnetic field and the platinum strip on the maximal value of HBAR frequency shift (Δf_n) and ISHE voltage (U_{ISHE}) has been studied in detail.

We found that, in contrast to the standard sinusoidal dependence of U_{ISHE} versus angle φ between the magnetizing field and Pt strip observed at electromagnetic excitation by cavities or striplines, the angular dependence of $U_{\mathrm{ISHE}}(\varphi)$ at ASP in HBAR is subject to more complex law. This is because only transverse acoustic waves with the components of particle displacement parallel to the bias field are able to excite magnetic oscillations. A model is proposed to explain the observed behavior of $U_{\mathrm{ISHE}}(\varphi)$ and $\Delta f_n(\varphi)$. Fitting the experimental curves with the obtained theoretical dependences allowed us to determine the location of projection of ZnO texture axis in the plane (111) of YIG. The locations extracted from $U_{\mathrm{ISHE}}(\varphi)$ and $\Delta f_n(\varphi)$ measurements are in good agreement with each other. It is concluded that in order to obtain the maximal value of U_{ISHE}, the piezoelectric texture axis of ZnO should be oriented towards the direction that is perpendicular to the axis of the platinum strip and parallel to the crystallographic axis $<1\,\bar{1}\,0>$ of YIG film.

1. M. Weiler, H. Huebl, F.S. Goerg, F.D. Czeschka, R. Gross, and S.T.B. Goennenwein. "Spin pumping with coherent elastic waves". Phys. Rev. Lett., **108**, 176601 (pp. 1-5), 2012.
2. K. Uchida, H. Adachi, T. An, T. Ota, M. Toda, B. Hillebrands, S. Maekawa, and E. Saitoh. "Long-range spin Seebeck effect and acoustic spin effect". Nature Mater., **10**, pp. 737-741, 2011.
3. N.I. Polzikova, A.O. Raevskii, and A.S. Goremykina. "Calculation of the spectral characteristics of an acoustic resonator containing layered multiferroic structure". J. Commun. Technol. Electron., **58**, pp. 87-94, 2013.
4. N. Polzikova, S. Alekseev, I. Kotelyanskii, A. Raevskiy, and Y. Fetisov. "Magnetic field tunable acoustic resonator with ferromagnetic-ferroelectric layered resonator". J. Appl. Phys., **113**, 17C704 (pp. 1-3), 2013.
5. N.I. Polzikova, S.G.Alekseev, I.I. Pyataikin, I.M. Kotelyanskii, V.A. Luzanov, and A.P. Orlov. "Acoustic spin pumping in magnetoelectric bulk acoustic wave resonator". AIP Advances, **6**, 056306 (pp. 1-4), 2016.

Thin-film ruthenium microstructures for transition edge sensors

A.S. Ilin, I.A. Cohn, A.N. Vystavkin, A.G. Kovalenko
Kotel'nikov Institute of Radio Engineering and Electronics, Moscow, Russia, ailin@hitech.cplire.ru

The most widely used material for transition edge sensors (TES) working at He-3 cryostats' temperatures is titanium at the moment. The critical temperature T_c for a bulk *T*i sample is 0.39-0.45 K, depending on the purity of the material [1]. The main disadvantages of using titanium for thin-film TES are its relatively high chemical reactivity and gettering action. Therefore there is a large spread of superconducting properties of Ti microstructures produced by sputtering and lithography. It is common for the T_c to drop below the working temperature of He-3 cryostats [1]. In this paper we propose ruthenium as a material for said TES.

Ruthenium is substantially inert, and the T_c for bulk Ru samples is 0.49 K [2]. We investigated magnetron sputtered Ru thin films with thickness 13-300 nm on a Si substrate and TES samples based on the thin-film Ru microstructures. It has been found that the T_c for the thin-film TES is 0.55-0.70 K, and the width of the paraconductivity region is 1-5 mK. Furthermore, it was established that lithography process didn't affect the properties of the TES samples, so we were able to get consistent properties for several fabrication sessions. Therefore ruthenium is concluded to be a desirable material for the transition edge sensors.

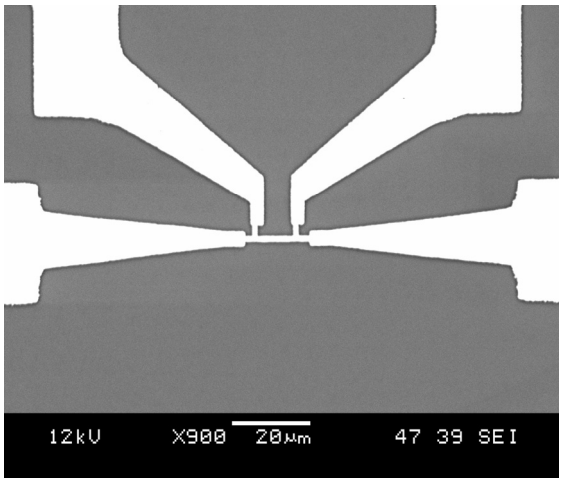

Fig. 1. SEM-picture of the TES sample.

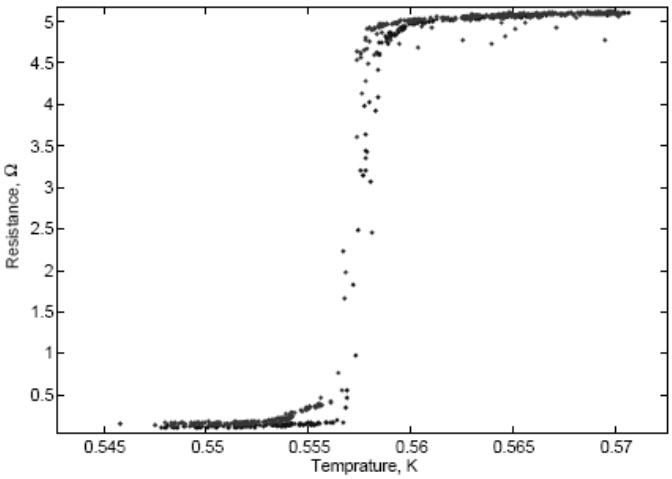

Fig. 2. *R*(*T*) characteristic of the TES.

1. A. Peruzzi, E. Gottardi, I. Peroni, G. Ponti, G. Ventura. "The influence of impurity concentration and magnetic fields on the superconducting transition of high-purity titanium". Nucl. Phys. B (Proc. Suppl.), **78**, pp. 576-580, 1999.
2. J.K. Hulm and B.B. Goodman. "Superconducting Properties of Rhenium, Ruthenium and Osmium". Phys. Rev., **106**, pp. 659-671, 1957.

Informational approach to the tomography of quadrature quantum states

Yu.I. Bogdanov[1,2,3], N.A. Bogdanova[1,2], G.V. Avosopyants [1,3], L.V. Belinsky[1,3], K.G. Katamadze[1,4], S.P. Kulik[4], V.F. Lukichev[1]

1. Institute of Physics and Technology, Russian Academy of Sciences, 117218, Moscow, Russia.
2. National Research Nuclear University "MEPHI", 115409, Moscow, Russia.
3. National Research University of Electronic Technology MIET, 124498, Moscow, Russia.
4. M.V. Lomonosov Moscow State University, 119991, Moscow, Russia.

The analysis of mutually complementary optical quadrature quantum measurements is presented. The approach is based on the Bohr principle of complementarity. In the framework of the root approach to quantum measurement we have developed new methods that improve the tomography of quantum states. Our approach is based on the quantitative analysis of information about the parameters of the quantum state, which is contained in the protocol of quantum measurement. The information contained in the quantum measurement allows one to strictly quantify reconstruction accuracy for each degree of freedom and for all states in general. The approach allows for detailed description of a wide range of practically important measurement protocols. The analytical calculations and numerical experiments showing the efficiency of developed methods are presented.

This work was supported by the Program of the Russian Academy of Sciences in fundamental research.

Broadband biphotons in the single spatial mode through high pump focusing and walk-off effect

K. G. Katamadze[1, 2], S. P. Kulik[1]
1. Faculty of Physics, M. V. Lomonosov Moscow State University, Moscow, Russia
2. Institute of Physics and Technology, Russian Academy of Sciences, Moscow, Russia

Correlated photon pairs, called biphotons, are a very useful tool in the quantum optics and quantum information tasks. Their spectral properties are very important for some quantum communication and metrological applications. Most of them require good biphotons coupling with some interferometers, microscopes and long-distance optical channels, so our goal is preparation of broadband biphotons in the single spatial mode.

The most effective biphoton source is based on the spontaneous parametric down-conversion (SPDC). There are some complicated biphoton broadening techniques, but the simplest way to obtain broadband biphotons is based on using short nonlinear media.

Single-mode biphoton generation rate $R_T \propto (L^2/W^2)\Delta\Omega$, where L is a crystal length, W is a waist of the pump beam and the target Gaussian mode and $\Delta\Omega$ is a spectral bandwidth of generated biphotons. In the case of high focusing the effective crystal length decreases to $L_{\text{eff}} \approx W/2\rho$, where ρ is a walk-off angle. So we obtain $R_T \propto \Delta\Omega/4\rho^2$. The spectral density remains constant, but the bandwidth $\Delta\Omega$ increases. Typically, $\Delta\Omega \propto L^{-1/2} \propto W^{-1/2}$ at the type-I phase matching and $\Delta\Omega \propto L^{-1} \propto W^{-1}$ at the type-II phase matching. So high pump focusing leads to increasing of the spectral bandwidth and total single-mode generation rate of biphotons.

Quantum states tomography with noisy measurement channels

Yu.I. Bogdanov[1,2,3], B.I. Bantysh[1,2], N.A. Bogdanova[1,2], A.B. Kvasnyy[1,3], V.F. Lukichev[1]

1. Institute of Physics and Technology, Russian Academy of Sciences, 117218, Moscow, Russia.
2. National Research Nuclear University "MEPHI", 115409, Moscow, Russia.
3. National Research University of Electronic Technology MIET, 124498, Moscow, Russia.

Quantum states tomography is an instrument for the quality control in quantum information systems. Real measurement systems are such that perform quantum state decoherence simultaneously with projection measurement. The aim of this work is the construction of methods and algorithms for precise quantum measurements with fidelity close to the fundamental limit. In the present work the notions of ideal and non-ideal quantum measurements are strictly formalized. It is shown that non-ideal quantum measurements could be represented as a mixture of ideal measurements. Based on root approach the quantum state reconstruction method is developed. Informational accuracy theory of non-ideal quantum measurements is proposed. The monitoring of the amount of information about the quantum state parameters is examined, including the analysis of the information degradation under the noise influence. The study of achievable fidelity in non-ideal quantum measurements is performed. The results of simulation of fidelity characteristics of the wide class of quantum protocols based on polyhedrons geometry with high level of symmetry are presented. The impact of different decoherence mechanisms, including qubit amplitude and phase relaxation, bit-flip, phase-flip and photon detectors finite quantum efficiency, is considered.

This work was supported by the Program of the Russian Academy of Sciences in fundamental research.

Schmidt decomposition and multivariate statistical analysis

Bogdanov Yu. I.[1,2,3], Bogdanova N.A.[1,2], Fastovets D.V.[1,2], Luckichev V.F.[1]

1. Institute of Physics and Technology, Russian Academy of Sciences
2. National Research University of Electronic Technology MIET
3. Moscow National Research Nuclear University "MEPHI"

The new method of multivariate data analysis based on the complements of classical probability distribution to quantum state and Schmidt decomposition is presented. It is shown that mathematical methods of quantum mechanics allow us to develop new effective tools of analysis of statistical dependences and relationships. The developed formalism allows us to analyze multidimensional systems and we have obtained analytical formulas for Schmidt decomposition of multivariate Gaussian states. We have considered the concept of partial and multiple correlation coefficients in quantum systems and examined their relationship to quantum entanglement. The presented formalism is the natural approach for the analysis of both classical and quantum multivariate systems.

This work was supported by the Program of the Russian Academy of Sciences in fundamental research.

Statistical reconstruction of compound Poisson mixtures of Fock states from quadrature measurements

Yu.I. Bogdanov[1,2,3], K.G. Katamadze[1,4], G.V. Avosopyants[1,3], L.V. Belinsky[1,3], N.A. Bogdanova[1,3], S.P. Kulik[4], V.F. Lukichev[1]

1. Institute of Physics and Technology, Russian Academy of Sciences, 117218, Moscow, Russia.
2. National Research Nuclear University "MEPHI", 115409, Moscow, Russia.
3. National Research University of Electronic Technology MIET, 124498, Moscow, Russia.
4. M. V. Lomonosov Moscow State University, 119991, Moscow, Russia.

We explore procedures for statistical reconstruction of a compound Poisson mixture of Fock states from quadrature measurements, based on maximum likelihood estimation and the method of moments. Using gamma distribution as a compounding distribution results in a model which can be applied to mixtures with various photon bunching regimes. We conducted experiments in generation and measurement of thermal quantum states as well as photon-subtracted thermal states, which are obtained as a result of an annihilation of a number of photons in a thermal mixture. Our results showcase the flexibility of this model in analysis of quantum optical experimental data. The goal of this research is the development of highly accurate procedures for generation and quality control of optical quantum states.

The work was supported by the Russian Science Foundation, grant no 14-12-01338.

Numerical characteristics of quantum computer simulation

A. Chernyavskiy[1,2], K. Khamitov[2], A. Teplov[2], V. Voevodin[2], Vl. Voevodin[2]
1. Institute of Physics and Technology of the RAS, Moscow, Russia
2. Lomonosov Moscow State University, Moscow, Russia

The simulation of quantum circuits is significantly important for the implementation of quantum information technologies. The main difficulty of such modeling is the exponential growth of dimensionality, thus the usage of modern high-performance parallel computations is relevant [1].

As it is well known, arbitrary quantum computation in circuit model can be done by only single- and two-qubit gates, and we analyze the computational structure and properties of the simulation of such gates.

We investigate the fact that the unique properties of quantum nature lead to the computational properties of the considered algorithms: the quantum parallelism make the simulation of quantum gates highly parallel, and on the other hand, quantum entanglement leads to the problem of computational locality during simulation.

We use the methodology of the AlgoWiki project (algowiki-project.org) to analyze the algorithm [2]. This methodology consists of theoretical (sequential and parallel complexity, macro structure, and visual informational graph) and experimental (locality and memory access, scalability and more specific dynamic characteristics) parts. Experimental part was made by using the petascale Lomonosov supercomputer (Moscow State University, Russia).

We show that the simulation of quantum gates is a good base for the research and testing of the development methods for data intense parallel software, and considered methodology of the analysis can be successfully used for the improvement of the algorithms in quantum information science.

This project is carried out with the financial support of the Russian Science Foundation, Agreement No 14-11-00190.

1. Bogdanov Yu.I. et al. "Modeling of quantum noise and the quality of hardware components of quantum computers" *International Conference on Micro-and Nano-Electronics 2012*. International Society for Optics and Photonics, 2013.
2. V. Voevodin, A. Antonov, and J. Dongarra. "AlgoWiki: an open encyclopedia of parallel algorithmic features." *Supercomputing frontiers and innovations* **2**(1), pp. 4-18, 2015.

Effective computation of quantum discord in a multiqubit spin chain

A. Chernyavskiy[1,2]
1. Institute of Physics and Technology of the RAS, Moscow, Russia
2. Lomonosov Moscow State University, Moscow, Russia

Quantum discord is a non-classical correlation beyond quantum entanglement, which is a possible resource for quantum information technologies. The computation of quantum discord is a difficult problem due to the necessity of global optimization. In [1] the discord of multiqubit spin chains is calculated for different model parameters. The computation is made numerically by the random mutations algorithm, moreover, the observation about the invariability of the minimum of conditional entropy for the considered model was presented.

We present the original semi-algebraic method for the effective computation of discord in the considered model. We use the random mutations algorithm in a non-standard way: not for the minimization, but for the verification of inequalities. More specifically, we use it to check the constancy condition mentioned above (we need to find a global minima only once for the fixed number of qubits). After that, the discord can be calculated effectively by the algebraic procedures, and we construct the discord surface for different values of the temperature and structural parameter of the model.

The considered approach for the verification of inequalities by global optimization algorithms can be used in a wide variety of applications, especially, in the theory of quantum correlations, which contains a lot of definitions based on minimums and maximums.

1. A.Yu Chernyavskiy, S.I. Doronin, and E.B. Fel'dman. "Bipartite quantum discord in a multiqubit spin chain." *Physica Scripta* **T160**, 014007, 2014.

Spectroscopic, kinetic investigations and preparation of pure quantum state of $^{167}Er^{3+}$ impurity ions in crystals $^{7}LiYF_4$ for implementing quantum memory protocol

K.I. Gerasimov, S.A. Moiseev, M.M. Minnegaliev, R.V. Urmancheev
Kazan Quantum Center, Kazan National Research Technical University, 10 K. Marx Street, Kazan 420111, Russia

Er^{3+} ions doped in to isotopically enriched crystals $^{7}LiYF_4$ have a record narrow spectral width of the optical transitions (~ 16 MHz) [1, 2]. These solid state mediums are the best candidates from rare-earth activated crystals known to date for implementing quantum memory protocol in the off-resonance Raman scheme [3]. In this work, we performed high-resolution magneto-optical spectroscopy of the hyperfine transitions of $^{167}Er^{3+}$ in an isotopically purified $^{7}LiYF_4$ crystal. Possible implementation of few tens of lambda-transitions is revealed in this crystal for spectral ranges of 800 and 1530 nm. We have also studied the kinetic characteristics of the radiative and nonradiative transitions of $^{167}Er^{3+}$ and identified effective schemes for preparation of the initial quantum states required for implementing quantum memory protocols.

1. Thiel C.W., Böttger T., and Cone R.L. Rare-earth-doped materials for applications in quantum information storage and signal processing. J. Lumin. **131**, pp. 353–361 (2011).
2. Gerasimov K.I., Minnegaliev M.M., Malkin B.Z., Baibekov E.I., and Moiseev S.A. High-resolution magneto-optical spectroscopy of $^{7}LiYF_4$:$^{167}Er^{3+}$, $^{166}Er^{3+}$ and analysis of hyperfine structure of ultranarrow optical transitions. In press: Phys. Rev. B (2016).
3. Moiseev S.A. Off-resonant Raman-echo quantum memory for inhomogeneously broadened atoms in a cavity. Phys. Rev. A **88**, 012304 (2013).

Broadband photon echo quantum memory in high quality optical cavity

S.A. Moiseev and E.S. Moiseev
Kazan Quantum Center, Kazan Scientific Research Technical University, 10, K. Marx, Kazan, 420111, Russia

We propose a new photon echo approach for broadband quantum memory based on atoms in resonant high quality optical cavity. Herein we analyze an efficient optical scheme providing broadband impedance matching condition for storage of signal light fields on the inhomogeneously broadened atomic transition. We show how this scheme and impedance matching conditions can be realized for resonant and Raman atomic transitions. Finally we discuss potential of this scheme for associative quantum storage of multi-mode light fields.

Long-lived photon echo quantum memory on quantum dots

S.A. Moiseev and S.O. Tarasov
Kazan Quantum Center, Kazan Scientific Research Technical University, 10, K. Marx, Kazan, 420111, Russia

We describe a protocol of photon echo quantum storage on a system of quantum dots. Here we derive Schrödinger approach for description of the quantum storage on the system of quantum dots with arbitrary optical thickness of inhomogeneously broadened resonant transition. The protocol contains the coherent control of the quantum dot dynamics by the sequence of short laser pulses in the external magnetic field when the long-lived storage is provided by the reversible transfer of the optical coherence to the electron spin states. The derived approach can be used for analysis of the light-atom dynamics for arbitrary quantum states of signal light fields. We also discuss the prospective of the studied quantum dot system for implementation in fast optical quantum storage and processing.

Metal-assisted chemical etching of silicon with different metal films and clusters: A review

O. Pyatilova[1], S. Gavrilov[1], A. Sysa[1], A. Savitskiy[1], A. Shuliatyev[1], A. Dudin[2], A. Pavlov[2]
1. National Research University of Electronic Technology, Zelenograd, Moscow, Russia, e-mail: 5ilova87@gmail.com
2. Institute of Nanotechnology Microelectronics INME of RAS, Moscow, Russia.

Micro-, meso- and macroporous silicon has a wide range of applications, what can be defined by its surface morphology. There are few methods to form nanostructured silicon (NS) layers with different type (porous silicon, nanowires) and porosity. In recent years, special attention is paid to simple and cheap method to form NS layers. It is metal-assisted chemical etching (MACE) with Ag, Au, Pt, Pd, etc. as catalyst [1-3]. The type and form of the metal mask influence on the morphological form of silicon (pores, wires, 3D structure). Considerable efforts have been devoted to integrate MACE to Si based technology. It is possible to replace noble metals with Cu, Fe, and Ni. But most of metals including noble metals or its reaction products can be remained on the etched Si surface [4, 5].

The investigation of the influence of the composition and form of the metal mask on the morphology and composition of etched silicon is important task.

1	***Metal mask***	Ag clusters	Ag film	Au clusters	Pt film	Ni film
2	***Film thickness***	-	50 nm	-	80 nm	25-100 nm
3	***Clusters diameter***	20-30 nm	-	100-120 nm	-	-
4	***Composition of etching solution***	$HF/H_2O_2/H_2O$ (25/10/4)	$HF/H_2O_2/H_2O$ (25/10/4)	HF/H_2O_2 (17/3)	$HF/C_2H_5OH/H_2O_2$ (3:1:0,1)	$HF/ H_2O_2/H_2O$ (2:1:10)
5	***Conductivity type***	*p, n*	*p, n*	*p, n*	*p, n*	*p*
6	***Structured silicon: porous layer, wires***	porous layer	porous wires	mesoporous silicon layer	mesoporous silicon layer	mesoporous silicon layer
7	***Diameter of Si pores***	no calculated	-	7-14 nm	3.8-5.0 nm for p-Si; 3.8-4.2 nm for n-Si	13-24 nm
8	***Length of silicon wires***	-	2-5 μm	-	-	-
9	***Rate of formation***	no calculated	depends on Ag^+ concentration	12 nm/min for p-Si	2 nm/sec for p-Si, 0.25 nm/sec for n-Si	7.5 nm/min
10	***Metal Contamination on Silicon surface***	Ag_2SiO_3	Ag_2SiO_3	Au clusters	Pt thin film	Metal free

Thus, it is shown that:
- spontaneous stop of the Ag-assisted chemical etching is due to Ag_2SiO_3 formation;
- the result of Ag-assisted chemical etching with clusters and continuous film as mask is porous layer and wires, respectively;
- porous layers formed by Pt-assisted chemical etching can be used for explosive devices;
- the result of Ni-assisted chemical etching of *p*-Si is black silicon what exhibits property of high absorptance. Enhanced light absorption results to photo-electrochemical formation of porous silicon.

The reported study was funded by RFBR (Russian Foundation for Basic Research), according to the research project No. 16-33-80157 mol_ev_a.

1. Z. Huang. “Metal-Assisted Chemical Etching of Silicon: A Review”. Adv. Mater. **23**, pp. 285–308, 2011.
2. X. Li. “Metal-assisted chemical etching in HF/H_2O_2 produces porous silicon”. Appl. Phys. Lett., **77** (16), pp. 2572-2574, 2000.
3. C. Chartier, S. Bastide, C. Lévy-Clément. “Metal-assisted chemical etching of silicon in $HF–H_2O_2$”. Electrochimica Acta, **53** (17), pp. 5509-5516, 2008.
4. F. Toor, J. Oh, and H.M. Branz “Efficient nanostructured ‘black’ silicon solar cell by copper-catalyzed metal-assisted etching”. Prog. Photovolt: Res. Appl. (2014) DOI: 10.1002/pip.
5. K.W. Kolasinski and J.W. Gogola “The mechanism of galvanic/metal-assisted etching of silicon” ECS Transactions, **33** (16), pp. 23-28, 2011.

Influence of treatment conditions on morphology and fractal characteristics of *por*-Si formed by metal-assisted chemical etching

A. Boyko[1], O. Pyatilova[1], R. Kalmykov[2], D. Gaev[2], S. Timoshenkov[1], S. Gavrilov[1]
1. National Research University of Electronic Technology, Moscow, Zelenograd, Russia, ant_nico@mail.ru,
2. Kabardino-Balkarian State University, Nalchik, Russia, dahir@mail.ru

Porous silicon (*por*-Si) is a material investigated very intensively due to its remarkable qualities and promising applications to production. Porous silicon is usually formed by etching of monocrystalline silicon resulted in a pore size from nanometers to microns. Surface orientation, type and doping level of a substrate as well as treatment conditions have a significant affect on physicochemical properties of *por*-Si. When different materials introduced into the pores it enables to produce composite materials, which are characterized by new features [1]. Due to large specific area *por*-Si can be used as a base of composite structures aimed for various sensors, catalysts, getters and so one. For *por*-Si characteristics of porosity have an important value and could give valuable information for controlled formation of porous layers. Another way for describing of morphological features relates to fractal geometry approaches, which allow to make both qualitative and quantitative texture analysis [2]. Fractal dimension is associated with internal structure of a matter and its physicochemical properties.

The influence of conductivity type and resistivity of monocrystalline silicon on morphology and fractal characteristics of *por*-Si was investigated. Test samples have been formed by metal-assisted chemical etching (MACE) with Pt as catalyst [3]. MACE is simple and productive method at the same time, the main benefit of the one, in comparison with the electrochemical etching, is providing of uniform supply of current to the etched surface. It summarized in capabilities of batch processing and productivity improvement. Porous layers were formed on *p*-Si (100) with ρ = 0.01 Ohm·cm and *n*-Si with ρ = 4.5 Ohm·cm using MACE's procedures. Thin films of Ti and Pt with thickness of 15 and 80 nm, respectively, were deposed onto passive side of the Si substrate by magnetron sputtering. The etching treatment was carried out under illumination of 230-240 lx in etch solution contained $HF(40\%)/C_2H_5OH(90\%)/H_2O_2(30\%)$ (volume ratio 3:1:0.1) and at temperature of 25 °C.

Morphology of porous layers was investigated by scanning electron microscopy (SEM) with Helios NanoLab 650. Specific area surface was S_{sp} studied with Quantachrome NOVA 3200e and calculated by multi-point model BET, because all the samples are of mesoporous texture [4]. SEM-results coupled with sorption measures reveal specific area value, pore size, pore shape and texture of porous layers under investigation. For *n*-Si and *p*-Si specimens specific surface values were about of 7 m^2/g and 13 m^2/g correspondently. For calculations of fractal dimension an algorithm proposed by B. Mandelbrot and called "slit islands" have been used [5]. According to that SEM-images of the surface were cut programmatically with different levels of image luminance, in the issue we get "islands" described by total area *S* and total length of "coastline" or perimeter *P*. Relationship between logarithmic perimeter and area values yields desired value of fractal dimension of the surface D_s, computation gives D_s = 2.52 for *n*-Si sample and D_s = 2.84 for *p*-Si sample. With the use fractal geometry an estimation of specific area of porous layers was done also, that gives S_{sp} = 24 m^2/g for *n*-Si sample and S_{sp} = 49 m^2/g for *p*-Si sample. The study exhibits correlation between characteristics of silicon substrates, treatment conditions and morphological features, porosity and fractal dimension of porous structures under investigation. The results can be used for creation of advanced nanomaterials.

The study was supported by the Russian Foundation for Basic Research, project №16-38-50099.

1. R. Herino, "Nanocomposite materials from porous silicon", Mat. Sc. and Eng. **B69-70**, pp. 70-76, 2000.
2. N.A. Torkhov, V.G. Bozhkova, I.V. Ivonin, V.A. Novikov, "Determination of the Fractal Dimension for the Epitaxial n-GaAs Surface in the Local Limit," Semiconductors, **43** (1), pp. 33-41, 2009.
3. C.R. Becker et al., "Galvanic Porous Silicon Composites for High-Velocity Nanoenergetics", Nano Lett., **11,** pp. 803-807, 2011.
4. S. Brunauer, P.H. Emmett, E. Teller, "Adsorption of gases multimolecular layers"; J. Am. Chem. Soc., **60**, pp. 309-319, 1938.
5. B. Mandelbrot, D. Passoja, A. Paullay, "Fractal character of fracture surfaces of metals", Nature, **308**, pp. 721–722, 1984.

The MBE growth of indium droplets and ring-like nanostructures

O.A. Ageev, M.S. Solodovnik, S.V. Balakirev
Southern Federal University, Institute of Nanotechnologies, Electronics, and Electronic Equipment Engineering, Department of Nanotechnologies and Microsystems, Taganrog, Russia, E-mail address: sbalakirev@sfedu.ru

Droplet epitaxy is one of the most promising growth methods to obtain self-assembled nanostructures in a wide range of material systems. A very important advantage of this technique is the possibility to form quantum dots in the lattice-matched systems as well as in a range of sub-critical thicknesses for lattice-mismatched crystals. The goal of this work was experimental study of droplet MBE growth modes to obtain the InAs quantum dots with acceptable geometrical parameters.

Experimental studies were carried out using modular MBE system STE35 (SemiTEq). GaAs(001) epi-ready wafers were used as growth substrates. After standard procedure of native oxide thermal desorption and GaAs buffer growth, the As_4 source was closed and indium was deposited on the GaAs surface. The growth temperature T was varied from 300 to 450 °C, the deposition rate V was 0.1-1 ML/s, and the effective thickness of the deposition H was 0.5-1.5 ML. After growth, the substrate immediately cooled to minimize the surface redistribution of the epitaxial material. Then samples were investigated by SEM and AFM.

It was shown the preferential formation of ring-shaped submicron nanostructures based on metallic In at high temperatures. So, at T = 450 °C, H = 1.5 ML and V = 0.5 ML/s ring-shaped In structure formed with density of about $5 \cdot 10^6$ cm^{-2} and average size of 500 nm in diameter. These structures were elongated along one direction and had octagonal shape. The decrease of growth temperature T to 300 °C resulted in the formation of solid-phase In nanostructures having the shape of regular octagons, the density to $2.5 \cdot 10^8$ cm^{-2}, with a diameter of 100-120 nm and 30 nm high at the same other growth parameters.

On the basis of combinations of contact and non-contact AFM modes, it was found that the obtained In nanostructures had a solid state of aggregation. Comparison of the AFM results with each other and with the MBE growth modes suggests that heterojunction “nanostructure–surface” is blurred with increasing of growth temperature and annealing time, which is due to the intensification of the diffusion mass transfer processes caused by the gradient of elements concentration on the boundary of a different phases.

This work was supported by the Russian Science Foundation Grant No. 15-19-10006. The results were obtained using the equipment of the REC and CCU “Nanotechnologies” of SFedU.

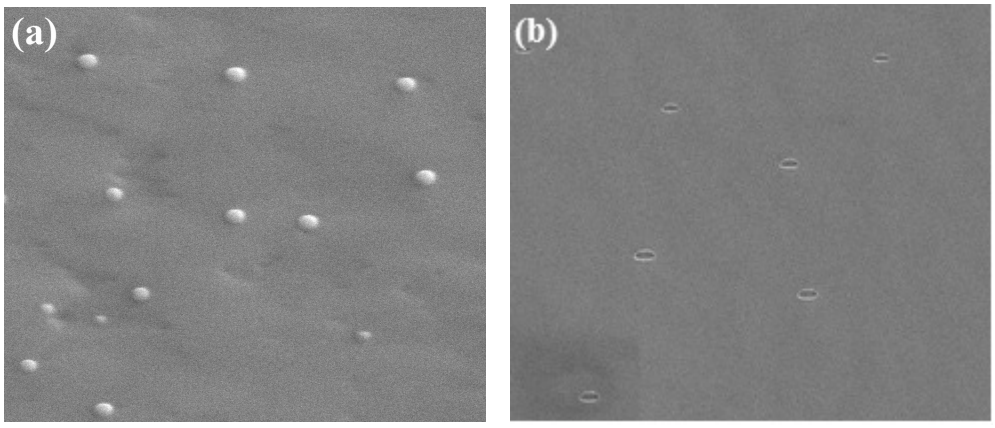

Fig. 1. SEM images of In structures obtained at T = 300 °C (a) and T = 450 °C (b).

Influence of the growth rate and As_4/Ga flux ratio on Ga surface diffusion during MBE of GaAs

O.A. Ageev, M.S. Solodovnik, S.V. Balakirev, M.M. Eremenko
Southern Federal University, Institute of Nanotechnologies, Electronics, and Electronic Equipment Engineering, Department of Nanotechnologies and Microsystems, Taganrog, Russia, E-mail address: sbalakirev@sfedu.ru

In the present work, the molecular beam epitaxial (MBE) growth of GaAs(001) is simulated by Monte Carlo method and the surface diffusion of Ga adatoms depending on the growth rate (v) and As_4/Ga flux ratio ($R_{As/Ga}$) is studied. As a basis, the kinetic Monte Carlo model of GaAs MBE growth on the GaAs(001)-β2(2×4) reconstructed surface [1] was used. The algorithm was developed to obtain the surface diffusion characteristics of Ga adatoms during growth via a flux of arsenic tetramers.

The simulation shows that islands preferentially form in the trench sites and favor elongation along the [1 -1 0] direction which is attributed to the Ga diffusion anisotropy. As shown in Fig. 1a, Ga diffusion length is larger at smaller growth rates. An increase in the growth rate as well as in the As_4/Ga flux ratio reduces Ga diffusion length. This behavior can be explained by the As_4/Ga flux ratio dependences of Ga surface lifetime (Fig. 1b). As the growth rate rises, Ga lifetime decreases essentially due to intensification of the incorporation processes. As the computations show, the diffusion coefficient increases on the contrary with increasing growth rate or As_4/Ga flux ratio (Fig. 1b). This indicates that the diffusion length is more effectively influenced by a decrease of Ga surface lifetime than an increase of the diffusion coefficient. The As_4/Ga flux ratio influence on the diffusion length and diffusion coefficient is stronger at $v = 0.01$ ML/s whereas this influence on the Ga surface lifetime is nearly the same at any v. The simulation results are in good agreement with previous theoretical and experimental data [2, 3].

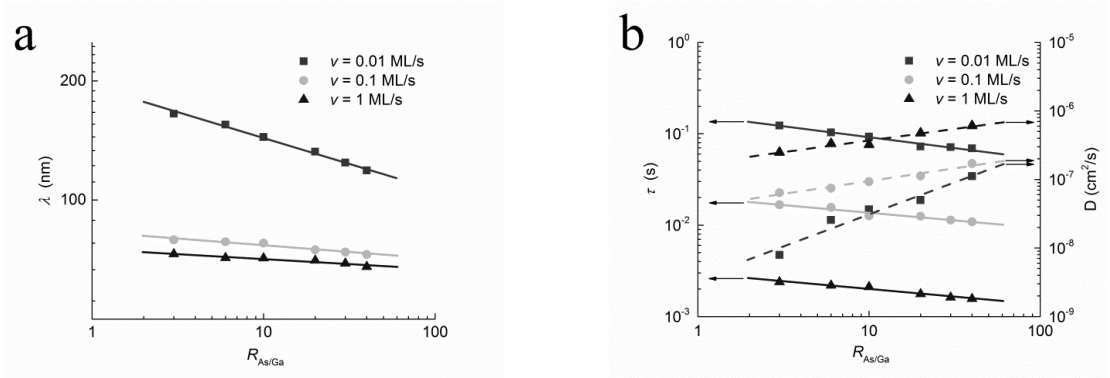

Fig. 1. As_4/Ga flux ratio dependences of (a) the diffusion length; (b) the diffusion coefficient and surface lifetime of Ga adatoms at $T = 580$ °C and different growth rates.

The reported study was funded by RFBR, according to the research project No. 16-37-60033 mol_a_dk.

1. O.A. Ageev, M.S. Solodovnik, S.V. Balakirev, M.M. Eremenko. "Kinetic Monte Carlo simulation of GaAs(001) MBE growth considering the V/III flux ratio effect". J. Vac. Sci. Technol. B, **34**, 041804, 2016.
2. Y. Kangawa, T. Ito, A. Taguchi, K. Shiraishi, T. Irisawa, T. Ohachi. "Monte Carlo simulation for temperature dependence of Ga diffusion length on GaAs(0 0 1)". Appl. Surf. Sci., **190**, pp. 517-520, 2002.
3. J.M. van Hove, P.I. Cohen. "Reflection high energy electron diffraction measurement of surface diffusion during the growth of gallium arsenide by MBE". J. Cryst. Growth, **81**, pp. 13-18, 1987.

Critical thickness for dislocation nucleation in $Ge_{1-x}Si_x$/Si(001) heteroepitaxial system

O.S. Trushin[1], E. Glazkov[2], E. Granato[3] and See-Chen Ying[4]

1. Yaroslavl Branch of the Institute of Physics and Technology of RAS, Yaroslavl, Russia, otrushin@gmail.com

2. P.G. Demidov Yaroslavl State University, Yaroslavl, Russia

3. LAS, National Institute for Space Research, São José dos Campos, Brazil

4. Department of Physics, Brown University, P.O. Box 1843, Providence, Rhode Island, 02912, USA

Heteroepitaxial systems play an important role in modern microelectronic technology. Due to the lattice mismatch between the film and the substrate, considerable elastic strain energy is accumulated in epitaxy. For sufficiently thick films, defects will form leading to the relaxation of strain energy and to the loss of coherent epitaxy. Controlling the film-substrate interface quality and preventing defect formation is an important problem of modern technology [1]. In this work we studied atomistic mechanisms of misfit dislocation nucleation in $Ge_{1-x}Si_x$/Si(100) heteroepitaxial systems (with x varying in the range from 0.1 up to 0.5). We explored these systems in three dimensions using molecular statics methods with Stillinger-Weber semi-empirical interatomic potential [2]. We used combination of Repulsive Bias Potential activation procedure and Nudget Elastic Band method for generating Minimum Energy Paths for transitions from the coherent epitaxial (defect free) state to the state containing an isolated defect (misfit dislocation, shown in fig.1). We have already used this method successfully before to study the process of dislocation nucleation in pure Ge film on Si(001) substrate [3]. In this work we extended the research to the random alloy $Ge_{1-x}Si_x$ thin films on Si(001) using similar methodology and model geometry. Start configurations of the $Ge_{1-x}Si_x$ films were prepared by random substitution of Ge atoms in the film according to the required chemical composition. For each composition of the film being studied, configurations containing a 90° dislocation have been generated using methodology described above. The energy of the final state containing the defect has been compared with initial coherent epitaxial state and energy gain due to strain relaxation been estimated. In such a way we were able to extract information about the dependence of critical thickness on the film composition (fig.2).

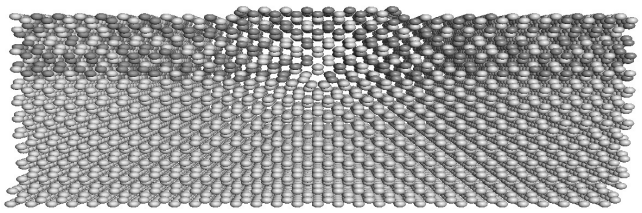

Fig. 1. Side view of the model with dislocation in the middle. Dark balls represent Ge atoms, white - Si.

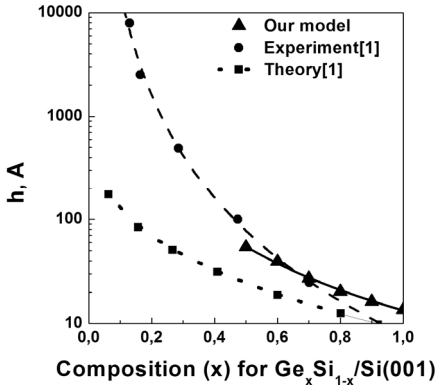

Fig. 2. Dependence of critical thickness on film composition.

In summary, we have used atomistic modeling to get systematic estimates of the critical thickness of $Ge_{1-x}Si_x$/Si(001) heteroepitaxial system as function of its composition. The results are in better agreement with available experimental data than those from an analytical theory based on a Matthew-Blakeslee continuum model, where the effective mismatch depends on the concentration of Ge [1].

1. R. Hull. "Misfit strain and accommodation in SiGe heterostructures", in a book *Germanium Silicon: Physics and Materials* (ed. by R.Hull and J. Bean), Academic Press, San Diego, 1999.

2. F. Stillinger, T. Weber. "Computer simulations of local order in condensed phases of silicon", Phys. Rev. B, **31**, pp. 5262-5271, 1985.

3. O. Trushin, E. Maras, A. Stukowski, E. Granato, S.-C. Ying, H. Jónsson, and T. Ala-Nissila "Minimum energy path for the nucleation of misfit dislocations in Ge/Si(001) heteroepitaxy", Modelling Simul. Mater. Sci. Eng. **24**, 035007, 2016.

DC-and AC-Electric and Dielectric Properties of Gallium Sulphide

S.M. Asadov[1], S.N. Mustafaeva[2]

1. Institute of Catalysis and Inorganic Chemistry named after M.F. Nagiyev, Azerbaijan National Academy of Sciences, Baku, Azerbaijan, E-mail: salim7777@gmail.com

2. Institute of Physics, Azerbaijan National Academy of Sciences, Baku, Azerbaijan, E-mail: solmust@gmail.com

An actual problem is to study regularities of the effect of (for example, X-ray, gamma-ray, as well as a stream of high-energy charged particles) on physical properties of layered or chain structure semiconductors. In this regard, semiconductors of type A^3B^6 are still poorly understood. In crystals with a layered or chain structure the role of defects is particularly important, such as severely deformed or even broken bonds, which tend to manifest acceptor properties. The existence of such defects is attributed to the high density of states near the Fermi level. Traps generated by a variety of defects in crystals, play a major role in charge transfer phenomena, particularly at low temperatures. Valuable information on localized states may be derived from conductivity measurements in the bandgap of the crystal.

According to *T*-x diagram of the system Ga-S two compounds GaS and Ga_2S_3 are creating. Gallium monosulfide melts congruently at 1235 ± 5 K. GaS single crystals are layered wide-gap semiconductors with a rather high dc-resistivity. The results of investigation of electrical, photoelectric, thermal and optical properties of these crystals were presented in the literature (for example, [1]). GaS-based materials, combining interesting electrical and optical properties, are potential candidates for use in various transducers, light modulators, and information storage units. The investigation of electric properties of semiconductor materials in dc-and ac-electric fields gives information about the nature of charge transport and localization states in forbidden gap. For the establishment of mechanism of charge transport it is necessary to know the temperature dependence of dc-conductivity.

The objectives of this work were to study the dc-and ac- electrical properties of GaS single crystals, to gain insight into the mechanism of charge transport in the crystals, and to evaluate the parameters of localized states in their band gap.

The layered GaS single crystals used for our study were grown by the Bridgman method and have hexagonal structure with lattice parameters: a = 3.58 Å, c = 15.47 Å at room temperature.

Thus, analysis of the experimental results of studying the processes of charge transport in GaS samples in the low-temperature range enables us to state that, in these crystals, hopping conduction takes place with variable hopping length passing into activationless hopping conduction [2].

It is revealed that GaS single crystals exhibit a variable-range hopping conduction along a normal to their natural layers at temperatures T = 140–238 K in a dc-electric field. Estimates are made for the density of states near the Fermi level ($N_F = 6.2\times10^{19}$ eV^{-1} cm^{-3}) and their energy spread (ΔE = 0.08 eV), the average jump distance (R_{av} = 46 Å), the activation energy of the hopping conductivity (ΔW = 0.07 eV) and the concentration of trapping states ($N_t = 5\times10^{18}$ cm^{-3}) responsible for the hopping dc-conductivity in GaS single crystal. Ac-electric and dielectric properties of the GaS single crystals were studied in a broad frequency range. The nature of dielectric losses and the hopping mechanism of charge transport in the GaS crystals were established, and the parameters of localized states in the forbidden gap of studied crystals have been evaluated from ac-electrical measurements.

1. S.N. Mustafaeva, M.M. Asadov. “Effect of Thallium Doping on the Parameters of Localized States in *p*-GaSe Single Crystals”. Inorganic Materials, **47** (9) pp. 941–944, 2011.
2. N.F. Mott and E.A. Davis. *Electron Processes in NonCrystalline Materials* (Oxford, Clarendon Press, 1979; Mir, Moscow, 1982).

Low temperature Ta/Al based ohmic contacts to high voltage GaN transistors for energy efficient power conversion

E. Erofeev[1], I. Fedin[2]

1. Tomsk State University of Control Systems and Radioelectronics, Tomsk, Russia, erofeev@sibmail.com

2. Research and Production Company Micran, Tomsk, Russia, fedin.iv@micran.ru

GaN HEMTs are generally promising candidates for switching power transistors due to their high breakdown strength and the high current density giving a low on-resistance [1]. Low-resistance ohmic contacts are needed to reduce losses and self-heating. Conventional ohmic contacts in GaN HEMTs use Ti and Al, along with a cap to avoid oxidation of the Al layer [2]. The cap often consists of Ni or Mo with Au. But these structures require the high annealing temperature (>800 ^{o}C) to achieve good ohmic properties, which can damage the performance of semiconductor heterostructure on which the HEMT action depends. These temperatures can also melt Al, creating unwanted surface roughness of the contact. Thus making it difficult to implement gate-first process, which is useful for the self-aligned process development. Alternative ohmic metals for use with nitride semiconductors are being sought using TiN, Hf or Ta, for example, which can be annealed at lower temperatures (<600 ^{o}C). They have shown a low contact resistivity and smooth surface morphology. In work [3] are presented ohmic metal contact scheme based on TiN/Ti/Al/Ti/TiN. The minimum contact resistance found for TiN ohmic contacts were 0.67 Ohm × mm after annealing at T = 550 ^{o}C during t = 90 s. In study [4] are presented a low thermal budget (<600 ^{o}C) Hf/Al/Ta (15/200/20 nm) ohmic contact scheme on unintentionally doped $In_{0.18}Al_{0.82}N$/GaN grown on Si substrate, which has demonstrated low contact resistivity (0.59 Ohm × mm) and smooth surface morphology. In addition, the $In_{0.18}Al_{0.82}N$/GaN HEMTs fabricated with Hf/Al/Ta ohmic contacts have shown significantly improved performance, compared to devices with traditional Ti/Al/Ni/Au ohmic contacts.

In this study, we report the Au-free low temperature Ta/Al based ohmic contacts to high voltage GaN transistors for energy efficient power conversion.

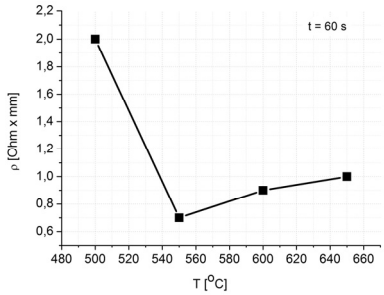

Fig. 1. The contact resistance of Ta/Al ohmic contacts versus annealing temperature in nitrogen.

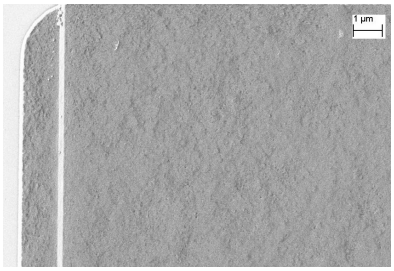

Fig. 2. SEM image of Ta/Al based contact surface after annealing at T = 550 °C during t = 60 s.

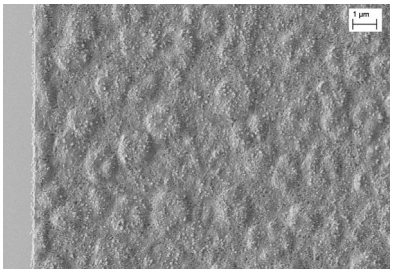

Fig. 3. SEM image of Ti/Al/Mo/Au based contact surface after annealing at T = 830 °C during t = 30 s.

That have been shown, the Ta/Al based ohmic contacts have the low contact resistance (0.7 Ohm × mm) after the low temperature annealing at T = 550 °C (fig. 1) and smooth surface morphology compared to conventional Ti/Al/Mo/Au based ohmic contacts (figs. 2 and 3). The fabricated high voltage GaN transistor based on the low temperature Ta/Al based ohmic contacts demonstrates the significantly improved source-drain breakdown voltage. The mechanisms responsible for discovered phenomenon have been discussed.

This work was financially supported by the Ministry of Education and Science of the Russian Federation, agreement no. 14.577.21.0204, unique project identifier: RFMEFI57715X0204.

1. J. Hudgins, R. Doncker. “Power semiconductor devices: For Variable Speed Drives“. Industry Applications Magazine, IEEE, **18**, pp. 18-25, 2012.

2. L. Wang, F. Mohammed. “Formation mechanism of ohmic contacts on AlGaN/GaN heterostructure: electrical and microstructural characterizations“. J. Appl. Phys., **103**, pp. 093516-09356-10, 2008.

3. A. Firrencieli, B. Jaeger, S. Decoutere. “Au-free low temperature ohmic contacts for AlGaN/GaN power devices on 200 mm Si substrates“. Jap. J. Appl. Phys., **53**, pp. 03EF01-1 – 04EF01-3, 2014.

4. Y. Liua and el. “Mechanisms of Ohmic Contact Formation and Carrier Transport of Low Temperature Annealed Hf/Al/Ta on $In_{0.18}Al_{0.82}N$/GaN-on-Si“. ECS J. Solid State Sci. Technol., **4**, 2, pp. 30-35, 2015.

Effect of point defects on the strength properties of interface formed by materials under the action of mechanical stresses

T.M. Makhviladze, M.E. Sarychev
Institute of Physics and Technology, Russian Academy of Sciences, Moscow, Russia, sarych@yandex.ru

The strength reliability of many layer structures that are used in the up-to-date nano- and microelectronics is one of the currently central problem [1]. That is why the adequate model development referred to delamination processes at the interfaces of joined materials under both the internal and external mechanical stresses is of great significance [2].

For this purpose we have developed an approach based on nonequilibrium thermodynamics methods. It should be mentioned that early these methods were successfully applied to investigate crack growth in homogeneous materials [3]. On these theoretical grounds we have advanced a new model which describes the kinetics of delamination due to crack formation and further its growth that takes place along the interface formed by two different monocrystalline materials. The kinetics of delamination in dependence on the concentrations of point defects in joint materials, temperature and on the rate of change of crack length has been investigated in detail. Within the framework of the model developed the situations have been revealed and analyzed when the defect concentration change can result in the replacement of delamination regime by crack healing regime. Estimations of critical values for crack lengths and defect concentrations are presented, these critical values serving as the boundary between these two regimes.

We discuss further the possibility of applying the developed model conceptions and results obtained to analyze and evaluate the impact of the effects of this type on the kinetics of oxygen precipitates growth in crystalline dislocation-free silicon. This process takes place in the stages of post-crystallization cooling and the subsequent heat treatment of silicon wafers while in the VLSI production. As shown in [4], the interface formed by precipitate particle and silicon matrix is exposed to the strong internal mechanical stresses due to the differences both in specific volumes and microstructures of materials. The combination of this factor along with the supersaturation of the silicon matrix with non-equilibrium point defects, which are in the form of atomic oxygen impurities and vacancies, can lead to the spontaneous formation and growth of cracks in the precipitate - silicon interface. It can significantly affect the growth rate of precipitate particles and the strength properties of the silicon wafers. In this regard the precipitates coalescence stage is of special interest because the oxygen supersaturation is already severely depleted and therefore is not a dominant source of growth precipitate phase. Instead, the coalescence is mainly due to the decay of the particles which sizes are less than the critical ones.

1. R.V. Goldstein, T.M.Makhviladze, and M.E.Sarychev. "Influence of electrical current on the stability of a conducting film surface". J. Surface, **9**, pp. 67-74, 2015.
2. R.V. Goldstein, T.M.Makhviladze, and M.E.Sarychev. "Modeling the kinetics of lattice defect adsorption into the interface of joint materials". J. Surface, **5**, pp. 712-717, 2011.
3. J.R. Rice. “Thermodynamics of the quasi-static growth of Griffith cracks”. J. Mech. Phys. Solids, **26**, pp. 61-78, 1978.
4. R.V. Goldstein, T.M.Makhviladze, and M.E.Sarychev. "Simulation of spatially heterogeneous oxygen precipitation in silicon with allowance for internal mechanical stresses". Russian Microelectronics, **43**, pp. 49-56, 2014.

Investigation of the phase formation from nickel coated nanostructured silicon

Yu.I. Shilyaeva[1], O.V. Pyatilova[1], A.Yu. Berezkina[1], A.V. Sysa[1], A.A.Dudin[2], and S.A. Gavrilov[1]
1. National Research University of Electronic Technology, Zelenograd, Moscow, Russia, shyliaeva@gmail.com
2. Institute of Nanotechnology Microelectronics INME of RAS, Moscow, Russia

Nickel coated porous silicon allows to implement a number of different applications. Nanocomposites of the "porous silicon – nickel" type are known to exhibit unique magnetic and magnetooptic characteristics and are promising materials for use in devices of silicon microelectronics [1]. Also, these materials are attracting considerable interest for gas sensing [2] and betavoltaic batteries [3].
On the other hand, due to the progressive trend of miniaturisation of electronic devices nanostructured nickel silicides are highly attractive materials in recent years [4]. The nickel silicide formation by solid-state synthesis typically includes nickel deposition on silicon surface and subsequent heat treatment. The solid-state synthesis based on nanostructured Si/Ni interface can provide significant reduction in silicide formation temperatures and a number of other features that require a detailed study.
In this regard, the aim of this work was to investigate the influence of the parameters of nickel deposition on nanostructured Si surface and further heat treatment conditions on the phase formation in the por-Si/Ni structures. For this purpose por-Si/Ni samples were formed by two methods:
1) metal-assisted chemical etching of *p*-type silicon with Ag film as catalyst and subsequent electroless nickel deposition using acidic solutions (Ni plating process in alkaline bath is not applicable in this case because it leads to a partial polishing of nanostructured Si surface);
2) electrochemical etching of *n*-type silicon and subsequent cathodic electrodeposition of nickel.
The obtained samples were characterized by means of scanning electron microscopy (SEM) and phase X-ray diffraction (XRD) analysis before and after heat treatment.
Energy dispersive X-ray analysis showed a significant amount of phosphorus impurity in the samples prepared by the first method. This fact is evidently explained by the composition of the solution used for electroless nickel plating, in particular, by the presence of sodium hypophosphite.
XRD patterns of the samples prepared by the first method indicate the presence of silicide phase Ni_2Si before heat treatment. It means that Ni_2Si is forming during the electroless nickel deposition on nanostructured Si surface at 90 □C. No peaks corresponding to silicide phases were detected for the reference samples prepared at the identical conditions using monocrystalline silicon. XRD patterns of the samples prepared by the second method show differences in phase composition in comparison with reference samples and samples prepared by the first method.
The performed studies allow to conclude that the electroless nickel deposition on nanostructured silicon surface is interesting for synthesis of nickel silicide nanostructures due to reduction in silicide formation temperatures. Moreover, the presence of silicide phase can improve the contact characteristics of the por-Si/Ni structures. Phosphorous impurity can be also useful when forming a *p-n* junction for betavoltaic devices. However, for investigation of silicide formation during heat treatment the electrochemical synthesis is preferred because it is allows to eliminate an influence of impurities.

Acknowledgement: The reported study was funded by RFBR according to the research project No. 16-33-00712 мол_а.

1. K. Rumpf, P. Granitzer, P. Polt. "Comparison of the magnetic behaviour between Co- and Ni-nanostructures embedded in silicon matrices". Phys. Stat. Sol., **5** (12), pp. 3798-3801, 2008.
2. I.M. Antropov, G.B. Demidovich, and S.N. Kozlov. Sensitivity of porous silicon-nickel composite to methane adsorption. Tech. Phys. Lett., **37** (3), pp. 213-215, 2011.
3. S.T. Revankar and T.E. Adams. "Advances in Betavoltaic Power Sources". J. Energy Power Sources, **1** (6), pp. 321-329, 2014.
4. J.-Y. Lin, H.-M. Hsu, and K.-Ch. Lu. "Growth of single-crystalline nickel silicide nanowires with excellent physical properties". Cryst. Eng. Comm., **17**, pp. 1911-1916, 2015.

Investigation of formation mechanism of Mo/Al/Mo/Au ohmic contact to AlGaN/GaN heterostructures

M.N. Kondakov[1,2], S.V. Chernykh[1,2], A.V. Chernykh[1,2], K.D. Shcherbachev[1], N.Yu. Tabachkova[1], D.A. Podgorny[1], N.B. Gladysheva[2], A.A. Dorofeev[2], S.I. Didenko[1]

1. National University of Science and Technology «MISiS», Moscow, Russia, kondakovmix@mail.ru.
2. Joint-Stock Company «Scientific & Production Enterprise «Pulsar», Moscow, Russia

Currently GaN-based high electron mobility transistors (HEMTs) are widely used in high-frequency, high-power and high-temperature electronics. The formation of ohmic contacts is one of the important part in the development of AlGaN/GaN HEMTs. At the same time the fabrication of ohmic contacts which meet the requirements on the contact resistance, surface morphology, edge quality and thermal stability is still under research.

The Ti/Al/Ni/Au metallization scheme is widely used as an ohmic contact to AlGaN/GaN heterostructures. The main disadvantage of this scheme is the high surface roughness due to the strong mixing between Au and Al. There are also many studies where Ti/Al/Mo/Au, Ti/Al/Ti/Au, V/Al/Mo/Au, Ta/Al/Ni/Au, Hf/Al/Ni/Au, Mo/Al/Mo/Au and other schemes are used as contact metallization. The possibility of obtaining low values of the contact resistance (less than 0.40 Ohm·mm) in the wide temperature range of rapid thermal annealing from 500 °C to 950 °C [1, 2] should be noted among the advantages of the latter scheme. However, the number of papers on the technological features of Mo/Al/Mo/Au contact formation is relatively small at the moment [1-4].

In this report results on study of the formation mechanism of Mo/Al/Mo/Au ohmic contacts to heterostructures AlGaN/GaN are presented. An epitaxial layer was grown using metal-organic chemical vapor deposition on a sapphire substrate. The epilayer consisted of 2.5 μm unintentionally doped GaN, 0.7 nm AlN and 15 nm undoped $Al_{0.26}Ga_{0.74}N$.

Electrical properties and the microstructure of the contacts were studied depending on annealing conditions and the composition of contact metallization. Current-voltage measurements on linear transmission line method (TLM) contacts were carried out at room temperature using an Agilent B 1500 semiconductor analyzer. The TLM structures design and fabrication technique of the experimental samples were presented in [5]. The contact microstructure was investigated with scanning and transmission electron microscopy, Auger electron spectroscopy, X-ray diffractometry and energy-dispersive X-ray spectroscopy.

It was determined that during thermal annealing of the contact there is a strong mixing between metals resulting in formation of intermetallic compounds – Al_2Au, Al_xMo_y, $GaMo_3$ and $GaAu_2$. Studies of the phase composition depending on thickness ratios of the metal layers and annealing temperature have shown that the Al_2Au phase formation negatively affects the contact morphology, and Al_xMo_y and $GaMo_3$ phases formation plays a crucial role in obtaining ohmic contact characteristics. It was found out that the formation of these phases does not occur when the Au layer is absent. Based on these results the model of the ohmic contact formation will be presented.

1. D. Selvanathan, F.M. Mohammed, A. Tesfayesus, I. Adesida, "Comparative study of Ti/Al/Mo/Au, Mo/Al/Mo/Au, and V/Al/Mo/Au ohmic contacts to AlGaN/GaN heterostructures". J. Vac. Sci. Technol. B, **22** (5), pp. 2409-2416, 2004.

2. A. Basu, F.M. Mohammed, S. Guo, B. Peres, I. Adesida, "Mo/Al/Mo/Au Ohmic contact scheme for $Al_xGa_{1-x}N$/GaN high electron mobility transistors annealed at 500 °C". J. Vac. Sci. Technol. B, **24** (2), pp. L16-L18, 2006.

3. J. Lee, M. Yan, B. Ofuonye, J. Jang, X. Gao, S. Guo, I. Adesida, "Low resistance Mo/Al/Mo/Au ohmic contact scheme to InAlN/AlN/GaN heterostructure". Physica status solidi (a), **208** (7), pp. 1538-1540, 2011.

4. Y. Ando, K. Ishikura, Y. Murase, K. Asano, I. Takenaka, S. Takahashi, H. Takahashi, C. Sasaoka, "Electron transport mechanism for ohmic contact to GaN/AlGaN/GaN heterostructure field-effect". IEEE Transactions on Electron Devices, **60** (9), pp. 2788-2794, 2013.

5. M.N. Kondakov, S.V. Chernykh, N.B. Gladysheva, A.V. Chernykh, A.A. Dorofeev, S.I. Didenko, K.D. Shcherbachev, N.Yu. Tabachkova, F.M. Baryshnikov, "Investigation of Mo/Al/Mo/Au metallization scheme as an ohmic contact to AlGaN/GaN heterostructures". Electronic Engineering, Series 2, Semiconductor Devices, **4** (238), pp. 38-48, 2015 (in Russian).

Low resistance Ti/Si/Ti/Al/Ni/Au ohmic contact for AlGaN/GaN HEMT

S. Shostachenko, R. Zakharchenko, R. Ryzhuk, N. Kargin
National Research Nuclear University MEPhI, Moscow, Russia, sashostachenko@gmail.com

Because of high electric conductivity, adherence and morphology, multilayer Ohmic contacts are often used in microelectronic applications. For Ohmic contact formation to n-type GaN semiconductor structure multilayer contacts based on Ti/Al (such as Ti/Al/Ni/Au) are often used. During the thermal treatment, they form compounds with low work functions [1]. Resistance of such contact annealed at temperature 800÷900 °C is 0.2÷0.5 mm [2].

The formation of conductive compound Ti_xN explains the formation of Ohmic contact to n-GaN, based on Ti/Al metal system [3]. This compound is formed by the deposition of titanium on the n-GaN surface and it extends for layer of metallization during the annealing. Ti_xN compound is formed at temperature 200÷1000 °C. Thus particles sprayed by various methods can form thick Ti_xN layer on the surface of semiconductor. Work function of Ti_xN is 3.74 eV and according to Schottky theory it corresponds to formation of Ohmic contact to n-GaN [3]. Resistance of metal-GaN Ohmic contact can reach 0.1÷1 $\mu\Omega\cdot cm^2$ at high charge carrier concentration in the semiconductor. This is due to the presence of nitrogen vacancies which are formed during the conductor interaction with contact metallization and produce high doped layer under contact [4].

This paper is dedicated to experimental investigation of Ohmic contacts to n^+-doped region of AlGaN/GaN transistor heterostructure based on Ti/Si/Ti/Al/Ni/Au metallization. Effect of annealing temperature on the specific resistance of Ohmic contact was studied. Ohmic contact with resistance of $3.4\cdot10^{-6}$ $\Omega\cdot cm^2$ was formed by optimization of the annealing temperature and introduction of the additional doping silicon layer. Such resistance is considered acceptable for Ohmic contacts [2, 3].

Acknowledgements
The study was supported by the Ministry of Education and Science of the Russian Federation (Agreement No. 14.578.21.0062 from 20.10.2014; unique identification number of the work is RFMEFI57814X0062).

Reference
1. P. Luther, S.E. Mohney. “Investigation of the mechanism for Ohmic contact formation in Al and Ti/Al contacts to n-type GaN”. Appl. Phys. Lett, **70**, pp. 57-59, 1997.
2 X. Kong. “Role of Ti/Al relative thickness in the formation mechanism of Ti/Al/Ni/Au Ohmic contacts to AlGaN/GaN heterostructures”. J. Phys. D: Appl. Phys, **45**, pp. 1-8, 2012.
3. A. Durbha, S.J. Pearton, C.R. Abernaty, J.W. Lee, P.H. Holloway, “Microstructural Stability of Ohmic Contacts to InxGa1-xN”. J. Vac. Sci. Tech B, 14, pp. 2582-2586, 1996.
4. H. Morko, S. Strike, G.B. Gao, M.E. Lin, B. Sverdlov, M. Burns. “Large-band-gap SiC, III-V nitride, and II-VI ZnSe -based semiconductor device technologies”. J. Appl. Phys, **76**, pp. 1363-1398, 1994.

Tungsten alloyed with rhenium as an advanced material for heat-resistant silicon ICs interconnects

A.N. Belov, Yu.A. Chaplygin, A.A. Golishnikov, D.A. Kostyukov, V.I. Shevyakov
National Research University of Electronic Technology, Russia, Shev@dsd.miee..ru

Currently Russian customers and manufacturers of electronic components (ECB) are in the need of development and manufacture of high-temperature silicon devices (operating at 200 °C and above) [1-2].
In terms of heat resistance metallization is the critical part of ECB.
One of its functional elements are interconnects, which are subject to new quality requirements associated with the reliability of the metallization system as a whole [3]. Recently researchers have shown interest for use of tungsten as a material for interconnects. Despite the fact that tungsten has a number of disadvantages, such as higher resistance; low adhesiveness associated with poor ductility; problems in outputs connection, etc., it has a significant advantage, namely advanced electromigration resistance.
So-called "Rhenium effect" is known, which manifests itself in the fact that when (5-10%) rhenium is added to the tungsten film it results in significant improvement of its plasticity. In particular, this effect is associated with the rhenium neutralizing the harmful effects of carbon contained in the tungsten.
This paper presents the results of comparative analysis of the electrical and mechanical characteristics of the tungsten and tungsten alloyed with rhenium films deposited on silicon, from the point of view of their use as interconnects in silicon ICs.
W and W (Re-5%) alloyed with rhenium films were made by magnetron deposition.
To measure sheet resistance of films well-known four-point probe method was used. Film thickness was measured by determining the values of the height difference with the help of profilometer by a step size relative to the contact profilometer substrate. Sheet resistivity for W and W (Re- 5%) was 13 and 27 Ohm·cm respectively.
Elemental composition the formed films was examined by Auger spectroscopy. The results of the experiment confirmed the presence of a uniformly distributed admixture of rhenium on the thickness of the W films (Re-5%)
To investigate the electromigration resistance of the conductors a methodology based on the accelerated electromigration testing at constant temperature was used [4]. Conductor integrity violation criterion was a change in its resistance ($R(t)$) by 20% relative to the initial value of the resistance in the steady state load current (R_0). As we expected, the electromigration resistance of W (Re- 5%) films was qualitatively higher in comparison, particularly, with the Al (Si, Cu) films.
We carried out a comparative analysis of the mechanical stresses in the W and W(Re - 5%) films. For this purpose we applied non-destructive method for optical laser scanning to measure the change of curvature, which appeared in the silicon wafer because of the deposited film. The results of a detailed study of mechanical stresses are given in the paper and a significant reduction in intrinsic stress in the W(Re - 5%) films is shown.
At the same time, these films explored their ability of adhesion to silicon and silicon oxide. It is shown that the pull force of the W(Re - 5%) films was ~1500 G/mm^2, of the W films ~700 G/mm^2.
Thus, the results of comparative analysis of electrophysical and mechanical characteristics of tungsten and tungsten alloyed with rhenium films deposited on silicon, from the viewpoint of their application as interconnects in heat-resistant silicon IP confirmed their recent promising use in this type of IC.

1. A.E I. Mehdi and K.K.J Brockschmidt. “A Case for High Temperature Electronics for Aerospace”, High Temperature Electronics Conference (HiTEC), pp. 14-15, 2006.
2. R.W. Johnson et al. “The changing automotive environment: high temperature electronics”, IEEE Transactions on Electronics Packaging and Manufacturing, **27** , pp. 164 – 176, 2004.
3. S. Tsukimoto, K. Ito, and M. Murakami. “Materials for ULSI metallization – Overview of Electrical Properties” Advanced Nanoscale ULSI Interconnects: Fundamentals and Applications, Springer Science+Business Media, pp. 131-143, 2009.
4. D. Munari, A. Scorzoni, F. Tamarri et al. “Drawbacks to using NIST electromigration test structures to test bamboo metal lines”, IEEE Trans. Electron. Dev. **41**, pp. 2280- 2288, 1994.

Mechanical properties of bimetallic one-dimensional structures

E. Smelova[1], I. Sitnikov[1], K. Tsysar[1], V. Andreev[1], V. Vdovin[2]
1. Moscow State University, Moscow, 119991 Russia, smelova_k_m@mail.ru
2. Kotel'nikov Institute of Radio Engineering and Electronics of RAS, Moscow, 125009 Russia.

The new problem of nanoelectronics is the study of stability of nanodevices. One of the most widespread systems of nanoelectronics is the one-dimensional structures (nanocontacts (NC) and nanowires (NW)) that can be used in low-dimensional storage devices [1]. These structures possess a high sensitivity to external mechanical stresses emerging, for example, under impact of powerful pulsed electro-magnetic fields on the structure [2]. The present work shows result of ab initio theoretical study of mechanical properties of freestanding Au-Mn nanowires and Au-Mn nanowire on copper substrate Cu(110). All calculations were carried out using the software package Vienna Ab-initio Simulation Package (VASP), which is based on the density functional theory (DFT) [3].

In Fig. 1a the total energy of the Au-Mn NW and forces per atom as function of average interatomic distance *d* are presented. We have shown that the interatomic distance about 3.0 Å is a breaking point of freestanding Au-Mn NW. The further increasing of the distance *d* results in decay of NW to the separate atoms.

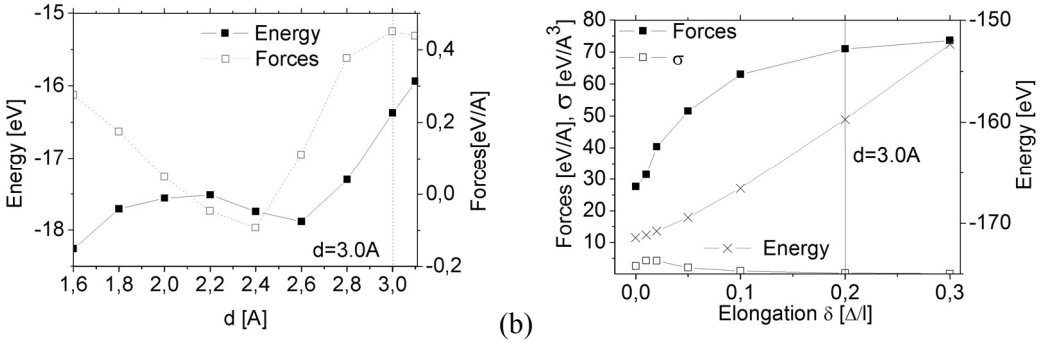

Fig. 1. Energy and forces in nanowire as function of average interatomic distance (a). Total energy, forces and stress of Au-Mn nanowire on copper substrate Cu(110) as function of elongation (b).

The influence of longitudinal deformation on mechanical properties of one-dimensional structures was studied in Au-Mn nanowire deposited on a copper substrate (Fig. 1b). The longitudinal deformation was applied to the copper substrate along the direction of nanowire formation. Forces on atom and elastic stress σ were calculated for longitudinal deformation along the nanowire axis. In Fig. 1b the total energy, forces and stress as function of relative elongation $\delta = \Delta/l$ were presented (l is the length of substrate, Δ its elongation). Elongation of copper substrate about 0.2% is crucial for deposited Au-Mn nanowire; at $\delta > 0.2\%$ the stress becomes zero. This deformation corresponds to average interatomic distance in Au-Mn nanowire about 3.0 Å, which is the breaking point of freestanding Au-Mn nanowire. Moreover, the longitudinal deformation of copper substrate exceeded 0.2% leads to critical changes of atomic structure of the system (the wire is dipped into the copper substrate). This study demonstrates the influence of longitudinal elastic deformation on the mechanical and atomic properties of the "wire-substrate" system.

The mechanical properties of the alloy 3-atomic Au-Co and Au-Ag nanocontacts represented by three atomic chains between two massive electrodes [4] were studied. The critical values of interatomic forces in the chain of nanocontact before its breaking were calculated for several types of atomic configurations of the chain. We found that dimer formation (Ag-Ag or Co-Co) in the nanocontact chain leads to the early break of NC. The Au-Co evenly mixed nanocontact possesses the maximal value of breaking force, however the rupture of nanocontact chain begins at interelectrodes distance exceeded 8.5 Å, which is less than in the Au-Ag nanocontact. We have found that the most stable configuration in respect to both these characteristics is evenly mixed Au-Ag nanocontact.

Work is supported by RFBR grants 16-07-01246, 16-29-09581

1. S. Loth et al., Science, **335**, p. 196, 2012.
2. V. Rodrigues and D. Ugarte, Phys. Rev. B, **63**, p. 073405, 2001.
3. G. Kresse and J. Furthmuller, Phys. Rev. B, **54**, p. 11169, 1996.
4. S. Egle et al., Phys. Rev. B, **81**, p. 134402, 2010; J. Bettini, et.al, Nature Nanotecnology, **1**, p. 182, 2006.

Analysis of contribution from various order diffraction maxima to complex magneto-optical Kerr effect from three-dimensional structures like magnetophotonic crystals

I.S. Zarev[1], N.Yu. Zvezdin[1], V.A. Paporkov[1], A.V. Prokaznikov[2]
1. Yaroslavl State Demidov University, Yaroslavl, Russia,
E-mail address: pva@univ.uniyar.ac.ru
2. Yaroslavl Branch of the Institute of Physics and Technology RAS, Yaroslavl, Russia,
E-mail address: prokaznikov@mail.ru

In the present time one of the widely spread investigation methods of magnetic and magneto-optical (MO) properties, especially in nanometer sizes region, is magneto-optical measurement of different characteristics and first of all is transverse magneto-optical Kerr effect (TMOKE). Periodic in space structures are of special interest. Such structures are called magnetophotonic crystals and they have a number of unique properties. At determined conditions of experiment a sharp increase of system response to external radiation was observed.

In this work the superposition of effects of different diffractional origins and orders by formation of resulting magneto-optical response from the structures like magnetophotonic crystals in the regions far from plasmonic resonances was investigated for the first time. The contributions into magneto-optical response from diffractional and interferential phenomena in maxima of different orders in three-dimensional systems like magnetophotonic crystals were studied. It was demonstrated that the usage of integral response in order to analyze magneto-optical effects results in disappearance of interference phenomena. Diffraction maximum of the zero order reflects represent magnetic component of magneto-optical response.

An important moment of electromagnetic radiation scattering on regular structures is the presence of resonance phenomena by fulfillment of conditions when multiplicity do a half of wave length for the incident radiation takes place for characteristic sizes of dispersers. This peculiarity connects with the fact that the bases of observed effects are interference and diffraction phenomena. The contribution into resulting response individual feature of elementary dispersers takes part as well as interference phenomena from different structure elements that have, generally speaking, different magnetic properties.

As a result of the presented investigations the conclusion can be done that the contribution into observed oscillating phenomena for different characteristics for maxima phenomena of different orders give interference along vertical direction of bulky structures. These interference phenomena in vertical direction reflect, in particular, properties of upper and bottom layers of the structure as well as characteristics of the walls of investigated three-dimensional structures. In the present work the structures are investigated like magnetophotonic crystals with vertical sizes much more than wave length of incident light. The investigation has demonstrated that zero diffraction maximum reflexes properly magnetic component of MO response. Moreover, zero order maximum makes possible to extract the information concerning vertical size of the structure. It was shown that by measuring of integral response, which is obtained by means of aperture lens, interference phenomena disappear on angle dependences of refraction rate.

The results of the present work can be used by analysis of signals from structures with complex topology what are important for elaboration of complex systems that contain components different with respect to structure and properties. In this connection it should be noted an interest to using of nanostructured systems as a dense arrays of regularly arranged vertical columns for creation of superdense magnetic memory. Reading of information from such a structure is closely connected with interaction effects of electromagnetic radiation with regularly structured magnetic medium (bit-pattered media). Obtained results testify concerning community of investigated phenomena that are related to a wide spectrum of diffraction and interference problems and they can be used in different technical and scientific aspects.

An exchange anisotropy effect in magnetic and magneto-resistive properties of epitaxial Fe/$Fe_{50}Mn_{50}$ film structures

L.A. Fomin, A.V. Chernykh, S.V. Pyatkin, G.M. Mikhailov
Institute of Microelectronics Technology and High Purity Materials RAS, Chernogolovka, Russia,
E-mail address fomin@iptm.ru.

It is known that antiferromagnetic $Fe_{50}Mn_{50}$ alloy is one of the materials that are most often used in film structures with a FM/AFM exchange anisotropy. A weak anisotropic permalloy $Fe_{20}Ni_{80}$ with fcc lattice as for $Fe_{50}Mn_{50}$ and close lattice parameters is widely used as a ferromagnetic layer. Such systems are most researched. Besides, epitaxial Fe(001)/$Fe_{50}Mn_{50}$(001) structures were not extensively studied argued by not quite good matching of crystal structure between the layers. However, it attracts interest as its realization leads to coexisting of two equal in-plane easy magnetization axes Fe[100] and [010] that may give new not studied exchange anisotropy configuration at a FM/AFM interface.

In this work the $Fe_{50}Mn_{50}$(80-150нм)/Fe(40нм)/Mo(5нм)/R-sapp structures were grown by pulsed laser deposition technique in an ultrahigh vacuum on R-sapphire substrates with Mo(001) seed layer. Discrete structures in a shape of rectangles, circles and crosses of different sizes ranged from 1 to 20 μm and different orientations against the substrate were fabricated by subtractive technology using grown multilayered films for magnetic structure studies by magnetic force microscopy (MFM). The subtractive technology included the etching of a film by Ar ions trough Al masks made on its surface by electron lithography [1]. Bridge-type structures were fabricated by deposition through a mask for magneto-resistive measurements. All samples were annealed in a vacuum at a magnetic field of 1000 Oe directed along Fe[100] axis followed by slow cool-down for a unidirectional anisotropy formation. Annealing temperature was 250 ^{o}C that exceeds the Neel temperature of $Fe_{50}Mn_{50}$.

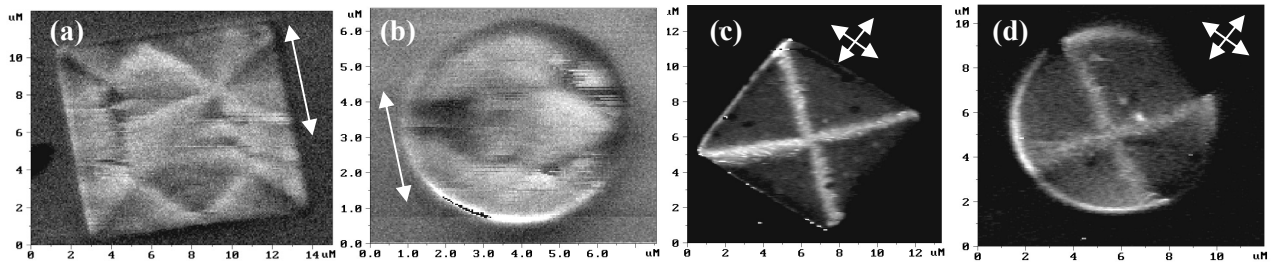

Fig. 1. MFM images of square and circle from Fe/ $Fe_{50}Mn_{50}$/Mo/R-sapp. (a), (b) and $Fe_{50}Mn_{50}$/Fe/Mo/R-sapp. (c), (d). Easy magnetization axes are indicated by arrows.

Magneto-resistance measurements showed that an exchange bias is observed in $Fe_{50}Mn_{50}$/Fe/Mo/R-sapp structures but does not in Fe/$Fe_{50}Mn_{50}$/Mo/R-sapp ones. However, by application of magnetic force microscope, a regular magnetic structure was found in all type microstructures although their domain structures were different. For structures with Fe-layer on the top of FeMn-layer, magnetic domains were arranged in such a way if the only in-plain easy axis of magnetization (EAM) directed perpendicularly to the unidirectional anisotropy axis that is formed during annealing exists (fig.1 a, b). This magnetic structure is usually observed [2] if an AFM plane is spin-compensated at the FM/AFM interface. For other structures (fig.1 c, d), where FeMn-layer is on the top of Fe-layer, two EAMs exist. The domain structure is the same as in epitaxial Fe structures without a $Fe_{50}Mn_{50}$ upper layer but slightly distorted due to an exchange field at the $Fe_{50}Mn_{50}$/Fe interface. The exchange field was directed along the magnetic field applied during annealing. Its value found in MFM measurements supplemented by an external magnetic field was 40 Oe and close to the exchange bias. The difference in domain structures is explained by a film epitaxy quality because high-quality epitaxy of Fe-layer on Mo seed-layer opposites to that on FeMn. This affects both on an exchange bias in magnetoresistance and on a MFM magnetic contrast distortion.

1. G.M. Mikhailov, L.I. Aparshina, S.V. Dubonos, Yu.I. Koval, I.V. Malikov, A.V. Chernykh, "Fabrication of monocrystalline refractory metal nanostructures capable of ballistic electron transport." Nanotechnology **9**, pp. 1–5, 1998.
2. A.I. Morosov, A.S. Sigov. "Frustrated multilayer ferromagnet-antiferromagnet structures: Beyond the scope of the exchange approximation (a review)." Phys. Solid State, **54**, pp. 219–242, 2012.

Infrared magnetoreflection in cobalt ferrite spinel

Yu. Sukhorukov, A. Telegin, N. Bebenin, A. Nosov, V. Bessonov, A. Buchkevich, V. Bessonova
M.N. Miheev Institute of Metal Physics Ural Branch of RAS, 620990, Ekaterinburg, Russia, imp.uran.ru

Currently there is intensive developing of a separate branch of spintronics – straintronics. It is a branch of physics that studies the change of the elastic properties of the material under application of a magnetic field and/or electric field. There are a large number of magneto-optical effects related to magnetoelastic properties of magnetic materials, but only in polarized light. Previously it was shown that magnetoreflection of natural light can reach giant values from units to tens of percent in magnetic semiconductors [1]. Magnetoreflection (MRf) is defined as relative change of intensity of light under application of a magnetic field.

In this paper we present the first report on the detection MRf of natural light in the IR region of the spectrum in the ferrimagnetic spinel $CoFe_2O_4$ with a large value of magnetostriction.

The $CoFe_2O_4$ single crystals (with inverted structure of the spinel - symmetry Fd3m) with a thickness of $d \sim 290$ μm, area of $S = 4\times4$ mm^2 (a = 8.38 Å) were grown by the radiational zone melting method. Conformity assessment of the composition of the samples to formula unit of $CoFe_2O_4$ was carried out using the microroentgen analysis method. It shown that the samples are single phase and chemical composition corresponds to the formula unit. The roughness of the polished surfaces was less than 1 μm. Measurements of reflection (R) and magnetoreflection (MRf) with a relative error of 0.2 % was carried out at angles of 7° to the normal falling of light in the infrared wavelength range from 0.8 to 30 μm and the temperature range $80 \le T \le 300$ K.

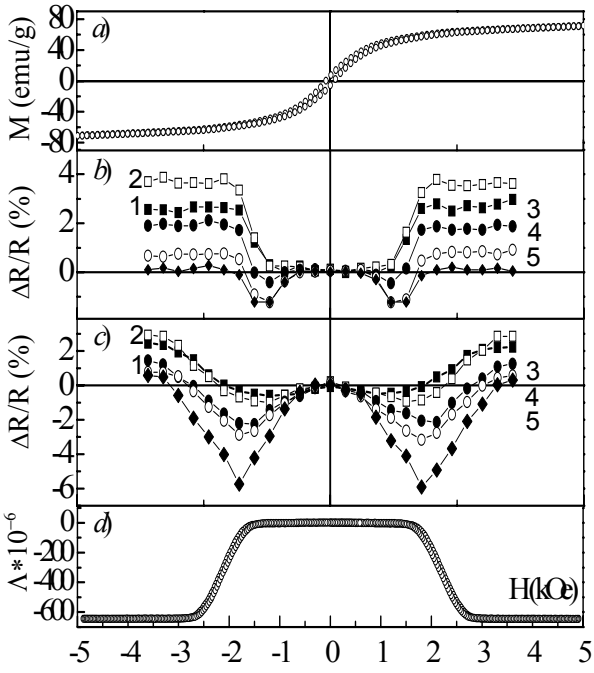

Fig. 1. The field dependences for H || (100) (a) of magnetization, (b) of magnetoreflection $\Delta R/R$ at T = 295 K, curve 1 – λ = 2.5 μm, 2 – 2.72, 3 – 2.96, 4 - 3.2, 5 – 3.4 μm, (c) $\Delta R/R$ at T = 80 K, curve 1 - λ = 2.5 μm, 2 – 2.72, 3 – 2.96, 4 – 3.2, 5 – 3.4 μm, (d) magnetostriction for $CoFe_2O_4$ single crystal.

Four physical mechanisms leading to the appearance of a giant magnetoreflection effect are known. The first mechanism is associated with the change of the interband transitions and the absorption edge shift in the magnetic field, the second – with the change of the impurity absorption, the third – with the influence of free charge carriers and the fourth – with the shift of the reflection minima near the phonon bands. The influence of deformation (elastic stress) on magnetoabsorption for ferromagnetic semiconductors are theoretically considered in the work [2]. Experimental work to study the effects of elastic stress on magnetoreflection and magnetoabsorption was expected.

It is shown that the effect of magnetoreflection is even relative to the magnetic field in contrast to the magnetization and saturates in fields above 2.5 kOe at room temperature and for H > 3 kOe at T = 80 K. In the spectral region $1.5 \le \lambda \le 4.5$ μm there is a similarity of the field dependences of the magnetoreflection and the magnetostriction. At a fixed wavelength it is indicated that value and sign of magnetoreflection in $CoFe_2O_4$ is possible to change only by the variation of the magnetic field amplitude due to the shift of the impurity absorption band under the field action.

1. A.V. Telegin, Yu.P. Sukhorukov, N.N. Loshkareva, E.V. Mostovshchikova, N.G. Bebenin, E.A. Gan'shina, A.B. Granovskii, "Giant magnetotransmission and magnetoreflection in ferromagnetic materials", JMMM, **383**, pp. 104-109, 2015.

2. N.G. Bebenin, "The deformation dependence of the light absorption coefficient in ferromagnetic semiconductors (Cd)$HgCr_2Se_4$ near the edge of the fundamental band", FTP, **25(9)**, pp. 1661-1663, 1991 (in Russian).

The features of CNT growth on catalyst-content amorphous alloy layer by CVD-method

S. Dubkov[1], S. Bulyarskii[2], A. Pavlov[2], S. Skorik[3], A. Dudin[2], E. Kitsyuk[3], P. Mierczynski[4], T. Maniecki[4], R. Ciesielski[4], S.Gavrilov[1], and D. Gromov[1]

1. National Research University of Electronic Technology, Moscow, Russia (sv.dubkov@gmail.com)
2. Institute of Nanotechnology of Microelectronics of the RAS, INME, Moscow, Russia
3. Scientific-Manufacturing Complex "Technological Center", Zelenograd, Moscow, Russia
4. Institute of General and Ecological Chemistry, Lodz University of Technology, Lodz, Poland

Carbon nanotubes (CNTs) were discovered by Iijima more than 25 years ago [1]. Today, there are numerous publications and monographs devoted to the study of the physical properties, synthesis and development of electronic devices on the basis of the carbon material [2].

CNT growth occurs on the catalytic metal clusters (the most commonly used metals Co, Fe, Ni), where the dimensions of CNTs depend on the size of clusters. The quality and reproducibility of the CNT growth also depends on the support layers, which are located clusters [3]. Typically, the surface preparation for CNT synthesis occurs in several stages: deposition support layers; deposition of the catalytic metal layer; CNT synthesis. Slight thickness variations of layers (5-10 nm) during the first two stages can lead to failure of all CNT synthesis process.

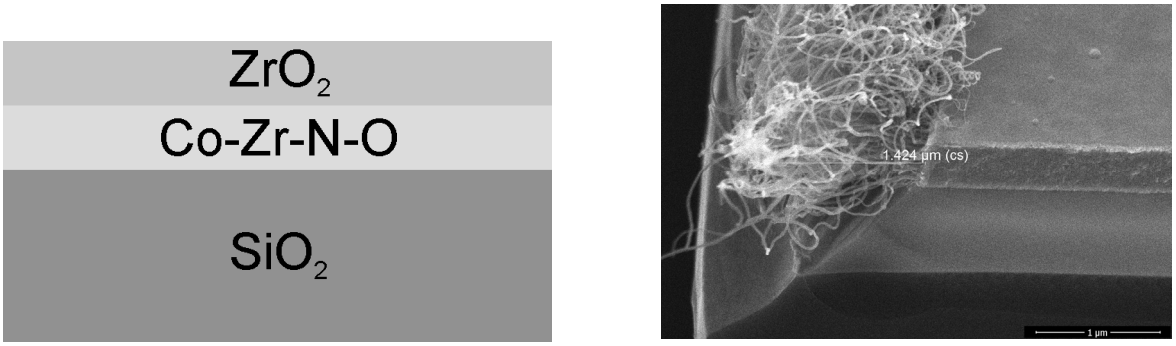

a b

Fig. 1. Schematic illustration of researched structure (a) and SEM picture of the sample after the synthesis of CNT (b)

In previous works [4] had demonstrated the synthesis of CNT thin films on the alloy Co-Zr-N-O with a low content of catalytic metal. The feature of this process is that it can be carried out on the alloy films of Co-Zr-N-O of varying thickness, making it technically attractive [5]. This work demonstrates that the use of an alloy Co-Zr-N-O allows growth of CNTs on an open end of the alloy, as shown in Fig. 1, which can be implemented to create a planar emission structure.

This work was funded by a grant BIOSTRATEG2/297310/13/NCBR/2016.

1. S. Iijima, "Helical microtubules of graphitic carbon," *Nature*, 1991, **354** (6348), pp. 56–58.
2. M. S. Dresselhaus, G. Dresselhaus, and P. Avouris, Eds., *Carbon Nanotubes*, Vol. 80. Berlin, Heidelberg: Springer Berlin Heidelberg, 2001.
3. H. Sugime, S. Esconjauregui, L. D'Arsié, J. Yang, A.W. Robertson, R.A. Oliver, S. Bhardwaj, C. Cepek, and J. Robertson, "Low-Temperature Growth of Carbon Nanotube Forests Consisting of Tubes with Narrow Inner Spacing Using Co/Al/Mo Catalyst on Conductive Supports," *ACS Appl. Mater. Interfaces*, 2015, **7** (30), pp. 16819–16827.
4. D.G. Gromov, S. Bulyarskii, A. Pavlov, S. Scorik, A. Shulyat'ev, and A.Y. Trifonov, "Catalytic CVD-growth of array of multiwall carbon nanotubes on initially amorphous film Co–Zr–N–O," *Diam. Relat. Mater.*, 2016, **64**, pp. 97–102.
5. D.G. Gromov, S.V. Dubkov, A.A. Pavlov, S.N. Skorik, A.Y. Trifonov, A.S. Shulyatev, Y.P. Shaman, and B.N. Rygalin, "Use of thin film of a $Co_{15}Ti_{40}N_{35}$ alloy for CVD catalytic growth of carbon nanotubes," *Russ. Microelectron.*, 2016, **45** (2), pp. 98–104.

Using functionalized CNTs for production of piezoelectric polymer composite films.

A.V. Sysa[1,2], Ju.P. Shaman[1,2], M.V. Silibin[1], L.V. Tabulina[3], A.A. Polohin[1], I.M. Gavrilin[1], A.A. Pavlov[4]

1. National Research University of Electronic Technology, Zelenograd, Russia, sysa.artem@yandex.ru;
2. Scientific-Industrial Complex Technological Center MIET, Zelenograd, Russia;
3. Belarusian State University of Informatics and Radioelectronics, Minsk, Belarus
4. Institute of Nanotechnologies of Microelectronics of RAS, Moscow, Russia;

At the present time composite materials attract huge interest. They combine the unique properties and ability to control and predict their chemical and physical parameters. Carbon nanotubes (CNTs) are a versatile component for such materials formation. Adding a small amount of CNTs in composites improves the operating characteristics due to their unique mechanical, chemical and electrical properties. For instance, introducing 0.1 wt. % of CNTs into piezoelectric polymer matrix a significant improvement in the electrical characteristics of the structures were observed [1].
To achieve uniform distribution of the CNTs in the polymer matrix choosing an effective method of introducing carbon nanoparticles in the polymer matrix is important, as well as formation process technological parameters optimization. The most important problem of polymer matrices with nanoinclusions CNT preparation process is the uniform distribution of the nanoparticles in the polymer matrix. Due to the large value of the surface energy of the CNTs, the size of the agglomerates up to several dozens of micrometers can be formed, which in turn leads to composite physical properties degradation [2]. Reducing the size of agglomerates of CNTs using ultrasonic method is quite effective way, but it has a limited effect [3]. In this regard, for better dispersion and uniform distribution of nanoinclusions in the polymer matrix combination of ultrasonic impact and chemical treatment for CNTs need to be used [4]. In this paper the role of CNTs oxidative treatments on the formation process of polymer composite piezoelectric films based on poly (vinylidene fluoride-trifluoroethylene) (P (VDF-TrFE)) was investigated.
Initial MWCNTs were synthesized on bimetallic Co-Mo catalyst on MgO core particles by chemical vapor deposition process supplied by methane pyrolysis. The resulting structures were processed in HCl solution to remove the metal catalyst particles. While chemical properties of the CNT surface should be changed functionalization in H_2O_2, H_2NO_3, H_2SO_4 solutions were performed. Obtained material was studied by TEM, FTIR and Raman spectroscopy methods. It was found that oxidized MWCNT (O-MWCNT) can form the highly stable suspensions based on polar solvents, which are used for dissolving P(VDF-TrFE), whereas suspensions with unmodified carbon nanotubes (U-MWCNT) showing degradation. This result is consistent with a large number of carboxyl groups which are formed on the surface in during oxidation process. A Fourier transform infrared (FTIR) spectra of O-MWCNTs confirms oxidation process with the presence of a peak at 1382 cm^{-1} related to the presence of OH due to bending deformation in -COOH. Other two bands are observed at 1735 cm^{-1} and 1154 cm^{-1} corresponding to C=O and C-O, respectively. Composites based on P (VDF-TrFE) matrices with different types of functionalizing CNTs have been prepared and their electrical parameters have been studied. It is shown that oxidative treatment of CNTs is necessary for polymer composite piezoelectric films formation.

This work was financially supported by the Ministry of Education and Science of the Russian Federation: reference number 2014/101.

1. G. Kim, S. Hong, Y. Seo. "Piezoelectric properties of poly(vinylidene-fluoride) and carbon nanotube blends: β-phase development". Phys. Chem. **11** (44), p. 10506, 2009.
2. S. Bal. "Dispersion and reinforcing mechanism of carbon nanotubes in epoxy nanocomposites". Bull. Mater. Sci. **33** (1), pp. 27-31, 2010.
3. J. Hilding, E. Grulke, Z. George, F. Lockwood. "Dispersion of carbon nanotubes in liquids". J. Dispersion Science and Technology. **24**, pp. 1-41, 2003.
4. J. Vera-Agullo, A. Glória-Pereira, H. Varela-Rizo, J. Gonzalez, I. Martin-Gullon. "Comparative study of the dispersion and functional proper ties of multiwall carbon nanotubes and helical-ribbon carbon nanofibers in polyester nanocomposites". Composites Science and Technology. **69**, pp. 1521-1532, 2009.

Formation of nanoporous structure in silicon substrate using two-stage annealing process

Yu. Denisenko, V. Rudakov
Institute of Physics and Technology, Yaroslavl Branch, Russian Academy of Sciences, Yaroslavl, 150007 Russia,
E-mail: den-yur55@mail.ru

The discovery of room temperature photoluminescence of porous silicon (PS) has produced a great interest with the perspective of development of silicon optoelectronic devices (light emitting diodes, photodetectors) formed using quantum dots. Besides, PS is intensively investigated for a variety of applications such as sensors, medical diagnostics, optical filters, micro reactors and fuel cells. A new class of PS materials created without the use of photolithographic or electrochemical processes are now of considerable interest from both technological and scientific points of view.

The aim of the present work is further development of engineering of PS layers. We consider the overall porosity of silicon can be increased by the way of bulk diffusion of excess vacancies generated during annealing in non-isothermal reactor. In the presence of grad *T*, the conditions for Frencel pair generation and division of point defects fluxes are created. This increases the chemical potential of vacancies, thus, increasing probability the appearance of viable nucleus of pores. The method involves preliminary creation of the surface impurity source with the help of co-implantation of P^+ and O^{2+} ions into (001)-oriented Si substrate and further two-stage annealing process. At the first stage, the substrate was annealed in non-isothermal reactor with process variables (substrate average temperatures $T = 800 \div 1100$ °C, 5 min, axial grad $T = \pm 35 \div 100$ K/cm). The characteristic property of this type of annealing is synergistic action of the many factors on impurity-defect subsystem of the substrate such as non-uniform thermal field, mechanical stress gradients, non-equilibrium concentrations of intrinsic point defects, complex self-organization processes within the boundary of diffusion zone. At the second stage, isothermal "evolution" of the substrates was continued in the conventional furnace (1150 °C, 4 h). The formation of two different kinds of nano-sized voids arrays on the cleaved samples has been exposed. The presence of the regularly spaced hollow tubes oriented along screw component of misfit dislocations (in the case of $T = 800 \div 900$ °C and grad $T = -35$ K/cm) had been reported earlier [1]. Within the scope of this work, the formation of porous structure in the surface layer (in the case of process variables $T = 1100$ °C and grad $T = -70 \div 100$ K/cm) is investigated. Corresponding information about the porous structure are presented as a photo collage of three SEM images in Fig. 1. The first SEM image (the top in Fig. 1) represents the data of visual inspection revealed that the silicon surface retains a mirror quality, but in some areas begin to form tetrahedral etch pits that originate from screw, edge, or mixed-type threading dislocations. The second SEM image made at an angle of 75° (the middle part in Fig. 1) shows the rhombic projection of the pore indicating the octahedral faceting along the {111} planes (in accordance with the table of projections in [2]). Faceted forms pores (single or double octahedron) also point to the information about the active participation of oxygen monolayers during formation the pore walls. In the bottom SEM image made at an angle of 90°, the pore boundaries within the phosphorus diffusion zone are clearly expressed too.

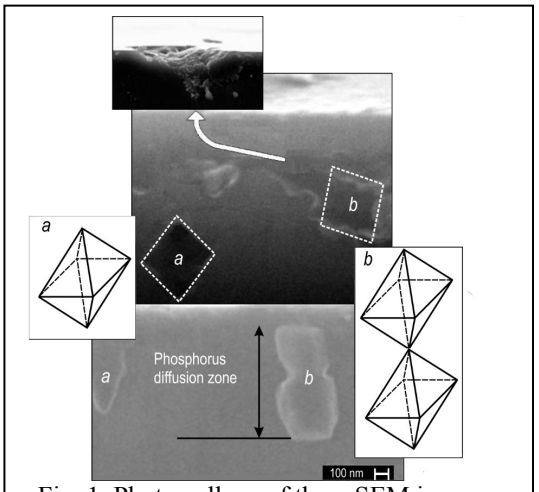

Fig. 1. Photo collage of three SEM images applied to the same cleaved specimen.

.

1. V. Rudakov, E. Bogoyavlenskaya, Yu. Denisenko, "Formation of nanovoids arrays in silicon substrate using non-isothermal annealing" Intern. Conf. ICMNE-2014: Book of Abstracts. Moscow-Zvenigorod, Russia, Oct. 2014. P1-01.
2. Cheremskoy P.G., Slezov V.V., and Betekhtin V.I. (1990). Pores in Solids, Energoatomizdat, Moscow (in Russian).

Luminescence properties of porous alumina films formed via Al anodization in selenic acid solution

Y. Nazarkina[1], A. Dronov[1], S. Gavrilov[1], S. Oleynik[1], D. Gromov[1], L.Lepnev[2]
1. National Research University of Electronic Technology, Bld. 1, Shokin Square, Zelenograd, 124498, Moscow, Russia, E-mail: engvel@mail.ru
2. Lebedev Physical Institute of the Russian Academy of Sciences, 53 Leninskiy Prospekt, 119991, Moscow, Russia

One-dimensional nanostructure arrays and nanostructured films attracted much attention due to its unique properties. Porous anodic alumina is a convenient inexpensive matrix for template synthesis and further investigation of such nanomaterials [1].
For formation of high quality nanostructure arrays, anodic alumina matrix should have ordered porous structure. Furthermore, specific requirements to the alumina matrix exist for each nanostructure investigation techniques. For example, for porous Al_2O_3 application for nanostructure properties characterization via spectroscopy techniques, Al_2O_3 matrices should introduce the smallest impact in the analyzed signal. This is a challenge, because porous oxides derived from commonly used self-ordering electrolytes (e.g. oxalic or phosphoric acid) are luminescent [2, 3]. It is caused either due to the luminescent ions incorporation or defect oxygen vacancy centers emersion during porous alumina growth. Therefore development of new electrolytes for formation of alumina matrices with specific properties is essential.
Recently it has been shown that ordered porous Al_2O_3 films can be formed in electrolyte based on selenic acid aqueous solution [4, 5]. Moreover, SeO_3^{2-}, SeO_4^{2-} ions are not luminescent. Hence, their incorporation within porous Al_2O_3 template should not introduce distortions in its optical response. In this work, this supposition was verified.
Self-ordered porous alumina films were obtained via anodization in selenic acid aqueous solution. The samples were prepared by both one-step and two-step anodization techniques. After anodization, specimens were annealed at different temperatures. Morphology of the samples was examined by scanning electron microscope JEOL JSM-7000F.
The luminescence properties of the samples were investigated by multichannel spectrometer S2000 (Ocean Optics). The pulsed nitrogen laser was used as the excitation light source (excitation wavelength = 337 nm). Measurements were performed both under room temperature and low temperature (77 K) conditions. The features of porous Al_2O_3 prepared in selenic acid based electrolyte luminescence spectra were considered. The effects of porous Al_2O_3 pretreatment (one- or two-step anodization) and posttreatment (annealing) procedures on its luminescence properties were studied. Additional samples formed in oxalic acid and sulfuric acids were fabricated. Luminescence spectra of matrices prepared in selenic acid based electrolyte were compared to the spectra of the samples synthesized in the oxalic and sulfuric acids.

The work was supported by grant of the President of the Russian Federation (MK-9536.2016.3).

1. S.A. Gavrilov, D.A. Kravtchenko, A. Zheleznyakova, V.Y. Timoshenko, P.K. Kashkarov, V. Melnikov, G. Zaitsev, L.A. Golovan. “Porous anodic alumina for photonics and optoelectronics” Proc. SPIE **5401**, Micro- and Nanoelectronics, pp. 235-241, 2003.
2. A. Brzózka, A. Brudzisz, K. Hnida, G.D. Sulka, “Chemical and Structural Modifications of Nanoporous Alumina and Its Optical Properties,” *Electrochemically Engineered Nanoporous Materials*, D. Losic, A. Santos (Eds.), **220**, Springer International Publishing, Switzerland, pp. 93–116, 2015.
3. I.S. Molchan, N.V. Gaponenko, R. Kudrawiec, J. Misiewicz, G.E. Thompson. “Influence of porous anodic alumina matrix upon europium luminescence from sol–gel-derived films”. Mater. Sci. Eng. B., **105**, pp. 37-40, 2003.
4. A. Baron-Wiechec, O. Ekundayo, S.J. Garcia-Vergara, H. Habazaki, H. Liu, P. Skeldon, G.E. Thompson. “Ion Migration and Film Morphologies in Anodic Alumina Films Formed in Selenate Electrolyte”. J. Electrochem. Soc., **159**, pp. C312–C317, 2012.
5. Y. Nazarkina, S. Gavrilov, H. Terryn, M. Petrova, J. Ustarroz. “Investigation of the Ordering of Porous Anodic Alumina Formed by Anodization of Aluminum in Selenic Acid”. J. Electrochem. Soc., **162**, pp. E166–E172, 2015.

Experimental study of optical coefficients of nanometer-thick copper and gold films in microwave frequency range

I. Khorin[1,2], N. Orlikovsky[1], A. Tatarintsev[1], S. Pronin[3], V. Andreev[3], V. Vdovin[4].
1. Institute of Physics and Technology of RAS (IPT RAS), Moscow, Russia, ivan-khorin@mail.ru,
2. Institute of Physics and Technology of Moscow Technological University (MIREA), Moscow, Russia,
3. Moscow State University, Moscow, 119991 Russia,
4. Kotel'nikov Institute of Radio Engineering and Electronics of RAS, Moscow, 125009 Russia.

The effect of abnormally high absorption of microwave radiation was observed recently in aluminum films of nanometer thickness [1]. This effect is most noticeable when the film thickness is comparable to the mean free path of the conduction electrons in the film. A significant difference between the experimental data and theoretical predictions for the films with thickness of several nm was noted. Our aim was to study in detail the reflection, absorption and transmission coefficients of the nanometer films of gold and copper at a wavelength of 3 cm. Both materials possess high electrical conductivity and are used widely in nanoelectronics.

Ultrathin copper films with different sputtering time were prepared on quartz (2×3.2 cm^2) and Si (100) substrates by using a magnetron sputtering in a Leybold Z-550 deposition system. The copper films were deposited from a 99.999 % purity Cu target by means of the DC magnetron sputtering with a 100 W power. The copper films thicknesses prepared on the quartz and Si substrates were 0.5, 1, 1.5, 2, 2.5, 3, 4, 5, 7.5, and 10 nm. The surface morphology of the copper films was observed using a Carl Zeiss Ultra scanning electron microscope (SEM) at 1 kV of acceleration with a Standard Everhart-Thornley secondary electron detector (SE2) and Annular on-axis Energy selective Backscatter electron detector (EsB). The SE2 highlights topographic contrast and the EsB highlights chemical (z) contrast.

Vector network analyzer R&S®ZVA 24 was used for the measurements of optical coefficients of the films. The films on the substrates were installed into the waveguide where reflected and transmitted amplitudes of microwave at a wavelength of 3 cm were measured.

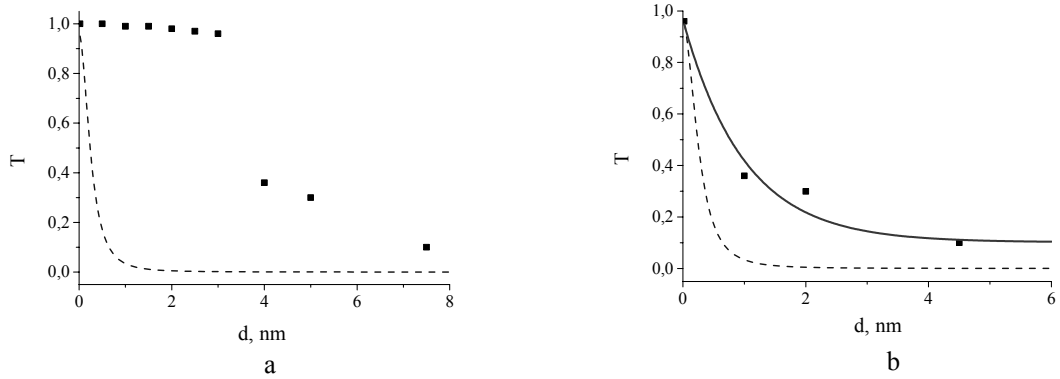

Fig. 1. Dependence of transmission coefficient on the copper film thickness *d*. Experimental data are shown by symbols, theoretical calculations for bulk conductivity $5.95\cdot10^7$ Sm/m and for $5.35\cdot10^6$ Sm/m are shown by dashed and solid lines.

The copper films with thicknesses up to 4-6 nm exhibit cluster-island structure and are characterized by low conductivity. A high percentage of the copper oxide in nanometer films also reduces their conductivity. A combination of these factors results in a significant difference between the experimental and theoretical results (see Fig. 1a) for the film thickness up to 3 nm. The introduction of an effective film thickness $d_{\text{eff}} = d$ - 3 nm, at which the film is considered to be formed, the experimental data for the transmission coefficient are in a good agreement with the model calculations (Fig. 1b). These results were confirmed by SEM images obtained in the films of different thicknesses.

This work was supported by RFBR grants 16-07-01246 and 16-29-09581.

1. Andreev V.G., Vdovin V.A., Voronov P.S. "An experimental study of millimeter wave absorption in thin metal films". Technical Physics Letters, **29**, pp. 953-955, 2003.

The features of charging -Z-cut single-domain ferroelectric $LiTaO_3$

K.E. Markovets[1], E.I. Rau[1], A.A. Tatarintsev[1, 2]
1. Faculty of Physics of M.V. Lomonosov Moscow State University, Moscow, Russia.
2. Institute of Physics and Technology RAS, Moscow, Russia.
tatarintsev@ftian.ru

In recent years integration of such active dielectric materials as ferroelectric, piezoelectric and pyroelectric in microelectronic technology has been increased. It allows to create the devices based on a new physical principle such as high-speed ferroelectric memories (FeRAM), random-access memory with a high integration (DRAM), microelectromechanical systems (MEMS), uncooled IR pyrodetector and others.

Creating a regular domain structures (RDS) configuration required in ferroelectric crystals is a practically important problem of using ferroelectricity. One of the most convenient ways to create the RDS of micron, submicron and (in very thin crystals) nanometer size is irradiation of a sample by focused electron beam in the electron beam lithography setup [1, 2]. However, the conditions of domain switching under electron irradiation, the further growth and fusion of adjacent domains have not yet been studied enough.

The present work aims to study the processes taking place in the ferroelectric material during electron beam irradiation. The experiments were performed on single-domain ferroelectric -Z-cut $LiTaO_3$ with different energy of the primary electron beam. According to our experiments under electron beam irradiation of a ferroelectric with the energy of E_0 = 200 eV and the current of I_0 = 100 pA on the area of 100×100 μm^2 in the initial moment of irradiation the sum of the displacement and leakage current I_{L+D} in magnitude was very similar to the current of the incident beam I_0, measured at the Faraday cup just before the start of the experiment. From a certain moment of time, the amount of I_{L+D} started to decrease, and at the same time a negative surface potential began to emerge.

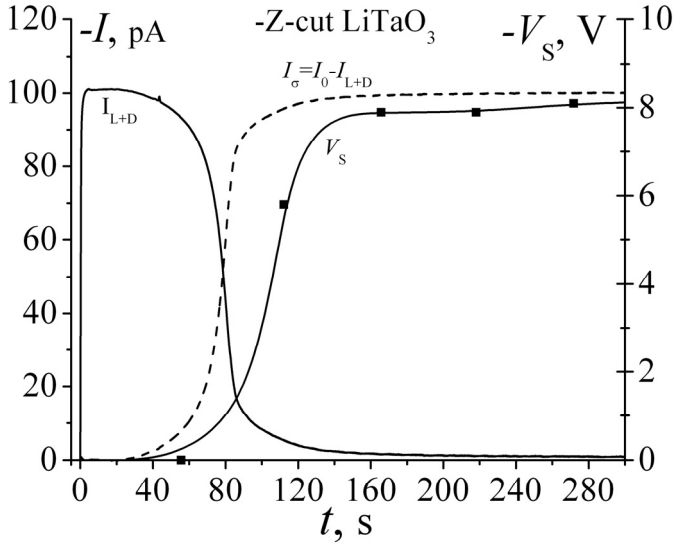

Fig. 1. Sum of leakage and displacement current I_{L+D} and surface potential $-V_S$ versus electron-irradiation time for primary electron energy E_0 = 200eV and current density $j_0 = 10^{-6}$ A/cm^2 measured on -Z-cut of $LiTaO_3$. Dash line shows the calculated data for secondary electron emission current from the currents balance: $I = I_0 - I_{L+D}$.

1. E.V. Emelin, A.I. Il'in, and L.S. Kokhanchik. "Recording of domains by an electron beam on the surface of +Z cuts of lithium niobate". Physics of the Solid State, **55** (3), pp. 540–546, 2013.
2. L.S. Kokhanchik, D.V. Irzhak. "Formation of regular domain structures and peculiarities of switching of the spontaneous polarization in lithium tantalate crystals during discrete electron irradiation". Physics of the Solid State, **52** (2), pp. 306–310, 2010.

Thermodynamic and Physical Properties of the New Layered Materials Based on $TlGaS_2$

M.M. Asadov[1], S.N. Mustafaeva[2]

1. Institute of Catalysis and Inorganic Chemistry named after M.F. Nagiyev, Azerbaijan National Academy of Sciences, Baku, Azerbaijan, E-mail: mirasadov@gmail.com

2. Institute of Physics, Azerbaijan National Academy of Sciences, Baku, Azerbaijan, E-mail: solmust@gmail.com

$TlBX_2$ type compounds (B = In, Ga; X = S, Se, Te) are formed in the quasi-binary sections of Tl_2X-B_2X_3 type of corresponding ternary systems. Materials based on these ternary compounds are promising for use as active elements in the various semiconductor devices of modern electronics. Representatives of these materials are single crystals of $TlGaS_2$, having a layered structure, which are characterized by strong anisotropy of physical properties. The report will present the results of the study of the physical properties of materials on the basis of crystals $TlGaS_2$.

Pure crystals. $TlGaS_2$ compound is a wide-gap layered *p*-type semiconductor with a melting point T_m = 1165 K, has a wide range of practically important physical characteristics, such as high photo- and X-ray sensitivity. In the process of semiconductor doping physical properties depend on what position the dopant takes. The substitution of cationic positions by metal atoms in ternary semiconductors is not fully understood.

Doped crystals based $TlGaS_2$. The following new results have been obtained. The layer single crystals on the base of $TlGaS_2$ were grown. This study presents the results of studying the frequency dependence of real (ε') and imaginary (ε") components of the complex dielectric permittivity, loss tangent (tan δ), ac-conductivity across the layers of obtained $TlGaS_2$<Ni> (1 mol. % Ni) samples at frequencies $f = 5\cdot10^4$–$3.5\cdot10^7$ Hz. The results demonstrate that the dielectric dispersion in the studied $TlGaS_2$<Ni> single crystals has a relaxation nature. The particular substitution of metal (Ga, Tl) atoms by Ni in $TlGaS_2$ single crystal leads to modification of ε'(*f*) and ε"(*f*) dispersion curves. At $f = 5\cdot10^4$–$3\cdot10^7$ Hz tanδ descends hyperbolically with an increase in frequency, which indicates conductivity losses in $TlGaS_2$<Ni>. The experimental dependence $\sigma_{ac} \sim f^{0.8}$ that we observed at $f = 2\cdot10^5$–10^7 Hz indicates that it is conditioned by hops of charge carriers between the states localized in the forbidden band of $TlGaS_2$<Ni>. We calculated the density of states at the Fermi level $N_F = 1.1\cdot10^{19}$ $eV^{-1}\cdot cm^{-3}$, the scattering of trap states near the Fermi level $\Delta E = 6.6\cdot10^{-2}$ eV, the average time of charge carrier hopping from one localized state to another τ = 0.2 μs, the average hopping distance *R* = 86 Å.

Solid solutions based on $TlGaS_2$. The liquidus in the *T*–*x* phase diagram of the system under consideration comprises two primary crystallization regions: those of the solid solutions based on the endmembers $TlGaS_2$ and $TlFeS_2$. Its solidus includes one eutectic horizontal, situated at 953 K. The melting point of the $TlGaS_2$ compound, which has a structure made up of layers of chains, is 1165 K, and that of $TlFeS_2$, which has a chain structure, is 900 K. The phase diagram has one eutectic, with a melting point of 953 K. The eutectic composition is 80 mol % $TlFeS_2$ + 20 mol % $TlGaS_2$. We calculated the boundaries of the solid solutions in the *T*–*x* phase diagram of the system $TlGaS_2$–$TlFeS_2$ by the thermodynamic method. We obtained single crystals of solid solutions and to study their physical properties. The unit cell parameters of $TlGaS_2$ crystals (monoclinic symmetry, sp. gr. *C*2/*c*) are *a* =10.772, *b* = 10.772, *c* = 15.638 Å, and β = 100.06°, and their density is ρ = 5.560 g/cm^3. The ternary compound $TlFeS_2$ is a magnetic semiconductor. $TlFeS_2$ crystals have a chain structure (monoclinic symmetry, sp. gr. $C2/m = C_2^3{}_h$) with the following unit cell parameters: *a* = 11.643, *b* = 5.306, *c* = 6.802 Å, β = 116.75°, *Z* = 16.

1. M.M. Asadov, S.N. Mustafaeva, A.N. Mamedov. "Dielectric Properties and Heat Capacity of $(TlInSe_2)_{1-x}(TlGaTe_2)_x$ Solid Solutions". Inorganic Materials, **51** (8), pp. 772-778, 2015.
2. M.M. Asadov, S.N. Mustafaeva, A.N. Mamedov. "Effect of Composition on the Properties of $(TlInSe_2)_{1-x}(TlGaTe_2)_x$ Solid Solutions". Inorganic Materials, **51** (12), pp. 1232-1236, 2015.

Effective optical constants of silver nanofilms calculated in wide frequency range

K. Tsysar[1], V. Andreev[1], V. Vdovin[2]
1. Moscow State University, Moscow, 119991 Russia, smelova_k_m@mail.ru
2. Kotel'nikov Institute of Radio Engineering and Electronics of RAS, Moscow, 125009 Russia.

In recent years the problem of the interaction of electromagnetic field with low-dimensional structures is of special interest. The most interesting part is the study of the interaction of electromagnetic field with thin metal films. In the recent study of Gong et al. the thickness dependent energy loss function was observed in ultrathin Ag nanofilms [1, 2]. The problem of influence of metal film thickness on the plasmon resonance is now extensively studied [1, 2]. The main attention in recent works is devoted to studies of visible range (300 nm – 1000 nm), but at the same time there is a lack of papers devoted to the long waves interaction with thin metal films. Present study is focused on dependence of conducting properties of Ag nanofilms on its thickness in wide frequency range: infrared and VHF range. All calculations were performed using the Vienna Ab-initio Simulation Package (VASP) code which is based on the density functional theory [3]. The most essential problem of experimental study of nanofilms is the problem of ultrathin film formation. With thickness of several nanometers the metal (Ag, Cu, Au) films have the islet or dendrite structure [2]. Type and shape of surface structure can significantly change the interaction of nanofilms with electromagnetic field in a whole range of wavelengths. In ultraviolet and visible range the island formation leads to the arising and enhancement of surface plasmon resonance (SPR) peaks and its displacement in long wave area. The VHF fields do not form new SPR peaks on surface islands due to strong decreasing of field frequencies. Thus for the radio waves dendrite and islet structure cannot drastically change conducting properties of the film but even so can lead to the strong changes of absorption and refractive properties of thin film as a whole. However, the SPR can be seen on perfectly flat surfaces in infrared range. Change in conductivity can be traced by changes of extinction coefficient (k) and refractive indexes (n) of the film. Annealing at high temperature (>200 °C) may lead to the surface alignment and vanishing of dendrite structure [2].

In present work the thickness dependence of k and n was studied for smooth Ag nanofilms without dendrite or islet structure as a perfectly formed annealed nanofilm.

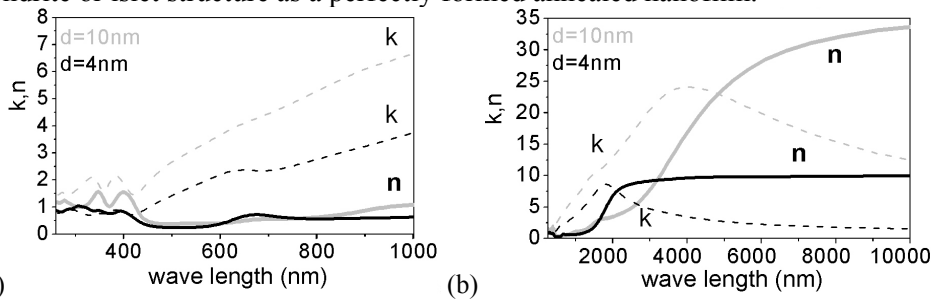

Fig. 1. The extinction coefficient (k) and refraction index (n) as function of wave length for visible range (300 nm – 1000 nm) (a) and infrared and VHF field (300 nm – 10000 nm) (b).

Fig. 1 illustrates the k and n for two different wave length ranges – visible (a) and infrared and radio waves (b) for two different film thickness – 4 and 10 nm. Our study revealed the strong difference of extinction coefficients (k) for ultrathin (4 nm) and thin (10 nm) Ag films in agreement with experimental work by J.Gong et al. [1]. In infrared and VHF range our calculation revealed the strong dependence of refractive index (n) on film thickness (Fig. 1b). Moreover, we found the displacement of surface plasmon resonant peak in long wave area with increasing of film thickness from 1000 nm - 3000nm for 4 nm smooth Ag films to 3000 nm – 7000 nm for 10 nm Ag film. Broadening of SPR with increasing of film thickness was detected.

Work is supported by RFBR grants 16-07-01246, 16-29-09581

1. J. Gong et al., Scientific Reports, **5**, p. 9279, 2015.
2. D. Kwon et al., Nature Nanotechnology, **5**, pp.148-153, 2010; I. Gladskikh et al., Journal of Optical Technology, **81** (5), pp. 280-284, 2014.
3. G. Kresse and J. Furthmuller, Phys. Rev. B, **54**, p. 11169, 1996.

The quantum-size Si dots in Si/SiO_2 multilayers formed by PECVD technique

A. Gismatulin[1,2], G. Kamaev[1], V. Volodin[1,2], I. Neizvestniy[1], S. Cherkova[1], A. Antonenko[2], S. Arzhannikova[1,2]

1. A.V. Rzhanov Institute of Semiconductor Physics SB RAS, Novosibirsk, Russia, E-mail address: kamaev@isp.nsc.ru

2. Novosibirsk State University, Novosibirsk, Russia

Attention to the nanoscale multilayer structures with quantum wells is risen due to appearance of quantum size effects even at room temperature (a negative differential resistance, charge effects, etc.). One of the applications of the Si/insulator structures is non-volatile resistive-based memory. Resistive switching in oxides can occur by different mechanisms: by conducting filament electrode of ions or due to the presence in the dielectric volume of various defects and impurities which alter electron transport. Introduction of Si nanoclusters in oxide should contribute to structuring the conducting channels and reduce the randomness of its formation.

In the present study, Si/SiO_2 multilayer nanoscale structures, which consist of alternating ultrathin layers of a-Si:H and SiO_2, were obtained on high doped n^{++}-type (resistivity of 0.002 Ω·cm) and p^{++}-type silicon substrates (resistivity of 0.003 Ω·cm) using inductively coupled plasma enhanced chemical vapor deposition technique. A silicon oxide layer of thickness ~30-35 Å was created by plasma enhanced oxidation of a silicon substrate. Then, the deposition of the amorphous silicon film with required thickness was carried out from monosilane-argon mixture. Afterwards α-Si:H film was oxidized up to required depth using plasma processes. As it was shown, ultra-thin α-Si: H film disintegrated into clusters during an oxidation process [1]. The cycles of deposition and plasma enhanced oxidation of α-Si:H were repeated as many times as it was needed to create multilayer structure. Subsequently, the structures were annealed at high-temperature in argon ambient.

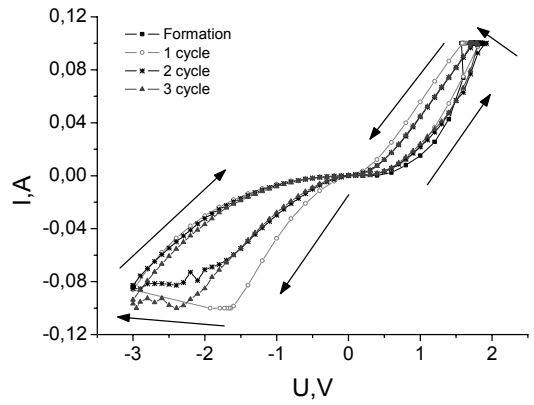

Fig. 1. *IV*–characteristics of Si/SiO_2 multilayer nanoscale structure on high doped n^{++}-type substrates

Measurements of capacity-voltage (CV) characteristics were carried out in a wide range of frequencies for the metal-insulator-silicon structures with embedded Si nanoclusters into the tunnel-thin insulator. There are some features on CV characteristics. One of these features is sharp increases of capacity while reducing the frequency of the measurement signal in the bias voltage corresponding to accumulation. This capacity surge is associated with the charge exchange between the substrate and surface-states in the dielectric. The magnitude of observed phenomena increases with increasing number of alternating layers of a-Si and SiO_2.

Measurements of static current-voltage (*IV*) characteristics in the studied structures show (see Fig. 1) the effect of the resistive switching in bipolar mode (besides the expected tunnel and charge-exchange effects). The switching process stabilizes after high-temperature annealing. The ratio of on/off resistance after annealing is no less than 2 orders of magnitude. The introduction of Si nanoclusters into the dielectric reduces the randomness of formation of a conducting channel. Intermediate metastable states are observed in *IV*–characteristics. This may prove to be important for multibit data storage.

1. A.A. Orlikovsky, I.G. Neizvestniy, V.A. Volodin, A.A. Gismatulin, G.N. Kamaev, A.H. Antonenko, A.G. Cherkov, V.G. Litovchenko, I.P. Lisovsky, I.Yu. Maidanchuk, "Formation of Si nanocrystals in SiO_x, SiO_x:C:H films and Si/SiO_2 multilayer nano-heterostructures by pulse laser treatments". Proc. SPIE, **9440**, 94400F, 2014.

Hydrogenated amorphous silicon based *p-i-n* structures with Si and Ge nanocrystals in *i*-layers

V.A. Volodin[1,2], G.K. Krivyakin[1], A.A. Shklyaev[1,2], S.A. Kochubei[1], G.N. Kamaev[1], A.V. Dvurechendkii[1,2], A. Purkrt[3], Z. Remes[3], R. Fajgar[4], T.H. Stuchliková[3], J. Stuchlik[3]

1. A.V. Rzhanov Institute of Semiconductor Physics, Russian Academy of Sciences, Lavrent'eva ave., 13, 630090, Novosibirsk, Russia, E-mail address: volodin@isp.nsc.ru;

2. Novosibirsk State University, Pirogova street, 2, 630090, Novosibirsk, Russia;

3. Institute of Physics ASCR, v. v. i., Cukrovarnická 10/112, 162 00 Praha 6, Czech Republic;

4. Institute of Chemical Process Fundamentals of the ASCR, v. v. i., Rozvojová 135, 165 02 Praha 6, Czech Republic.

The development of efficient and high-stability solar cells and light-emitting diodes based on the inexpensive and commonly used silicon thin-film technology remains a challenging problem. Semiconductor *p–i–n* structures are used for both types of optoelectronic devices. Plasma-enhanced chemical vapor deposition (PECVD) is the lowest-cost and most widespread method for manufacturing of thin films and structures. In the last few years, the efforts of researchers have been aimed to increase the efficiency of these devices by embedding various nanocrystalline inclusions into the undoped intrinsic layer (*i*-layers) of such structures [1–3]. Si and Ge nanocrystals (NCs) embedded in *i*-layers of *p-i-n* structures have perspectives for applications in such optoelectronic devices. The a-Si:H films were grown using the PECVD method from a monosilane (SiH_4) and hydrogen mixture at a temperature of 220 °C on non-refractory glass substrates. The film thickness was controlled by the deposition time and was checked using the data of ellipsometry and electron microscopy. Both undoped films and *n*- and *p*-type films were deposited. The as-deposited films contained 10-35 atomic % of hydrogen, depending on conditions of deposition.

Two types of structures were formed and studied. First type contains Si NCs, which were formed in the *i*-layers of *p–i–n* structures using pulsed laser annealing. An excimer XeCl laser with a wavelength of 308 nm and a pulse duration of 15 ns was used. The laser fluence was varied from 100 (below the melting threshold) to 250 mJ/cm^2 (above the threshold). The average sizes of NCs were estimated by analyzing of Raman spectra. The sizes were changed from 2.5 to 5 nm, depending on the laser-annealing parameters. Current–voltage measurements show that the fabricated *p–i–n* structures possess diode characteristics. An electroluminescence signal in the infrared range is detected for the *p–i–n* structures with Si NCs; the peak position (0.9–1 eV) varies with the laser-annealing parameters. Radiative transitions are presumably related to defects or states on nanocrystal/amorphous-matrix interface.

The second type of structures contains Ge and GeSi NCs embedded in *i*-layers. Amorphous or nanocrystaline Ge layers were grown on *i*-layer of semi-ready *p-i* structure using low-temperature (300-450 ^{o}C) molecular beam epitaxy. The analysis of phase and elemental composition of deposited GeSi heterostructures was also carried out using Raman spectroscopy [4]. Optical properties of GeSi heterostructures was studied using photoluminescence spectroscopy. Both as-deposited and laser treated structures were studied. It is shown that applying pulsed laser annealing allows varying the elemental composition and size of the Ge NCs formed from solid alloys of germanium and silicon. Structural properties of the films were studied using atomic force microscopy, scanning tunneling microscopy and electron microscopy. Then, the *p-i-n* structures were formed (*i*-layer, *n*-layer and contacts were deposited) and the samples were studied using current–voltage measurements and electroluminescence spectroscopy.

The proposed approaches can be used to produce light-emitting diodes or solar cells on non-refractory substrates.

1. N.G. Galkin, K.N. Galkin, I.M. Chernev, R. Fajgar, T.H. Stuchlikova, Z. Remes, and J. Stuchlik. Phys. Status Solidi C, **10**, p. 1712, 2013.

2. N.G. Galkin, K.N. Galkin, I.M. Chernev, R. Fajgar, T.H. Stuchlikova, J. Stuchlik, and Z. Remes. JJAP Conf. Proc., **3**, 011104, 2015.

3. G.K. Krivyakin, V.A. Volodin, S.A. Kochubei, G.N. Kamaev, A. Purkrt, Z. Remes, R. Fajgar, T.H. Stuchliková, and J. Stuchlik. Semiconductors, **50**, p. 935, 2016.

4. A.V. Dvurechenskii, V.A. Volodin, G.K. Krivyakin, A.A. Shklyaev, S.A. Kochubei, I.G. Neizvestnyi, and J. Stuchlik, (2016, in press).

Electronic properties modification of silicon heterostructures by microwave plasma

R. Yafarov[1], V. Timoshenkov[2], S. Timoshenkov[2], S. Orlov[3]
1. Saratov Branch of the Kotel'nikov Institute of Radio Engineering and Electronics of RAS, Saratov, Russia
2. National Research University of Electronic Technology, MIET, Zelenograd, Moscow, Russia, valeri04@hotmail.com;spt@miee.ru;
3. Molecular Electronics Research Institute JSC, Zelenograd, Moscow, Russia, sorlov@mikron.ru

Actual problems of modern semiconductor materials are obtaining atomic-clean surfaces, creating quantum-well layers and heterojunctions with given composition and structural perfection. This is due to the high sensitivity of the electronic properties of materials to defects and inhomogeneities in the structure. In this study we investigated the effect of low-energetic plasma-treating of the crystal surface in various gases on the electronic properties of heterostructures "tunnel-thin films on silicon". Electronic properties near the surface of the semiconductor crystal are very different from the electronic properties in crystal volume. Experiments were carried out in the vacuum system using a microwave plasma ion source. The power of the microwave radiation and the magnetic field corresponding to the appearance of electron cyclotron resonance (ECR) were respectively 250 W and 875 Gs. The pressure of the working gas was 0.1 Pa. The plasma ionization degree was about 5% which corresponds to ECR conditions.

Monocrystal p-type silicon wafers with crystallographic orientation of (100) were used in the experiments. Silicon surface has been modified under the influence of low-energy microwave plasma processing in various gas atmospheres. Freon-14, hydrogen and argon were used as working gases. The values of the substrate accelerating voltage at the plasma etching processes of the silicon were constant (-100V). The processing of silicon wafers with natural oxide were performed in next modes: ion-plasma etching in the case of using of argon, reactive-ion etching (RIE) in the cases of using Freon-14 or hydrogen. As a result of plasma-chemical in the Freon-14 environment processing the chemisorbed SiC and SiF complexes are formed on silicon surface. These complexes passivate the dangling (unsaturated) chemical bonds of the silicon surface atoms and decrease their surface density. Hydrogenated amorphous silicon carbide (a-SiC: H) layer with 10 nm thickness was deposited in vapor mixture of ethanol and silane in microwave plasma at the same vacuum process cycle after plasma cleaning of the silicon wafers. Then, the metal contacts were formed on the surface of the heterostructure by vacuum thermal deposition.

Field emission properties of the emitter on base heterostructures using a-SiC: H (10 nm)/Si were investigated. The presence of the surface potential can significantly reduce the threshold of electron emission from the surface of the heterostructure and increase the maximum field-emission currents. The surface of the carbon emission centers contains adsorbed atoms that can exchange electrons with the amount of the cathode structure of the matrix. The adsorbed atoms can donate electrons, turning into positive ions, or to take over the additional electrons are negatively charged, depending on what is energetically favorable. Thus, the electronic exchange between the adsorbed atoms and the amount contributes the occurrence of electric potential in the surface layer of the structure. Surface potential can significantly change the electrical conductivity in the surface layer of the semiconductor, as well as to weaken or strengthen the external electric field in the electron field emission. In addition, the presence of surface states has a great influence on the surface recombination velocity. The surface recombination of carriers can lead to their destruction, and reduce the size and stability of the field emission currents. Therefore, reliable stabilization of the surface and its protection from external influences of the atmosphere is one of the important tasks of emission electronics.

We may conclude that influence of low- energetic plasma processing of the crystal surface in various gases on the electronic properties of heterostructures of «tunnel-thin film on silicon» was studied. The plasma processing of silicon crystal of p-type may to lead to the surface formation of positively charged silicon ions. The revealed features of carrier transport in semiconductor crystal structures with built-in electrostatic potential show the fundamental possibility of the formation various electronic devices. Heterostructure with built-in potential and the cutoff voltage from 1 to 5 and above can be used as a voltage limiter.

Some important aspects in the glass structure of chalcogenide system

V. Minaev, S. Timoshenkov, V. Kalugin, N. Korobova
National Research University of Electronic Technology, MIET, Zelenograd, Moscow, Russia, korobova3@mail.ru

Chalcogenide glasses are used in various fields of technology where their different properties are employed. As the range of clearly defined properties of these materials becomes wider, it leads to a greater potential for their use in specific technical applications in devices, circuits, and systems. In seeking glasses with desired properties, it is extremely important to forecast new glass-forming compositions. In our opinion, there are two ways to solve the glass-formation prognosis problem in the absence of a unified concept of glass-formation that connects its structural-chemical, kinetic, and thermodynamic aspects [1].

The most important feature of glass-formation is the polymerization of structural fragments of which the glass is built. The necessary and sufficient condition of glass-formation are follows: (1) presence of localized paired electrons bonds in the structure; (2) construction of the main polymeric network from endless polymeric complexes; (3) connection of structural complexes only through a single bridge bond, i.e. the presence of bonds in the structure that can be called swivel bonds.

Structural-chemical and energetic factors of glass-formation, together with the relaxation conditions of glass-forming ability (GFA) with increase in atomic numbers of elements have been considered as a starting point for the development of the structural-energetic concept of glass formation. Glass-forming phase diagrams of binary systems are usually diagrams with low temperature eutectics in the range adjoining chalcogen. Such systems are Al-Te, Ge-Se, Si-Te, As-S, P-Se, Cs-Te, and others. Glasses in ternary systems are formed, as a rule, when among the participating binary systems there is one, two, or all three systems that are characterized by glass- formation phase diagrams. This simple rule, without any additional data allows predicting of a possibility of glass-formation in any ternary system if the phase diagrams of the binary systems constituent in the ternary system are known. When phase diagrams can be obtained, it is easy to find out points where the process of glass-formation is more or less probable. As the criterion of the actual (concrete experimental) glass formation, the average value of the GFA of boundary compositions (glass-crystal) of glass formation regions of the same type of glasses obtained at a certain cooling rate was taken. In telluride compositions glasses were formed in the case of cooling rate $V_c \sim 10^2$ K·s^{-1} at GFA $\geq 0.270 \pm 0.010$ kJ mol^{-1}·K^{-1}; in the case of cooling rate $V_c \sim 10^6$ K·s^{-1} at GFA $\geq 0.250 \pm 0.010$ kJ·mol^{-1} K^{-1}. Criterion of the concrete experimental glass formation cannot be formulated without taking into account the kinetic factor expressed in this case through cooling rates of melts.

Glass formation is realized due to co-polymerization of fragments of different structure – nanoheteromorphous fragments without an LRO which are not able to form a crystalline substance because of their heteromorphous character. In the paper analyzed glass systems show a genetic relationship between the polymeric polymorphoid glass structure concepts that was applicable to ICSs. More general concept of polymeric nanoheteromorphous glass structure was applicable to multicomponent systems as well. The main thesis of the new concept can already be started as nanoheteromorphism and nanoheteromorphous co-polymerization are necessary and sufficient conditions of glass formation in any substance[1]. This concept was successfully implemented for the analyses of structure, properties, and relaxation processes in some one-component oxide and halogenide substances as well as in halcogenides $GeSe_2$, GeS_2, SiS_2, $SiSe_2$, $As_{50}Se_{50}$, and Se. Nanoheteromorphism is also typical for multi-component glass-forming systems, binary in particular – simultaneous presence of different structural fragments of the nanometric scale without LRO in a vitreous polymer [1].

Authors hope that the proposed polymeric nanoheteromorphous glass structure concept will stimulate the further development of thermodynamic and kinetic approaches to glass formation, and to promote future unification of these approaches with structural – chemical approach in a joint general theory of glass formation.

1. V.S. Minaev, *Semiconductors and Semimetals*, Vol. 78, Chapter 4. ELSEVIER Inc., San Diego, 2004.

Properties of Ge-Sb-Te thin films for high read/write performance and reliability

A. Sherchenkov, P. Lazarenko, A. Babich, S. Timoshenkov, N. Korobova, D. Terekhov, A. Yakubov

National Research University of Electronic Technology, MIET, Zelenograd, Moscow, Russia, korobova3@mail.ru

The use of electrically writable and erasable phase change materials, i.e., materials that can be electrically switched between generally amorphous and generally crystalline states or between different resistive states while in crystalline form, for electronic memory applications is well known in the art. Today the use of phase change materials is disclosed, but many International conferences indicate generally the state of the art, and to contain a discussion of the current theory of operation of chalcogenide materials.

Chalcogenide glassy semiconductor of Ge-Sb-Te (GST) system, in particular $Ge_2Sb_2Te_5$ (GST225), is most widely used as a programmable material for PCM. However PCM technology must be improved for the successful commercialization and effective methods for controlling electrical properties of PCM materials are needed. But a lot of questions related to the mechanism of charge carrier transport are still open and need to be investigated. Thus, the aim of this work is the investigation of electrical, thermoelectric properties and transport mechanism for the amorphous thin films of GST system.

The alloys GST225, GST124, and GST147 were synthesized with using of quenching technique. Thin films were prepared by thermal evaporation of the synthesized materials in vacuum. Substrate temperature during the deposition did not exceed 50 °C.

Dependencies of Seebeck coefficient and resistances of the films GST147, GST124, and GST225 on annealing temperature were obtained. Samples were annealed in the temperature range from room temperature to 325 °C during 30 min in air. In the first range from room temperature up to 100 °C material exist in the amorphous state and Seebeck coefficient is highly negative in the range from -600 to -1000 μV/°C. Crystallization in the temperature range 100-150 °C is accompanied by the sharp change of the Seebeck coefficients, which are nearly independent on the following increase of the annealing temperature. However, the Seebeck coefficient remains negative indicating on the dominating p-type conductivity. The negative sign of thermoelectric power and the resulting value of the Seebeck coefficient for the amorphous thin films are consistent with the data of [2]. With moving along the quasi-binary line GeTe-Sb_2Te_3 in the direction from GST147 to GST225 the value of Seebeck coefficient changes, however type of the conductivity remains the same**.**

With using of the Mott-Davis model, and taking into account experimental results, the energy band diagrams for amorphous GST thin films were proposed. The current-voltage characteristics in the middle electric field intensity range has power dependences for all investigated compounds, which indicates on the dominating of the space charge limited current. The densities of states and positions of energy levels restricting the current transport were estimated. Thus, electrical and thermoelectric properties, and transport mechanisms in thin films of chalcogenide semiconductors on the quasi-binary line GeTe-Sb_2Te_3 ($Ge_2Sb_2Te_5$, $GeSb_2Te_4$ and $GeSb4Te_7$) for phase change memory application were investigated. Influence of the composition variation along the quasi-binary line GeTe-Sb_2Te_3 on electrical, thermoelectric properties and transport mechanism were studied. Three regions with different current-voltage dependencies were established. Composition dependence of the energy diagrams was analyzed. Position of the trap levels controlling transport mechanisms, and density of traps were estimated. Obtained results showed that electrical and thermoelectric properties of thin films can be sufficiently varied with moving along the quasi-binary line, which is important for the optimization of PCM technology.

1. A. Sherchenkov, P. Lazarenko, A. Babich, N. Korobova, S. Timoshenkov, A. Yakubov, D. Terekhov, A. Shuliatyev, S. Kozyukhin, O. Boytsova, "Electrical Properties and TransportMechanisms in Ge-Sb-Te Thin Films for Nanoelectronics" in Proc. IEEE 15th International Conference on Nanotechnology, Roma, 2015, pp.885-888.

2. J. Lee, T. Kodama, Y. Won, M. Asheghi, K.E. Goodson, "Phase and Temperature Dependent Thermoelectric Properties of $Ge_2Sb_2Te_5$ Films down to 25 nm Thickness", J. Appl. Phys., 2012, **112**, 014902, pp. 1-6.

Analysis of changes in the composition of lithium niobate crystals under long-term impact of high vacuum

E. Pantelei, V. Paranin
Samara National Research University, Samara, Russia, mekachiku-san@mail.ru

Lithium niobate is an electrooptical ferrolectric with the $LiNbO_3$ chemical formula widely used as substrates of integral optical circuitry, in devices of up-to-date optical and acoustical electronics. Devices on the basis of LN crystals are used in aircraft and space systems and, as a consequence, are exposed to temperature and pressure gradients. The popularity of LN is accounted for by the unique combination of its properties which may vary depending on the composition and crystalline structure. The impact of the above parameters leads to degradation of the crystalline structure and variation of the crystal composition, which has a negative effect on the operation of target devices.

The aim of the study is the investigation of changes in the composition of lithium niobate crystals under long-term exposure to vacuum of the order of 10^{-5} Pa using various direct and indirect methods.

To assess the changes in the composition of the crystals the following methods were used: X-ray fluorescence analysis, energy-dispersive analysis and the method of optical spectroscopy in the visible and infrared ranges.

The X-ray fluorescence method was applied with the help of the X-MET 5100 analyzer that registered elements starting with 12 (Mg-magnesium) to 92 (U-uranium) of the periodic table with sensitivity up to 0.1 per cent. The method made it possible to recognize the presence of niobium Nb, zirconium Zr and molybdenum Mo in the same proportions both for the crystals exposed to vacuum and reference specimens. The method has limitations and cannot recognize many elements including oxygen O and lithium Li, which make up a considerable part of the crystal composition.

Energy-dispersive analysis is one of such methods. The investigation was carried out with the use of a Hitachi TM3030Plus scanning electronic microscope with an add-on device for energy-dispersive microanalysis Thermo ScientificCompact EDS NSS. The elements being defined are in the interval from 5 (B-boron) to 92. Measurements of the composition did not reveal any significant differences in the content of niobium Nb and oxygen O for all specimens. The method can be regarded as being more reliable compared to the X-ray fluorescence analysis since such elements as zirconium Zr and molybdenum Mo, mistakenly revealed in the previous method were not discovered by energy-dispersive analysis.

The method of optical spectroscopy in the visible and infrared ranges was implemented using ShimadzuUV-2450 and Shimadzu IRPrestige 21 spectrometers. Detection of organic impurities, including hydrogen, as well as information on some optical properties of a specimen are distinguishing features of the method. The measurements were of qualitative nature. The absorption band in the transmission spectra of reference specimens contained 3% more hydrogen H than the crystals exposed to vacuum.

Summarizing the results of investigation it can be inferred that vacuum did not affect the content of niobium Nb atoms with a greater atomic radius or the oxygen O atoms bound with lithium Li and niobium Nb. This gives grounds to assume that the structure of the crystal remained unchanged. Impurity atoms, such as hydrogen H and others responsible for the photorefraction properties and laser radiation tolerance were affected.

Promising design of hyperbolic metamaterial for optical spectral range

I. Gasenkova[1], N. Mukhurov[1], V. Lukichev[2], K. Rudenko[2], A. Miakonkikh[2], I. Ryzhikov[3], I. Bykov[3]
1. State Research and Production Association "Optic, Optoelectronic and Laser technique",
E-mail: n.mukhurov@ifanbel.bas-net.by.
2. Institute of Physics and Technology, 34 Nakhimovsky Ave., Moscow, Russia
3. Institute for Theoretical and Applied Electromagnetics of RAS, 13/19Izhorskaya str., Moscow, Russia

Materials with special properties designed to work in the optical range of wavelengths are intensively investigated [1, 2]. Such metamaterials (MM) has artificial structure that modifies the optical characteristics in certain wavelength range. Among the known MM's designs it can be distinguished two ones for using in the optical band: the MM-structure consisting of an alternation of layered metal-dielectric nanostructures and the MM-structure based on ordered unidirectional nanowires. Each of these designs is intended for a narrow wavelength band.

Inner structure of proposed hyperbolic metamaterial [3] for optical applications comprises a dielectric substrate (thickness greater than 30 μm) with periodic system of nanosized holes from 30 to 50 nm diameter over the entire surface filled by noble metals forming metallic nanowires height of 3 to 10 diameters nanoholes inside. This surface is facing to the source of electromagnetic radiation. The anodic aluminum oxide (AAO) with regular nanopores is intended to be used as substrate material. However, quite high surface roughness of such substrate causes unacceptable scattering and absorption of electromagnetic radiation in a wide wavelength range. This effect will result in decreased efficiency for MM over operating range of wavelengths and angles of incidence of the electromagnetic radiation.

We have implemented the option to reduce the roughness of the surface of the dielectric substrate and the surface inside nanoholes. It includes the technique of atomic layer deposition (ALD) on the substrate surface and in the nanoholes the thin layer of Al_2O_3, which is close in properties to AAO. The samples were made from dielectric substrate of alumina ceramics with thickness of 40 μm and periodic system of nanoholes with diameter in the range of 70 to 150 nm. Both surface and inside part of nanoholes were covered by dense layer of 20 and 50 nm ALD-Al_2O_3 with same chemical composition as the substrate AAO. Dense and conformal non-porous layer of Al_2O_3 on AAO samples resulted in flattening the surface and significant dropping of roughness. Because of surface coverage with same material the good fitting of the coefficients of thermal expansion, adhesive properties, and insignificant mechanical stresses of such structures were observed. That implies nanostructured composite AAO+ALD-film is applicable when exposed to elevated temperatures, thermo-mechanical loads and other extreme environmental conditions.

The ellipsometric measurements were made with the ellipsometer САГ-1891 model. The optical constants for prepared material are effective parameters. Both surfaces of the AAO-structures have significantly lower refractive index than the bulk amorphous sapphire. This is understandable, since the material is substantially nano-porous. The results of the measurements of refraction and absorption coefficients at two angles of incidence at 45° and 60° and under three rotations around the normal have confirmed the significant reduction in roughness of the proposed design of ALD-AAO combination. It opens wide prospects for development of a hyperbolic metamaterial.

1. W. Cai and V. Shalaev. Optical Metamaterials: Springer, 2010.
2. C.R. Simovski, P.A. Belov, A.V. Atrashchenko, Yu.S. Kivshar. Wire Metamaterials: Physics and Applications // Adv. Mater. 2012. P.1-20.
3. N. Mukhurov, M.A. Binhussain, I. Gasenkova, N. Kazak, V. Belyi. The construction of hyperbolic metamaterial for an optical spectral range // 9th International Congress on Advanced Electromagnetic Materials in Microwaves and Optics Metamaterials 2015 / Oxford, United Kingdom, 7-12 September 2015. P.523-525.

Retardance of alumina nanoporous thin films in visible and near infrared spectral region

V. Dlugunovich[1], A. Zhumar[1], N. Mukhurov[2], I. Gasenkova[2], M. Binhussain[3]
1. B.I. Stepanov Institute of Physics of National Academy of Sciences of Belarus
68 Nezavisimosti ave., 220072 Minsk, Belarus
2. State Research and Production Association "Optic, Optoelectronic and Laser technique",
E-mail: n.mukhurov@ifanbel.bas-net.by.
3. The National Center of Building Systems, KACST, Riyadh 11442, Saudi Arabia

The phenomenon of form birefringence caused by phase anisotropy arising as light passes through a certain ordered system of particles in the optically isotropic material when the size of particle is larger than the size of the molecules but smaller of the light wavelength has well-known [1, 2]. Rapid development of technologies of making various nanocomposite materials with desired ordered structures [3, 4] allows researchers to fully investigate this phenomenon. The creating inconvertible to changing environmental conditions achromatic phase plates with variable retardance to control the polarization characteristics of the radiation is actual. The main aim of this research was to study the form birefringence phenomenon due to pore anisotropy of nanocomposite nanoporous alumina films (NAF) by Stokes polarimetry method and to create on their basis the achromatic phase plates with variable retardance of 0 to λ/2. The absolute uncertainties of Stokes parameters, as well as the retardance (Δ) do not exceed 0,015 and 3° correspondingly. The Stokes parameters measurements of the radiation passing through NAF were carried out the lasers at the wavelength 400, 633, and 808 nm, correspondingly, at the azimuth of the incident linearly polarized radiation 45°. The angle between the optical axis of the Stokes polarimeter and the normal to the film surface (α) varied in the range from 0 to 75°. NAF had a pore size 40−50 nm, axle base of pores was 80−100 nm. The film thickness was varying 10−30 μm. It was taken into account the effect of the film amplitude anisotropy to evaluate the retardance. In the visible region, the variation of retardance from 0 to λ/2 as a function of the incidence angle is observed for thickness of 30 microns. It was found that the shorter wavelength of the incident radiation, the smaller angles of incidence is necessary to receive the retardance close to λ/4 or λ/2. So for the wavelength 400 nm, Δ = λ/4 corresponds to the angle of incidence 34°, for 633 nm − 49°, and for 808 nm − 53° respectively. The angle, in which there were the retardance variations from λ/4 up to λ/2, was invariant value in visible region and equal 23±1°. It was not possible to receive the retardance equal to λ/2, at near-infrared wavelengths.

1. M. Born, E. Wolf. *Principles of Optics*. Oxford, London, Pergamon Press (1970).
2. L.A. Golovan, V.Yu. Timoshenko, P.K. Kashkarov. Physics-Uspekhi (Advances in Physical Sciences) **50**, pp. 595–612 (2007).
3. T. Kikuchi, O. Nishinaga, Sh. Natsui, R.O. Suzuki. Electonica Acta **156**, pp. 235–243 (2015).
4. L. Micheli, N. Sarmah, H. Luo, K.S. Reddy, T. Mallick. Renewable and Sustainable Energy Reviews **20**, pp. 595–610 (2013).

Features of $CuInS_2$ formation process by SILAR method

A. Borisova, M. Kuzmicheva, A. Dronov, D. Dronova, A. Zheleznyakova, S. Gavrilov
National Research University of Electronic Technology, Bld. 1, Shokin Square, Zelenograd, Moscow, Russia, 124498, stushka@bk.ru

Copper-indium sulfide (CIS) is the $A^IB^{III}C^{VI}_2$ type semiconductor which is the closest analogue to $A^{II}B^{VI}$ type semiconducting materials by electronic and crystallographic structure. The compound has good photoelectrochemical stability, narrow band gap 1.3÷1.6 eV and does not contain toxic elements [1]. Ability of $CuInS_2$ layers to absorb solar radiation efficiently allows creating solar cells with an efficiency of up to 11-13%. $CuInS_2$ can be either p-type or n-type semiconductor. N-type can be obtained after heat treatment with indium in excess, and p-type - with an excess of sulfur and copper. Solar cells based on $CuInS_2$ have a high absorption coefficient - 10^5-10^6 cm^{-1}. Also, they are not sensitive to radiation damage or impurities. According to that effective radiation detectors and photodetectors based on copper-indium sulfide can be created [2]. As the components of this compound are quite common on the planet, manufacturing of photovoltaic energy converters based on $CuInS_2$ should be rather cheap.

Up to date, the most common methods for obtaining $CuInS_2$ layers are conventional vacuum methods such as sputtering, vacuum evaporation, atomic layer deposition, and molecular beam epitaxy. One of the perspectives, low-temperature methods of copper-indium sulfide formation is SILAR [3]. This method is based on sequential chemical reactions of cations and anions from precursor solutions at the substrate - solution boundary where insoluble compound precipitate forms. The method is simple and accessible. The main advantage of SILAR method is to control the growth rate by changing various parameters such as concentrations, pH, temperature and number of process cycles. As the substrates a wide range of materials can be used, including glasses, plastics, nanostructured materials and other heat sensitive substrates, since the deposition occurs at ambient or near ambient temperature and at atmospheric pressure. However, it is necessary to optimize the deposition process parameters to obtain layers with good quality in particular precursor solutions concentration, pH of the precursors, concentration and type of complexing agents, absorption, reaction and duration. In this paper, features of CIS microparticles formation by SILAR method have been investigated for use as an absorbent material in solar cells with extremely thin absorber (ETA-cell) [4].

During the formation 0.01 M indium chloride and 0.01 M copper sulfate solutions were used in a different ratio. To study the structure and properties of deposited copper - indium sulfide silicon wafers with a titanium adhesion layer were used as substrates. SEM and AFM techniques were used to study the morphology of obtained CIS microparticles. Investigations of elemental composition of the microparticles were provided by Auger spectroscopy. Also, the effect of heat post treatment on composition and roughness of the obtained samples was studied.

During the research ETA-cells with $Ti/TiO_2/In_2S_3/CuInS_2/CuSCN/ITO$ structure were formed where $CuInS_2$ microparticles were deposited by SILAR method and their basic photoelectric characteristics were measured.

This work was supported by the Russian Science Foundation (project № 16-19-10625).

1. A.S. Wochnik, C. Heinzl, F. Auras, T. Bein, C. Scheu “Synthesis and characterization of $CuInS_2$ thin film” Journal of Materials Science, **47** (4), pp. 1669–1676, 2012.
2. S.V. Bulyarsky, L.N. Vostretsova, and S.A. Gavrilov, “Photodetectors based on $CuInS_2$,” Semiconductors, **50** (1), pp. 106–111, 2016.
3. S. Gavrilov, A. Zheleznyakova, A. Dronov, A. Presnukhina, and E. Popova, “Different methods of forming multicomponent metal sulfide by SILAR-techniques,” International Conference on Micro- and Nano-Electronics 2014, Dec. 2014.
4. S.A. Gavrilov, A.A. Dronov, V.I. Shevyakov, A.N. Belov, and E.A. Poltoratskii, “Ways to increase the efficiency of solar cells with extremely thin absorption layers,” Nanotechnol. Russia, **4** (3–4), pp. 237–243, 2009.

Investigation of germanium nanowires arrays formation process by electrochemical deposition

I.M. Gavrilin, V.A. Smolyaninov, A.I. Savitsky, A.A. Dronov, S.A. Gavrilov
National Research University of Electronic Technology, Moscow, Russia, gavrilin.ilya@gmail.com

In the present time germanium nanowires shows great interest among science community. Due to the excellent electrophysical properties such structures can be used in energy storage and generation applications and optoelectronics [1]. However, the high cost and technological complexity of nanostructured Ge manufacturing process limits its production [2].

Recently in [3] a new method of preparing crystalline filamentary Ge nanostructures has been proposed. Described method based on electrochemical deposition of Ge from aqueous solutions at room temperature, where as an electrode catalyst metals having low melting points such as Hg and Ga are used. However, usage of these metals is technologically complicated. Moreover, controlling the dimensions of the formed structures is also difficult.

In this paper, we demonstrate a simple method of Ge filamentary nanostructures formation by electrochemical deposition using indium nanoparticles as a catalyst material. Indium nanoparticle arrays are formed by vacuum thermal evaporation and condensation of material small batches using molybdenum vaporizer. This method allows controlling the density and size of In nanoparticles, which in turn makes possible to control the dimensions of the Ge nanowires.

The work presents results of influence of particle size indium catalyst on the morphology and phase composition of the obtained germanium structures. The morphology of the samples was investigated using SEM, phase and elemental analysis were made by Auger spectroscopy and XRD.

This work was supported by the Russian Science Foundation (project № 16-19-10625).

1. N. Dasgupta, J. Sun, C. Liu, S. Brittman, S.C. Andrews, J. Lim, H. Gao, R. Yan, P. Yang. “25th Anniversary Article: Semiconductor Nanowires – Synthesis, Characterization and Applications”. Adv. Mater., **26**, pp. 2137–2184, 2014.
2. Kolasinski K.W. “Catalytic growth of nanowires: Vapor−liquid−solid, vapor−solid−solid, solution−liquid−solid and solid−liquid− solid growth”. Curr. Opin. Solid State Mater. Sci., **10**, pp.182−191, 2006.
3. A. Carim, S. Collins, J. Foley, S. Maldonado. “Benchtop Electrochemical Liquid-Liquid-Solid Growth of Nanostructured Crystalline Germanium”. J. Am. Chem. Soc., **133**, pp.13292–13295, 2011.

writing of micro- and nanostructures for optics with using new e-beam lithography principle

E. Zhikharev[1], M. Bruk[2*], A. Rogozhin[1]
[1]*Institute of Physics and Technology of RAS, Moscow 117218, Russia*
[2]*L.Ya. Karpov Institute of Physical Chemistry, Moscow 105064, Russia*
**Corresponding author: bruk@cc.nifhi.ac.ru*

Lithographic techniques, including electron-beam lithography (EL) is often used in the formation of micro- and nanostructures for optical applications. The traditional "wet" EL technology is usually used in this techniques, having a number of important advantages, among which the main one is high lateral resolution. However, when this technology is applied to the optics elements creation, there are significant drawbacks. These include: 1) the need for large doses of exposure, causes a relatively poor performance of the lithographic process and its high cost; 2) the difficulty of obtaining relief structures with a well-rounded profile of a given shape; 3) the relatively low accuracy in the vertical direction (Z-axis) of the 3D-structure. The authors of the presentation earlier [1] proposed a new "dry" method of EL (DEBER method), largely devoid of the above disadvantages. The method is based on the chemical chain depolymerization reactions in the polymer during the electron beam irradiation in a vacuum at temperatures above the glass transition temperature of the resist, these reactions are accomplished by release of volatile products (monomer) which are removed from the resist. In this process an additional free volume in the exposed resist area arises which leads to a relaxation (shrinkage) of the polymer, and to the direct formation of images on the positive type (there is a "selfdeveloped" image).
The presentation shows that DEBER method allows you to: 1) hundreds of times increase sensitivity of PMMA resist in the electron-lithographic process compared to "wet" EL technology, which offers the prospect of creating a more productive and low-cost technology; 2) obtain high quality well rounded profile relief with a predetermined shape (aspherical, sinusoidal, etc.) in one-step process 3) form spatial 3D-structure with very high vertical resolution (about 1 nm) and low surface roughness. On the other hand the main disadvantage of the DEBER method include low lateral resolution (about 100 nm) and the difficulty of obtaining structures with a strictly rectangular cross section profile. The presentation provides examples of the microstructures formation by method DEBER in the PMMA resist and in poly-α-methylstyrene with various well-rounded cross-section profiles such as 3D-ladder structures (Fig. 1) and binary lattices (Fig. 2). Also examples of resist relief transfer into silicon and tungsten layer presented.
The data obtained shows that DEBER method can be used to generate a wide range of components and devices including optics and optoelectronics elements.

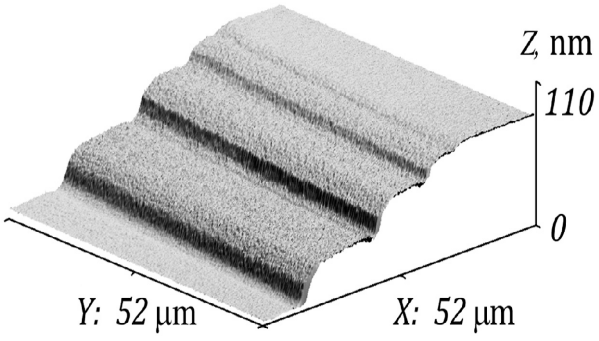

Fig. 1. 3D-ladder structure.

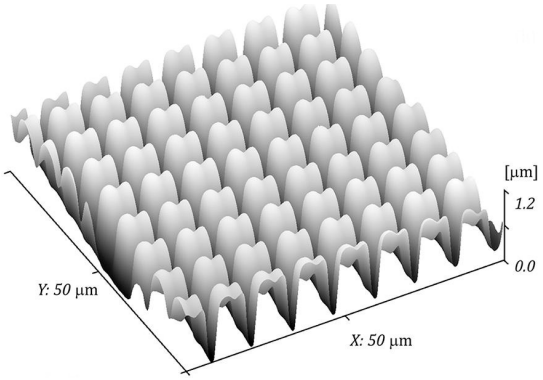

Fig. 2. Binary lattice.

1. M.A. Bruk, E.N. Zhikharev, D.R. Streltsov, V.A. Kalnov, A.V. Spirin. "The new dry method of mask (relief) formation by direct electron-beam etching of resist". Microel. Eng. **112**, pp. 1-4, 2003.

A resistless electron beam lithography based on charge accumulation in dielectric films

E. Kelm, D. Zubov, S. Kazmishchev, R. Milovanov, S. Sokolov
Institute of Nanotechnology of Microelectronics, Russian Academy of Science, Russia, 119991 Moscow, Leninsky Prospekt, 32A, milovanov_r@inbox.ru

Modern electron lithography demonstrates a significant breakthrough in resolution of nanostructures, formed on the surface. However, the use of this method currently don't implemented in manufactured of integrated circuit. The one of main problems is related with the lower selectivity SiO_2; Si_3N_4; Al/electron resist etching in comparison with a photoresist.

In our work we considered the possibility of using effect of charge accumulation on the dielectric films (such as SiO_2; Si_3N_4) under the electron beam for a subsequent charge selectivity etching of surface, as a forming method of surface structures. HF based solutions were selected as etchants.

The main idea of this technique is: the occurrence of the electric double layer reduces etching rate in case of negatively charged dielectric layer; the attraction of HF_2^- etching ions to the surface increase etching rate in case of positively charged dielectric layer.

In this work we used thermal-SiO_2 films with thickness of 140 and 600 nm on Si wafers for lithography (1, 5, 10, 15 kV were tested), and HF(49% aqueous):CH_3COOH(100%) as a developer etchant. Mixtures of HF:CH_3COOH – 1:8; 1:12; 1:16 were investigated. Admixture $[C_{16}H_{33}C_5H_5N]^+Cl^-*H_2O$ was used to increase the shielding effect of electric double layer (100 and 200 mg per 10 ml HF:CH_3COOH solution). Optical surface profiler and laser scanning microscope (LSM) were used to analyze the results of etching (fig. 1a). To confirm the results of optical methods, samples were treated in RIE and analyzed using SEM (fig. 1b).

a) b)

Fig.1. LSM image after developer etching (a) and SEM image of RIE silicon wafer through SiO_2 mask (b).

Electro-optical converter of zero-order and second-order Bessel laser beams for the photolithography systems

V. Paranin[1], S. Khonina[1,2]
1. Samara National Research University, Samara, Russia, vparanin@mail.ru.
2. IPSI RAS – Branch of the FSRC "Crystallography and Photonics" RAS, Samara, Russia, khonina@smr.ru

Bessel laser beams are widely used in the high-resolution photolithography [1], optical micromanipulation [2], laser ablation [3]. Further improvement of optical processing technique of materials requires dynamic control of laser beam properties. The use of linear electro-optical effect is one of the ways of solving this problem. Electro-optical effect allows creation of high-speed optical modulators and switches for application in photolithography systems.

The aim of this work was theoretical research of the electrically tunable transformation of zero-order Bessel beam with maximum intensity in central part to the second-order Bessel beam with zero intensity in central part. The electro-optical crystal $Sr_{0.75}Ba_{0.25}Nb_2O_6$ (SBN:75) with a high sensitivity of refraction indexes to electric field is selected for this project.

The optical setup for tunable conversion contains laser, the spatial filter – an beam expander, diffraction axicon, a *z*-cut of SBN:75 crystal and the focusing optics. The transparent electrodes are formed on an input and output surface of a crystal. Applying of electrical voltage causes changing of refraction indexes of a crystal n_o, n_e and of an output Bessel beam. For calculation of output beam intensity for the crystal lighted by a diffraction axicon formulas [4, 5] were used. Refraction indexes are equal to $n_o = 2.3117$, $n_e = 2.2987$, wavelength $\lambda = 632.8$ nm, electro-optical coefficients $r_{13} = 67$ pm/V, $r_{33} = 1340$ pm/V, the period of an axicon $d = 1.3$ μm, crystal thickness $h = 9.7$ mm. Radial intensity distribution is presented in fig. 1.

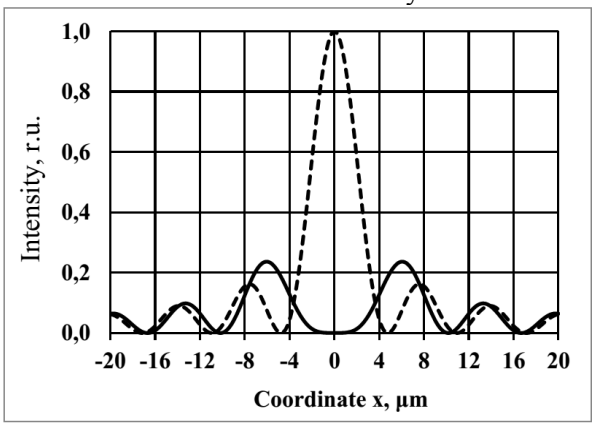

Fig. 1. Intensity of an output beam: dotted line - $U = 0$, solid line - $U = 800$ V.

It follows from these results that full transformation of Bessel beams occurs at a voltage near $U = 800$ V. Field $E_z \approx 0.8$ kV/cm is required and this value is less than coercive field $E_c \approx 1$ kV/cm for $Sr_{0.75}Ba_{0.25}Nb_2O_6$ crystal. It makes possible the creation of such electrically tunable optical switches and modulators for high-resolution photolithography technique.

This work was financially supported by Russian Foundation for Basic Research (grant 16-29-11698).

1. E. Cagniot, M. Fromager, T. Godin et al. "Transverse superresolution technique involving rectified Laguerre-Gaussian $LG(p)^0$ beams". J. Opt. Soc. Am. A., **28**(8), pp. 1709-1715, 2011.
2. V. Soifer, V. Kotlyar, S. Khonina. "Optical Microparticle Manipulation: Advances and New Possibilities Created by Diffractive Optics", Physics of Particles and Nuclei, **35**(6), pp. 733–766, 2004.
3. S. Alferov, S. Karpeev, S. Khonina et al. "On the possibility of controlling laser ablation by tightly focused femtosecond radiation", Quantum Electronics, **44**(11), pp. 1061-1065, 2014.
4. S. Khonina, S. Volotovsky, S. Kharitonov. "Features of nonparaxial propagation of Gaussian and Bessel beams along the axis of the crystal", Computer Optics, **37**(3), pp. 297-306, 2013.
5. S. Khonina, S. Kharitonov. "Comparative investigation of nonparaxial mode propagation along the axis of uniaxial crystal", Journal of Modern Optics, **62**(2), pp. 125-134, 2015.

Comparative study of CF_4- and CHF_3-based plasmas for dry etching applications

A. Efremov[1], K.-H. Kwon[2], A. Morgunov[3], D. Shabadarova[4]
1. Ivanovo State University of Chemistry & Technology, Ivanovo, Russia, amefremov@mail.ru.
2. Korea University, Sejong, South Korea, kwonkh@korea.ac.kr
3. Ivanovo State University of Chemistry & Technology, Ivanovo, Russia, amefremov@mail.ru
4. Ivanovo State University of Chemistry & Technology, Ivanovo, Russia, amefremov@mail.ru

Fluorocarbon gases, including CF_4 and CHF_3, are widely used in the microelectronic industry for the dry patterning of silicon and silicon-based dielectrics (SiO_2, Si_3N_4). In most of the existing processes, these gases are combined with Ar or O_2 in a form of binary or ternary gas mixtures with the aim of accelerating the physical etching pathway, increasing the F atoms' yield and suppressing polymerization. In current state, many commercial dry etching processes require optimization in order to satisfy the increasing requirements to both device dimensions and performance. One of the evident pathways for the optimization of the plasma etching process is the correct choice of the chemically active fluorine-containing gas which determines the types of plasma active species as well as their fluxes on the treated surface. This task cannot be solved without deep understanding of plasma chemistry in various fluorine-containing gas systems.

The goal of this work was the combined (experimental and model-based) comparative study of $CF_4/O_2/Ar$ and $CHF_3/O_2/Ar$ inductively coupled plasmas under one and the same operating conditions. The main attention was focused on the formation-decay kinetics for plasma active species, steady-state plasma compositions and the relationships between gas mixing ratios and the efficiencies of both chemical and physical etching pathways.

The experiments were carried out in a planar inductively-coupled 13.56 MHz plasma reactor. The process conditions were: total gas flow rate (q) of 40 sccm, gas pressure (p) of 6 mTorr, input ICP power (W) of 700 W, and bias power (W_{dc}) of 200 W. Langmuir probe diagnostics provided the data on electron temperature (T_e), ion current density (J_+) and total positive ion density (n_+). The feed gas mixture compositions were set by adjusting the partial gas flow rate of the components within p = const. Particularly, we kept the constant 50% fraction of CF_4 or CHF_3, but varied the ratio between O_2 and Ar within the remaining 50%. Accordingly, the variation of O_2 content in a feed gas in the range of 0–50% corresponded to the transition between $CF_4(CHF_3)$/Ar and $CF_4(CHF_3)/O_2$ gas systems. In order to determine the absolute densities and fluxes of plasma active species, the simplified global (zero-dimensional) plasma model operating with volume-averaged plasma parameters and a Maxwellian approximation for the electron energy distribution function was applied. The model directly involved the experimental data on T_e and n_+ as input parameters.

It was found that the main feature of the CHF_3-based plasmas is the domination of HF over other neutral fluorine-containing species. Such situation is provided by the direct formation of HF from the original CHF_3 molecules in electron-impact dissociation process as well as by the fast conversion of both CHF_3 and their first-step dissociation products, such as CF_3 and CHF_2, in atom-molecular reactions. Under one and the same operating conditions, the $CF_4/Ar/O_2$ plasma provides the systematically higher F atom densities compared with the $CHF_3/O_2/Ar$ gas system. Therefore, in the case if the etching process is not influenced by the fluorocarbon polymerization and is driven by the chemical etching pathway only, the CF_4-based plasma allows one to expect higher etching rates compared with the CHF_3-based one. At the same time, the CHF_3-based plasma provides the systematically higher densities of polymerizing radicals (CF_2, CF, and CHF) compared with the CF_4-based one. Taking into account that the densities and fluxes of O atoms in both gas systems are quite close, the CHF_3-based plasma is expected to be more polymerizing system. The obtained conclusions are in good agreement with the independent experimental data [1, 2].

1. A.J. Roosmalen, J.A.G. Baggerman, S.J.H. Brader. *Dry etching for VLSI*. Plenum Press. New-York. 1991.
2. M.T. Kim. "Pressure dependence of the radical densities in fluorocarbon discharges". J. Electrochem. Soc., **149**, pp. G218-G225, 2002.

Investigation of the reactive ion etching of $Ge_2Sb_2Te_5$ thin films

A. Shulyatev, A. Sherchenkov, D. Gromov, P. Lazarenko, A. Sysa, A. Kozmin
National Research University of Electronic Technology, ashuliatyev@gmail.com

Phase change memory (PCM) is a promising technology, which can successfully replace flash memory technology due to the better characteristics. PCM has better scalability, operation rate, endurance and radiation proof than flash memory. The most perspective material for PCM application is $Ge_2Sb_2Te_5$ (GST225) compound. However, PCM technology is needed to be improved, and one of the challenges is connected with the development of the dry etching process of GST225. So, the goal of this work was investigation of the dry etching of GST225 thin films with using of different etching conditions.

GST225 thin films were deposited by thermal evaporation of synthesized GST225. Residual pressure in the chamber was 10^{-4} Pa. The maximum temperature during evaporation was not more than 630 C, while the substrate temperature did not exceed 50 °C. XRD study (D8 ADVANCE Bruker and Rigaku Smart Lab.) showed that the synthesized material had a polycrystalline structure, while as deposited thin films were amorphous. According to the Rutherford Backscattering Spectroscopy (RBS) and Energy Dispersive X-Ray Analysis (EDXRA) compositions of the synthesized material and thin films were close to GST225.
Reactive ion etching (RIE) system with inductively coupled plasma (ICP) source (NII TM RIT) was used for dry etching. In experiments wafers with deposited GST225 thin films were partly covered by Si substrate.

RIE power was 200 W, and etching time was 1 minute in all cases. Following etching gas mixtures were tested during the experiments: i) Ar (2 l/h) + O_2 (0.6 l/h); ii) Ar (2 l/h) + SF_6 (0.6 l/h); iii) Ar (2 l/h) + Freon-218 (0.6 l/h); iv) Ar (2 l/h) + O_2 (1 l/h) + Freon-218 (0.6 l/h); v) Ar (2 l/h) + O_2 (1 l/h) + SF_6 (0.6 l/h).
The thicknesses of the films were determined by the atomic-force microscopy (AFM). It was found that etching rates were in the range from 17.5 nm/min for the second mixture to 41.1 nm/min for the last one.

The surfaces of the films were checked by scanning electron microscopy (SEM), and showed planar structure and absence of the defects for the etched layers. In Fig. 1, which illustrates SEM investigation, right part was etched, while left one was masked by Si substrate.

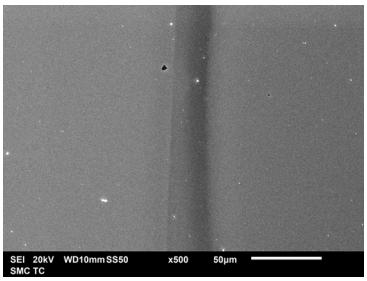

Figure 1. SEM of GST225 thin film after etching.

EDXRA measurements showed that compositions of the etched films coincide with those of the original layers. It means that components of GST225 forms volatile compounds and are equally removed from the layers.

So, influence of different gas mixtures on the dry etching process of GST225 thin films was investigated. Etching rates for different conditions were determined; structures and compositions of the etched layers were investigated.

This work was supported by Ministry of Education and Science of Russian Federation (project ID: RFMEFI57814X0085).

A study of the vertical walls and the surface roughness GaAs after the operation in the combined plasma etching

O.A. Ageev, V.S. Klimin, M.S. Solodovnik, A.V. Eskov, S.Y. Krasnoborodko
Southern Federal University, Institute of Nanotechnologies, Electronics, and Electronic Equipment Engineering, Department of Nanotechnologies and Microsystems, Taganrog, Russia, E-mail address: sbalakirev@sfedu.ru

One of the promising methods of etching structures A3B5 is the method of plasma chemical etching. The advantage of this method compared with liquid is high anisotropy etching process and the absence of the need for additional steps for removing the reaction products from the surface outside and the impurities contained in the initial reagents.
The aim of this work was to study the surface of the etching rate of gallium arsenide, for different values of power inductively coupled plasma in a chlorine-containing environment.
As experimental samples were used GaAs substrates having a standard liquid surface after polishing. Samples were treated for 1, 2, and 3 minutes at different values of the power inductively coupled plasma. The etching was carried out for three groups of samples at the source of the power values of inductively-coupled plasma 200, 400 and 600 watts. All other process parameters remained unchanged.
The results of experimental studies have been built according to the thickness of the layer is etched by the etching time for different values of power inductively coupled plasma.
Thus, according to the results of studies of the dependences presented in Figure 2, we can estimate the rate of etching. Gallium arsenide etch rate was 28.2 nm/min, 24.9 nm/min, 27.8 nm/min, the power values of 200 W, 400 W, and 600 W respectively.
In this work we studied the influence of plasma chemical etching process conditions in the combined plasma etched layer thickness, roughness of the etched surface and the anisotropy of the process in an environment of technological gases BCl_3 and Ar.
Determined etching rate at different values of output capacitance and inductively coupled plasma. The values of the mean square roughness for the modes are shown in the work. It was found that for large values of the source of inductively-coupled plasma etched layer thickness of the power will be increased, this effect is associated with a large number of particles which are responsible for the formation of volatile compounds with the products reactive-ion etching reactions. By increasing the capacitance of the plasma source power increases the etch rate, but the etching rate at thicknesses not exceeding 500 nm, differ slightly.
It was also found that when the power source is inductively coupled plaza burr remains relatively constant, while reducing capacitive plasma source power and bias voltage decreases accordingly decreases the roughness of the etched surface.
Also in the work they were estimated value of the etching rate in different crystallographic directions, which allows us to estimate the anisotropy of the process in a combined plasma. Using the experimental results, we can find the optimal etching modes, which allow the most precise control over the thickness of the etched layer and the surface roughness of the etched considering the process of anisotropy.

This research has been supported by the Results obtained using the Center for collective use of equipment and the Research and Education Center, "Nanotechnologies" South Federal University..This work was supported by the Russian Science Foundation Grant No. 15-19-10006.

The formation of photoresist film with thicknesses from 0.7 to 100 μm on surfaces with considerable relief by spray coating on the heated substrate

A.V. Romashkin, D.D. Levin, R.Yu. Rozanov, V.K. Nevolin
National Research University of Electronic Technology, Moscow, Russia, skaldd@yandex.ru

In contrast to the integrated circuit, elements of MEMS and NEMS significantly non-planar, that increases the requirements for the coating of photoresist (PR): PR uniformity in the horizontal and side surfaces, the optimum thickness for photolithography (PL), in conjunction with the incomplete filling of micron- and submicron-sized in plane grooves.

Existing systems and spray-coating techniques provide formation of thick film PR is not less than 3 μm in considerable (10-100 μl/s) aerosol stream [1], which in combination with a low viscosity (<20 cSt) and very low content of PR material (4-15%) makes it difficult uniform coating of the side walls of the grooves with angle more 50° by PR, nor PR filling narrow (< 1 μm) in the width of the grooves formed in the process such as plasma etching. In this case the solvent leaving from bulk of the thick film is not uniform in softbake process and as a result the formation of inhomogeneity in properties in the thickness of the PR film was occurred, resulting in degradation parameters of PR edge during PL. Thus, the existing spray-coating technology requires a specific recipe of PR solution containing easily-vaporized component.

Decreasing the flow rate of the aerosol, and changing recipe of PR by introduction into its composition mixture as easy and hard vaporized component can form a uniform film thickness of PR from about 0.5 μm to 100 μm on surfaces with considerable relief using almost any PR source used for spin-coating. In work the composition of the solution PR FP3515 (analogue of s1813), which is diluting of the original PR with a mixture as easy and difficult evaporated solvents, for coating by spray method was proposed. The effect of the mutual concentration of the solution component, and the parameter of boiling point of the solvent used on the uniformity of thin (<1 μm) thick films of PR was investigated. Chosen mutual concentration of the components of the solution allows to form a uniform PR film 0.7 μm thick by coating with a flow less than 2 μl/s on Si wafers with depth of grooves ~ 6 μm obtained by liquid etching (Figure 1). That structure was investigated by AFM in area that include edge of etched groove with and without PR, that was successfully opened from PR (thickness 0.7 and 6 μm) by exposed that area by the use of proprietary design laser PL system with software pattern and development of that in KOH solution.

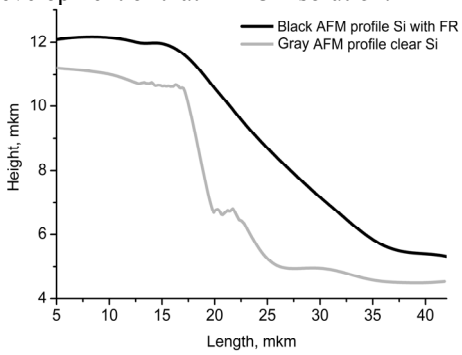

Figure 1. Cross-section of edge of etched groove in Si with and without coating of PR.

Using techniques of coating PR solution with a low flow rate in which solvent is vaporized from the formed on the surface micro-droplets, instead of a thick layer of the entire film, allows achieving acceptable solvent evaporation rate, surface roughness and nonuniformity of film thickness, combined with the ability to form thin films of PR.

In combination with layer by layer coating with heat treatment of each layer up to 65 °C, that techniques allows to provide the uniformity of solvent content along of thickness of the PR film, the uniformity of the coating of side walls of the grooves with width up to 1 μm, and also allows to refuse from process subsequent softbake of PR film.

Thus, the proposed technique by spray coating PR from original solution with low flow rate allows to form a uniform film with thickness less than 1 μm on substrates with any geometrical dimensions and a height difference between structural elements on substrate of at least 6 μm and above, with spread in the substrate film thickness about 10-16%, with maximum the film thickness is limited only by the ability of PR to be exposed at a given depth.

This work is supported by the Ministry of Education and Science of the Russian Federation, contract N 14.578.21.0113 (unique ID RFMEFI57815X0113)

1. N.P. Pham, J.N. Burghartz, P.M. Sarro. “Spray Coating of Photoresist for pattern transfer on high topography surfaces”. J. Micromech. Microeng., **15**, pp. 691-697, 2005.

Deposition of polymers on structures of nano-gap in carbon nanotubes on SiO_2 creating by focusing ion beam implantation and etching

A.V. Romashkin, A.V. Emelianov, K.A. Tsarik, I.I. Bobrinetskiy
National Research University of Electronic Technology, Moscow, Russia, romaleval@gmail.com

The difference of physicochemical properties of surface with dimensions in plane even less than 2 μm with the nanometer scale film thickness has significantly affects to the properties and film uniformity, particularly when heating the polymer over the glass transition temperature [1], which is used to improve the structuredness of films when forming the organic electronics elements. An alternative factor for distribution of material on substrate is to implantation the charge into the substrate [2].

However, for nano-sized structures of carbon nanotubes (CNTs) on the surface of SiO_2 with a significant difference physicochemical properties the formation of ultrathin films and deposition of polymer molecules in the nano-gap between the CNTs there are some features, that must be taken into account to form a conductive molecular channel. The gap ~ 30 nm was formed by etching the CNT by focused ion beam (FIB). At low exposure doses at first swelling of SiO_2 was occurred due to created defects and small sputtering of material at area ~ 25-35 nm, comparable to the actual width of the etching region, and ion distribution in the substrate [3] (this area coincides with the size of the gap in the CNT), and only then - at a dose of more than $2.5 \cdot 10^{15}$ cm^{-2} SiO_2 is etched (Fig. 1a). Additionally it is necessary noted that the dose for etching single walled CNTs with diameter less than 1.5 nm coincides with the depth of etching SiO_2. In addition, the etching and the formation of a gap in the CNT makes a significant charge of the ions Ga^+. During the deposition of polymers from solution onto the structure with a residual charge when the charge relaxation was not carried out by annealing, the essential features were observed in polymer deposition not only in whole gap between the metal micro-contacts on SiO_2, but especially near etching line. In the case of deposition of polyaniline (PANi) (M_w ~ 10 kDa) from solution of n-methylpyrrolidone (~ 10 μg/ml), it preferential deposition occurred directly in the center region FIB etching and gaps between CNTs, although in the form of unstructured large particles (Fig. 1b); and in the case of non-polar polymer molecules from toluene solution deposition occurred to the alongside of main line of etching (Fig. 1c), which is consistent with other results [2].

Thus, by long-term stored in the insulator charge (in the absence of annealing above 300 °C) deposition molecules from a solution in predetermined regions at leveling differences in physicochemical properties of the substrate can be provided, that can be used for directional deposition of molecules and the formation of molecular channels with field effect showing significantly better mobility, than in the macro-scale, and allowing to investigate transport of low molecular structures in nano-scale contacts based on CNTs.

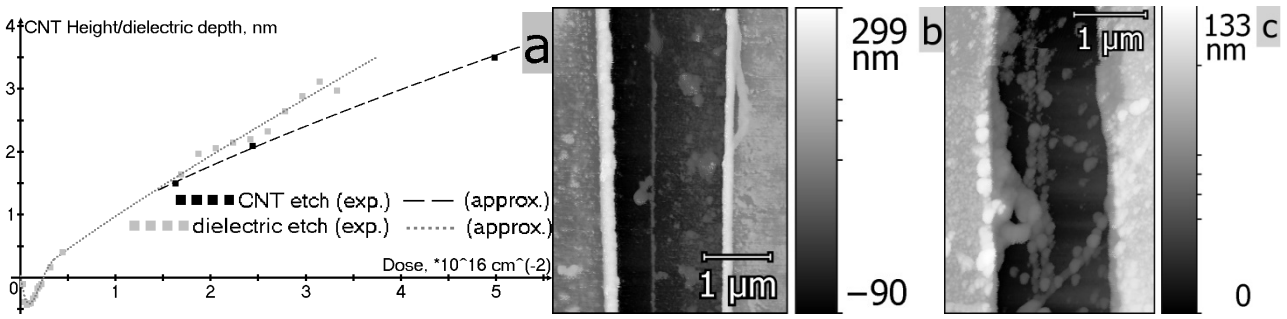

Fig. 1. a – dependence of CNT height/SiO_2 depth with dose; AFM of PANi (b) and non-polar polymer (c) deposited on structure of FIB line etching area in gap between micro-contacts from solution of polar N-methylpyrrolidone and non-polar toluene respectively.

1. C. Luo, et al. "Ordered droplet formation by thin polymer film dewetting on a stripe-patterned substrate" J. Colloid and Interface Science, **269,** pp. 158–163, 2004.

2. C.W.J. Berendsen, et al. "Dielectrophoretic deformation of thin liquid films induced by surface charge patterns on dielectric substrates". Soft Matter, **9**, pp. 4900–4910, 2013.

3. I.I. Bobrinetskii, et al. "A distribution of Ga^+ ions in a silicon substrate for nano-dimensional masking". Russian Microelectronics, **43**, pp. 15–20, 2014.

Modelling energy gaps of graphene nanoribbons (GNRs) by DFT

N. Savinski[1], U. Logachev[2]
1. Yaroslavl Branch of the Institute of Physics and Technology, Russian Academy of Sciences, Moscow, Russia.
2. P.G. Demidov Yaroslavl State University, Yaroslavl, Russia.

Graphene nanoribbons (GNRs) have one-dimensional structures with hexagonal two-dimensional carbon lattices, which are stripes of graphene. Their structures and their electronic and magnetic properties have been intensively studied both experimentally and theoretically. Due to their various edge structures, GNRs present different electronic properties ranging from normal semiconductors to spin-polarized semimetals, which open the possibility of GNRs as electric devices. After the successful isolation of graphene, its amazing properties make it become a potential candidate for post-silicon electronics and photonics. However, as we know, graphene is a zero-gap semiconductor. To extend the real applications, an energy gap is needed, which enables the basic electric logic states: on and off. When graphene is etched or patterned along one specific direction, a novel quasi one-dimensional (1D) structures obtained, which is a strip of graphene, referred as graphene nanoribbon (GNR). There are some critical questions about such GNRs: How do they organize the structures? Do they have energy gaps? And is there any magnetic state in these GNRs?
Graphene is a zero-bandgap material; however, cutting the graphene sheet into small pieces (GNRs or GQDs), making defects or introducing chemical modification in graphene can induce a band gap. Graphene oxide has been intensively studied recently owing to its fundamental properties and potential applications [1, 2]. The oxidation of graphene serves as an example for chemical modification of graphene, which is of great interest to tune the electronic, mechanical, and optoelectronic properties of graphene. GNRs have been reported as a promising material for applications of spintronic devices that is related to the half-metallic behavior of GNRs. In this work, we studied a series of rectangular GNRs with oxygen-containing groups and we notated the ribbons with NxM convention, where N and M represents the number of rows and columns across the GNRs width and length, respectively. In addition, oxygen-containing groups mean the type of groups substituted on the edge, including -OH, -COOH, and –COO.
We conducted spin-polarized ground-state calculations using the screened exchange hybrid functional HSE06 and polarized 6-31G** basis set, which has been tested on many materials and has been verified to accurately reproduce the experimental band gaps. Therefore, all the geometry optimizations and electronic properties of the GNRs with oxygen-containing groups were implemented using the HSE06.

1. Savinski N., Vasiliev S., Naumov V., Soloviev M., Shvircova N.”The oxidation of exfoliated graphite” Bulletin of the Yaroslavl State University. A series of Natural and technical Sciences, **4**, pp. 73-79, 2013 (in Russian).
2. Savinski N., Vasiliev S., Naumov V., Soloviev M., Shvircova “Microwave heating of intercalated graphite” Bulletin of the Yaroslavl State University. A series of Natural and technical Sciences, **4**, pp. 80-86, 2013 (in Russian).

Electrochemical exfoliation for the scalable production of high-quality graphene

N. Savinski[1], D. Puhov[1], M. Lebedev[1], S. Vasilev[1], O. Trushin[1], M. Soloviev[2], A. Surovtsev[3]
1. Yaroslavl Branch of the Institute of Physics and Technology, Institution of Russian Academy of Sciences
2. Yaroslavl State Technical University
3. Joint Stock Company Research Institute "Yarsintez"

The exceptional electronic, thermal, optical, and mechanical properties of graphene render it a remarkable candidate for the next generation of electronic and optoelectronic devices [1].
Consequently, techniques for the scalable production of high-quality, solution - processable graphene are needed. Among the numerous protocols employed to date, the exfoliation of bulk graphite is most common for harvesting graphene sheets on a large scale because of its low process complexity and costs.
Direct exfoliation in the solid state (e.g., scotch-tape cleavage, ball milling or in a liquid phase (e.g., liquid phase sonification, shear force exfoliation, also known as physical exfoliation, provides feasible means for producing graphene with a low number of defects. In comparison, chemical exfoliation, which generally relies on Hummers' method, offers a wide range of flexibility for the production of graphene oxide (GO) and related materials because of the potential scalability, impressive conversion efficiency (~100%), and superior processability [2]. Unfortunately, the unique physical properties of graphene are seriously compromised and cannot be sufficiently recovered, even upon reduction, because of the appreciable fraction of oxygen groups and defects that are left behind. These oxygen groups restrict its usage in fine applications [3].
Electrochemical exfoliation has recently emerged as a promising strategy for producing graphene on an industrial scale with high efficiency, at low cost, and in an environ-mentally friendly manner.
Anionic intercalation (primarily in aqueous electrolytes) is less time demanding and can take less than 1 h. However, the graphene produced is generally decorated with functional oxygen groups that occur due to the positive potentials used, especially with acidic electrolytes. Nevertheless, the radicals (e.g., HO•) generated from water electrolysis will unavoidably disrupt the graphitic structure during the exfoliation process [4]. Therefore, it is highly desirable to eliminate these radicals to ultimately improve the quality of the graphene. In this study, the electrochemical exfoliation of graphene is carried out in the presence of a series of antioxidants (such as ascorbic acid, hydrazine, sodium borohydride, dimethylsulfoxide (DMSO), (2,2,6,6-tetramethylpiperidin-1-yl)oxyl (TEMPO)), 2,2,6,6-tetramethyl-4-one-piperidin-1-yl)oxyl (IPON), Dimer (2,2,6,6-tetramethylpiperidin-1-yl)oxyl-fulvalene (YARSIM-0215) in a neutral aqueous electrolyte (ammonium sulfate) to suppress the formation of radicals from water electrolysis. Remarkably, using TEMPO, the electrochemically exfoliated graphene (EG) produced is of exceptionally high-quality, and the process gives high exfoliation efficiencies.

1. Novoselov K.S., Geim A.K., Morozov S.V., Jiang D., Zhang Y., Dubonos S.V., Grigorieva I.V., Firsov A.A. "Electric Field Effect in Atomically Thin Carbon Films." Science, **306**, p. 666, 2004.
2. Savinski N., Vasiliev S., Naumov V., Soloviev M., Shvircova N."The oxidation of exfoliated graphite" Bulletin Of The Yaroslavl State University. A series of Natural and technical Sciences, **4**, pp.73-79, 2013 (in Russian).
3. Savinski N. ,Vasiliev S., Naumov V., Soloviev M., Shvircova N. "Microwave heating of intercalated graphite" Bulletin Of The Yaroslavl State University. A series of Natural and technical Sciences, **4**, pp. 80-86, 2013 (in Russian).
4. S. Yang, S. Brüller, Z.-S. Wu, Z. Liu, K. Parvez, R. Dong, F. Richard, P. Samorì, X. Feng, K. Müllen "Organic radical-assisted electrochemical exfoliation for the scalable production of high-quality grapheme". J. Am. Chem. Soc., **137**, pp. 13927−13932, 2015.

Direct laser patterning of graphene-based biosensors

I.A. Komarov[1], A.V. Golovin[2], E.I. Rubtsova[1], T. Kholina[2], N. Otero[3], P. Romero[3], I.I. Bobrinetskiy[1]

1. National Research University of Electronic Technology, Moscow, Russia, master_kom@mail.ru.
2. Lomonosov Moscow State University, Moscow, Russia, golovin@gmail.com.
3. Laser Applications Centre, AIMEN, Porriño, Spain, promero@aimen.es

One of today's most promising materials is graphene and its derivatives like graphene oxide and reduced graphene oxide. Due to outstanding electrical and dimensional properties and flexibility graphene is a highly promising material for different sensors for personal healthcare monitoring systems. It is possible to use graphene and its derivatives as a platform for detection biological agents [1] in case of decorating graphene surface with bio sensitive materials like antibodies, aptamers etc.

We designed a graphene based platform for biosensors on a flexible polymer substrate. As sensitive substance we used aptamers - short oligonucleotides features high specificity to the target along with stability and possibility high yield chemical synthesis for mass production. We used two types of graphene materials for sensor platform. In one case we put CVD graphene on the top of polymer substrate and covered it with lamination. In other design we used graphene oxide reduced by direct laser patterning (LrGO) (fig. 1). This pattern also provides easy connection to the standard socket for flexible cables and the control of the reduction level i.e. the number of oxidized group in graphene lattice. Higher laser energies provide total removal of graphene providing concept of both physical and chemical mask-less patterning of graphene (fig. 2). We put aptamers only inside sensing area by noncovalent bonding through a special linker.

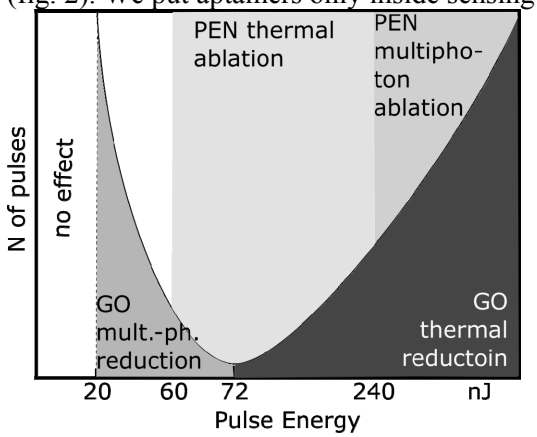

Fig. 1 – Parameter map for laser reduction from graphene oxide on polymer substrate.

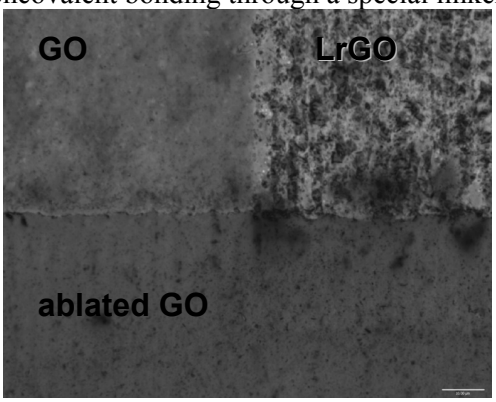

Fig. 2 – Photography of laser patterned GO: lift top – pristine, right top – LrGO, bottom –ablated.

We measured dependence of biosensing platforms resistance on time. CVD graphene based structures shows good stability and relatively low resistance 3-4.5 kOhm. In case of reduced GOx biosensors have resistance from 2.2 to 5.3 MOhm and lower stability. We think reduced GOx have much higher resistance due to not a full reduction. In that case most of resistance generates from contacts between graphene flakes. Also depending on pulse energy and number of laser pulses it will be different surface topology. Better results will be in case of high energies and pulse number. Raman spectroscopy in all cases shows decrease of signal intensity with aptamers. This means that binding reaction goes well.

Thus, we have demonstrated the mask-less technology based on laser patterning for graphene biosensor manufacturing.

1. Y.H. Kwak, D.S. Choi, Y.N. Kim, H. Kim, D.H. Yoon, S.-S. Ahn, J.-W. Yang, W.S. Yang, S. Seo. "Flexible glucose sensor using CVD-grown graphene-based field effect transistor". Biosensors and Bioelectronics, **37**, pp 82–87, 2012.

Silicon wafer temperature switching waves in a lamp-based chamber

V. Ovcharov, A. Kurenya, V. Rudakov, V. Prigara
Yaroslavl Branch of the Institute of Physics and Technology RAS, Email:ovcharov.vlad@gmail.com

In the thermal processing of semiconductor wafers in a thermal lamp-based chamber there are such modes of heat exchange possible, during which the wafer can exhibit optical and temperature bistabilities [1]. The salient feature of the temperature bistability in a silicon wafer is occurrence of two stable steady states in the wafer. The first of which is a lower-temperature state when the wafer is much of the transparent one to heat radiation. And the second state is the upper-temperature one for the entirely opaque wafer. Switching process of semiconductor samples caused by laser-induced radiation from the lower-temperature state to upper-temperature state and reverse of it have been studied at the end of the last century in connection with a problem of developing the optical transistor. It was found that these processes take in analogy to the phase transition of the first type [2] that it allows to introduce the concept of high-temperature and low-temperature phase. At the distinct parameters of the laser-induced beam a nucleus of a new temperature phase is formed on the surface of the semiconductor sample. The extension of the nucleus is accomplished by propagation of the switching wave of temperature along the wafer surface. Parameters of the switching waves depend on both thermo-physical properties of the sample and heat input and removal modes of heat exchange during the interaction of the sample with laser-induced radiation. Unlike switching the semiconductor sample under the effect of laser-induced beam, the entire semiconductor wafer is switched in the lamp-based chamber being exposed by uncoherent thermal radiation in the wide spectral interval under the conditions of heat exchange with the elements of the lamp-based reactor. In such conditions the problem of the switching the semiconductor wafers has not been carried out until now. Study of the switching the lightly-doped silicon wafer in the process of interacting of the lamp radiation with the optical inhomogeneity on the wafer surface is the essence of the present work.

The doped layer on one half of the silicon wafer surface was used as the material of the optical inhomogeneity on its face surface. The silicon wafer with the doped layer on its surface on being heated is switched into upper-temperature state at the less heater temperatures than in the case of the silicon wafer without the doped layer [3]. In this case, the doped layer acts as the nucleus of the upper-temperature phase that initiates the switching of the entire wafer into upper-temperature state. The switching process must be followed by propagating the switching wave of temperature across the surface of the wafer. Parameters of the switching wave are defined by numerical simulation of the switching process of the wafer with regard to its temperature dependence of thermal capacity and heat conductivity coefficients. These results were compared with theoretical evaluations. It is shown that in this situation the boundary conditions on the end edge surface of the wafer have no essential effect on the process of origin of the high-temperature phase and on the propagating the switching wave along the wafer.

For the comparison of the simulation results with the results of the experiment into upper-temperature phase formation on the optical inhomogeneity and switching wave propagating across the silicon wafer there was a general procedure developed for controlling the switching wave propagating by pyrometer measurements. Using this procedure there was detected propagating the switching wave across the surface of the silicon wafer doped by boron with resistivity 12 Ohm·cm having the heavy-doped layer on one half area of its face surface. The velocity of the switching wave in order of magnitude corresponds to simulation results and theoretical evaluations.

1. V.I. Rudakov, V.V. Ovcharov, A.L. Kurenya, V.P. Prigara. ”Bistable behavior of silicon wafer in rapid thermal processing setup”. J. Microelectron. Eng., **93**, pp. 67-73, 2012.
2. N.N. Rozanov. *Optical bistability and hysteresis in distributed nonlinear systems*. Fysmatlit, Moscow, 1997 (in Russian).
3. V.P. Prigara, V.V. Ovcharov, V.I. Rudakov. ”Temperature bistability in a silicon wafer with a doped layer on lamp-based heating”. Materials Science in Semiconductor Processing, **34**, pp. 312-325, 2015.

Critical parameters of lamp-based annealing in high-power flux of incoherent radiation

V. Prigara, V. Ovcharov, V. Rudakov, A. Kurenya
Yaroslavl Branch of the Institute of Physics and Technology RAS, Email:ovcharov.vlad@gmail.com

Thermal processing is an integral part of the micro- and nanoelectronics technology. It involves promising processes of wafers treatment by incoherent radiation. A temperature bistability effect in a silicon wafer can result from letting high-power fluxes of incoherent radiation through the wafer [1]. The essence of the effect implies that the wafer temperature whose emissivity increases non-linearly with the increase of the temperature of the wafer, takes different values under its heating and cooling for distinctive relations between the input and output from the wafer heat fluxes [2]. Such effect can be responsible for a difference between planned and real wafer temperature magnitudes and requires to be taken into account in thermal treatment processes on lamp-based heating chambers. Here the object is to determine controlling parameters corresponding to temperature bistability effect initiation and break-down in the silicon wafer, and also the dependence of the controlling parameters on the characteristics of the heat system elements (a heater, an absorber, and a cold stream) and a working wafer.

The heat exchange between the silicon wafer and the elements of the lamp-based chamber is simulated by use of the numerical solution of the heat balance equation. Those solutions of heat balance equation for which the temperature bistability effect is obtained for the working wafer have the appearance of the surface with a fold [3]. As a result of the solution, a bifurcational surface, termed as a fold, is plotted on the plane of the heater temperature and effective heat exchange coefficient [3]. It is found that the full projection on the controlling parameters plane represents a finite convex domain. This domain is limited over the effective heat exchange coefficient axe from the left and right sides by two points that we will call as critical points, and a vector joining the left and right points and defining an orientation of the bistability domain will be called a critical parameters vector. The critical values of the controlling parameters are important characteristics of the solution of the heat balance equation for the silicon wafer at the bistable behavior of the wafer. The bistable mode of thermal treatment corresponds to the controlling parameters values limited on the interval between the critical values, outside this interval there are monostable modes. These modes can be called as pre- and afterbistable modes, correspondingly. It is shown that the change of the optical characteristics of the heat system elements corresponds to the change in an orientation of the vector of critical parameters, whereas, the change in an optical characteristics of the working wafer corresponds to the change in the length of the vector on remaining of its orientation. Caused by temperature variations in optical characteristics of the silicon wafer the change in long of the critical parameters vector is made possible from its both sides. So, the experimental observation of the afterbistable mode has become available as a result of the shortening the critical parameters vector on the side of the afterbistable parameter (the end of the vector). The vector of the critical parameters may be lengthened on the prebistable critical parameter side (the origin of the vector), thus making it possible to raise the question of the temperature bistability in a vacuum condition.

As a result of simulating wafer behavior in the vacuum condition of a heat system, where an absorber is an absolute blackbody plate and a heater is a plate from tungsten, emissivity spectrum of which is limited by 5 μm, it is found that bistability can be observed in a highly doped silicon wafer (with impurity concentration up to 10^{15} cm^{-3}) at the thickness of the wafer above 700 μm. The result of the present work allow setting up the problem of the observation of the temperature bistability in the silicon wafer in conditions of purely radiation heat exchange between the working wafer and the elements of the heat system.

1. V.I. Rudakov, V.V. Ovcharov, V.P. Prigara. “Bistability in radiation heat exchange”. Thech. Phys. Lett., **34** , pp. 718-721, 2008.
2. V.I. Rudakov, V.V. Ovcharov, A.L. Kurenya, V.P. Prigara. “Bistable behavior of silicon wafer in rapid thermal processing setup”. J. Microelectron. Eng., **93**, pp. 67-73, 2012.
3. V.P. Prigara, V.V. Ovcharov, V.I. Rudakov. “Temperature bistability in a silicon wafer with a doped layer on lamp-based heating”. Mat. Sci. in Semcond. Proc., **34**, pp. 312-325, 2015.

Influence of reactor wall conditions on the silicon etching rate in SF_6 plasma processing

O.V. Morozov, A.V. Postnikov
Yaroslavl Branch of Institute Physics and Technology, Russian Academy of Sciences, Yaroslavl, Russia;
moleg1967@yandex.ru

SF_6 plasma has been widely used for silicon etching in microsystem technologies. In this plasma, decomposition of SF_6 produces F radicals that etch silicon spontaneously (isotropically) by formation of volatile SiF_4. SF_6 plasmas are particular used to achieve fast isotropic etching for release procedure of various suspended structures [1]. In addition F-based Bosch-process is often preferred to perform directional deep reactive ion etching (DRIE) of silicon for bulk micromachining. This process can be briefly described as consisting of sequential etch (SF_6 plasma) and passivation (fluorocarbon plasma) steps [2]. Fluorocarbon polymer film is deposited on the reactor walls at passivation step, which could cause DRIE instability. The some DRIE tools are equipped with a heated liner to prevent polymer deposition on the reactor walls [3]. Temperature of a liner may also affect on the density of F radicals in SF_6 plasma processing step and on silicon etching rate. A global model for SF_6 plasma predicts a significant impact of loss SF_x radicals by deposition of a fluoro-sulfur film on the reactor walls on degree of decomposition of SF_6 [4]. This work studies influence of the DRIE-tool equipped with a liner on silicon etching rates in single step SF_6 plasma processing.

To determine the etch rate we carried out the etching of the trenches into bulk of silicon wafer. Silicon dioxide was used for masking. Masking layer 0.44 μm thick was patterned with line-and-space and etched in HF solution. The lines were 40 μm wide, with 60 μm space between them. Experiments were carried out with home-built radio frequency (13.56 MHz) inductively coupled plasma (ICP) source. The feed gases were introduced at the top side of the source. Downstream the ICP source, a diffusion chamber which includes the wafer holder (Alcatel RDE-300) is located. Distance from a highest density ICP point to the holder is approximately 200 mm. The system is pumped using two 400 l/s turbomolecular pumps backed by a mechanical pump. A liner (thin-walled aluminum tube 220 mm in diameter) was placed inside the diffusion chamber. It has poor thermal contact with other parts of the chamber. During SF_6 plasma processing the time dependence of the liner temperature and the process pressure were measured with a thermocouple and with a capacitance manometer, accordingly. The silicon etching rate was measured with real-time trench depth measurement based on laser interferometry technique [5]. The results presented here were obtained at different SF_6 flow rates of 25, 50, 100, 150 sscm and at constant inductive power level of 900 W. At this power level a liner was heated in 15 minutes from room temperature to the equilibrium temperature of about 553 K.

The silicon etching rate is significantly increased in the progress of SF_6 plasma processing in our experiments. The raise of the etch rate may amount to as much as 2.3 times. This ratio depends on the process flow rate. The lower the flow rate the smaller the raise of the etch rate (of 1.6 times at 25 sscm). The initial silicon etching rate (at room temperature liner) ranged from 1.5 to 5.4 um/min under varied flow rates from 25 to 150 sscm, accordingly. The time dependence of the process pressure correlates well with etching rate behavior, i.e., the pressure was increased in the progress of processing. Therefore, the raise of the etch rate is the result of the increasing the SF_6 decomposition efficiency concerned with reactions on liner surface. Experimentally, the etch rate is controlled by at least two comparable factors: the liner temperature and the process duration after O_2 plasma cleaning. Second unexpected factor was detected when the measurement was started at various liner temperatures after O_2 plasma heating. To eliminate the temperature factor the time dependence of the etch rate was measured without a liner at the same flow rates. The time dependences of the etch rate are less pronounced in these experiments but for 25 sscm the etch rate was almost constant. With that the initial etch rates relatively higher as mach as 1.4 times in all settings. Thus, application of a liner is advantageous to increase etch rate at the high liner temperature and at long processing time.

1. A. Tserepi, et.al. J. Micromech. Microeng. **13**, pp. 323–329, 2003.
2. R. Abdolvand, F. Ayazi. Sensors and Actuators A, **144**. pp. 109–116, 2008.
3. H.V. Jansen, et.al. J. Micromech. Microeng. **19**, pp. 1-41, 2009.
4. G. Kokkoris, et.al. J. Phys. D: Appl. Phys. **42**, pp. 1-15, 2009.
5. http://micromagazine.fabtech.org/archive/04/10/grange.html

Cleaning of Si sidewall surface of high aspect ratio trenches in oxygen and hydrogen peroxide plasma

I. Amirov, M. Izuymov, L. Mazaletsky
Yaroslavl Branch of the Institute of Physics and Technology, Yaroslavl, Russia, E-mail:ildamirov@yandex.ru

Cleaning the side walls of the micro- and nanostructure from the fluorocarbon impurities obtained in the processes of deep reactive ion etching (DRIE) in fluorocarbon containing plasma is important for the manufacture of various elements of microelectromechanical systems. It is essential operation in through-silicon-via (TSV) technology of creation 3-dimensional silicon substrate interconnects [1]. In the TSV technology through-hole interconnects in Si with dimensions of 2 to 100 μm with a different aspect ratio are used. For removal of fluorocarbon films using oxygen plasma with the addition of H_2O, with followed by a series of wet cleans to remove organic and inorganic contaminants. Treatment in oxygen plasma cannot completely to remove residues.

This paper presents results of study cleaning sidewalls of narrow and wide trenches (width 3, 10, and 200 μm) with an aspect ratio of 13, 8, and 1, respectively, in a dense plasma O_2 and H_2O_2 of RF inductive discharge. The presence of hydrogen in the plasma should promote more complete removal of carbon residues. The composition of a passivation film on a side wall Si before and after cleaning was determined from energy dispersive X-ray (EDX) data, using INCA Oxford Instruments EDX spectrometer mounted in the Supra 40 microscope. The top and bottom parts of the etched sidewall were analyzed. The analyzed region was 5 × 5 μm^2.

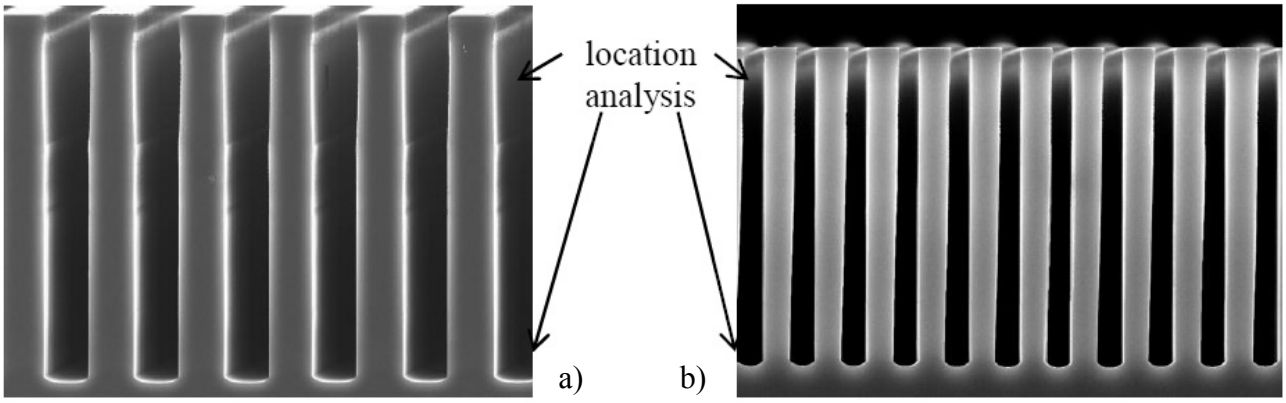

Fig. 1. SEM image trenches width 10 μm (a) and 3 μm (b).

Etching trenches of different width in C_4F_8/SF_6 plasma (DRIE Bosch process) was performed in mode when on the top of wide trenches is formed the fluorocarbon film of large thickness (100-200 nm). Results of semiquantitative EDX analysis of the sidewall surface of wide and narrow grooves after treatment (t = 300 s) in plasma H_2O_2 and O_2 are shown in Table. EDX: 5 kV, at. %.

	3 μm (H_2O_2 plasma)		10 μm (H_2O_2 plasma)		200 μm (O_2 plasma)		Cleaning flat Si surface (H_2O_2 plasma)	
	C	O	C	O	C	O	C	O
Top	2.37	3.12	2.19	4.03	2.29	6.89	2.27±0.12	4.21±0.22
Bottom	2.31	1.87	2.12	1.59				

After the plasma treatment the carbon content on the sidewall is not more than on clean surface Si. These data show that treatment in plasma H_2O_2 leads to an effective cleaning of side wall trenches of the different width.

1. J.P. Gambino, S.A. Adderly, J.U. Knickerbocker. An overview of through-silicon-via technology and manufacturing challenges. Microelectronic Engineering, **135**, pp. 73-106, 2015.

Effect of low energy ion-plasma treatment on the internal stresses in three-layer Pt/Ti/SiO_2 microcantelevers

I. Amirov, R. Selyukov, V. Naumov
Yaroslavl Branch of the Institute of Physics and Technology, Yaroslavl, Russia, E-mail:ildamirov@yandex.ru

The sensitivity of biosensors, sensors, infrared radiation devices based on two-, three-layer microcantilevers (MC) depends on the mechanical properties of materials used for their fabrication. Therefore, the ability to control internal stresses in the films is important to improve the performance of the devices. One effective way to influence the tension in the film is ion-plasma treatment [1, 2]. It was shown that the bombardment of Pt film surface by ions Ar^+ with energies above 500 eV leads to the change of stresses from compressive to tensile [2]. However, at high energy of ions the film is sputtering. It is a negative factor of such treatment. In this work the results of studies of low-energy ion (E_i < 30 eV) treatment three-layer Pt/Ti/SiO_2 microcantilever in dense plasma Ar on the internal stresses in the metal film are presented. Stress in Pt film was determined from the measured bending curvature of MC using the Stoney formula. In addition, tension in the film was determined from the data of X-ray diffraction (XRD) Pt films, by measuring the interplanar distances of Pt (111).

The sets of Pt/Ti/SiO_2 (thicknesses 80/10/850 nm) MCs with length 10-100 μm and width 2-10 μm were fabricated using micromachining process. Ion-plasma treatment was carried out in high density Ar plasma of RF inductive discharge [3]. The energy of bombarding ions was below 30 eV. Ion energy was determined by the potential of RF-electrode on which the specimens were installed. The treatment of MC was carried out at room temperature and at the T = 100-250 °C.

Fabricated samples MK slightly deviated downward in the direction of the silicon substrate. This indicates that the stresses in Pt film and Ti/SiO_2 bi-layer are almost compensated. Measurements of stresses in Pt film by XRD are showed compression stress up to 900 MPa. Plasma treatment MC at room temperature and low-energy ions (15-20 eV), showed that with the increase processing time deviation MC down increases, reaching 9 μm after 300 s treatment. This indicated that the ion bombardment of the Pt surface at room temperature leads to an increase compression stress. Ion treatment at the high-temperature (100-250 °C) leads contrary to the development of tensile stresses. Short-time treatment (t = 60 s) led to the strong (25-33 μm) deflection of MC's free end away from substrate. The internal tensile stresses in Pt film, determined by Stoney formula were 450-600 MPa. XRD measurements of stresses in Pt films showed the existence of tensile stress of 730 MPa. These higher residual stresses Pt, what their values are defined by the formula Stony due to the fact that at MC fabrication was a partial relaxation of stresses.

Thus, it was shown that ion-plasma treatment of Pt/Ti/SiO_2 microcantilever by ions with energy below the sputtering threshold enables to control the stresses in film. Depending on the substrate temperature in Pt film may develop compressive or tensile stresses.

1. E. Chason, J.W. Shin, S.J. Hearne, and L.B. Freund. "Kinetic model for dependence of thin film stress on growth rate, temperature and microstrucutre". J. Appl. Phys., **111**, 083520, 2012.
2. W.-L. Chan, K. Zhao, N. Vo, Y. Ashkenazy, D.G. Gahill, and R.S. Averback. "Stress evolution in platinum thin films during low-energy ion irradiation". Phys. Rev. B., **77**, 205405, 2008.
3. I.I. Amirov, V.V. Naumov, M.O. Izyumov, and R.S. Selyukov. "The effect of ion energy on the surface morphology of platinum film under high-frequency ion plasma sputtering". Tech. Phys. Lett.., **39**, pp. 130-133, 2013.

Elements for Hard X-ray Optics Produced by Cryogenic Plasma Etching of Silicon

A. Miakonkikh[1], A. Rogozhin[1], K. Rudenko[1], V. Lukichev[1], V. Yunkin[2]
1. Institute of Physics and Technology of Russian Academy of Sciences, Moscow, Russia, miakonkikh@ftian.ru
2. Institute of Microelectronics Technology RAS, Chernogolovka, Russia

A number of different hard X-ray optics elements such as refractive lenses, refractive bi-lenses and multilens interferometers, mirror interferometers can be made of Silicon [1]. The optical performance of these elements depends on the quality of refracting and reflecting surfaces. It concerns both shapes and roughness. Significant advantages can be obtained using the method of plasma cryogenic etching of silicon, which can be successfully applied for etching of high aspect sub-50 nm trenches [2]. Those nanoscale etched features indirectly gives a proof for extremely smooth sidewalls. It was experimentally shown that the peculiarities of profiles depend on the cryo-process parameters of etching.

Optimised continuous cryo-etching of Silicon based on $SF_6 + O_2$ plasma was applied to etch multilens structures through silicon oxide mask (t = 300 nm) using Plasmalab System 100 tool (OIPT, UK). Three step process of etching was developed. Low pressure plasma of 10 mTorr was used and sample temperature was established at -110 °C. After ignition step combined with breakthrough step, the step eliminating the notch/undercut of Silicon under the mask was applied. This step is followed by increasing oxygen contents in plasma. Next step lasts for 20-100 sec and provide overpassivation of top part of walls of lens structure which is subject to strongest long time bombardment by plasma species during the etching. The main etch step lasts for 15-80 min and characterized by lower content of oxygen in plasma mix.

We have considered the use of Silicon oxide and Aluminium oxide as hard masks. The advantage of Aluminium oxide provides its enormous stability in fluorine based cryo-process. The following parameters were reached: selectivity (Al_2O_3) of 30000, the slope of the walls of 89.3° with mask undercut of 50 nm, etch rate up to 1.5 μm/min. It should be noted that since the Alumina releases smaller amount oxygen during the etching, it leads to change of optimal oxygen content in feeding gas relatively SiO_2 mask. Cross section of etched multilens structure is shown on Fig. 1.

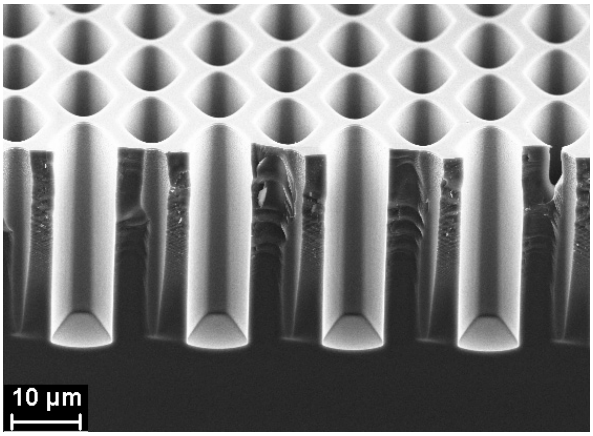

Fig.1. Cross section of multilens structure of bi-lenses depth of 40 um etched by cryogenic process

The investigation of sidewall roughness was provided on specially prepared samples of etched multilens structures by AFM and by optical interferometer Zygo New View 5000. Geometrical parameters of structures were measured by SEM. It was observed that roughness of inner sidewalls of etched structures does not exceed 3 nm/um (RMS) and deviation from vertical profile was within 30 nm along 20 um depth.

The reported study was partially supported by RFBR, research project 15-07-09290.

1. M. Lyubomirsky, I. Snigireva, S. Kuznetsov, V. Yunkin, and A. Snigirev, Hard x-ray single crystal bi-mirror. Optics Letters, **40**, pp. 2205-2208 (2015).
2. J. Parasuraman, A. Summanwar, F. Marty, P. Basset, D. E. Angelescu, T. Bourouina. Deep reactive ion etching of sub-micrometer trenches with ultra high aspect ratio. Microelectronic Engineering, **113**, pp. 35–39 (2014).

Evolution of structural and optical properties of Si(001) multilayers containing He bubbles by low-temperature annealing

A. Lomov[1], K. Shcherbachev[2], Y. Chesnokov[3], V. Denisov[4], A. Kirichenko[4], A. Miakonkikh[1]

1. Institute of Physics and Technology of Russian Academy of Sciences, Moscow, Russia, E-mail lomov@ftian.ru

2. National University of Science and Technology MISiS, Moscow, Russia, E-mail chterb@mail.ru

3. National Research Centre "Kurchatov Institute", Moscow, Russia, E-mail chessyura@yandex.ru

4. Federal State Budgetary Institution "Technological Institute for Superhard and Novel Carbon Materials", Moscow, Russia, E-mail denisovvn@tisnum.ru

Creation of semiconductor materials with advanced physical properties and engineering of shallow junctions and strained layers with a depth of less than several tens of nm are the main trends for ultra-large scale integration circuits (ULSI) [1]. Nowadays this intention can be realized by forming nanoscale silicon layers in a different phase state by high dose Plasma-immersion ion implantation (PIII) [2] with low energies (0.5-5keV). For modification of structural and electrical properties of semiconductor substrates noble gas ions are very promising [3]. Unfortunately crystal lattice damages and structural defects created during implantation and subsequent annealing change electrical and optical properties of such layers. Metrological control of low-dimension multilayers both fabrication and post technological treatment is required.

In this work we investigated structural changes of He^+ PIII implanted silicon layers after thermal annealing. To study structural evolution of the layers high-resolution X-ray reflectivity (HRXRR), diffraction (HRXRD) and transmission electron microscopy (TEM) were used. Optical properties of the samples were taken by Raman spectroscopy with Renishaw spectrometer in the mapping mode.

Samples 20 × 20 mm^2 in size were cut out from p-type (ρ = 12 Ω cm) Cz-Si(001) wafer. The high-dose ($D = 5\times10^{17}$ cm^{-2}) implantation of He^+ ions was performed at room temperature by applying 10-μs rectangular pulses of negative accelerating potential (2 or 5 kV) with a frequency of 1 kHz in a plasma-immersion low-voltage ion implanter (FTIAN RAN), equipped with an inductively coupled plasma source. After implantation the samples were annealed in vacuum at 580 and 800 °C for 30 min. The structural changes into the sample subsurface layer after implantation and the annealing were studied in vicinity 000, 004 reflection by using a complementary techniques: multipurpose SmartLab (Rigaku Corp.) diffractometer equipped by 9 kW copper rotating anode and TITAN 80-300 transmission scanning electron microscope (FEI, United States).

Our results show that due to PIII treatment multilayer structures consisting of three sublayers (amorphous, buried bubble-porous, defective or deformed) were formed. The structural parameters of as implanted sublayers: thickness (Table 1), profile of density and deformation, He-bubble size in the porous sublayer of the samples were derived.

Table 1. Sublayer thickness of the surface structures versus energy He implantation. L_A - amorphous, L_{BP} - bubble-porous, L_{DS} - with structural defects, L_{DD} - deformed

E, keV	TEM			X-ray		
	L_A, nm	L_{BP}, nm	L_{DS}, nm	L_A, nm	L_{BP}, nm	L_{DD}, nm
5	38(2)	67(3)	53(2)	30-35	75-85	60
2	15(1)	33(3)	42(3)	12-15	25-32	50

Comparison of XRR and HRXRD results showed that the helium filled bubbles located in low-density sublayer at the depth of about R_p is a major source of the tensile strain in the damaged layer. The characteristic bubble size is estimated to be 2–20 nm. The middle bubble size is smaller for low energy implanted sample, what may be explained by remarkable surface influence. Due to thermal annealing tensile strain is changed. Its value is function of PIII and annealing regimes. The Raman spectra were excited with the 532 nm laser line. We have observed the new line at 502 cm^{-1} assigned to nanocrystalline silicon in agreement with the phonon confinement model.

This research was partially financed by RFBR (Grant № 15-07-01228).

1. International Technology Roadmap for Semiconductors (ITRS) 2014 http://www.itrs.net/Links/2014ITRS/

2. W. Ensinger, "Semiconductor processing by plasma immersion ion implantation", Materials science & Engineering A, **253** (1–2), pp. 258–268, 1998.

3. Doyle B.S. et al. "Method of increasing the mobility of MOS transistors by use of localized stress regions" Patent US #6.228.694_B1.

Optical emission 2D-tomography of plasma: case of rectangular two-view scanning and diagonal symmetry of inhomogeneities

A.V. Fadeev, K.V. Rudenko
Institute of Physics and Technology of RAS, Moscow, Russia, rudenko@ftian.ru

Plasma technologies for microelectronics currently are applied to processing 300 mm wafers and should be transferred to 450 mm wafers in future. Lateral homogeneity of the plasma particles density supports the uniform particle fluxes to wafer and makes the process rates (for etch or deposition) uniform on area. The 2D-diagnostics of uncharged chemically active radicals is an issue for industrial-like plasma chambers with limited number of diagnostic ports. It seems that spectrally resolved optical emission 2D-tomography of plasma could solve this problem but it can be implemented only in few-view scanning method.

The few-view tomography task is highly under-determined, so mathematically it is ill-posed problem. Number of attempts (in [1] for instance) have been undertaken to improve few-view reconstruction algorithms. As a rule, those attempts were the modifications of well-known approaches [2] and did not provide the desirable qualities of reconstruction for certain symmetry of inhomogeneities relatively points of view/scanning. To overcome drawbacks of few-view tomography of plasma we have proposed algorithm based on local inhomogeneities model [3]. The 2D-density of particles is represented as the sum of a constant distribution and finite number of non-interacting inhomogeneities of density. Method of local inhomogeneities has good results on the set of tomographic phantoms and in the test experiments.

Strict diagonal inhomogeneities symmetry for two points of view (Fig. 1a) is insoluble in principle because of equal values for beam integrals from scanning sensors for equivalent rectangular cases. Fig. 1b demonstrates the drawbacks of phantom (1a) reconstruction by well-known classical maximum entropy method. However, absolute symmetry is not occurs in practice. Deviations may appear from physical reasons even from the fact that recorded intensity actually depends on the distance from the point radiation sources (plasma particles). This paper shows an opportunity to reconstruct objects with a small deviation of symmetry relative to points of view. In order to do that we have enhanced accuracy of extraction of local inhomogeneities in model [3] by taking into account reducing the intensity from the radiation source with distance, as well as improved the principle of iterative calculations optimization. The result of the tomographic reconstruction with proposed algorithm using rectangular two-view fun beam geometry can be seen in Fig.1c. Initial phantom (Fig. 1a) consists from 3 overlapped Gaussian peaks; stronger of them has clear diagonal symmetry. Fig. 1c shows result of applied algorithm of reconstruction proposed in this study. The reconstruction error does not exceed 1%.

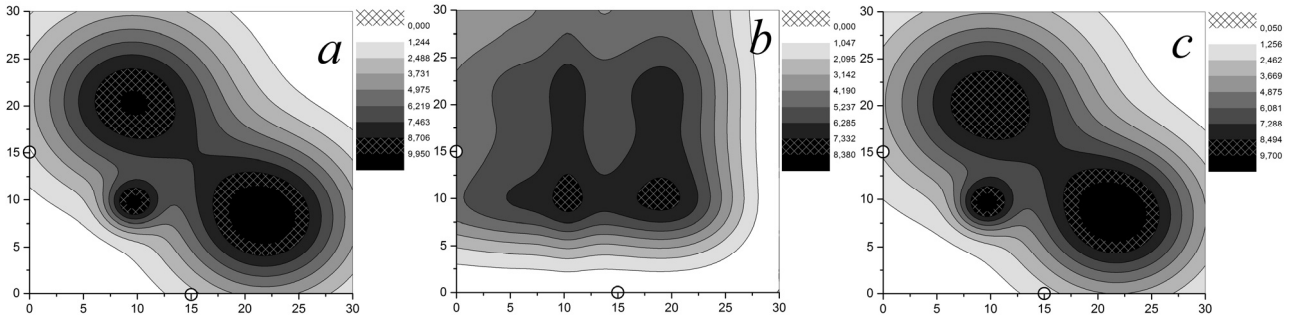

Fig. 1. *a*) initial tomography phantom, *b*) maximum entropy technique reconstruction, *c*) reconstruction with proposed algorithm (error = 0.4%). ○ - positions of points for fan-like scanning.

1. N.V. Denisova. "Two-view tomography". J. Phys. D: Appl. Phys, **33**, pp. 313–319, 2000.
2. G.T. Herman. *Image reconstruction from projections*. Academic Press. New York, 1980.
3. A.V. Fadeev and K.V. Rudenko. Investigation of the BF_3 Plasma Particle's Lateral Distribution Using Two-View Emission Tomography". Russian Microelectronics, **43**, pp. 407–412, 2014.

Two methods of improving dopant contrast for semiconductor structures under thin surface layers in scanning electron microscope

E. Rau[1], A. Tatarintsev[1, 2], S. Kupreenko[1], V. Karaulov[3], S. Kolybin[3]
1. Moscow State University, Moscow, Russia, E-mail: rau@phys.msu.ru
2. Institute of Physics and Technology of RAS, Moscow, Russia
3. JSC "NPO Sernia", Moscow, Russia

The development of modern nanotechnology requires of adequate accompanying diagnostic parameters and physical properties of submicron device structures. High-local methods of scanning electron microscopy are becoming more popular for this purpose. Methods of measuring the degree of doping and the spatial distribution of implanted impurities in semiconductor crystals are great of interest [1-3]. It is necessary to determine the type and concentration of impurities in the range of 10^{16}-10^{20} cm^{-3} with a spatial resolution of nanometers to tens of nanometers.

Studied structures usually are covered with thin dielectric coatings or surface contamination layers. All of these factors decrease already weak contrast. Dopant mapping of such structures and explanation of contrast mechanisms are main problems of this work.

Task of dopant visualization can be solved by two methods. The first is based on detection of energetically filtered secondary electrons by toroidal electron spectrometer [1]. The second one is based on scanning mirror electron microscopy [4].

Images of test sample, which is a n-type silicon wafer with locally doped regions with p-type impurity (impurity concentration is 10^{18} cm^{-3}), are depicted on Fig. 1. Energy filtration of secondary electrons increases dopant contrast to values of about 40 % (Fig. 1a), what is the record in scanning electron microscopy. But sample covered with oxide film (20 nm of SiO_2) demonstrate poor contrast (Fig. 1b). We will discuss this artifact in our report for the purpose of choosing suitable method of dopant mapping.

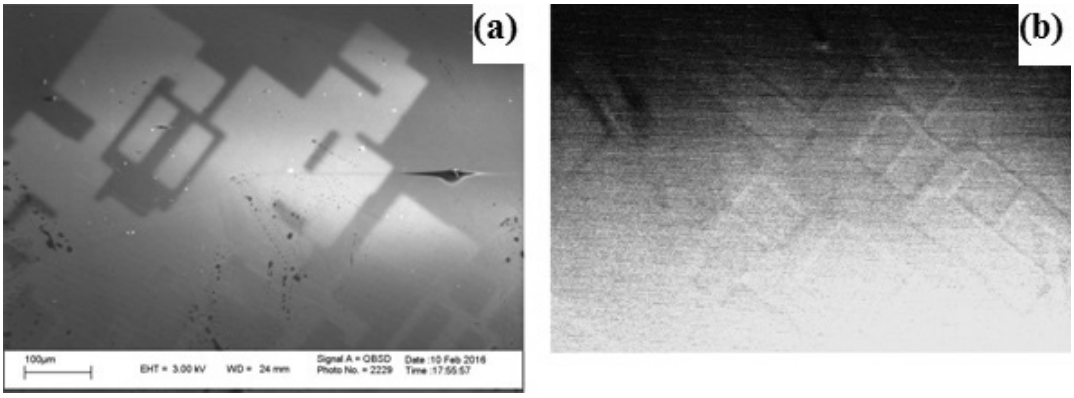

Fig. 1 Images of test sample (a) and the same sample covered with oxide film (b)

This work was funded thanks to the support of RFBR (grant 15-02-01557)

1. M. El-Gomati, F. Zaggout, H. Jayacody, S. Tear, K. Wilson. "Why it is possible to detect doped regions of semiconductors in low voltage SEM: a review and update". Surf. Interface Anal., **37**, pp. 901-911, 2005.
2. C. Rodenburg, M.A.E. Jepson, E.G.T. Bosch, M. Dapor. "Energy selective scanning electron microscopy to reduce the effect of contamination layers on scanning electron microscope dopant mapping". Ultramicroscopy, **110**, pp. 1185-1191, 2010.
3. A.V. Gostev, N.A. Orlikovskii, E.I.Rau, A.A. Trubitsyn. "Updating of the toroidal electron spectrometer intended for a scanning electron microscope". Technical Physics, **58**, 3, pp. 447-454, 2013.
4. G.V. Spivak, V.P. Ivannikov, A.E. Luk'yanov, E.I. Rau. "Development of scanning mirror electron microscopy for quantitative evaluation of electric microfields". J. Microsc. Spectrosc. Electron., **3**, pp. 89-100, 1978.

Reduction in protrusion width values under scanning in a low voltage SEM

Yu.V. Larionov[1], Yu.V. Ozerin[2]
1. A.M. Prokhorov Institute of General Physics, Moscow, Russia, luv@kapella.gpi.ru
2. JSC Mikron, Zelenograd, Russia, yozerin@mikron.ru

Protrusions in a material linewidth measure for SEM are subjected to multiply and frequently durable scanning. An important requirement for measure protrusions is geometric parameter constancy in time. However protrusion width is able to increase due to formation of contamination film on its surface even in a high vacuum SEM. Our work discovered that a protrusion width value is able to decrease as a result of multiply consecutive scannings in a low voltage and high vacuum SEM.

The phenomenon is investigated using a test- object similar to MShPS-2K measure (with a gentle sloping structures) in a S4800 SEM and polysilicon protrusions with almost vertical slopes in a S9260A SEM. Results are presented on Fig. 1A and 1B.

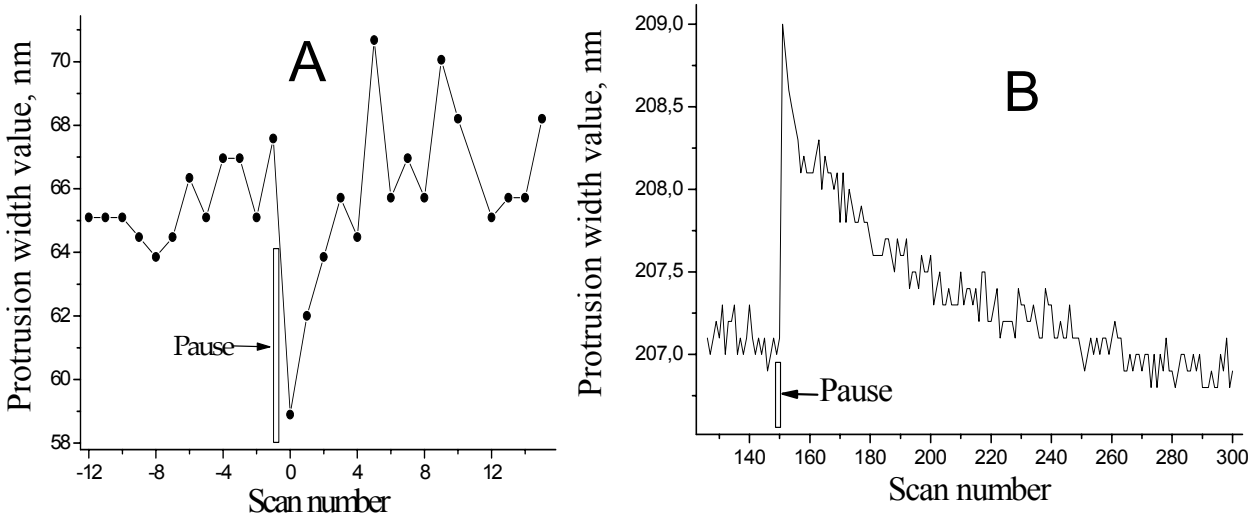

Fig. 1. Width size variations under consecutive scannings for a gentle sloping structure (A) and with almost vertical slopes (B).

One can see size jumps in consecutive scans after pauses followed by slow variations in size. The pause duration is as long as some minutes. We attribute the protrusion width value changes to a known phenomenon of structure size variation due to inducing electric charges under this structure surface [1]. The reduced width values of polysilicon and silicon protrusions after pauses in irradiation demonstrate phenomenon versatility and different characters of curves in Fig. 1 testify that different structure geometries and surface state influence the curve form. The surface state is shown to change its properties as a result of surface clean procedure.

The discovered size changes are comparable with the maximum permissible error of protrusion width value for MShPS-2K measure (±2 nm, [2]).

1. Y.-Uk Ko et al, "Monte Carlo Simulation of Charging Effects on Linewidth Metrology", Scanning, **20**, pp. 447-455, 1998.
2. *Certificate on pattern approval of measuring instrument,* RU.C. 27.010. A №26441, pp.1-4, Federal Agency on Tech. Reg. and Metrology, Moscow, 2012.

Determination of mechanical stress in the silicon nitride films with a scanning electron microscope

N. Dyuzhev, E. Gusev, A. Dedkova, N. Patiukov
National Research University of Electronic Technology, 124498, Moscow, Zelenograd, Shokina square, 1,
bubbledouble@mail.ru

Contemporary techniques of mechanical stress measurement are based on wafer bending detection (such as profilometry), or evaluation of lattice parameters (X-ray diffractometry, transmission electron microscopy). In this paper we suggest a method of determining a value of mechanical stress in thin films of various materials, that is based on visual analysis of thin film fragment after it's been released from substrate. Algorithm for determining stress in MEMS structures with a SEM includes developing layout, preparation of structures, measuring linear dimensions of film fragment before and after removal of the substrate, and stress analysis by Hooke's law. Balk structure geometry is shown in figure 1.

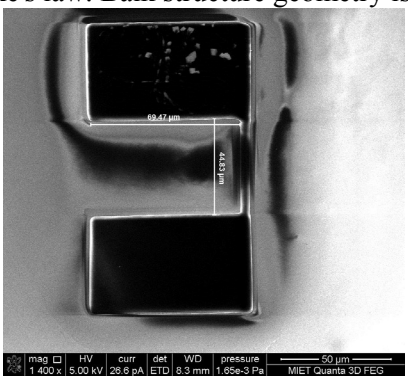

Fig. 1. Geometry of the formed balk structure.

During the process flow after removal of underlayer, film fragment is released, and structure will compress or stretch depending on the sign of mechanical stress. Consequently, the value of the gap between periphery and edge of the balk is changed. Formula (1) [1] is used to calculate mechanical stress:

$$\sigma = -\frac{L - L_0}{L} \cdot \frac{E_f}{1 - \mu_f} \qquad (1)$$

where L is the length of free end of the balk after the extension/compression, L_0 is initial length of balk, μ_f is the Poisson's ratio of the film, E_f is the Young's modulus of the film.

Preparation of structures was carried out using a focused ion beam. Measurements of mechanical stress in silicon nitride with developed method gives the value of- 1.64 GPa, the relative error is 1.2%. The numerical value of mechanical stress correlate well with data obtained by wafer bending measurement using profilometer [2] and other methods. It is proved that bending of balk structure based on Si_3N_4 is insignificant for the described method.

Method can be used for various materials that are being used in MEMS technology. There are several advantages that used technique of preparing test structures is providing: silicon etching time is significantly reduced by replacing wet etching [1, 3] with plasma chemical etching; use of maskless lithography (focused ion beam) allows you to locate the area of stress measurement and research on operating wafers.

Research is executed on the equipment CCU MCT and ECB MIET with support of the RF Ministry of Education GK № 14.578.21.0007 (RFMEFI57814X0007)

1. Conru H.W. Measuring small area Si-SiO_2 interface stress with SEM. J. Appl. Phys., **47** (5), pp. 2079-2081, 1976.
2. N.A. Dyuzhev, A.A. Dedkova, E.E. Gusev, A.V. Novak. Method measurement mechanical stress in thin films on wafer using an optical profilometer. Proceedings of the universities. Electronics. 2016, №4 (in Russian).
3. S.C.H. Lin and I. Pugacz-Muraszkiewicz. Local stress measurement in thin thermal Si-SiO_2 films on Si substrates. J. Appl. Phys., **43** (1), pp. 119-125, 1972.

Extraction of differential inverse inelastic mean free paths in solids from electron energy loss spectra

V. Afanas'ev[1,2], A. Gryazev[1], D. Efremenko[3], P. Kaplya[1]
1. National Research University "Moscow Power Engineering Institute", Moscow, Russia, GryazevAS@gmail.com
2. Joint Institute for High Temperatures of the RAS, Moscow, Russia, v.af@mail.ru
3. Deutsches Zentrum für Luft- und Raumfahrt (DLR), Institut für Methodik der Fernerkundung (IMF), Oberpfaffenhofen, Germany

Knowledge of differential inverse inelastic mean free paths (DIIMFPs) in solids is of utmost importance for surface analysis by means of electron spectroscopy. It is quite challenging to compute this quantity from basic physical principles since the *many-body quantum theory* should be involved. In this regard, it seems to be more feasible to extract information on DIIMFPs by filtering out multiple scattering signal from electron energy loss spectra. In this work, we are particularly focused on DIIMFP retrieval from reflected electron energy loss spectra (REELS) and photoelectron spectra (PES).

The extraction of cross-sections from the multiple scattering signal is a severely ill-posed deconvolution problem [1]. Direct numerical deconvolution algorithms usually fail to get physically relevant DIIMFPs. To obtain numerically stable results, a new retrieval algorithm is designed in which the DIIMFPs are parametrized on the base of linear respond theory. Unknown parameters of the model are found by means of the fitting procedure which minimizes the residual between simulated spectra and measurements. For simulating energy loss spectra, an efficient forward model based on the invariant imbedding method is developed. The partial intensities of k-fold inelastically scattered electrons are found as solutions of the Riccati and Lyapunov equations. This technique is validated against Mote-Carlo simulations and yields accuracy below 0.5 % in partial intensities. The computational time for generating a set of 1000 electron spectra does not exceed 2 minutes on Intel Xeon E5-1620 3.60 GHz. Thus, the fitting procedure is quite robust and the performance of the forward model is not really an issue for the retrieval.

In addition, we reexamine the concept of the surface excitation parameter (SEP) [2, 3] which is used to account for surface plasmons. A multilayer model [4, 5] is adopted for a consistent description of inelastic energy losses as well as multiple scattering processes in bulk and surface layers. It is shown that the multilayer model is efficient for interpreting electron energy spectra for transition metals, e.g. Nb. According to theory developed by Ritchie [6], the number of layers corresponds to the number of surface excitation frequencies (plasmons) while the layer thicknesses are inversely proportional to the respective frequencies. These relations are used as additional constrains in the retrieval procedure. This model is applied for analyzing both REELS and PES. Good agreement is found between DIIMFPs of Nb retrieved from REELS and PES, which shows the consistency and numerical stability of the retrieval algorithm.

1. V.A. Tikhonov, V.Ja. Arsenin. *Method of the solution of incorrect problems*. Nauka, Moscow, 1986.
2. K. Salma, Z.J. Ding, H.M. Li, Z.M. Zhang. "Surface excitation probabilities in surface electron spectroscopies". Surf. Sci., **600**, pp. 1526-1539, 2006.
3. M.R. Went, M. Vos, W.S.M. Werner. "Extracting the Ag surface and volume loss functions from reflection electron energy loss spectra". Surf. Sci., **602**, pp. 2069-2077, 2008.
4. V.P. Afanas'ev, O.Yu. Golovina, A.S. Gryazev, D.S. Efremenko, P.S. Kaplya, "Photoelectron spectra of finite-thickness layers". J. Vac. Sci. Technol. B, **33**, pp. 03D101, 2015.
5. V.P. Afanasyev, D.S. Efremenko, A.V. Lubenchenko, M. Vos, M.R. Went. "Extraction of cross-sections of inelastic scattering from energy spectra of reflected atomic particles". Bull. Russ. Acad. Sci.: Phys. **74**, pp. 170-174, 2010.
6. R.H. Ritchie. "Plasma Losses by Fast Electrons in Thin Films". Phys. Rev. **106**, pp. 874-881, 1957.

Reflected electron spectroscopy for depth profiling

V. Afanas'ev[1,2], Yu. Andriyanova[1], A. Gryazev[1], P. Kaplya[1]
1. National Research University "Moscow Power Engineering Institute", Moscow, Russia, GryazevAS@gmail.com
2. Joint Institute for High Temperatures of the RAS, Moscow, Russia, v.af@mail.ru

Development of quantitative methods of surface analysis is important task of electron spectroscopy. Qualitative methods of surface composition determination such as Auger electron spectroscopy and X-Ray photoelectron spectroscopy are well known. These methods are based on the assumption of exact correlation between quantity of the element atoms in the surface with the elastic peak intensity formed by electron which didn't experienced inelastic scatterings [1]. The inaccuracy of such methods is too large to treat them as quantitative [2]. The only we to determine the quantity of the atoms in the surface is to investigate the energy loss range of about 100-150 eV near the elastic peak [2].

Proposed method isn't limited by energy analyzer precision [3-5], based on the analysis of samples in a wide energy range [3] and leads to up to sub-monolayer accuracy of layer thickness determination.

The most precise results for sputtered surface layer profiling can be achieved if one can measure reflected electron spectra for the semi-infinite homogeneous layer of the surface material by itself and the substrate [3]. The described method can be generalized for the multilayer structures of thee and more layers.

The goal of the current work is to develop the universal method of depth profiling using reflected electron spectroscopy. The thickness of the surface layer is determined by the fitting procedure. The data for the differential elastic and inelastic cross-sections is needed for the fitting procedure to execute. Differential elastic cross-section data can be found in NIST database, but not the inelastic cross-sections. The other goal of the work is to develop method of reconstruction the differential inelastic cross-sections from the reflection electron spectroscopy experiments.

The research is focused on the creation of the new and development of the common depth profiling techniques. Comparison of the theoretical and experimental results of depth profiling is presented.

1. S. Hofmann. *Auger- and X-Ray Photoelectron Spectroscopy in Materials Science.* Springer, Berlin/Heidelberg, 2013.
2. S. Tougaard, "Surface nanostructure determination by X-ray photoemission spectroscopy peak shape analysis". J. Vac. Sci. Technol. A, **14**(3), pp. 1415-1423, 1996.
3. V.P. Afanas'ev, D. Naujoks. "Energy spectra of electrons reflected from layered targets". Z. Phys. B Cond. Mater., **84,** pp. 397-402, 1991.
4. V.P. Afanas'ev, A.V. Lubenchenko, M.V. Lukashevsky, M. Norell, A.B. Pavolotsky. "Study of Al/Nb interface by spectroscopy of reflected electrons". J. Appl. Phys., **101**, 064912, 2007.
5. E.I. Rau, S.A. Ditsman, S.V. Zaitsev, N.V. Lermontov, A.E. Luk'yanov, S.Yu. Kupreenko. "Analysis of Formulas for Calculating the Main Characteristics of Backscattered Electrons and How They Compare to Experimental Results". Bull. Russ. Acad. Sci.: Phys. **77**, pp. 951-958, 2013.

Method of stress and measurement modes for research of thin dielectric films of MIS structures

V.V. Andreev[1], V.V. Maslovsky[2], D.V. Andreev[1], A.A. Stolyarov[1]

1. Bauman Moscow State Technical University, Kaluga branch, Bazhenov St. 4, 248600, Kaluga, Russia, E-mail: vladimir_andreev@bmstu.ru

2. Institute of Physical Problems, proezd 4806, 6, 103460, Moscow, Russia, E-mail: acdmaslovsky@mail.ru

One of the major methods to observe the quality of thin dielectric films of MIS structures under stress conditions are the methods based on high-field injection of electrons into dielectric [1–3]. These methods are widely used for research of degradation processes, charge effects, and defectiveness of dielectric films. Besides, they are used to evaluate the stability of dielectric films to high-field, radiation, and other stress conditions. When usage of these methods, high-field injection of charge usually is realized in conditions of constant current or constant voltage maintenance. At the same time, a change of MIS structure charge state is monitored by using the time dependence of voltage or current on current or voltage, respectively [1]. Therefore, an increasing of information capability and accuracy of these methods is an important problem of modern micro- and nanoelectronics especially when control of thin high-k dielectric films and stacks based on such dielectrics.

In this paper, we introduce new method of stress and measurement modes to research thin dielectric films of MIS structures. This method suggests that the main injection of charge into gate dielectric is realized during stress modes at which maintenance of constant current, flowing through dielectric, or constant voltage, applied to the gate, takes place. In order to acquire an additional information about change of MIS structure charge state, the process of stress injection is interrupted in certain time and MIS structure observed is switched to measurement mode. In measurement mode, we monitor changes of electrical fields at the dielectric/semiconductor and dielectric/gate interfaces, by using of which we calculate density of charge accumulated, centroid of charge accumulated, observe generation and relaxation processes in dielectric. In order to improve accuracy of the method and reduce influence of switch effects in measurement mode, density of measurement current should be much less than density of stress current. Account of processes of MIS structure charging and processes of trapping of charge in MIS structure gate dielectric enables highly increase metrological characteristics of the method and reduce errors, which taking place when determination characteristics of MIS structures. We developed models, which describe a change of charge state of MIS structures in both charging of capacitance and charge injection modes. Use of these models allows to choose an optimal algorithm of stress influence and to improve accuracy of measurements.

The proposed method, assuming receipt of the C-V [2, 3] and I-V characteristics, allows to control the parameters of the charge degradation immediately after the high-field stress injection. That reduces the influence of relaxation processes. Special test setup is developed for realization of the method. This method is used for quality control of thin dielectric films of different MIS structures, including high-k dielectrics and dielectric stacks.

1. JEDEC Standard, JESD35–A: Procedure for the Wafer–Level Testing of Thin Dielectrics. (2001).
2. V.V. Andreev, G.G. Bondarenko, V.M. Maslovsky, A.A. Stolyarov. "Multilevel current stress technique for investigation thin oxide layers of MOS structures". IOP Conf. Series: Materials Science and Engineering, **41**, 012017(pp. 1-6), 2012.
3. V.V. Andreev, G.G. Bondarenko, V.M. Maslovsky, A.A. Stolyarov, D.V. Andreev. "Control current stress technique for the investigation of gate dielectrics of MIS devices". Phys. Status Solidi C. **12**, pp. 299–303, 2015.

Classification Automation of Thermoplastic Particles in a Cured Epoxy Matrix According to Their Size on Microscopic Images

Victoria A. Sablina[1], Alexander N. Varnavsky[1], Andrei N. Varnavsky[2]
1. Ryazan State Radio Engineering University, Ryazan, Russia, sablina.v.a@evm.rsreu.ru
2. M.V. Lomonosov Moscow State University, Moscow, Russia, varnavskii.a.n@gmail.com

Microscopy images have wide applications for carrying out various scientific researches of organic and inorganic material characteristics. In particular, the scientific interest is the study of the structure of the cured epoxy matrix modified thermoplastics by microscopic images, obtained with a scanning electron microscope. This paper is dedicated to process automation of processing and analysis of such image.

The aim is to development the method for automatic classification of thermoplastic particles in a cured epoxy matrix according to their size on microscopic images obtained using a scanning electron microscope.

An example of a microscopy image for experiments is represented in Figure 1, a.

To determine characteristics of the investigated material it is required to establish the presence or the absence of the particles there, their number and parameters. In this case we considered for existing particles the task of classification by their size in the microscopy image. To solve the assigned task we need to implement digital image processing methods and algorithms [1]. Image processing is done in several stages, i.e. the selection of the objects in the microscopy image, the determination of occupied area for each object, the distribution of the objects to classes by size. The experiments are carried out in MATLAB®. The result of the particle classification by size for the microscopy image in Figure 1,a is represented in Figure 1, b.

In Figure 1,b the classification result is visualized using pseudocolors: small particles are highlighted by the cold colors, big particles are highlighted by the warm colors. The computation of the threshold to perform the image segmentation to the desired objects and the background is executed using the Otsu's method [2].

As the main classification parameter the area occupied by an object in pixels is selected. The size distribution histogram for the particles (except very large particles) is represented in Figure 1, c. In the analyzed image 2113 objects were found. These objects were divided into 6 classes depending on the size. Numbers and rates of the objects for each class are represented in Table 1.

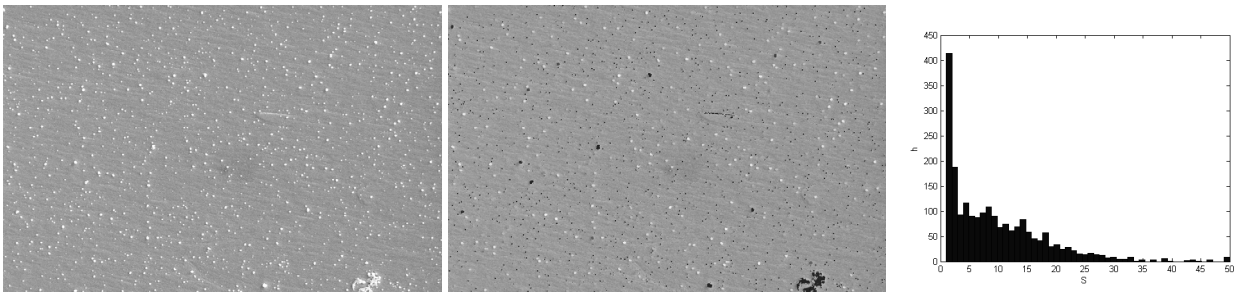

a b c

Figure 1. Particle classification by size:
a – an original epoxy microscopy image; b – the classification result; c – the particle size distribution histogram

Table 1. Particle size classification result

Object area in pixels	1 to 10	11 to 20	21 to 30	31 to 40	41 to 50	More than 50
Object number	1350	552	162	31	9	9
Object rate	63,9 %	26,1 %	7,7 %	1,5 %	0,4 %	0,4 %

So we can notice in the given specimen the big rate of the small size particles, the fewer rates of the average size particles and quite a little rate of the large size particles. In further work it is advisable to continue this research to implement an automatic intellectual comparative analysis of the epoxy specimen images acquired from the scanning electron microscope.

1. R.C. Gonzalez, R.E. Woods, and S.L. Eddins, *Digital Image Processing Using MATLAB*, 2nd ed., 827 p., Gatesmark Publishing, Knoxville, TN, 2009.
2. N. Otsu, "A Threshold Selection Method from Gray-Level Histograms," IEEE Transactions on Systems, Man, and Cybernetics, 1979, **9** (1), pp. 62-66.

Plasma parameters and active species kinetics in $CF_4/O_2/Ar$ gas mixture: Effects of CF_4/O_2 and O_2/Ar mixing ratios

J. Lee[1], K.-H. Kwon[2], A. Efremov[3]

1. Korea University, Sejong, South Korea, lee_jm@korea.ac.kr

2. Korea University, Sejong, South Korea, kwonkh@korea.ac.kr

3. Ivanovo State University of Chemistry & Technology, Ivanovo, Russia, amefremov@yandex.ru.

Various fluorocarbon (FC) gases are widely used in the microelectronic industry for the dry patterning of silicon and silicon-based dielectrics (SiO_2, Si_3N_4). In most of the existing processes, these gases are combined with Ar or O_2 in a form of binary gas mixtures with the aim of accelerating the physical etching pathway, increasing the F atoms' yield and suppressing polymerization. Recently, many dry etching processes require optimization in order to satisfy the increasing requirements to both device dimensions and performance. Particularly, the three-component (or ternary) gas systems provide more pathways to change the gas mixing ratios and thus to achieve the optimal process conditions. For example, for the $FC/O_2/Ar$ has mixture, one can one can fix the fraction of one component, but change the mixing ratios of the remaining two gases. Since the composition of the feed gas in each case appears to be different compared with the conventional FC/Ar or FC/O_2 mixtures, some principal differences in plasma parameters and densities of plasma active species can take place.

The goal of this work was the study of $CF_4/O_2/Ar$ inductively coupled plasmas with an aim of understanding how the CF_4/O_2 and O_2/Ar gas mixing ratios influences on the plasma parameters and densities of active species. The focus was on the parameters directly connected with the dry etching mechanisms, such as the ion energy flux, F atom density, and the CF_x (x =1-3) radical density.

The experiments were carried out in a planar inductively-coupled 13.56 MHz plasma reactor. The process conditions were: total gas flow rate (q) of 40 sccm, gas pressure (p) of 4–10 mTorr, input ICP power (W) of 800–900 W and bias power (W_{dc}) of 150–200 W. Langmuir probe diagnostics provided the data on electron temperature (T_e), ion current density (J_+) and total positive ion density (n_+). The relative changes in densities of some neutral species were controlled by optical emission spectroscopy via I/I_{Ar} ratios. In order to determine the absolute densities and fluxes of plasma active species, the simplified global (zero-dimensional) plasma model operating with volume-averaged plasma parameters and a Maxwellian approximation for the electron energy distribution function was applied. The model directly involved the experimental data on T_e and n_+ as input parameters. The feed gas mixture compositions were set by adjusting the partial gas flow rate of the components within p = const. In one experimental series, we kept the constant 50% fraction of Ar, but varied the ratio between O_2 and CF_4 within the remaining 50%. Therefore, the variation of O_2 content in a feed gas in the range of 0–50% corresponded to the transition between CF_4/Ar and O_2/Ar gas systems. Another experimental series assumes the constant 50% fraction of CF_4 and the variable fractions of O_2 and Ar. Accordingly, the variation of O_2 content in a feed gas in the range of 0–50% corresponded to the transition between CF_4/Ar and CF_4/O_2 gas systems.

It was found that the change of CF_4/O_2 mixing ratio in $CF_4/O_2/Ar$ plasma results in the non-monotonic (with a maximum) change in F atom density, as was repeatedly mentioned for the binary CF_4/O_2 as system. The reasons are 1) the concurrence between the decreasing density of CF_4 molecules and increasing their dissociation degree due to the atom-molecular processes involving O and $O(^1D)$ and 2) the non-monotonic densities of fluorine-containing reaction products, such as CF_xO_y and F_2, which contribute the total F atom formation rate through electron-impact dissociations. At the same time, the change in O_2/Ar mixing ratio at constant fraction of CF_4 in a feed gas do not result in the non-monotonic effects in the F atom formation rate and thus, leads to monotonically increasing F atom density. In both cases, the ratio between the fluxes of polymerizing species (CF_x radicals with more than 2 free bonds) and O atoms decreases toward more oxygenated plasmas. This directly means the suppressing of surface polymerization. The above data on plasma parameters and composition were clearly confirmed by the etching experiments for Si and SiO_2. The differences in the etching kinetics for both Si and SiO_2 were analyzed.

Technology for fabrication of sub-20 nm Silicon planar nanowires array

A. Miakonkikh, A. Tatarintsev, A. Rogozhin, and K. Rudenko
Institute of Physics and Technology of Russian Academy of Sciences, Moscow, Russia, miakonkikh@ftian.ru

Silicon one-dimensional structures are perspective for application in nanoelectronic devices like nanoscale field effect transistor, solid state structures for quantum computing, photonics and for THz applications.
Precision of modern plasma etching technologies allows forming Silicon structures with critical dimensions as low as 10 nm, but defects produced by ion bombardment during etching lead to significant decrease of carrier mobility in silicon nanostructure even at walls faced along ion flux from plasma. That is why we employ three technology steps sequentially: precise plasma etching of Silicon over e-beam resist by highly selective process, thermal oxidising of surface layer, and then removal of oxidised defected layer by selective wet etching. The thickness of oxide layer was additional parameter for tuning final diameter of Silicon nanowires.
At first we developed a process for Si nano-fin fabrication on SOI substrate Si(50 nm)/SiO_2(200 nm)/Si. Hydrogen silsesquioxane (HSQ) XR-1541 resist was used as a negative-tone electron beam resist with good etch-resistance, high resolution and high mechanical stability. Lithography process was held on Raith 150 EBL system with 30 kV acceleration voltage. This process was optimized to produce mask with critical size up to 11 nm with e-beam size ~1 nm. Samples with developed resist were baked at ambient for 30 min at 400 °C, which significantly improves selectivity of Silicon etch process respectively to resist. Longer annealing did not show any improvements.
Plasma etching was performed in RIE tool PlasmaLab 100 (OIPT, UK) in mix of SF_6 and C_4F_8. By changing the ratio SF_6:C_4F_8, the sidewall profile angle have been controlled thoroughly. Increasing the ratio improves the etch rate, reduces the selectivity, and decrease profile angle. Increasing the forward power again reduces the selectivity with a slight improvement in etching rates. Gas mixture composition was optimized in separate experiment to obtain vertical profile of sidewalls for fins, and was 5:9 SF_6:C_4F_8. This process allows achieving the selectivity of Silicon etching over XR-1541 resist up to 14 [2]. Process was preliminary investigated on bulk silicon (Fig. 1) and SEM reveals no undercut and deviations from vertical walls. Then process was adopted for SOI structures without noticeable notch effect.

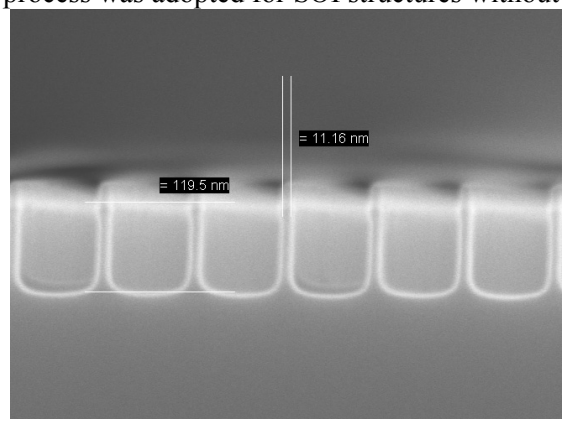

Fig. 1. Cross-sectional SEM of 11 nm Si-fins with the remaining resist after RIE.

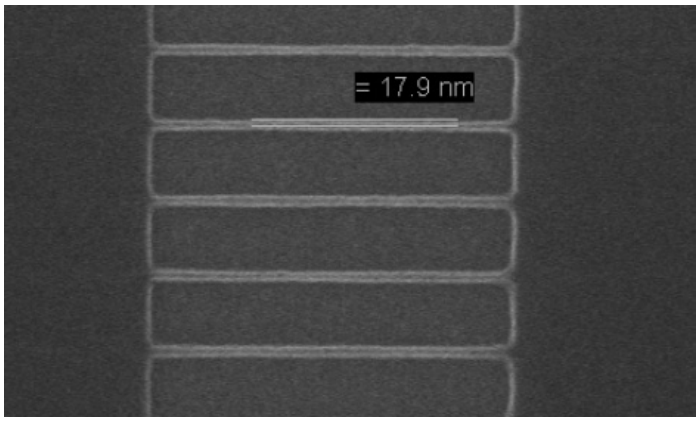

Fig. 2. Final structure of planar Si-nanowires diameter of 18 nm on SOI substrate.

Oxidation of Si-fins was performed in AnnealSys AS-One tool with controlled flow of dry oxygen and water vapour. Oxidation rate was precisely controlled by ex-situ spectral ellipsometry. Resulting Si-nanowires are shown at Fig. 2
The reported study was partially supported by RFBR, research project 16-29-09510.

1. Yang J.K.W., Berggren K.K. J. Vac. Sci. Tehcnol. B, **25** (6), p. 2025, 2007.
2. I.P. Ivanenko, V.A. Kalnov, A.V. Miakonkikh et al. Int.Conf. "Micro- and nanoelectronics - 2014" (ICMNE-2014). Book of Abstracts. Moscow. October 6th-10th, 2014. p. O1-13

Cellular-automata model of oxygen plasma impact on porous low-K dielectric

A. Rezvanov[1, 2*], I.V. Matuyshkin[2, 3], O.P. Gutshin[2]
1. Moscow Institute of Physics and Technology, Dolgoprudny, Russian Federation
2. Molecular Electronics Research Institute, Moscow, Russian Federation
3. National Research University of Electronic technology, Moscow, Russian Federation
** arezvanov@mikron.ru*

One of the most common low-K dielectrics are porous organo-silica glasses (SiOCH), which are widely use in technological nodes beyond 45 nm [1, 2]. During some operations in back-end-of-line (BEOL) interconnect technological flow the low-K materials undergo plasma exposure. In particular, one of the most crucial steps is the photoresist stripping in oxygen plasma. Oxygen atoms deep penetrate into pores and replace hydrophobic methyl groups by hydrophilic OH-groups [3]. As a result, the k-value and leakage current are dramatically increasing (growth about 30%) [4]. The present work investigates the imitative simulation of this system, which allows predicting the oxygen atoms penetration depth into pores of low-K at given conditions and also to determine the change in the intrinsic permittivity.

In our model, we restrict ourselves in consideration of one isolated pore, which is simulated by cylinder with length L = 200 nm and radius R = 1 nm, ignoring the curvature factor. The model is the interaction of a pair of cellular-automata, the first one is 1D, which locates in the middle of cylinder and represents a pool of molecules inside the pore volume. The second automaton is 2D with a hexagonal grid, which is rolled on the surface of the cylinder, and simulates the surface diffusion processes (taking into account the activation thermokinetic) and chemisorption interaction in the discrete atomic level. The reaction process of oxygen atoms with methyl groups is considered by two-steps mechanism [5]:

$$\begin{aligned} O + CH_3Si &\rightarrow OH + CH_2Si + P^*,\ k_1 = 5*10^{-18} cm^3/s, \\ O + CH_2Si &\rightarrow CH_2O + Si,\ k_2 = 8{,}4*10^{-11} cm^3/s. \end{aligned} \quad (1)$$

The space step is 6 Å, which is characteristic to the distance between the adjacent methyl groups on the pore surface. The mathematical model is intermediate between the quantum-chemical and continuous approaches, thus it is not necessary to use a small time step. Therefore, the time step was selected as 10^{-6} s. The simulation was performed for 2 million steps of automaton, which corresponds to 2 seconds of the real process time. The first results show, that the number of oxygen atoms in the 1D automaton (depot) lineally reduces with depth. Behavior of the average quantity (on the belt of automaton) of O atoms in 2D automaton with penetration depth indicates, that with the increasing of exposure time the number of oxygen atoms in pore surface layer increases considerably (the maximum at depth about 8 nm), followed by a monotonic decrease with depth. Extrapolating the results to the long time, more and more -OH groups will replace by $-CH_3$ groups, and over time almost all methyl groups will leave the pore surface (at 2 seconds of the real process time on the first 40 nm depth is present no more than 20% of the initial quantity). However, at the same time the formation of free silicon bonds will occur.

As a conclusion, at physically proven parameters the assumption that during the exposure degree of chemical transformation does not reach unity has been confirmed. Moreover, the possibility of transformation of Si-CH_3 groups not only in Si-OH groups, but also in dangling Si- bonds, which concentration increases, has been shown.

References

1. G.Ya. Krasnikov. *Structural and technological features of submicron MOSFETs*. Part 2. Moscow, 2011 (in Russian).
2. K. Maex et al. J. Appl. Phys., **93**, p. 8793. 2003.
3. E. Kondoh et al. J. Vac. Sci. Technol. *B*, **18**, p. 1276, 2000.
4. M. Darnon et al. J. Vac. Sci. Technol. *B*, **26**, pp. 1964-1970, 2008.
5. O.V. Braginsky et al. J. Appl. Phys., **108**, p. 073303, 2010.

Low-damage plasma etching of porous low-k films in CF_3Br and CF_4 plasmas under low-temperature conditions

A. Miakonkikh[1,2], I. Clemente[1,2], A. Vishnevskiy[3], K. Rudenko[1,2], M. Baklanov[4]

1. Institute of Physics and Technology Russian Academy of Sciences, Moscow, Russia

2. Moscow Institute of Physics and Technology, Dolgoprudny, Russia

3. MIREA, Moscow, Russia

4. IMEC, Leuven, Belgium

Low-damage (LD) plasma etching is one of the key challenges for successful integration of porous low-k dielectrics in advanced interconnects. Plasma processing degrades the low-k properties because of impact of chemically active radicals, ions and VUV photons. Increase of the k-value is caused by film densification, changes in chemical composition and bonds configuration, i.e. destruction of $Si-CH_3$ bonds, forming dangling bonds and the following moisture adsorption [1].

This paper presents the results of cryogenic plasma etching of ultra low-k (ULK) films in CF_3Br and CF_4 plasma. The first gas, CF_3Br, form a plasma with low F* concentration, the main plasma species are CF_3* and Br* in neutral and ionized forms. The low volatile byproducts ($SiBr_xF_y$ etc) can condense in the pores protecting ULK film against the plasma damage. The second gas, CF_4, forms fluorine rich plasma and no formation of low volatile compounds is expected. However, this plasma contains high concentration of CF_2 radicals that can form fluorocarbon polymers on porous low-k surfaces and to prevent the penetration of F* radicals. These two approaches are compared experimentally.

200 nm thick organosilicate (OSG) films were spin-on deposited on Si wafer and thermally cured at 400°C. The etch process was performed in dense remote ICP plasma with controlled biasing and with wafer temperature range -100÷0 °C. The etch rates of low-k films and their refractive indices were measured by spectral ellipsometry. The chemical bonds in low-k films were monitored by Fourier transform infrared spectroscopy (FTIR), and the changes in porosity and hydrophilic properties by ellipsometric porosimetry.

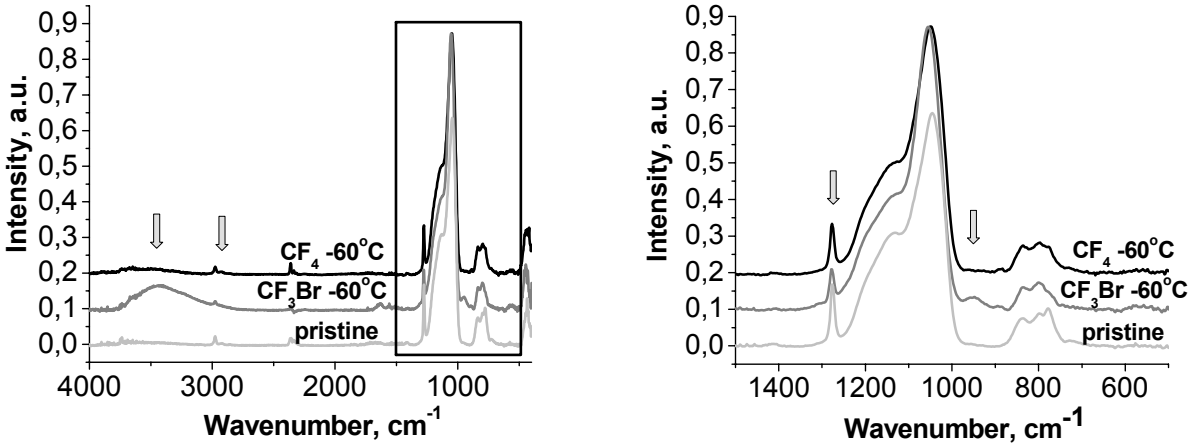

Fig. 1. FTIR spectra of ULK films plasma after the etching in CF_3Br and CF_4 plasmas and annealing.

Fig. 1 shows the change of chemical composition during the etching and the following thermal annealing. The pristine sample has a structure typical for OSG with strong absorption peak at 1050-1100 cm^{-1}, which corresponds to Si-O-Si vibrations. An important feature of OSG low-k materials is the presence of hydrophobic $Si-CH_3$ groups (around 1270 cm^{-1}) and CH_x groups (2800-3000 cm^{-1}).

Analysis of the presented results allows us to conclude that both types of cryogenic processing shows a decrease of plasma induced damage with the decreasing the sample temperature. The films etched in CF_4 plasma show significantly less damage at moderate cryo regime. Therefore, characteristics of traditional etch chemistry based on CF_4 plasma might be significantly improved at cryogenic temperature because of activated nature of diffusion of fluorine containing species through fluorocarbon polymer.

The reported study was partially supported by RFBR, research project # 16-07-01233.

1. M.R. Baklanov, J.-F. de Marneffe, D. Shamiryan et al J. Appl. Phys. **113**, 041101 (2013).

Nanoscale patterning using redeposition on sidewall microstructure

I. Amirov, A. Shumilov, A. Kupriyanov, V. Naumov
Yaroslavl Branch of the Institute of Physics and Technology, Yaroslavl, Russia, E-mail:ildamirov@yandex.ru

Currently being developed different methods of fabrication nanostructures without the use of nanolithography methods. One of these methods is an edge lithography (EL) [1, 2]. It is based on the use of nanostructures formation near the edges of original mask. There are several variations of EL method, depending on the method of forming new nanomask. In this work we propose a new method of formation of nanostructures using redeposition of material on the side walls original mask during the ion-plasma sputtering. Implementation of the method was carried out using the photoresist mask as well as Si mask. Here new method is demonstrated on the example of formation of Cr nanowire on the Si surface using the polySi mask.

The fabrication process of the Cr nanowire structures using poly-Si mask include the following: 1. The formation in resist layer coated on the poly-Si/Cr (1 μm/50 nm) structure a pattern of grating with pitch 3 μm by photolithography. 2. Formation of poly-Si mask by anisotropic his etching in plasma SF_6/C_4F_8. 3. Photoresist mask etching of in an oxygen plasma. 4. Ion-plasma sputtering of Cr film (not until the end) through poly-Si mask in Ar plasma. During sputtering on the sidewall Si mask is formed by redeposition Cr film thickness ~ 50 nm and ~0.9 μm in height. 5. The isotropic etching of poly-Si in SF_6 plasma. Further, to obtain Cr nanowire on Si an additional etching Cr film is carried out (Fig. 1). Smoothness of nanowires (Fig. 2) is determined by the edge roughness of the wall resist mask.

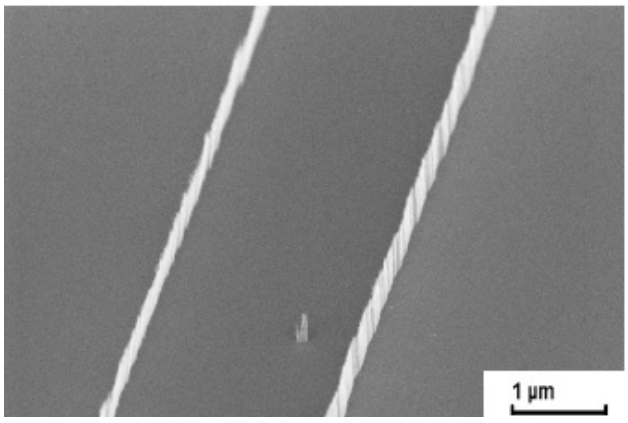

Fig. 1. SEM image of the Cr nanowire on the Si.

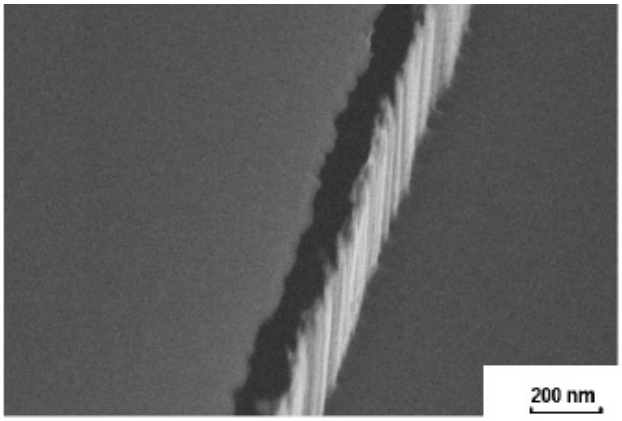

Fig. 2. A magnified image of a Cr nanowire.

A diversity of parallel Cr nanowires of different shapes produced by this method is determined by films Cr and poly-Si thickness. Cr sputtering conducted in a reactor of density plasma described in detail in [3].

Using software complex simulations of sputtering process was performed the 2D modeling of Cr redeposition process on the side wall of the mask during ion sputtering depending on the sticking coefficient of Cr atoms and output function of the angle of the sputtered particles. The width and geometry of formed Cr structures was determined by these two parameters. A satisfactory agreement with the experimental data is obtained with a coefficient of adhesion of 0.4 and $\cos^n$ distribution of the sputtered atoms Cr.

1. Y. Zhao, E.Berenschot, H. Jansen, N.Tas, J. Huskens, M. Elwenspoek. “Multi-silicon ridge nanofabrication by repeated edge lithography”. Nanotechnology, **20**, 315305, 2009.
2. H. Mao, W. Wu, Y. Zhang, G. Zhai, J. Xu. “Fabrication of high-compact nanowires using alternating photoresist ashing and spacer technology”. J. Micromech. Microeng., **20**, 085029, 2010.
3. I. Amirov, M. Izyumov, and V. Naumov. “Low energy selective etching of metal films in oxygen-containing high-density argon plasma. Journal of Surface Investigation: X-ray, Synchrotron and Neutron Techniques, **10**, pp. 855–859, 2016.

Diffraction gratings and 2D photonic crystals fabrication in a SOI waveguide by plasma and wet etching of Si

M. Barabanenkov[1,2], A. Il'in[1], V. Volkov[1], A.Gruzintsev[1]

1. Institute of Microelectronics Technology RAS, Chernogolovka, Moscow Region, Russia, barab@iptm.ru

2. Molecular Electronics Research Institute, Zelenograd, Moscow, Russia

The integration of micro and nanophotonic devices on the traditional CMOS platform holds promises for overcoming the limitations of traditional silicon electronics. It is well known that employing waveguide configurations for couplers [1], optical filters [2] and mode modulators [3] would open up wider potentialities of optical integration and its compatibility with CMOS processing techniques [4]. For instance, Etched Silicon - On - Insulator (SOI) Bragg gratings have been successfully demonstrated in recent years [3].

In the currently presented report a fabrication process is described including electron beam (EB) lithography, plasma and wet etching of Si for polycrystalline Si strip-like waveguides, waveguide lamellar diffraction grating and 2D photonic crystal structures tuned to an electromagnetic wave with the wavelength 1.5 μm. The SiO_2 layer is produced by dry oxidation of the Si wafer. A polycrystalline Si layer was deposited by EB evaporation of a Si target. Strip-like waveguides are fabricated on the basis of $Si/SiO_2/Si$ or SiO_2/Si substrates (Fig 1(a)). The waveguides have thickness from 150 to 260 nm, widths from 1.5 to 15 μm at lengths to 800 μm. The waveguide lamellar diffraction gratings have grooves with a thickness from 40 to 265 nm and the pitch from 340 to 600 nm (Fig 1(b)). The photonic crystals are composed of either Si pillars (Fig. 1(c)) or cylindrical pores (Fig. 1(d)) in the Si waveguide which is situated on the surface of a SiO_2 (1 μm thick)/Si-wafer substrate.

The measured attenuation coefficient of the polycrystalline Si waveguide is estimated to be 0.17 dB/mm at wavelength of 1.5 μm. This losses value is typical of thin films of amorphous Si [5].

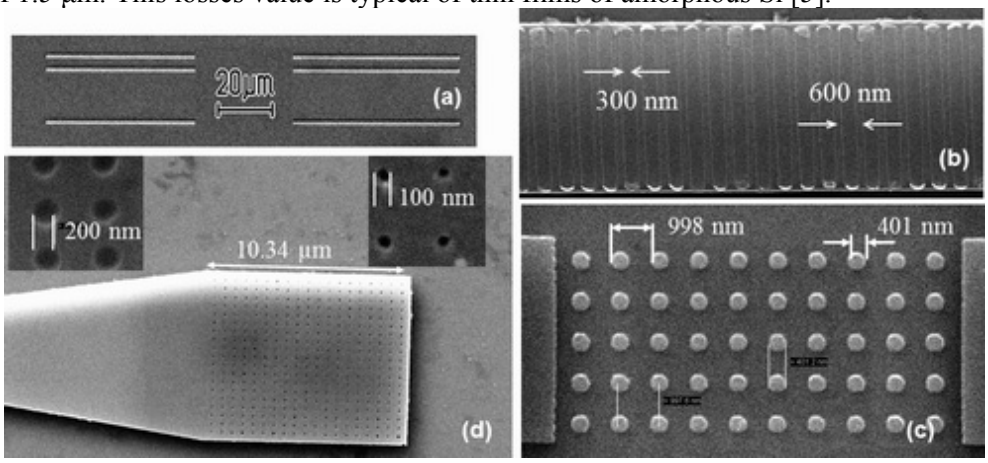

Figure 1. SEM images of strip-like waveguides 5 μm wide and 220 nm thick (a) with an integrated lamellar diffraction grating with grooves thickness of 45 nm, the pitch of 600 nm and 50 % fill-factor (b), and a 10×5 Si pillar array with a pillar diameter of 400 nm, height of 220 nm and a pillar pitch of 1 μm (c), and a 19×19 pore array in an extended part of the 5 μm wide strip-like waveguide (d), the pores with the diameter 100 and 200 nm (see the inset) constitute a rectangular lattice with the periods 610 and 500 nm.

1. G.Z Masanovic, G.T. Reed, V.M.N. Passaro, W.R. Headley, B. Timotijevic, R.M.H. Atta, M. Josey, G.Ensell, A.G.R. Evans, "Preliminary experimental results of a dual grating-assisted directional coupler on SOI," Proc. SPIE, **5730**, pp.173-180, 2005.

2. T.E Murphy, J.T. Hastings, H.I. Smith, "Fabrication and characterization of narrow-band Bragg-reflection filters in silicon-on-insulator ridge waveguides", J. Lightwave Technology, **19**, pp. 1938-1942, 2001.

3. C.A. Barrios, V.R. Almeida, R. Panepucci, M. Lipson, 'Electrooptic modulation of silicon-on-insulator submicrometer-size waveguide devices", J. Lightwave Technology, **21**, pp. 2332 – 2339, 2003.

4. G.T. Reed (ed). *Silicon Photonics: The State of the Art.*, Willey, Blackwell, 2008.

5. M.J.A. de Dooda, A. Polman, T. Zijlstra, van der Drift E.W.J.M., "Amorphous silicon waveguides for microphotonics", J. Appl. Phys., **92**, pp. 649 – 653, 2002.

Quantum well FPA's of 384×288 and 640×512 elements

M.A. Dem'yanenko, D.G. Esaev, I.V. Marchishin, A.I. Toropov, V.N. Ovsyuk, N.A. Valisheva, A.V. Latyshev
Institute of Semiconductor Physics, Russia, Novosibirsk, 630090 Lavrentyva Ave., 13
esaev@isp.nsc.ru.

The repot of design and fabrication of Quantum well infrared photodetectors (QWIP) on the basis of GaAs/AlGaAs multiple quantum well heterostructures are presented. The format of QWIPs was as 384×288 with 25 μm pitch and 640×512 with 20 μm pitch, consecutively.

High-quality photosensitive GaAs/AlGaAs heterostructures were produced by molecular beam epitaxial method on the semi-insulated GaAs substrates. Low concentration of growing defects (100-200 cm^{-2}) and small size of its (less than 5-8 μm) were achieved.

The Focal plane arrays were fabricated by using HF-plasma dry etching for the formation of a two-dimensional diffraction grating and mesa structures. The Ge-Au-Ni-Au alloy was used as contacts to the bottom and top conduction layers of the structure. The indium bumps both on a focal plane array (FPA) and on silicon read-out integral circuit (ROIC) was produced by lift-off lithography. The assembly of QWIP was occurred by flip-chip technology. After intermediate testing of QWIP assembly the thinning of GaAs substrate was performed by lapping, chemical-mechanical polishing and wet etching. At the last step the anti-reflection coating were performed.

QWIP structure was mounted in the vacuum dewars which are integrally interfaced with Stirling cryocoolers. The operation temperature of FPA detectors was about 70 K. The noise equivalent temperature difference (NEDT) of the QWIP detectors were reached up to 20-30 mK and operability – (99.6-99.9)%. A typical results of the photosensitive QWIP multilayer structure, individual pixel with the diffraction grating, spectral response and a thermal image registered by 640×512 QWIP FPA are presented below.

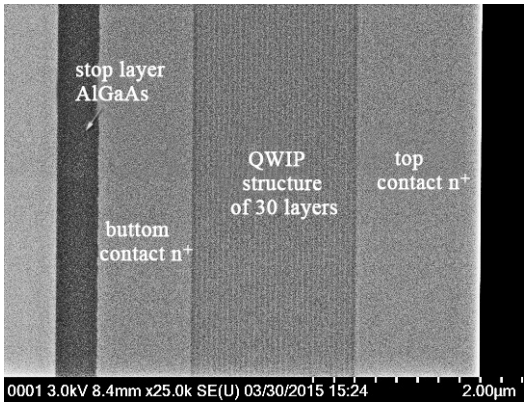

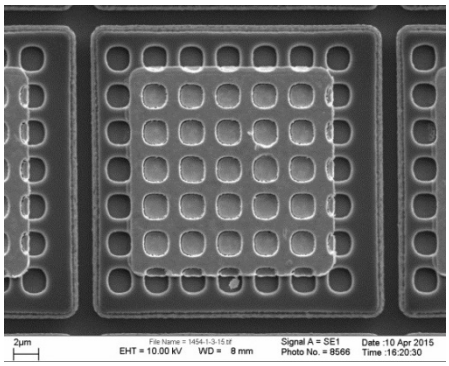

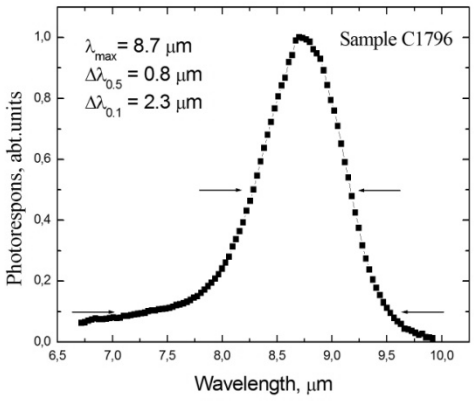

Terahertz bolometer based on Sn nanothreads in GaAs

I. Semenikhin[1], V. Vyurkov[1], A. Bugayev[2,5], R. Khabibullin[2,5], D. Ponomarev[2,5], A. Yachmenev[2], P. Maltsev[2], M. Ryzhii[3], T. Otsuji[4], V. Ryzhii[2,4,5]

1. Institute of Physics and Technology, Russian Academy of Sciences, Moscow, Russia; vyurkov@ftian.ru
2. Institute of Ultra High Frequency Semiconductor Electronics of RAS, Moscow, Russia
3. Department of Computer Science and Engineering, University of Aizu, Aizu-Wakamatsu, Japan
4. Research Institute for Electrical Communication, Tohoku University, Sendai, Japan
5. Center for Photonics and Infrared Technology, Bauman Moscow State Technical University, Moscow, Russia

We propose and evaluate the terahertz hot-electron bolometers (HEBs) based on gated GaAs structures like the field-effect transistor with the array of the Sn nanothreads. Such structures can be fabricated via delta-doping of vicinal GaAs surface by Sn atoms with a subsequent regrowth. That results in the formation of the chains of Sn atoms at the terrace edges [1]. The operation of the HEBs is associated with an increase of the delocalized electrons due to their heating by the incoming terahertz (THz) radiation. Therefore, for higher sensitivity the Fermi level must be immersed fairly deep into potential wells by a negative gate voltage when most electrons are confined in nanothreads (Fig. 1).

We developed two device models. The quantum model accounts for the quantization of the electron energy spectrum in the self-consistent two-dimensional electric potential, herewith the electron density distribution in nanothread arrays for different gate voltages is calculated. The classical model ignores the quantization and electrons are distributed in space according to 3D density of states and Fermi-Dirac statistics. It turned out that qualitatively both models demonstrate similar behavior, nevertheless, the classical one is in better quantitative agreement with experimental data. Feasibly, the quantization could be ignored because Sn atoms are randomly placed along the thread axis.

In Fig. 2 the fraction of delocalized electrons vs. gate voltage for different dispersion a is plotted. It was supposed that Sn ions were distributed around the thread axis according to the Gaussian function with a space dispersion a including $a = 0$ (delta-doping). The lowest curves the best way match the experimental I-V curves when the current flows perpendicular to threads. It could be regarded as an indirect confirmation that nanothreads really exist.

The doubtless advantage of the proposed bolometer is its significant polarization sensitivity, i.e. whether the electric field in THz wave is parallel or perpendicular to nanothreads.

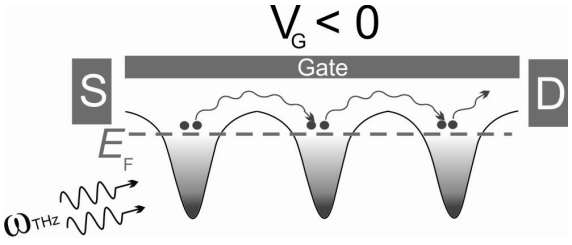

Fig. 1. Principle of a bolometer functioning.

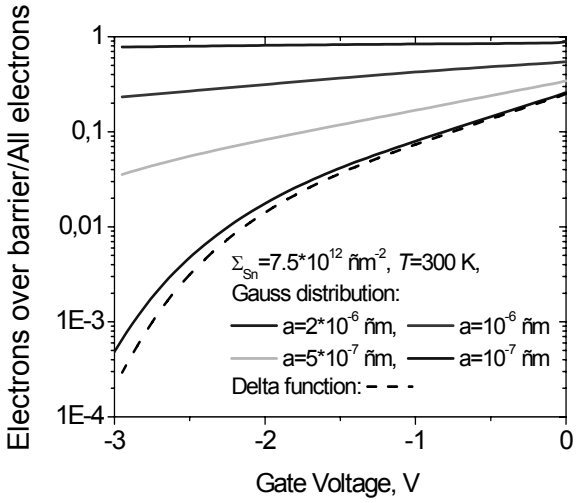

Fig.2. Fraction of delocalized electrons vs. gate voltage for different dispersion a.

1. R.A. Khabibullin, A.E. Yachmenev, D.V. Lavrukhin, D.S. Ponomarev, A.S. Bugayev, and P.P. Maltsev. "Pseudomorphic HEMT with Sn nanowires on a vicinal GaAs substrate". Semicond. Sci. Technol., **30**, 085009, 2015.

Diffraction gratings for optoelectronics by dry e-beam etching of resist

A. Rogozhin[1, 3], E. Zhikharev[1], M. Bruk[2], S. Averkin[1]
1. Institute of Physics and Technology of RAS, Moscow 117218, Russia, rogozhin@ftian.ru
2. L.Ya. Karpov Institute of Physical Chemistry, Moscow 105064, Russia
3. Moscow Institute of Physics and Technology (MIPT), Moscow, Russia.

Micro- and nanostructures formation of special well-rounded shape using an e-beam lithography is a huge task. Usually stair-like profile is used instead that complicates the process immensely. The problem can be solved using the dry method of relief formation in some positive resists during electron-beam exposure in vacuum (DEBER method) proposed by Bruk et al. [1]. The method is based on the chain depolymerization reaction, which takes place in the polymer resists during e-beam exposure at the glass-transition or higher temperatures. The volatile reaction products (monomers) are pumped out during exposure.
Three main technologies are used for diffraction grating formation: ruling, holographic technology and replication [2]. Master grating for replication could be obtained by ruling, holographic or DEBER method. Ruling is a complex and low-productive process but it provides the grating of the highest efficiency. Moreover very large grating can be obtained by ruling. On the other hand light scattering could be relatively high for ruled gratings.

Holographic gratings have sinusoidal shape. Their efficiency could be high for the radiation of some wavelength range. Holographic gratings may offer advantages to spectroscopic systems in which light scattered from the grating surface is performance-limiting. Holographic method is high-productive. Only some special resists could be used for holographic method.
Simple gratings obtained by DEBER method are quite similar to holographic gratings. They also have sinusoidal shape and limited efficiency. Throughput for DEBER method is lower than ruling or holographic method but it is high enough for small gratings production. DEBER exposure time of 3×3.9 mm^2 is about 10-100 s (exposure dose 0.1-1 μC/cm^2). DEBER method is extremely accurate due to e-beam system exploitation. Moreover the shape of the grating produced by DEBER method could be modified. The shape of the grooves could be skewed, for example. Also complex grating like binary gratings could be produced by DEBER method if e-beam lithography or FEBIP system is used. Large set of positive resists could be used with DEBER method.
In this work different diffraction gratings obtained by DEBER method are presented and their parameters are analysed.

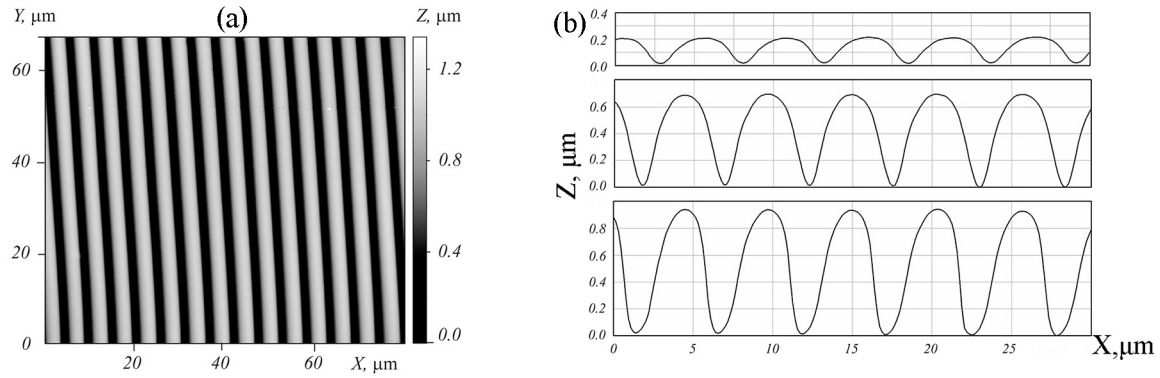

Fig. 1. AFM image (a) and profiles (b) of diffraction gratings obtained by DEBER method.

1. M.A. Bruk, E.N. Zhikharev, D.R. Streltsov, V.A. Kalnov, A.V. Spirin, Microelectronic Engineering, **112**, pp. 1-4, 2013.
2. Loewen E. *Diffraction Grating Handbook* (New-York: Newport Corp.) 2005.

Simulation of field-effect transistors and resonant tunneling diodes based on graphene

I. Abramov, V. Labunov, N. Kolomejtseva, I. Romanova
Belarussian State University of Informatics and Radioelectronics, Minsk, Belarus, E-mail: nanodev@bsuir.edu.by

Graphene is a nanomaterial that due to unique properties has attracted great interest for various applications, in particular, for development of nanoelectronic devices [1]. In the paper the graphene field-effect transistors (GFET) and resonant tunneling diodes (RTD) are analyzed with the use of proposed models.
First, simulation of dual-gate field-effect transistor based on monolayer graphene with the use of proposed combined model is considered. In the model the following important factors such as quantum capacitance, hole and electron mobility difference, drain and source resistances are taken into account. Investigations of dependence of a drain current on drain voltage for various top-gate-to-source voltages are performed. Influence of channel length, source and drain resistances on output characteristics of the device is analyzed. Comparison of calculation results with simulation ones obtained with the known models was carried out.
Secondly, simulation of graphene-based nanostructures on hexagonal boron nitride, silicon carbide and silicon dioxide substrates was performed using proposed self-consistent numerical model, based on effective wave function formalism [2, 3]. The developed models in detail were described in our previous works [4, 5]. The possibility of using a proposed self-consistent model for double- and triple-barrier graphene-based RTD simulation was illustrated. As well as it was investigated the influence of different parameters on IV-characteristics of graphene-based RTDs. It was shown that it is necessary to take into account extended (passive) regions for adequate simulation of these devices.
The programs realizing proposed models of dual-gate graphene field-effect transistors and graphene-based resonant-tunneling diodes were included in the nanoelectronic devices simulation system NANODEV [6, 7] developed in BSUIR since 1995.

1. A.C. Ferrari, F. Bonaccorso, V. Fal'ko, K.S. Novoselov et al. "Science and technology roadmap for graphene, related two-dimensional crystals, and hybrid systems". Nanoscale, **7** (11), pp. 4598-4810, 2015.
2. I.I. Abramov. *Bases of micro- and nanoelectronic devices simulation*. Saarbrücken: LAP LAMBERT Academic Publishing. 2016. 444 pp. (In Russian).
3. I.I. Abramov "Problems and principles of physics and simulation of micro- and nanoelectronics devices. V. Resonant-tunneling structures". Nano- i mikrosistemnaya tekhnika, N 3, pp. 57-70, 2007 (in Russian).
4. I.I. Abramov, N.V. Kolomejtseva, V.A. Labunov, I.A. Romanova "Simulation of graphene resonant tunneling diodes on the substrates of various types". Nano- i mikrosistemnaya tekhnika, N 11. pp. 3-10, 2015 (in Russian).
5. I.I. Abramov, V.A. Labunov, N.V. Kolomejtseva, I.A. Romanova "Simulation of resonant tunneling devices and nanostructures based on graphene". Proceedings of the 25th International Crimean Conference "Microwave & Telecommunication Technology", 6-12 Sept., **2**, pp. 711-712, 2015 (in Russian).
6. I.I. Abramov, I.A. Goncharenko, S.A. Ignatenko, A.V. Korolev, E.G. Novik, A.I. Rogachev. "NANODEV: A nanoelectronic-device simulation software system". Russian Microelectronics, **32** (2), pp. 97-104, 2003.
7. I.I. Abramov, A.L. Baranoff, I.A. Goncharenko, N.V. Kolomejtseva, Y.L. Bely, I.Y. Shcherbakova. "A nanoelectronic device simulation software system NANODEV: New opportunities". Proc. of SPIE, **7521**, edited by Kamil A. Valiev, Alexander A. Orlikovsky, pp. 75211E1-1-11, 2010.

Collapse of resonances as a manifestation of *PT*-symmetry breaking in resonant tunneling heterostructures

A.A. Gorbatsevich[1,2], N.M. Shubin[2]

1. P.N. Lebedev Physical Institute of the Russian Academy of Sciences, Moscow, 119991, Russia.

2. National Research University of Electronic Technology, Zelenograd, Moscow, 124498, Russia.

Recently the new type of symmetry breaking (SB) phenomenon has been discovered – PT-symmetry breaking (PT-SB) in quantum systems, described by a pseudo-Hermitian Hamiltonian, which is symmetric with respect to both time reversal (T) and space inversion (P) [1, 2]. In the PT-symmetric state such a Hamiltonian has real eigenvalues and symmetric eigenvectors, while in a symmetry broken state eigenvalues become complex and symmetry of eigenvectors breaks either. Physical realization of systems with pseudo-Hermitian Hamiltonians is a nontrivial task because of T-breaking terms, which correspond to creation/annihilation (gain/loss) processes. Because of this, all experiments on PT-symmetry breaking phenomena presented in the literature up to now have been based on photonic or bosonic systems [3]. In this report we present fermionic model based on a dissipationless symmetric resonant tunneling heterostructure (RTS) demonstrating a coalescence of resonances. At the coalescence point spatial symmetry of electron probability distribution in RTS is broken. Such a behavior in fermionic system can be described as a PT-SB of certain auxiliary Hamiltonian [4].

We analyze transmission properties of a multi-well dissipationless RTS in Keldysh formalism within tight-binding approximation. Classically, transmission coefficient can be written as a fraction with characteristic polynomial of system's effective non-Hermitian Hamiltonian in denominator, which describes decaying states of open quantum system (this is a well-known result from Feshbach studies of open quantum systems). Eigenvalues of effective non-Hermitian Hamiltonian coincide with poles of scattering matrix in complex energy plane. For narrow and well-separated resonances real parts of complex eigenvalues of effective Hamiltonian define positions of transmission peaks. However, exact positions of overlapping resonances cannot be figured out from eigenvalues of effective Hamiltonian. The key point of our consideration is introduction of an auxiliary pseudo-Hermitian Hamiltonian, which can be derived straightforwardly from effective one, and rewriting the transmission coefficient in the following form:

$$T = P^2/(P^2 + Q^2), \qquad (1)$$

where Q is a characteristic polynomial of auxiliary Hamiltonian. Thus, energies of unity transmission peaks coincide *exactly* with real eigenvalues of auxiliary pseudo-Hermitian Hamiltonian. This relation holds true for strongly interacting resonances, which can coalesce. In the case of symmetric structure auxiliary Hamiltonian becomes PT-symmetric and collapse of resonances effect [4, 5], accompanied by symmetry breaking of electron wavefunction distribution profile, is described just as a PT-SB of auxiliary Hamiltonian. We show that SB takes place in dissipationless systems with even number of quantum wells, while in the case of odd number of wells collapse of resonances is not accompanied by SB. Results of numerical solutions of the effective mass Schrödinger equation via the transfer matrix approach are presented to demonstrate the difference between systems with even and odd number of wells. Also we classify collapse of resonances in symmetric RTS from the catastrophe theory point of view and show that introduction of dissipation (scattering) destroys (smoothens) PT-SB.

1. C.M. Bender and S. Boettcher, "Real Spectra in Non-Hermitian Hamiltonians Having PT Symmetry", Phys. Rev. Lett. **80**, pp. 5243-5246, 1998.

2. C.M. Bender. "Making sense of non-Hermitian Hamiltonians", Rep. Prog.Phys. **70**, pp. 947-1018, 2007.

3. A. Guo, G.J. Salmo, D. Duchesne, R. Morandotti, M. Volatier-Ravat, V. Aimez, G.A. Siviloglou, and D.N. Christodoulides. "Observation of PT-Symmetry Breaking in Complex Optical Potentials", Phys. Rev. Lett. **103**, 093902, pp. 1-4, 2009.

4. A.A. Gorbatsevich and N.M. Shubin. "PT-symmetry breaking in resonant tunneling heterostructures", JETP Letters, 2016, DOI: 10.1134/S0021364016120031.

5. A.A. Gorbatsevich, M.N. Zhuravlev, and V.V. Kapaev. "Collapse of resonances in semiconductor heterostructures as a transition with symmetry breaking in an open quantum system" JETP **107**, pp. 288-301, 2008.

Numerical modeling of microwave switchers with subpicosecond time delay

B. Konoplev, E. Ryndin
Southern Federal University, Taganrog, Russia, rynenator@gmail.com

The important elements of the monolithic microwave integrated circuits which find wide application in the high-speed broadband data transmission systems are the microwave switchers. The development of digital technologies requires a switching time was comparable with the period of switched microwave signals [1].
To solve this problem the variants of the topology and structure of the microwave switchers based on the managed electron density maximum rearrangement in multi-contacts functionally integrated active region were proposed in [3] and [4]. The basis of the microwave switcher is a normally opened HEMT-structure with multiple Schottky gates and the corresponding number of switching ohmic contacts that provide a full technological compatibility with the manufacture routes of microwave integrated circuits.
In this research two-dimensional finite-difference physical and topological model of the microwave switchers, which allows to analyze the transient processes of managed electron density rearrangement in a functionally integrated active region is proposed. A distinctive feature of the proposed model is a combination of two different sets of variables and explicit first-order upwind discretization scheme for the normalized continuity equation:

$$
\begin{aligned}
n^{*}_{i,j} = n_{i,j} + \Delta t_m \Bigg\{ & \frac{2}{\Delta x_i + \Delta x_{i-1}} \Big[\Big(\mu_{ni+1,j} e^{\varphi_{i+1,j} + V_{ni+1,j}} \theta\left(\Phi_{ni,j} - \Phi_{ni+1,j}\right) + \mu_{ni,j} e^{\varphi_{i,j} + V_{ni,j}} \theta\left(\Phi_{ni+1,j} - \Phi_{ni,j}\right) \Big) \times \\
& \times \frac{\Phi_{ni+1,j} - \Phi_{ni,j}}{\Delta x_i} - \Big(\mu_{ni,j} e^{\varphi_{i,j} + V_{ni,j}} \theta\left(\Phi_{ni-1,j} - \Phi_{ni,j}\right) + \mu_{ni-1,j} e^{\varphi_{i-1,j} + V_{ni-1,j}} \theta\left(\Phi_{ni,j} - \Phi_{ni-1,j}\right) \Big) \frac{\Phi_{ni,j} - \Phi_{ni-1,j}}{\Delta x_{i-1}} \Big] + \\
& + \frac{2}{\Delta y_j + \Delta y_{j-1}} \Bigg[\Big(\mu_{ni,j+1} e^{\varphi_{i,j+1} + V_{ni,j+1}} \theta\left(\Phi_{ni,j} - \Phi_{ni,j+1}\right) + \mu_{ni,j} e^{\varphi_{i,j} + V_{ni,j}} \theta\left(\Phi_{ni,j+1} - \Phi_{ni,j}\right) \Big) \frac{\Phi_{ni,j+1} - \Phi_{ni,j}}{\Delta y_j} - \\
& - \Big(\mu_{ni,j} e^{\varphi_{i,j} + V_{ni,j}} \theta\left(\Phi_{ni,j-1} - \Phi_{ni,j}\right) + \mu_{ni,j-1} e^{\varphi_{i,j-1} + V_{ni,j-1}} \theta\left(\Phi_{ni,j} - \Phi_{ni,j-1}\right) \Big) \frac{\Phi_{ni,j} - \Phi_{ni,j-1}}{\Delta y_{j-1}} \Bigg] - R_{i,j} \Bigg\},
\end{aligned}
\tag{1}
$$

where $n_{i,j}$ is the electron density at the moment t_m; $n^{*}_{i,j}$ is the electron density at the moment t_{m+1}; $\varphi_{i,j}$ is the electrostatic potential; $\Phi_{ni,j}$ is the exponent of quasi-Fermi level for electrons; $N_{i,j}$ is the effective impurity concentration; $V_{ni,j}$ is the heterostructural potential; $\mu_{ni,j}$ is the electron mobility; $R_{i,j}$ is the difference between the generation and the recombination rates; Δx_i, Δy_j are the steps of coordinate grid; Δt_m is the time grid step; θ is the Heaviside step function.
The obtained results of numerical modeling show that even with relatively large gate length of 500 nm the switching time of the switcher using the principles of electron density maximum rearrangement three times less (up to 0.1 ps) compared to switching time of the conventional switcher. The results obtained without taking into account the parameters of external circuits, which can be considered in the circuit modeling.
The results have been obtained using the equipment of the Shared Equipment Center and the Research and Educational Center “Nanotechnology” of the Institute of Nanotechnologies, Electronics and Electronic Equipment Engineering, Southern Federal University (Taganrog, Russia). This research is supported by the Russian Foundation for Basic Research (Grant 16-07-00018) and the Ministry of Education and Science of the Russian Federation (Project 8.797.2014K).

1. I. Vikulov. "Monolithic microwave integrated circuits. Technological basis of APAA". Elektronika: nauka, tekhnologiya, biznes, **7**, pp. 60-73, 2012 (in Russian).
2. B.G. Konoplev, E.A. Ryndin, and M.A. Denisenko. "Components of Integrated Microwave Circuits based on Complementary Coupled Quantum Regions". Russian Microelectronics, **44**, pp. 190-196, 2015.
3. B.G. Konoplev and E.A. Ryndin. "Functionally integrated microwave switcher with spatial rearrangement of electron density maximum". *25th Int. Crimean Conference "Microwave & Telecommunication Technology"*, IEEE Cat. Nr. CFP 15788, pp. 713-714, Sevastopol, 2015.

Development of Drift-Diffusion Numerical Models of High-Speed On-Chip Photodetectors with Heterojunctions

I.V. Pisarenko, E.A. Ryndin
Southern Federal University, Institute of Nanotechnology, Electronics, and Electronic Equipment Engineering, Taganrog, Russia, ivan123tgn@yandex.ru (I.V.P.), rynenator@gmail.com (E.A.R.)

In this paper we consider the problem of research and development of the high-speed photodetectors designed for the operation as parts of the integrated inter-core optical commutation systems for multi-core ULSIs together with the $A^{III}B^{V}$ nanoheterostructure lasers-modulators [1, 2]. This research is aimed at the development of numerical models, modelling methods, and applied software allowing simulation of the transient processes taking place in structures of integrated photodetectors with heterojunctions during the detection of subpicosecond laser pulses. We have described the processes of charge carrier transport and accumulation applying the drift-diffusion approximation of semiclassical approach to the simulation of semiconductor devices. The drift-diffusion equation system of semiconductor written for structures with heterojunctions has the following form [3]:

$$\frac{\partial n}{\partial t} = -\nabla\left\{\mu_{\mathrm{n}}\left[n\cdot\nabla\left(\varphi+V_{\mathrm{n}}\right)-\varphi_{\mathrm{T}}\cdot\nabla n\right]\right\}+G-R\,; \tag{1}$$

$$\frac{\partial p}{\partial t} = \nabla\left\{\mu_{\mathrm{p}}\left[p\cdot\nabla\left(\varphi-V_{\mathrm{p}}\right)+\varphi_{\mathrm{T}}\cdot\nabla p\right]\right\}+G-R\,; \tag{2}$$

$$\nabla\left(\varepsilon\cdot\nabla\varphi\right)=\frac{q}{\varepsilon_0}\left(n-p-N_{\mathrm{D}}+N_{\mathrm{A}}\right), \tag{3}$$

where n, p are the electron and hole concentrations; μ_{n}, μ_{p} are the electron and hole mobilities; t is time; q is the elementary charge; φ is the electrostatic potential; φ_{T} is the temperature potential; V_{n}, V_{p} are the heterostructure potentials in the conduction and valence bands; G, R are the generation and recombination rates of electron-hole pairs; ε is the dielectric permittivity of semiconductor; ε_0 is the permittivity of vacuum; N_{D}, N_{A} are the concentrations of the ionized donors and acceptors. We have taken into account the different mechanisms of electron-hole pair generation and recombination and the influence of semiconductor temperature, impurity concentration and electric field intensity on mobilities of charge carriers. We have developed the non-stationary drift-diffusion numerical simulation technique for the implementation of the aforementioned models. This technique combines the implicit difference scheme and the Newton method and has the optimized balance between the adequacy of the simulation results and the consumption of time and computational resources for their obtainment. We have developed specialized applied software in the GNU Octave program using the MATLAB programming language. This software implements the aforementioned models and modelling methods for the simulation of on-chip heterostructure photodiodes with different electrophysical, constructive, and technological parameters. We have applied the proposed simulation aids for the research of transients taking place in p^{+}-$Al_{0.3}Ga_{0.7}As$/i-GaAs/n^{+}-$Al_{0.3}Ga_{0.7}As$ structures and Schottky-barrier photodiodes with $Al_{0.3}Ga_{0.7}As$/GaAs heterojunctions at the edges of near-contact and heavily-doped regions. According to the simulation results, the photodetectors being considered can be applied for the detection of rectangular laser pulses with the duration of 1 ps and above. The results have been obtained using the equipment of the Shared Equipment Center and the Research and Educational Center “Nanotechnology” of the Institute of Nanotechnologies, Electronics and Electronic Equipment Engineering, Southern Federal University (Taganrog, Russia). This research is supported by the Russian Foundation for Basic Research (Grant 16-07-00018) and the Ministry of Education and Science of the Russian Federation (Project 8.797.2014K).

1. B.G. Konoplev, E.A. Ryndin, and M.A. Denisenko. "Components of integrated microwave circuits based on complementary coupled quantum regions". Russian Microelectronics, **44**, pp. 190–196, 2015.
2. B.G. Konoplev, E.A. Ryndin, and M.A. Denisenko. "Diffusion-drift model of the transport of charge carriers and photons in injection lasers". Tech. Phys. Lett., **41**, pp. 587–590, 2015.
3. I.I. Abramov. "Problems and Principles of Physics and Simulation of Micro- and Nanoelectronics Devices. II. The Models of Semiclassical Approach". Nano- and microsystem technology, **9**, pp. 26–36, 2006 (in Russian).

Calculation of the high-frequency conductivity and the Hall constant of a thin semiconductor film

O.V. Savenko[1], D.N. Romanov[2], I.A. Kuznetsova[3]
1. P.G. Demidov Yaroslavl State University, Yaroslavl, Russia, cryak92@mail.ru
2. P.G. Demidov Yaroslavl State University, Yaroslavl, Russia, romanov.yar357@mail.ru
3. P.G. Demidov Yaroslavl State University, Yaroslavl, Russia, kuz@uniyar.ac.ru

In present work the kinetic calculations of the high-frequency conductivity and the Hall constant of a thin semiconductor film are carried out. The alternative electric field is applied along the film, and the constant magnetic field is applied perpendicular to the film. Skin effect is neglected (the film thickness is assumed to be much less than the skin layer depth). The electric and magnetic fields are supposed to be homogeneous. This task are decided by using the kinetic method, therefore the ratio between the film thickness and the mean free path of charge carriers is supposed to be arbitrary. At room temperatures the mean free path of charge carriers lies in the range 10 – 100 nm for typical metals and 10 – 1000 nm for typical semiconductors. The quantum size effects are neglected, because the considered film thickness is supposed to be much more than de Broglie wavelength of charge carriers. The value of de Broglie wavelength of charge carriers is of the order to 10 nm for typical semiconductors and of the order to interatomic distance for typical metals. The time-periodic electric field acts on charge carriers and induces the deviation of its distribution function from Fermi distribution function. Non-equilibrium distribution function is found by solving of Boltzmann kinetic equation in time relaxation approximation and in linear in the external field approximation. The diffuse-specular scattering of charge carriers from film surfaces is considered. The mirrority coefficients of the upper and lower surfaces of film are supposed to be equal. The expression of non-equilibrium distribution function permits to find the current density, conductivity and Hall constant.

The dependences of module and argument of dimensionless conductivity and Hall constant on dimensionless parameters: electric field frequency, magnetic field induction, film thickness and mirrority coefficient of film surfaces are investigated. The comparison of obtained results with known calculations for the case of a metal film is made. The nontrivial character of behavior of dependences of dimensionless conductivity and Hall constant on dimensionless electric field frequency, magnetic field induction and film thickness becomes more pronounced with mirrority coefficient decreasing (with increasing of the relative amount of diffusely reflected electrons). It is shown that with dimensionless electric field frequency increasing dimensionless conductivity module decreases monotonically. This dependence caused that the electron gas hasn't time to respond to high-frequency oscillations of the electric field intensity and behave as the bound charge complexity. These bound charges don’t contribute to the conductivity. The dimensionless conductivity argument increases with dimensionless electric field frequency increasing. At large values of the electric field frequency dimensionless conductivity argument seek to $\pi/2$ and the conductivity becomes purely imaginary value.

The oscillations of the dependences of the dimensionless conductivity module and argument on the dimensionless magnetic field induction are observed. Also the dependences of the dimensionless Hall constant module and argument on the dimensionless magnetic field induction and the dimensionless electric field frequency have the oscillating character. These oscillations attenuate with increasing of the dimensionless magnetic field induction and the mirrority coefficient of the film surfaces. These dependences are less pronounced oscillations for the case of a semiconductor film, because the dependences for this case oscillate with a larger period than the dependences for the case of a metal film. At large values of the dimensionless parameters the dimensionless Hall constant module seek to 1, and Hall constant argument seek to zero. When the dimensionless magnetic field induction is equal to the dimensionless electric field frequency, the resonant-like behavior of the dependences of dimensionless Hall constant argument is observed. With mirrority coefficient decreasing the difference between the dimensionless conductivity and the dimensionless Hall constant for the case of a metal film and for the case of a semiconductor film increases.

Comparative study of diamond FETs with contact Schottky barriers and SiC source-drain regions

V.P. Popov[1], M.A. Ilnitskii[1], A.V. Sheremetiev[1], V.A. Kagadei[2], E.V. Shesterikov[2]
1. Institute of Semiconductor Physics, SB RAS, Novosibirsk, Russia
2. Micran, Tomsk, Russia

Diamond is very attractive semiconductor material for high power and high frequency field effect transistors (FETs) because it offers wide band gap energy (5.45 eV), high electric breakdown field (10 MV/cm), high carrier mobility (μ_e: 2000 cm^2/V s; μ_h: 1000 cm^2/V s), and high thermal conductivity (22 W/cm K) [1, 2]. But up to now the problem of its doping did not been solved following deep boron acceptor level (E_v + 0.32 eV) and even deeper phosphorous donor level (E_c - 0.62 eV). Additional difficulties create very low impurity diffusivity and graphitization of implanted regions during high temperature annealing [3]. However, the researches already have demonstrated metal-semiconductor FETs (MESFETs) based on so called "transfer" doping using hydrogen terminated diamond surface for operation at maximal frequencies higher than 50 GHz [4]. But long term stability of properties for such transistors is still unreached especially at moderate temperatures ≥ 450 K.

Numerical simulation is a power tool in order to optimize metal-oxide-semiconductor FET (MOSFET) construction for silicon and silicon dioxide based devices. Unfortunately many charge carriers properties for diamond needed for such simulation do not known. In our work we used instead of missing the well verified data of charge carrier transport for silicon and silicon carbide to simulate by TCAD Synopsys I-V drain-gate characteristics of metal-insulator-semiconductor FET (MISFET) with Schottky barrier (SB) or SiC source-drain regions for the comparison of their properties with experimentally published I-V curves for MESFETS with H-transfer doping. The advantages of MISFETs are their stability even at operating temperatures higher than 600 K that is impossible in the case of MESFETs.

The results of MISFET simulation using SB source-drain contacts show the I_{on}/I_{off} relation higher than twelve orders and saturation current I_{on} as high as 100 mA/mm for optimized SB height. This value is about 10 times higher than in MESFETs with H-transfer doping. Using highly doped SiC source-drain regions leads to drastic decrease in I_{on} up to ten orders of magnitude due to high conduction and valence band mismatches in heterostructure SiC/C/SiC up to 1.6 eV and low tunneling rate. It is shown that I_{on} can be increased by p^+-SiC source and n^+-SiC drain as in the tunnel FET (TFET) due to band-to-band tunneling. On-state current I_{on} for TFET can be increased on few orders of magnitude at the same value of I_{off}.

1. I. Akimoto, Y. Handa, K. Fukai, N. Naka, High carrier mobility in ultrapure diamond measured by time-resolved cyclotron resonance. Appl. Phys. Lett. **105**, pp. 032102(4), 2014.
2. J.R. Olson, R.O. Pohl, J.W. Vandersande, A. Zoltan, T.R. Anthony, W.F. Banholzer, "Thermal conductivity of diamond between 170 and 1200 K and the isotope effect". Phys. Rev. B **47,** pp. 14850-14856, 1993.
3. J.F. Prins. "Implantation-doping of diamond with B^+, C^+, N^+ and O^+ ions using low temperature annealing". Diamond Relat. Mater., **11,** pp. 612-617, 2002.
4. S. Russell, S. Sharabi, A. Tallaire, D.A.J. Moran. "RF Operation of Hydrogen-Terminated Diamond Field Effect Transistors: A Comparative Study". IEEE TED**, 62**, pp. 751-756, 2015.

Fundamentals of the fast neutral beams diagnostics

V. Kudrya, Yu. Maishev
Institute of Physics and Technology, Moscow, Russia; E-mail address: kvp@ftian.ru

Development and optimization of both fast neutral beam sources and neutral beam technologies need the methods to measure and control the neutral beam parameters. Such parameters are: (1) number n of the beam components, their kinds and contents $r_i(x, y; z)$; (2) total flux density $F(x, y; z)$; (3) energy distribution functions (EDFs) for every component $f_i(E; x, y; z)$. Here z is the beam direction. This set of parameters allows us to calculate any local and integral (over the beam cross section) technological characteristics of fast neutral beams. For example, the energy flux density can be calculated as

$$W(x,y;z) = F(x,y;z)\sum_{i=1}^{n} r_i(x,y;z)\int_0^{\infty} \mathrm{d}E f_i(E;x,y;z)E \ .$$

The beam composition can be determined using ionization by electrons following mass-spectrometry of the products, high resolution optical spectroscopy, and chemical probes. But only the first method is universal. Besides only the ionization method with an energy analyzer can provide measuring the EDFs of the beam components. It should be noted that the measured (positive ionic products) EDF links with the original EDF of the neutral component by the relation:

$$f^{\text{neutral}}(E;x,y;z) \sim f^{\text{measured}}(E;x,y;z)\sqrt{E} \ .$$

Another problem of the ionization method is dissociative ionization that changes the beam composition. For example, a molecular oxygen beam (O_2) after ionization will contain positive ions O_2^+ and O^+. We have developed a method to extract the necessary information from experimental data obtained using some energy analyzer and mass-spectrometer. The two component beam case is considered in detail.

We also consider such probes based on calorimetry, secondary neutral-electron emission, and sputtering (quartz oscillator probe). Let S be the probe work surface area. Then the secondary emission probe current is

$$I(x,y;z) = SF(x,y;z)\sum_{i=1}^{n} r_i(x,y;z)\int_0^{\infty} \mathrm{d}E f_i(E;x,y;z)\gamma_i(E) \ ,$$

where $\gamma_i(E)$ is the secondary neutral-electron emission coefficient. The power transferred from the beam to the work plate of the calorimetrical probe is

$$W(x,y;z) = SF(x,y;z)\sum_{i=1}^{n} r_i(x,y;z)\int_0^{\infty} \mathrm{d}E f_i(E;x,y;z)E\kappa_i(E) \ ,$$

where $\kappa_i(E)$ is the fraction of incident particle energy transferred to heat. At last, the mass loss rate due to sputtering (or etching) is

$$\frac{\mathrm{d}m(x,y;z)}{\mathrm{d}t} = SF(x,y;z)\sum_{i=1}^{n} r_i(x,y;z)m_i \int_{E_i^{\text{th}}}^{\infty} \mathrm{d}E f_i(E;x,y;z)Y_i(E) \ ,$$

where $Y_i(E)$ is the sputtering coefficient, m_i is the sputtered particle mass, E_i^{th} is the threshold energy for sputtering by ith particles. These equations become non-trivial in the cases of non-monoenergetic neutral beams.

Application of spectral ellipsometry to *in situ* diagnostics of atomic layer deposition of dielectrics on silicon and AlGaN

I. Clemente[1,2], A. Miakonkikh[1,2]

1. Institute of Physics and Technology Russian Academy of Sciences, Moscow, Russia, miakonkikh@ftian.ru
2. Moscow Institute of Physics and Technology, Dolgoprudny, Russia

Atomic layer deposition (ALD) of Al_2O_3 and HfO_2 on Si and AlGaN substrates was studied in situ by means of spectral ellipsometry. The method was used for optimization of process of atomic layer deposition.

Atomic layer deposition technique became the most prominent method for deposition of ultrathin metal and dielectric layers in semiconductor applications [1]. Decrease of the gate dielectric electrical thickness providing physical thickness which is enough for suppressing tunneling current lead to implementation of high-k metal oxides as the gate dielectric of silicon based transistors [2]. On the other hand oxides produced by ALD are widely used as passivation layers in HEMT AlGaN high power UHF electronics and as gate dielectric in MISHEMT [3].

ALD allows to produce ultrathin films with atomic level control of film thickness (only monatomic layer is deposited in each step of process), low level of volume and surface defects, and excellent conformal coverage. Although dependence of growth parameters from substrate temperature, kinetics of surface reactions and nucleation phase on different substrates are still under research. Spectral ellipsometry has precision limit as low as 0.1 nm, but its application *in situ* is complicated by changes temperature of sample which affects optical properties of substrate, and, in case of AlGaN, transparency of substrate leads to difficult models of multilayer structures.

In present work Al_2O_3 and HfO_2 films were deposited in FlexAl ALD tool from Oxford Instruments plasma technology. Wafers were placed on heated chuck with controllable temperature (250-400 °C). The films were deposited in plasma assisted ALD process with TEMAH ($Hf(N(C_2H_5)(CH_3))_4$) and TMA ($Al(CH_3)_3$) as metal precursors and O_2 as a non-metal plasma precursor. Plasma was excited at pressure of oxygen 15 mTorr with applied power of 250 W. This process is truly self limited and hence process dependence on external parameters (stage temperature, duration of the process, pressure) is flat in wide interval. That provides “process window”, in which stable and reproducible film properties can be achieved.

Spectral ellipsometry was performed *in situ* by Woollam Co M2000X 65 degrees ellipsometer in 245-1000 nm range. Measurements were done on every half of ALD cycle (after metalorganic precursor dosage and after oxygen plasma exposure as well) which allows measuring of sorption of precursor on the surface and its subsequent oxidation. Special corrections were done to take into account sample tilt which cannot be adjusted in reactor chamber.

Developed model were used to measure *in situ* temperature of wafer before the process and its change during the deposition. Completeness of plasma oxidation reaction was proven by spectral ellipsometry measurements showing saturation of oxide thickness for plasma durations longer than 2 sec. Spectral ellipsometry was used to determine initial nucleation lag of film growth which is different on silicon and AlGaN surface. Rate of surface plasma enhanced reactions in different process conditions were determined and time of process saturation was calculated which could help to optimize process. Dependence of precursor desorption rate on silicon surface were measured depending on substrate temperature.

1. S.M. George. Atomic layer deposition: an overview. Chem. Rev., **110**, 111 (2010).
2. J.H. Choi, Y. Mao, J.P. Chang. Development of hafnium based high-k materials—A review. Materials Science and Engineering: R: Reports, **72**, 97–136 (2011).
3. R.C. Fitch et al. Comparison of passivation layers for AlGaN/GaN high electron mobility transistors. J. Vac. Sci. Technol. B, **29**, 061204, pp. 1-6 (2011).

TDR method for determination of IC's parameters

V. Timoshenkov, D. Rodionov, A. Khlybov
National Research University "MIET", Zelenograd, Russia

Frequency domain simulation is a widely used approach for determine integrated circuits parameters. This approach can be found in most of software tools used in IC industry. Time domain simulation approach shows intensive usage last decade due to some advantages. In particular it is applicable for analysis of nonlinear and nonstationary systems where the frequency domain is inapplicable. But time domain research methods require ultrawideband signal generators and oscilloscopes for experiment. It is disadvantage. Recent years show us a significant improvement in time domain measurement equipment. High frequency (up to 70 GHz) generators, oscilloscopes, receivers are available. It gives researchers new opportunities to use time domain method for determine spatial heterogeneity in to device under test (DUT). Resolution of time domain systems allows see heterogeneities on distance ~1 mm ($L_{min} = t_r v/2$, where v is a signal velocity) and determine its parameters and properties.

Field effect transistor technology scaling up to 30-60 nm gate length and ~10 nm gate dielectric, heterojunction bi-polar transistors with 10-30 nm base width allows fabricate digital IC's with 20 GHz clock frequency and mm-/μw-IC's with tens GHz bandwidth. Such devices and operation speed suppose transit signal by use microwave lines. There are local heterogeneities can be found inside of the signal path due to connections between different parts of signal path (stripe line-mm/μw-connector pin, stripe line – IC package pin). These heterogeneities distort signals that cause bandwidth decrease for μw-devices. Time domain research methods of signal transmission gives the opportunities to determine heterogeneities, it properties, parameters, built up equivalent circuits. It allows improve device construction.

This paper contains result of signal path research on PCB used for 12 GHz RF chips. Experimental results are provided and show possibility for inductance and capacitance measurement up to 25 GHz. Also dielectric constant as function from frequency was measured up to 35 GHz.

Non-destructive determination of thickness of the dielectric layers using EDX

S. Sokolov, E. Kelm, R. Milovanov
Institute of Nanotechnology of Microelectronics, Russian Academy of Science, Russia, 119991 Moscow, Leninsky Prospekt, 32A, sokol481@rambler.ru

The importance of the thin films in semiconductor, microelectronics, photonics, microsystems and other engineering industries is well known. In this regard, the determination of thin film thicknesses is highly interesting challenge. Many different techniques can be used to measure the thickness of thin films [1].The main requirement for these methods is locality of measurements and also methods should be non-destructive. Energy dispersive X-ray spectroscopy (EDX) Spectroscopy satisfies these requirements. However, the existing methods for determining the thickness of thin films using EDX have several disadvantages [2].
In this work a non-destructive method for measuring the thickness of the dielectric layers consisting of silicon oxide and silicon nitride has been developed using a scanning electron microscope (SEM) equipped with energy dispersive X-ray spectrometer (EDS).
The main idea of our method consists in the following. An increase of accelerating voltage of electron beam leads to an increase in the depth of generation of the characteristic X-ray. If the signal intensity ratio of one of the substrate elements to the background equal to 3 suggests that the depth of generation of the characteristic X-ray coincides with the thickness of the overlying film. Dependence of the thickness of the overlying film on the accelerating voltage may be plotted (fig.1a). Validation of the results was carried out using the Bette equation:

$$R = \frac{27.6AE_0^{1.67}}{\rho Z^{0.89}} \qquad (1)$$

The volume of generation of the characteristic X-Ray was simulated using a CASINO program [3] (fig.1b). The simulations are in good agreement with the experimental results for small thicknesses.
Thickness determination carried out on samples of integrated circuits PIC16F876A. Samples were treated in RIE (reactive ion etching) to reduce the thickness of the dielectric layers. Cross-section (fig.1c), performed using FIB (focused ion beam), and SEM images were used to confirm thickness of the dielectric layers after RIE.

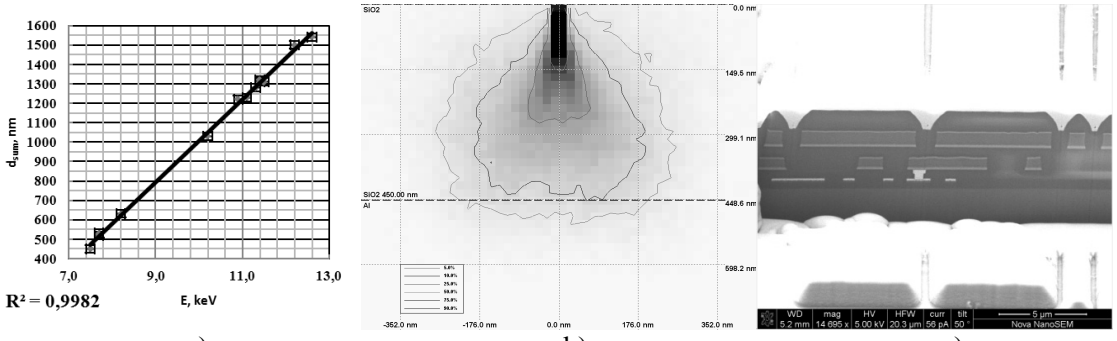

a) b) c)

Fig.1. Calibration curve (a), results of simulation in Monte-Carlo program (b) and SEM image of cross-section PIC16F876A (c).

1 A. Piegari and E. Masetti, “Thin film thickness measurement: a comparison of various techniques,” Thin Solid Films, **124**, pp. 249-257, 1985.
2. G. Love, W. A. Nicholson, A. Armigliato. *Modern Developments and Application in Microbeam Analysis.* Springer, New York, 1998.
3. P. Hovington, D. Drouin, R. Gauvin. "CASINO: A New Monte Carlo Code in C Language for Electron Beam Interaction —Part I: Description of the Program". Scanning, **19**, pp. 1-14, 1997.

The use of multi-scale imaging solutions for microelectronics

M. Chukalina[1,2,3], S. Zaitsev[2], A. Buzmakov[1], D. Zolotov[1], I. Shelokov[2], Ya. Shabelnikova[2], A. Ingacheva[1], V. Asadchikov[1]

1. Shubnikov Institute of Crystallography Russian Academy of Sciences, Moscow, Russia
2. Institute of Microelectronics Technology RAS, Chernogolovka, Russia, chukalinamarina@mail.ru
3. Moscow Institute of Physics and Technology (State University), Dolgoprudny, Russia

Idea to use multi-scale imaging solutions for microelectronics certainly is not new [1]. However, the idea to combine essentially different tomographic techniques (Fig.1) for materials and process characterization looks original and promising. In the report, we plan to answer three questions: why we proposed these 3 measurements for our goals, what is a result of each measurement and why we are not able to construct proposed hardware-software complex for quality control of technologies today? We will give the answer last question as the direct problem statement. After the approach to solving the problem will be suggested by mathematicians, it is possible to think about the metrology complex.

We combine X-ray computed tomography with the cone beam, apparatus X-ray fluorescence tomography [2] and X-ray computed tomography with asymmetric crystals magnification [3] to reconstruct 3D structure of the full object, to scan its ROI in fluorescence mode and to reconstruct ROI with magnification.

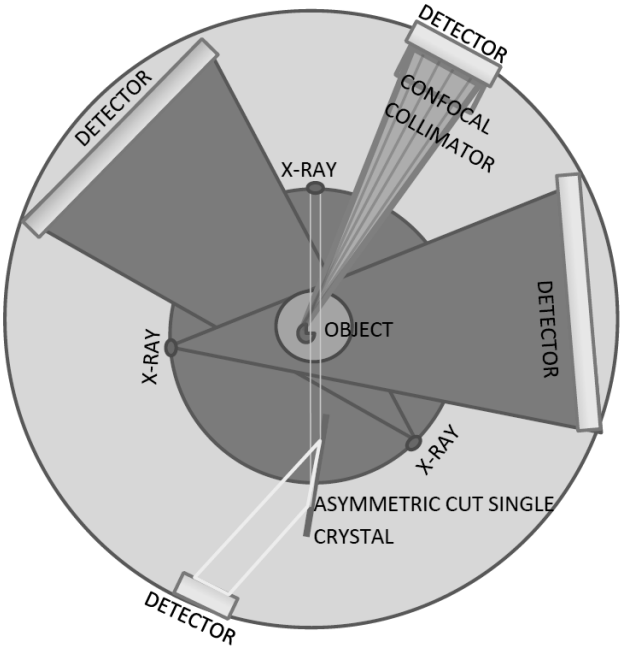

Fig.1. Multi-scale tomography set-up.

Experimental and/or simulation results for each technique are presented and discussed. Reconstructed images (each measure reconstructed image and the final one) contain the set of artifacts. Classification of the artifacts, sources of its appearance, network of the sources and artifacts quantitative description [4] are given. The geometry requirements, sensitivity and resolution estimations is presented.

In the conclusion we present the comparison table for currently used techniques to control the technology processes in-situ and to make final control of the microelectronics products. X-ray techniques look promising today from one side because of the properties of the structure is not changed during the X-ray probing and from the other side the X-ray table sources are on the market.

This work was partly supported by Russian Foundation for Basic Research (grant 16-32-00498) and the Russian Ministry of Education and Science (grant RFMEFI61614X0005).

1. Z. Ehrenfried, N. Sven, L. Markus, W. M. Jürgen, "Multi-scale X-ray tomography for process and quality control in 3D TSV packaging". Int. Microelectronics and Packaging Society, 47th International Symposium on Microelectronics, IMAPS, pp. 184-187, 2014.
2. M. Chukalina, S. Zaitsev, A. Simionovici, C.J. Vanegas, “Two X-ray fluorescence microtomography experimental set ups: standard and confocal collimator apparatus”. Spectrochimica Acta, Part B, **62** (6-7), pp. 544-548, 2007.
3. A. Andreev, V. Asadchikov, A. Buzmakov, A. Konovko, S. Kuzin, A. Pertsov, Yu. Ponomarev, R. Senin, I. Smirnov, S. Shestov, V. Shkurko, "Two times magnified image obtained by X-ray microscope with assymetric crystals". Lett. J. Exper.&Theor. Phys., **85**(1), pp. 106-108, 2007.
4. D. Nikolaev, A. Buzmakov, M. Chukalina, I. Yakimchuk, A. Gladkov, A. Ingacheva, “CT Image Quality Assessment based on Morphometric Analysis of Artifacts”, Proc. ICMRV-2016, Moscow, Sept. 2016 (in press).

3D X-ray topo-tomography imaging of defects in crystalline materials

D. Zolotov, V. Asadchikov, A. Buzmakov, F. Chukhovskii
Shubnikov Institute of Crystallography of Federal Scientific Research Centre "Crystallography and Photonics" RAS , Moscow, Russia, E-mail address: zolotovden@crys.ras.ru

Nowadays the development of modern microelectronics is due to the permanent improvement of non-destructive X-ray diffraction methods for studying microelectronics devices and semiconductor crystalline materials, which are used for. Intrinsic crystal structure defects often cause the deterioration parameters and characteristics of microelectronics. In this regard, identification of the imperfections of the spatial crystal structures is one of the most important study issues, particularly, from viewpoint of the development of non-destructive methods of diagnostics and control of the real structure of crystalline objects.
As is well known, the conventional X-ray topography is a powerful tool for a number of materials of interest. The X-ray topography technique allows visualizing single dislocations, block boundaries, the impurities clusters, stacking faults and so on. At the same time, that has certain restrictions. Firstly, by using laboratory X-ray equipment the exposure time for observing single frame can be up to tens of hours. Secondly, what is most important, the obtained 2D diffraction image strongly complicates the defect structure analysis.
In the last years, the modern X-ray synchrotron radiation sources are widely used for developing the X-ray diagnostic methods, especially, for the so-called X-ray topo-tomography crystal structure imaging [1].
The key idea of the X-ray topo-tomography is the following. The crystal sample is rotated around the axis, which is directed along the diffraction vector. It enables to register a number of 2D diffraction image projections. It is essential that the numerical algorithms, which are usually used in the conventional X-ray absorption tomography, can be applied for reconstructing 3D defects images.
In this work, it is shown that the X-ray diffraction tomography technique can be realized with using the laboratory X-ray tube source [2]. The X-ray topo-tomography measurements have been carried out in the Laue diffraction geometry by means of the Lang method [3], for which a moderate absorption of incident radiation $\mu t < 1$ is a necessary condition for the contrast of the observed defects (μ is the linear absorption coefficient, t is the crystal thickness along the incident X-ray beam).
The main challenge in the X-ray topo-tomography is the quantitative determination of the 3D deformation field distribution related to single defects of crystal lattices.
In the present work, based on the X-ray topo-tomography method elaborated, experimental and theoretical studies are described in application to linear defects in single crystals Si. The corresponding 2D topographic dislocation images are numerically simulated and analyzed by use of the numerical solutions of the Takagi-Taupin equations that describe the two-wave X-ray diffraction by distorted crystals [4]. The 3D-image quantitative reconstruction of the dislocation half-loop near the crystal surface is done with estimating the dislocation sizes [5].

1. W. Ludwig, P. Cloetens, J. Härtwig et al. "Three-dimensional imaging of crystal defects by topo-tomography". J. Appl. Cryst., **34**, pp. 602-607, 2001.
2. D.A. Zolotov, A.V. Buzmakov, V.E. Asadchikov et al. "Study of the internal structure of lithium fluoride single crystal by laboratory X-ray topo-tomography". Cryst. Rep., **56**, pp. 393-396, 2011.
3. A.R. Lang. "The projection topograph: a new method in X-ray diffraction microradiography". Acta Cryst., **2**, pp.249-250,1959.
4. I.S. Besedin, F.N. Chukhovskii, V.E. Asadchikov. "Study of the diffraction contrast of dislocations in X-ray topo-tomography: a computer simulation and image analysis" Cryst. Rep., **59**, pp. 323-330, 2014.
5. D.A. Zolotov, A.V. Buzmakov, D.A. Elfimov et al. "The possibility of identifying spatial location of single dislocations by method topo-tomography on laboratory setups". Cryst. Rep., **61**, 2016, in press.

Silicon ohmic lateral-contact MEMS switch for RF applications

A. Rogozhin[1, 2], A. Miakonkikh[1, 2], A. Tatarintsev[1], K. Lebedev[1], V. Kalnov[1], K. Rudenko[1, 2], V. Lukichev[1, 2]

1. Institute of Physics and Technology of RAS (IPT RAS), Moscow, Russia, rogozhin@ftian.ru.
2. Moscow Institute of Physics and Technology (MIPT), Moscow, Russia.

Application variety and huge potential market of RF MEMS switches guarantee relentless research interest to the field. There are lots of different types of MEMS switches. Direct contact MEMS switches are simple for integration then capacitive MEMS switches [1]. Lateral technology considerably simplifies the formation process [2]. The objective of this research is to estimate characteristics of the simple direct-contact lateral MEMS switch and to understand improvement directions.

MEMS switches were fabricated on the SOI wafers by e-beam lithography, dry etching and wet HF-etching. E-beam lithography and dry etching were used to form the cantilever and electrodes on the buried oxide layer. The structure with two control electrodes was used. IV characteristics were measured by Keithley 4200-SCS. The distance between cantilever and control electrodes was 100 nm (fig. 1, left).

From the obtained IV characteristics it is clear that the devices switch at about 60 V (fig. 1, right). High control voltage could be explained by the large distance between cantilever and control electrode, and high rigidity of the cantilever.

Following simulation in COMSOL Multiphysics showed that the control voltage could be decreased to lower than 3 V by adding of spring element to the cantilever and reduction of the distance between cantilever and control electrodes to 40-60 nm.

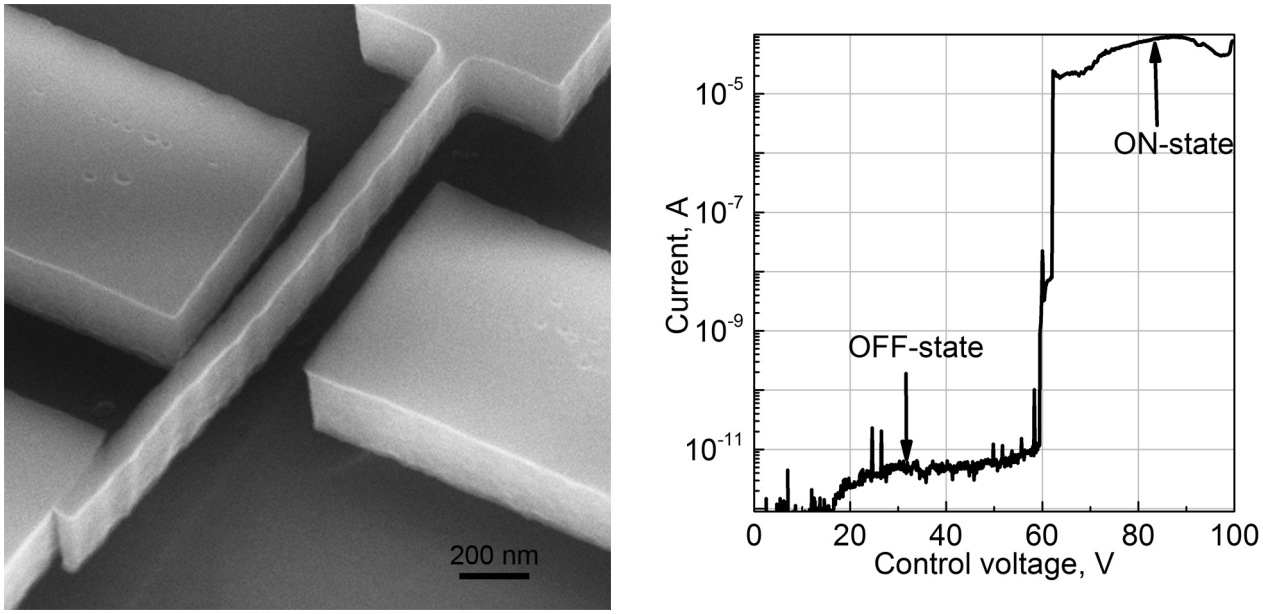

Fig. 1. SEM image of MEMS switch (left) and obtained IV characteristic (right).

1. Y. Wang, et al, “Low-voltage lateral-contact microrelays for RF applications,” IEEE MEMS, 2002.
2. Y. Shi, S.-G. Kim, “A Lateral, Self-cleaning, Direct Contact MEMS Switch,” IEEE MEMS, 2005.

Research of the micromechanical three-axis accelerometer

B. Konoplev, I. Lysenko, E. Ryndin, O. Ezhova, F. Bondarev
Southern federal university, Taganrog, Russia, ingvarlys@gmail.com

Micromechanical accelerometers find broad application in the modern technical devices of different function: from specialized products of space equipment to household appliances, such as cell phones and game platforms of new generation. For registration of the linear accelerations the biaxial and monoaxial micromechanical devices on one substrate are manufactured. They are located on three mutually orthogonal axes of sensitivity that leads to increase of the substrate space occupied by them. To solve this problem, to improve dimensional characteristics of microsystems, to provide a possibility of registration of the linear acceleration of mobile object on three axes of sensitivity the integral multiaxial micromechanical accelerometers are used. The accelerometers are manufactured on one substrate in one fabrication cycle [1].
In work [2] design of the micromechanical accelerometer with three axes of sensitivity is offered. The distinguishing characteristic of the offered design of the micromechanical accelerometer is its structural ability to register the linear acceleration on three axes of sensitivity by method of direct conversion or compensation conversion on two axes.
Within the sphere of this work parametrizable mathematical models of the offered device were developed, results of simulation are received, the experimental devices (fig. 1) are made and analysed.

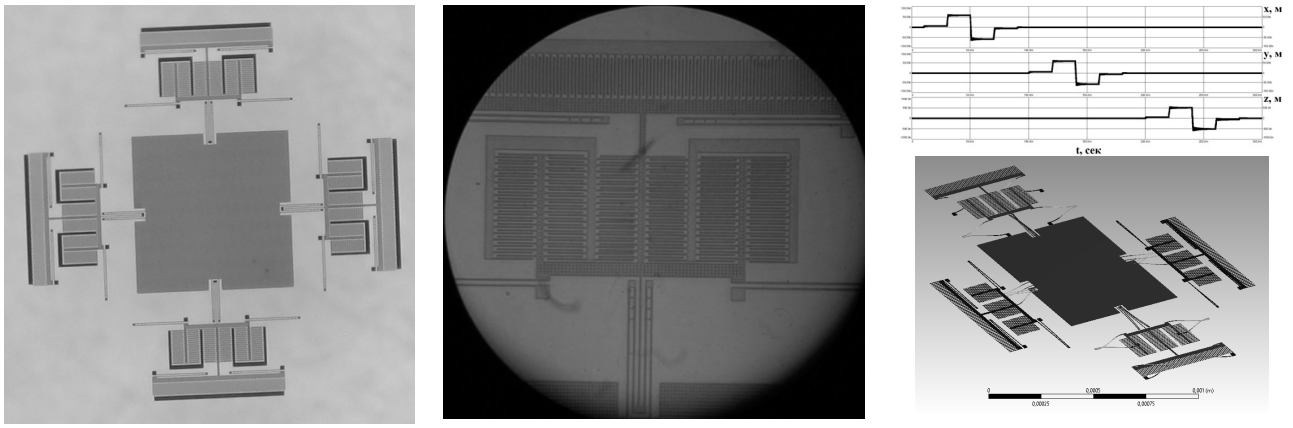

Fig. 1. Topology (MUMPS technology), fragment of the prototype and results of the micromechanical accelerometer researches

As a result the parameters of the micromechanical accelerometer are confirmed. The parameters were planed at the design stage: quantity of axes of sensitivity – 3; the range of the measured accelerations – ±10 g; level of suppression of cross interference – at least 50 dB; sensitivity of the capacity micromechanical transformer – at least 0.5 fF/g, sensitivity of the signal processing devices over 800 kHz/fF. Novelty of the received results consists in a solution of the problem of increase of the functional capabilities of micromechanical accelerometers by using of the principle of the functional integration. This approach provides increase of the functional capabilities of sensors and allows to register the linear accelerations on three axis of sensitivity.
The results have been obtained using the equipment of the Shared Equipment Center and the Research and Educational Center “Nanotechnology” of the Institute of Nanotechnologies, Electronics and Electronic Equipment Engineering, Southern Federal University (Taganrog, Russia). This research is supported by the Ministry of Education and Science of the Russian Federation (the project No. 213.01-11/2014-12).

1. S.P. Timoshenkov, B.B. Kalugin, E.S. Kochurina, C.A. Anchutin, V.A. Kalinin, K.A. Stroganov. "Various Ranges of Linear Accelerations Microaccelerometers for Using in the Inertial Navigation Systems". Nano- and microsystem technique, **8**, pp. 32-35, 2012. (in Russian)
2. B.G. Konoplev, O.A. Ezhova. "Integrated micromechanical accelerometer-clinometer". Patent №2279092, 2006 (in Russian)

Highly sensitive devices for primary signal processing of the micromechanical capacitive transducers

B. Konoplev, E. Ryndin, I. Lysenko, M. Denisenko, A. Isaeva
Southern federal university, Taganrog, Russia, rynenator@gmail.com

Micromechanical gyroscopes and accelerometers are widely used in modern devices in different fields, such as aerospace engineering, defense industry, mobile phone and game console development. Gyroscopes and accelerometers with micromechanical capacitive transducers (MMCT) are prevalently used [1]. Micromechanical components production with using of integrated technology leads to capacity minimization. Capacitance change that occurs under the influence of angular velocities and linear accelerations decreases too. So, the high sensibility is the main performance requirement that makes to MMCT signal processing device. Circuit with the charge amplifiers are usually used to provide higher sensibility. However, charge amplifiers sensitive to noise as well as to signal, which limits specifications of the signal processing device. In a paper [2] the method of micromechanical capacitive transducers signal processing device design is proposed. This method provides the complex solution of the sensibility increasing and noise immunity problems. The finding of the difference frequency of signals, which are formed by two identical generators with micromechanical capacitive transducers in frequency control circuits are the base of this method.
In this study the analog and digital versions of the highly sensitive signal processing devices circuits with frequency output were developed. The breadboards of these devices are fabricated and studied and the project of their integral realization is designed (Fig. 1).

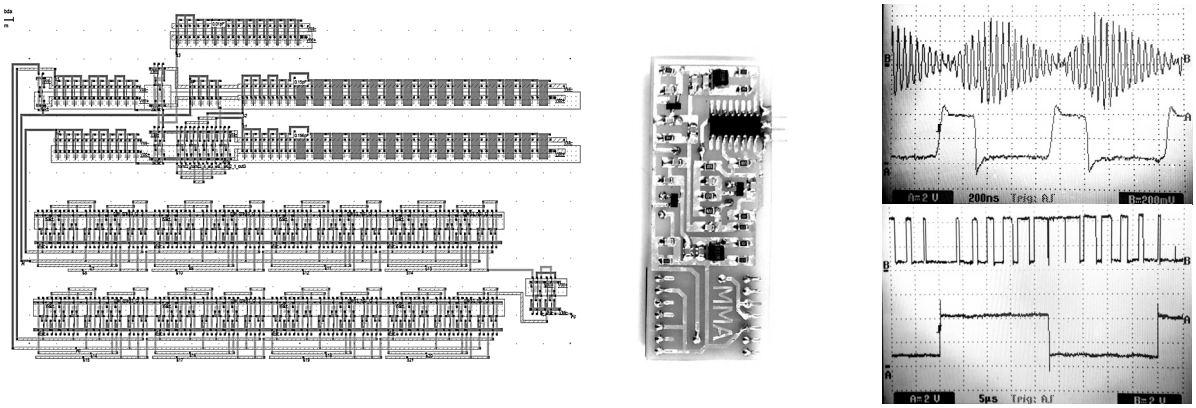

Fig. 1. Layout (CMOS-90 nm), breadboard and studying results of primary signal processing devices of the MMCT.

As a result of the difference principle of output signal forming, decreasing of MMCT capacitances provides a quadratic increasing of sensitivity of the signal processing devices (39.6 kHz/pF for breadboards and 842 MHz/pF for integral realization with nonlinearity coefficient 1.8 %). A noise immunity of the devices (due to the fact that the fluctuations of charge and current noise have a greater influence on the shape of the generating signals, but not on their frequency) can significantly reduce the threshold of the measured capacitance. Moreover, the difference principle of an output signal forming provides increasing stability of the signal processing devices when destabilizing factors act upon.
The results have been obtained using the equipment of the Shared Equipment Center and the Research and Educational Center “Nanotechnology” of the Institute of Nanotechnologies, Electronics and Electronic Equipment Engineering, Southern Federal University (Taganrog, Russia). This research is supported by the Ministry of Education and Science of the Russian Federation (contract №14.575.21.0045 from June 30, 2014, RFMEFI57514X0045).

1. V.D. Verner, P.P. Malcev, A.A. Reznev, A.N. Saurov, Yu.A. Chapligin. "Modern Tendencies in Development of Micro System Technique". Nano- and microsystem technology, **8**, pp. 2-6, 2008 (in Russian).
2. I.E. Lysenko, E.A. Ryndin, N.K. Dudin "Signal Processing Devices of Micromechanical Components Capacitor Converters". Nano- and microsystem technology, **7**, pp. 48-51, 2012 (in Russian).

Computer Simulation of Heavy Charged Particles Radiation Damage on Microsystems

V. Shakhnov, A. Glushko, V. Makarchuk, L. Zinchenko, V. Terekhov, S. Mikhaylichenko
Bauman Moscow State University, Moscow, Russia, E-mail address: lzinchenko@bmstu.ru

Microelectromechanical systems (MEMS, microsystems) are widely used in space missions. It should be noted that special design techniques have to be used for systems design for the applications. Environment conditions: thermal cycling, vacuum, shock and vibration, and radiation are crucial factors in systems design for space missions. The first factors are well investigated. However, radiation damage on MEMS functionality has to be studied in more detail.

Experimental radiation damage tests are expensive and dangerous. Therefore, simulation of radiation damage is more preferable. Simulation results of radiation damage on silicon transistors have been published in [1]. However, MEMS are fabricated using different materials including silicon, glass, ceramics, metals, polymers etc. Moreover, different physical effects (electrostatic, piezoresistive, piezoelectric, electrothermal, optical etc.) are used in MEMS design. In [2], an approach to multi-scale optimization of radiation tolerant MEMS has been proposed. However, the algorithm [2] has been applied to optical and piezoelectric MEMS only.

In our paper, we discuss our experience of application of SRIM and TCAD Sentaurus software [3] for microsystems simulation. SRIM tool has been used to evaluate the energy loss function and parameters of spatial distribution of generated charge using the predefined energy of ions. Then TCAD Sentaurus has been applied for transient processes simulation.

In the paper, we summarize our results for computer simulation of heavy-ion radiation damage on electrostatic MEMS because electrostatic MEMS are the most sensitive devices to the radiation. It causes a change in device calibration and even device failure. Details of charging and a transient electric current depend on the geometry and the materials.

It should be noted that self-similarity is observed for many objects in the real world. Recently, a novel MEMS fractal inductor based on Hilbert Curve has been proposed in [4]. Our focus is on fractal electrostatic microsystems. We propose to use self-similarity for radiation tolerant microsystem design. We compare a radiation tolerance of three microsystems geometry: a parallel plate capacitor, a stepped capacitor based on the Cantor set and a capacitor based on the Koch snowflake. We have chosen silicon capacitor plates. A dielectric spacer is made of silicon dioxide. We simulated heavy-ion radiation damage on the three microsystems. It is obvious that transient current in the stepped capacitor based on the Cantor set is reduced by a factor of 30 in average in comparison with the parallel plate capacitor. It is remarkable that the transient current in the capacitor based on the Koch snowflake is reduced by a factor of 300 in average in comparison with the stepped capacitor based on the Cantor set.

Finally, conclusions about heavy-ion radiation degradation of fractal electrostatic MEMS are envisaged. It is noteworthy that the Koch snowflake curve is the most promising geometry. However, more research of fractal microsystems radiation tolerance is required.

1. A.A. Glushko, L.A. Zinchenko, and V.A. Shakhnov. “Simulation of the impact of heavy charged particles on the characteristics of field-effect silicon-on-insulator transistors”. Journal of Communications Technology and Electronics, **60**, pp. 1134-1140, 2015.
2. V. Shakhnov, L. Zinchenko, I. Kosolapov, I. Filippov. “Modeling and Optimization of Radiation Tolerant Microsystems”, *EMS '14 Proceedings of the 2014 European Modelling Symposium*, pp. 484-489, 2014.
3. A.A. Glushko, *Device and Process Simulation in TCAD Sentaurus System*. BMSTU Press, Moscow, 2015 (in Russian).
4. G. Wang, L. Xu, and T. Wang, "A Novel MEMS Fractal Inductor Based on Hilbert Curve". *Fourth International Conference on Computational Intelligence and Communication Networks*, pp. 241-244, 2012.

Computer modeling of elastic tension fields of MEMS tensoconverters with micro-perforated membrane structure

L.V. Sokolov[1], N.A. Agafonova[2]
1. JSC «Scientific Research Institute of Aircraft Equipment», Zhukovsky, Russia.
2. LLC «Research and Engineering Company», Zhukovsky, Russia.

There is the trend of introduction of microelectromechanical (MEMS) devices based on silicon and heterostructures silicon on insulator (SOI) (e.g. microaccelerometers, microgyros, microelectronic sensors of pressure) in inertial and aerometric system of aircraft and UAV instead of traditional electromechanical transducers in recent years. As a result consumption energy and dimensions and weight characteristics reduce, also main time between failures (MTBF) of control and navigation systems significantly increases.
Design of transducers with microprofiling membrane structure can significantly increase tensosensitivity of sensors [1], but there is the necessity of accurate positioning of strain gauges bridge measuring circuit in local regions of the microprofiling membrane with equal quantities of elastic tension. Only in this case it is possible to provide a sufficiently high linearity of the converter characteristic that is accuracy of measurement [2]. Methods of modeling of elastic tension fields of MEMS tensoconverters with microprofiling membrane structure still insufficiently were investigated.
There are researches of distribution of elastic tension fields of MEMS tensoconverters with microprofiling membrane structures in this paper. Software package COMSOL FEMLAB was used for modeling that allows solving problems in the field of deformable solid using method of finite elements.
As a result of computer modeling experimental batches of tensoconverters of pressure which based on microprofiling membrane structure on silicon with a rigid center and on the SOI structure with a monolithic tensoframe were designed and manufactured.

1. Sokolov L.V. *Bases of designing silicon MEMS integrated tensoconverters of pressure and microsystems with microprofiling triangular membrane structure*. Petit, Zhukovsky, 2009 (in Russian).
2. Sokolov L.V., Zhukov A.A., Kapustyan A.V. Proceedings of the Conf. on Actual Problems of Rocket-Spase Instrumentation and Information Technologies. Fizmatlit, Moscow, pp. 364-366, 2009 (in Russian).

Effect of crosstalk on QBER in QKD in urban telecommunication fiber lines

V.L. Kurochkin[1], Y.V. Kurochkin[1], A.V. Miller[1], A.S. Sokolov[1], A.A. Kanapin[1,2]
1. Russian Quantum Center, Skolkovo, Moscow reg., Russia, v.kurochkin@rqc.ru
2. Moscow State University, Moscow, Russia

Quantum key distribution (QKD) as a technology is being actively implemented into existing urban telecommunication networks. QKD devices are commercially available products. While sending single photons through optical fiber, adjacent fibers, which are used to transfer classical information, might influence the amount of "clicks" of single photon detectors. This influence is registered, since it directly introduces a higher quantum bit error rate (QBER) into the final key [1-3].

Our report presents the results of the first tests of the QKD device, developed in the Russian Quantum Center. These tests were conducted in Moscow, and are the first of such a device in Russia in urban optical fiber telecommunication networks.

The device in question is based on a two-pass autocompensating optical scheme, which provides stable single photon transfer through urban optical fiber telecommunication networks [4, 5]. The single photon detectors ID230 by ID Quantique were used. They operate in free-running mode, and with a quantum effectiveness of 10% have a dark count ~10 Hz. The background signal level in the dedicated fiber was no less than 4 fWt, which corresponds to $1.2 \cdot 10^3$ detector clicks per second. The single mode fiber length in Moscow was 30.6 km, the total attenuation at 11.5 dB. The sifted quantum key bit rate reached values of 1.9 kbit/s at the QBER level of 4-6%. Methods of lowering the influence of crosstalk on the QBER are considered.

This work is supported by the Federal Program «Research and development in priority areas of Russian scientific and technological complex for 2014-2020» (Agreement 14.582.21.0009).

1. K.A. Patel, J.F. Dynes, I. Choi et al. "Coexistence of High-Bit-Rate Quantum Key Distribution and Data on Optical Fiber" Phys. Rev. X, **2**, 041010, 2012.
2. S. Wang, W. Chen, Z.-Q. Yin et al. "Field and long-term demonstration of a wide area quantum key distribution network". Opt. Express, **22**, pp. 21739–21756, 2014.
3. A. Ciurana, J. Martínez-Mateo, M. Peev et.al. "Quantum metropolitan optical network based on wavelength division multiplexing," Opt. Express. **22**, pp. 1576–1593, 2014.
4. D. Stucki, N. Gisin, O. Guinnard, G. Ribordy, and H. Zbinden. "Quantum key distribution over 67 km with a plug&play system," New J. Phys. **4**, p. 41, 2002.
5. V.L. Kurochkin, A.V. Zverev, Yu.V. Kurochkin et al. "Long-distance fiber-optic quantum key distribution using superconducting detectors". Optoelectronics, Instrumentation and Data Processing. **51**, pp. 548–552, 2015.

Single-photon detector design features

S.V. Zaitsev[1,2], V.L. Kurochkin,[1], Y.V. Kurochkin[1]
1. International Center for Quantum Optics & Quantum Technologies, Moscow region, Skolkovo,
2. Femto Vision LLC, Moscow region, Skolkovo, E-mail: s.zaitsev@rqc.ru.

In the report are discussed the laboratory test results of SPAD detectors with InGaAs/InP avalanche photodiodes, operating in Geiger mode. The detectors are intended for communication equipment to receive and transmit quantum information QKD over optical lines. Device operating in synchronous mode with the dead timer setting for proper working conditions of photodiodes.
The report materials will showing the functional block diagram of the detector, real operating signals in the receiver path and clock circuits and main results of measurements.
The input signal of the synchronous detector is the clock, which determines the time positions of expected photons arrival. Increasing the clock speed 1 ... 300 MHz or getting more time positions of the time grid, we provide increased capacity for time position code of signals, when QKD information transmitted over the nets.
At the same time, the maximum attainable speed of photon reception is limited by diode dead time. Diode quantum noise is minimized by inclusion of a special time interval – dead time 0.1 ... 10 μs, after each received and registered a photon. The lowest attainable value of the dead time is determined as a compromise between transients in electrical circuits, passive avalanche «quenching» circuit and thermal transients cooling crystal diode, after each avalanche pass though photodiode. Achievable time and speed parameters are discussed with specific examples of detectors.
In final part of the report, we discuss the technological equipment required for the measurements and detector characterizations.
Optical path forming pulse signals up to 80 ps with an output power level of 1.0 ... 0.01 photons per pulse and a clock frequency 1 ... 300 MHz was designed and made.
Desktop fixture for cooling of diodes was manufactured to provide several possibilities - rapid diode exchange, tuning the signal boards, the input control of diodes and the detector characterization over the temperature range + 25 ... - 70 °C.

This project supported by the Ministry of Education and Science of the Russian Federation in the framework of the Federal Target Program (Agreement 14.579.21.0103).

1. Y.V. Kurochkin, V.L. Kurochkin. Single-photon detectors based on avalanche photodiodes. Proceedings of the Universities, Series Physics, **54** (2), pp. 202-205, 2011 (in Russian).
2. S.V. Zaitsev, V.L. Kurochkin, Y.V. Kurochkin. Research noise characteristics of InGaAs/InP avalanche photodiodes in synchronous and asynchronous mode, single-photon detector. 15th International Youth Conference on Luminescence and Laser Physics, Arshan, July 18-24, 2016. Abstracts of Lectures and Presentations, Irkutsk, 2016, p. 74 (in Russian).
3. S.V. Zaitsev, A.V. Miller, A. Losev, V.L. Kurochkin, Y. Kurochkin. Development of a single-photon detector for quantum communication lines based on InGaAs/InP avalanche photodiodes and measuring their performance. Proceedings of the 17th International Conference "Optica lazerov- 2016", 27 June - 1 July 2016. Abstracts, St. Petersburg, 2016 (in Russian).

Computer simulation of quantum effects in Tavis-Cummings model and its applications

V.Y. Ladunov[1], Y.I. Ozhigov[2], N.A. Skovoroda[3]
1. Moscow State University (MSU), ladunoff@gmail.com
2. MSU, FTIAN, ozhigov@cs.msu.su
3. MSU, chalkerx@gmail.com

We show the effective computer program for simulation of quantum effects in Tavis - Cummings model for the ensemble of two level atoms in the optical cavity. Daphasing assisted transport, quantum bottleneck and the effect of darkness - these purely quantum effects are contra intuitive and can have applications in nano electronics. We show the exact simulation of CSign quantum gate on two cavities with decoherence made by our program, and the effect of dark and almost dark states in this model that can accumulate the energy of atomic excitations and keep it for a long time. We investigate numerically the decay of dark states induced by thermal noise or mechanical shift of atoms, and the influence of dephasing and decoherence on the mentioned quantum effects. Our program is made in Mathematica and Python; it contains the kernel and special modules, which can be elaborated independently that makes the whole program complex flexible and ready for parallel realization.

Structure of dark subspace in Tavis-Cummings model

Y.I. Ozhigov
MSU, FTIAN, ozhigov@cs.msu.su

Dark state of a group of two-level atoms in Tavis-Cummings model can neither absorb nor emit a photon. They can serve as an energy reservoir, from which we can extract photons by the by differentiated impact on atoms, for example by their spatial separation. These states have numerous applications. We calculate the dimension of the subspace of dark states and proved that any dark state is a linear combination of tensor products of EPR-singlet states. This explicit description of singlets supplements the result of the work quant-ph/0201138, where singlets are defined as stationary points of the tensor degree of group SU(2). We also show the example of almost-dark states, in which atoms do not emit photons for a long time, for sufficiently small energy of atomic excitation.

The death of local realism and the idea of quantum computation

V.V. Aristov and A.V. Nikulov
Institute of Microelectronics Technology, Russian Academy of Sciences, 142432 Chernogolovka, Moscow District, Russia. E-mail: nikulov@iptm.ru

According to "Science" [1], one of the breakthroughs of the 2015 year is the experimental result [2] which, according to [3], has hammered final nail in the coffin of local realism. The claim about the dethronement of realism is based [3] on a new loophole-free Bell inequality violation [2]. The author [3] writes fairly that "*Bell inequalities are named after John Bell, the physicist who discovered in 1964 that the predictions of quantum mechanics are incompatible with the local-realism hypothesis*". But this author as well as most other contemporary authors don't want to know that according to John Bell violation of his inequalities "*is the real problem with quantum theory: the apparently essential conflict between any sharp formulation and fundamental relativity*" (see his Introductory remarks "Speakable and unspeakable in quantum mechanics" at Naples-Amalfi meeting, May 7, 1984, p. 172 [4]) rather than the death of local realism. Unfortunately most contemporary authors as well as the authors [1-3] don't want to understand that the incompatibility of quantum mechanics with realism was obvious long before the famous Bell paper [5]. Einstein has concluded that Born's interpretation of the Schrodinger wave function implies '*spooky action at a distant*' and conflict with the relativity postulate long before Bell, as far back as 1927, during the discussion at the Fifth Solvay Conference [6]. But most physicists could not understand this logical deduction made by Einstein. Only few scientists could realize also that Bohr claimed a real 'spooky action at a distant' in his reply [7] on the famous EPR paper [8]. John Bell, who was among these few scientists, "*felt that Einstein's intellectual superiority over Bohr, in this instance, was enormous as vast gulf between the man who saw clearly what was needed, and the obscurantist*" [9]. Bell understood that Bohr [7] rejected the premise - 'no action at a distance' - rather than refuting the EPR argument [10]. Most contemporary authors, in contrast to Einstein, Schrodinger, Bell and other critics of quantum mechanics, misinterpret the essence of the conflict between quantum mechanics and realism. For example, the author [3] interprets the EPR correlation just realistically: "Entanglement is a holistic property of a system of quantum particles that can persist even when the particles are far apart". Whereas Schrodinger has defined the EPR correlation as *entanglement of our knowledge* as far back 1935 [11]. The true understanding of the conflict between quantum mechanics and realism has not only fundamental but also practical importance due to the crucial role of the EPR correlation for the idea of quantum computation. It will be shown in the present work that the EPR correlation is deduced logically from Born's interpretation and Dirac's jump as a result of a spooky non-local influence of the mind of the observer on quantum state of observed system. According to this logical deduction quantum computer cannot be real according to the orthodox quantum mechanics, contrary to almost universal belief.

1. A. Cho, "Quantum weirdness confirmed", Science **350**, p. 1463, 2015.
2. B. Hensen at al., Loophole-free Bell inequality violation using electron spins separated by 1.3 kilometres. Nature **526**, pp. 682–686, 2015.
3. H. Wiseman, Death by experiment for local realism. Nature **526**, pp. 649–650 (2015).
4. J.S. Bell, *Speakable and unspeakable in quantum mechanics. Collected papers on quantum philosophy*. Cambridge University Press, Cambridge, 2004.
5. J.S. Bell, On the Einstein-Podolsky-Rosen paradox. Physics **1**, pp. 195-200 (1964).
6. A. Einstein, Electrons et photons. Rapports et discussions du cinquieme Gonseil de physique- Bruxelles du 24 au 29 octobre 1927 sous les auspices de 1' Institut International de physique Solvay, pp. 253-256. Paris, Gautier-Villars et Gie, editeurs 1928.
7. N. Bohr, Can Quantum-Mechanical Description of Physical Reality be Considered Complete? Phys. Rev. **48**, pp. 696-702 (1935).
8. A. Einstein, B. Podolsky, N. Rosen, Can Quantum-Mechanical Description of Physical Reality Be Considered Complete? Phys. Rev. **47**, pp. 777-780 (1935).
9. J. Bernstein, Quantum Profiles. Princeton, 1991.
10. J.S. Bell, Bertlmann's socks and the nature of reality. Journal de Physique, pp. **42**, 41-61 (1981).
11. E. Schrodinger, Die gegenwartige Situation in der Quantenmechanik. Naturwissenschaften **23**, pp. 823-828, (1935).

No-go theorems and the idea of superconducting quantum bits

A.V. Nikulov
Institute of Microelectronics Technology, Russian Academy of Sciences, 142432 Chernogolovka, Moscow District, Russia. E-mail: nikulov@iptm.ru

The idea of superconducting quantum bits is based on the pet assumption of Sir Anthony Leggett about possibility of macroscopic quantum coherence. The title of the paper [1] emphasizes that this assumption contradicts to macroscopic realism. It emphasizes also that the superconducting loop with Josephson junctions can be indeed considered as quantum bit (persistent current [2] or flux [3] qubit) only if the flux is not there when nobody looks. The question in the title of [1] "Is the flux there when nobody looks?" represents the essence of the contradiction of quantum mechanics with realism: the magnetic flux and the persistent current in the loop don't exist when nobody looks according to the orthodox quantum mechanics. Whereas the realists, such as Einstein, would like to think that the flux (or the moon) exists independently on the mind of the observer. The creators of quantum mechanics have rejected realism because of the impossibility to describe realistically some quantum phenomena, for example the Stern-Gerlach effect [4]. Bell wrote that "*Phenomena of this kind made physicists despair of finding any consistent space-time picture of what goes on the atomic and subatomic scale… Going further still, some asserted that atomic and subatomic particles do not have any definite properties in advance of observation. There is nothing, that is to say, in the particles approaching the magnet, to distinguish those subsequently deflected up from those subsequently deflected down. Indeed even the particles are not really there*"[5]. The validity of the realism rejection is proved with the help so-called no-go or no-hidden-variables theorems [6]. One of the first no-go theorems was proposed by von Neumann as far back as 1932 [7]. Greta Hermann pointed out a glaring deficiency of von Neumann's argument as far back as 1935 [6]. But her work was entirely ignored. "*A third of a century passed before John Bell, 1966* [8]*, rediscovered the fact that von Neumann's no-hidden-variables proof was based on an assumption that can only be described as silly – so silly, in fact, that one is led to wonder whether the proof was ever studied by either the students or those who appealed to it to rescue them from speculative adventures*" [6]. John Bell disproving Neumann's no-go proof in his first paper [8] has proposed other no-go theorem in his second paper [9], which is well known now as the Bell inequalities. The possibility of superconducting qubits should be proved with a no-go theorem. Some authors [10] are sure that experimental violation [11] of the Leggett–Garg inequality [1] can both disprove realism and prove the possibility of superconducting qubits. These authors misinterpret the LG inequality as a Bell's inequality in time although it was noted as far back as 1987 [12] that the analogy between the Bell type of inequalities and the LG inequalities is misleading, because of a key role of the locality demand in the deduction of Bell's inequalities. It will be accentuated in the present work that the LG inequality [1] is analogue of von Neumann's rather than Bell's no-go theorem. This fact calls the idea of superconducting qubits in question.

1. A.J. Leggett and Anupam Garg, Quantum mechanics versus macroscopic realism: Is the flux there when nobody looks? Phys. Rev. Lett. **54**, pp. 857–860 (1985).
2. J.E. Mooij, T.P. Orlando, L. Levitov, L. Tian, C.H. van der Wal, S. Lloyd, Josephson Persistent-Current Qubit. Science **285**, pp. 1036-1039 (1999).
3. I. Chiorescu, Y. Nakamura, C.J.P.M. Harmans, J.E. Mooij, Coherent Quantum Dynamics of a Superconducting Flux Qubit. Science **299**, pp. 1869-1871 (2003).
4. W. Gerlach, O. Stern, Das magnetische Moment des Silberatoms. Zeitsch. fur Phys. **9**, pp. 353-355 (1922).
5. J.S. Bell, Bertlmann's socks and the nature of reality. J. de Physique, **42**, pp. 41-60 (1981).
6. D. Mermin, Hidden variables and the two theorems of John Bell. Rev. Mod. Phys. **65**, pp.803–815 (1993).
7. J. von Neumann, Mathematishe Grundlagen der Quantem-mechanik. Springer, Berlin, 1932.
8. J.S. Bell, On the problem of hidden variables in quantum mechanics. Rev. Mod. Phys. **38**, pp. 447-452 (1966).
9. J.S. Bell, On the Einstein-Podolsky-Rosen paradox. Physics **1**, pp. 195-200 (1964).
10. J.E. Mooij, Quantum mechanics: No moon there. Nature Physics **6**, pp. 401-402 (2010).
11. A. Palacios-Laloy et al., Experimental violation of a Bell's inequality in time with weak measurement. Nature Physics **6**, pp. 442–447 (2010).
12. L.E. Ballentine, Realism and quantum flux tunneling. Phys. Rev. Lett. **59**, pp. 1493–1495 (1987).

Ambipolar Memristor-Based Oscillator

V. Rakitin[1], A. Rakitin[2]
1. Institute for Design Problems in Microelectronics, Moscow, Russia, vlarak@rambler.ru,
2. Lomonosov Moscow State University, Moscow, Russia, alexander.v.rakitin@gmail.com.

The memristor is a passive two-terminal device with a resistance that varies depending on the passing charge. Memristors are compatible with silicon CMOS technology and can be used to extend the capabilities of data processing systems. The memristor can also be used to improve various circuits and is particularly effective in oscillators [2]. Of particular importance are nonreactive memristor oscillators, i.e. oscillators that do not contain reactive elements like inductances or capacitances [3-5]. These oscillators are typically constructed using a window comparator. In this paper we consider the possibility of building nonreactive memristor oscillators using devices with a negative differential resistance (NDR). An oscillator consisting of a basic linear drift memristor [1], resistor, and window comparator only permits monostable oscillation when using NDR devices as the load due to the linearity of the "instantaneous" I-V characteristic of the memristor for a given control characteristic. The requirements for the active load can be lowered by introducing ambipolarity into the "instantaneous" I-V characteristic. Any change of the voltage sign in an ambipolar memristor (aM) leads to a reduction of its conductivity. As a result, a single-threshold comparator with hysteresis or a diode with NDR can serve as the load in an oscillator with an ambipolar memristor.

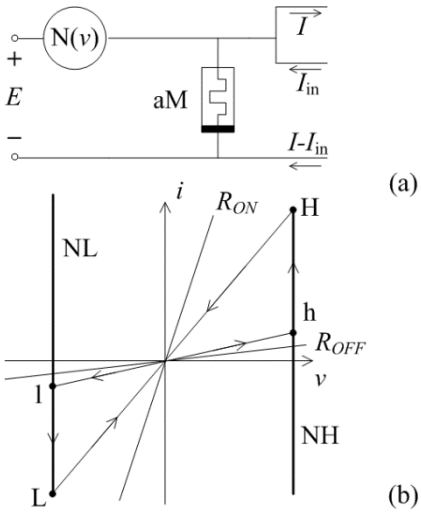

Fig. 1. Memristor oscillator with an N-diode, phase portrait of the I-V characteristic for an N-type oscillator.

We consider using N- and S-diodes with piecewise-constant I-V characteristics as the load in aM-based oscillators. If the threshold values for conductivity are presented as $(G_m + g_0)$ and $(G_m - g_0)$, the oscillation period for an N-type aM-oscillator is

$$T_N = 4g_0/\beta \cdot E, \quad (1)$$

with β being the inertia of change in the memristor's conductivity with the dimension $[C/V^2]$. The oscillation period is not dependent on the input current. The constant voltage component is zero because of central symmetry of the I-V plot. For an S-type oscillator the constant component of the output current is

$$\bar{I} \simeq I_m(1 - g_0/G_m). \quad (2)$$

We conclude that there is a possibility of using an S-type aM-oscillator with a current input acting as a modulator. An N-type aM-oscillator has the same properties, if the memristor component has its resistance controlled by voltage.

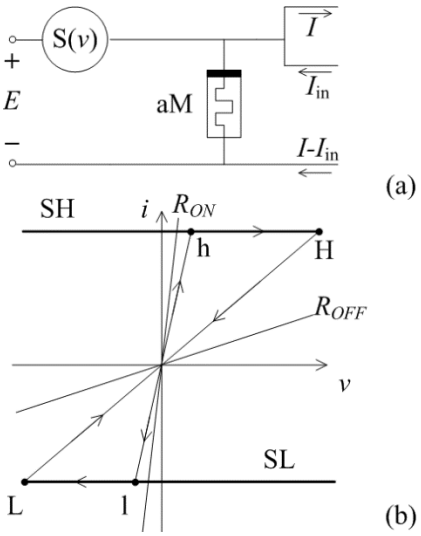

Fig. 2. Memristor oscillator with an S-diode, phase portrait of the I-V characteristic for an S-type oscillator.

We propose a more general statement: a modulator that uses an aM and a diode with NDR must have the memristor's changeable property controlled by the ambiguous variable. Thus, the aM in conjunction with NDR devices facilitates the creation of nonreactive oscillators that allow a simple integrated implementation.

1. D. Strukov, et al., "The Missing Memristor Found," *Nature*, **453**, pp. 80–83, 2008.
2. M. Itoh, L. Chua, "Memristor Oscillators," *Int. J. Bifur. and Chaos*, **18(11)**, pp. 3183–3206, 2008.
3. M. Fouda, A. Radwan, "Memristor-based voltage-controlled relaxation oscillators," *Int. J. Circuit Theory and Appl.*, **42(10)**, pp. 1092–1102, 2014.
4. M. Zidan, et al., "A family of memristor-based reactance-less oscillators," *Int. J. Circuit Theory and Appl.*, **42(11)**, pp. 1103–1122, 2014.
5. A. Mosad, et al., "Improved memristor-based relaxation oscillator," *Microel. J.*, **44(9)**, pp. 814–820, 2013.

Application of Triple Modular Redundancy for Soft Error Mitigation in 65-28 nm CMOS VLSI

A.P. Skorobogatov
Federal State Institution «Scientific Research Institute for System Analysis of the Russian Academy of Science», Moscow, Russia, E-mail address: skorobog_a@cs.niisi.ras.ru

One of the main tasks for the design of space integrated circuits (IC) is to ensure their tolerance to a single event upset (SEU), which is the switching of individual logical elements under the heavy ion strike [1]. The probability of multiple failures from a single particle increases in modern high-performance VLSI with an increase of integration scale. Besides, single event transient (SET) pulse increase with shrinking technology node from 250 nm to 130 nm [2].

Heavy ion induces electron-hole pairs when passing through the semiconductor. As a result, due to the drift and diffusion processes of charge collection, ionization current occurs in IC element [3]. In this paper, we use the model of charge collection from heavy ion track with sensitive area considered as a cylinder with effective radius end height [4]. The circle with effective radius is the sensitive area for modeling.

The problem of multiple soft errors plays a major role in modern VLSI. For sub-100 nm designs we can consider the effective sensitive area size as 2 μm [5, 6]. E.g., on TSMC 65 nm design with 10-track cells we get multiplicity of failure up to 4 [7] (modeling was performed for failure in data registers). In TSMC 28 nm node tracks are narrower, so we get multiplicity up to 6 or even up to 8 (for 9-track cells).

One of the main methods for the decrease of soft error rate is structural redundancy including triple modular redundancy [8]. We used register transfer level (RTL) based global triple modular redundancy with 3 majority elements in each node. But even this method is not effective in design with a great many of multiple errors because one multiple fault can cover cells in more than one path in triplicated scheme. Consequently, for 65 nm and lower we propose a method to use component separation along with triple modular redundancy. The separation distance should be equal to the sensitive area size or more.

1. A.I. Chumakov. *Deistvie cosmicheskoi radiatsii na IS*. Radio and Svyaz, Moscow, 2004, 320 pp. (in Russian).
2. J.M. Benedetto, P.H. Eaton, D.G. Mavis, M. Gadlage. “Digital Single Event Transient Trends With Technology Node Scaling”. IEEE Transactions on Nuclear Science, **53** (6), pp. 3462-3465, 2006.
3. M. Raine, G. Hubert, M. Gaillardin, L.T. Artola et al. “Impact of the Radial Ionization Profile on SEE Prediction for SOI Transistors and SRAMs Beyond the 32-nm Technological Node”. IEEE Transactions on Nuclear Science, **58** (3), pp. 840-847, 2011.
4. K.V. Zolnikov, K.I. Tapero, V.A. Smerek, T.P. Belyaeva. “Model radiatsionnih effectov vozdeistviya tyajelih yadernih chastits v KMOP-elementah mikroshem”. Programmnie Producti I Sistemi, №3, pp. 17-21, 2001 (in Russian).
5. O.A. Amusan. “Analysis of Single Event Vulnerabilities in a 130 nm CMOS Technology”. M. S. Thesis, Vanderbilt University, Nashville, Tennessee, USA, 2006.
6. L. Entrena, A. Lindoso, E.S. Mill´an, S. Pagliarini et al. “Constrained Placement Methodology for Reducing SER under Single-Event-Induced Charge Sharing Effects”. Radiation and Its Effects on Components and Systems (RADECS) papers, 2011.
7. A.P. Skorobogatov. “Metodika razneseniya komponentov SBIS dlya preodoleniya mnogokratnih sboev pri vozdeistvii TZCh”, Voprosi atomnoi nauki i tehniki, issue “Fizika radiatsionnogo vozdeistviya na radioelektronnuyu apparaturu”, vol. 4, pp. 5-11, 2015 (in Russian).
8. V.A. Ostreikovsky. *Teoriya nadejnosti.* Visshaya Shcola, Moscow, 2003, 128 pp. (in Russian).

Graphene Field Effect Structure Manufacturing and Characterization

S. Shostachenko, R. Zakharchenko, G. Zebrev, V. Razumny, N. Kargin
National Research Nuclear University MEPhI, Moscow, Russia, sashostachenko@gmail.com

The graphene field effect structure was investigated in this report. Graphene film was manufactured by the CVD onto a substrate of the copper foil 60 um thick, at atmospheric pressure using methane as a hydrocarbon precursor [1]. The graphene synthesis was carried out at 1050 °C as a carrier gas was a mixture of argon and hydrogen. The copper foil was dissolved after synthesis process in the solution of $FeCl_3$. After washing in the distilled water, the graphene film was transferred to the SiO_2/Si substrate with a thermally formed oxide thickness of 300 nm. Back gate contact to the silicon oxide film represented by a continuous metal layer to the reverse side of the plate. The SiO_2 film at the same time played the role of the lower gate dielectric. The graphene film etching to form a transistor structure was conducted in an oxygen plasma (200 W, 6 minutes) by the Diener Nano. The metal Ti/Au (20/200 nm) drain, source and the gate were deposited by the electron beam evaporation. The resistance of ohmic contacts was $5.6 \cdot 10^{-5}$ Ohm·cm^2. The current voltage characteristics of graphene samples with $W/L \cong 24/18$ μm were measured at different drain voltages.

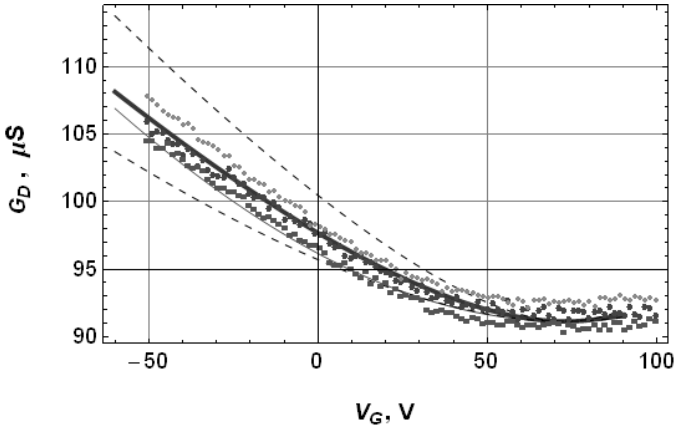

Fig.1. Experimental conductance measured at different V_{DS} (points) and simulation results (lines). The model fitting parameters are mobility ~ 30 cm^2/(V s), residual carrier concentration at the neutrality point ~ 1.6 10^{13} cm^{-2}, mean interface trap capacitance 54 fF/ μm^2.

The experimental results were simulated with the model, which allows taking into account the interface trap density [2]. This work is aimed to development of preliminary technology of graphene field effect transistor manufacturing. The further work is needed to improve the graphene film technology and device parameters.

Acknowledgements
The study was supported by the Ministry of Education and Science of Russian Federation (a unique identification number of the work is RFMEFI58414X0001).

References

[1] I. Komissarov, "Micro Raman Investigation of Graphene Synthesized by Atmospheric Pressure CVD on Copper Foil from Decane". Physics Procedia, **72**, pp. 450 – 454, 2015.
[2] G.I. Zebrev et al., "Interface Traps In Graphene Field Effect Devices: Extraction Methods and Influence on Characteristics," chap. 26, in Graphene Science Handbook, Vol. 5. CRC Taylor and Francis Group, LLC, 2016.

Single-electron transistor based on intramolecular single-atom charge center

V. Gaydamachenko, E. Beloglazkina, R. Petrov, I. Sapkov, E. Soldatov, S. Dagesyan
M.V. Lomonosov Moscow State University, Moscow, Russia, 1994vg@gmail.com

In the last decade a new direction of nanoelectronics devoted to single-electronics on single atoms is actively developing. A promising branch of this trend is a fabrication of single-electron transistors based on single molecules containing monoatomic accentuated charge centers. Development and research of nanoelectronic devices based on such objects can lead to the creation of computing devices working on new physical principles (quantum computers, charge cellular automata) and offers new ways of processing and transmission of information. Thus, a creation of single-electron transistors based on single molecules, which contain monoatomic emphasized charge centers, and researching of their properties is currently very actual problem.

In this paper approaches to creation such molecular single-electron transistors based on complex compounds of rhodium (Rh (III)) and terpyridine molecules are developed. Also new method of fabrication single-electron transistors with nanogaps (<5 nm) between gold electrodes "suspended" over the substrate was developed.

System of such transistor nanoelectrodes was formed from gold nanowires with 18×40 nm^2 cross section in the region of maximum constriction. Gold nanowires were fabricated by photo- and electron-beam lithography. Suspending of nanowire over the substrate was obtained by wet etching in 10% HF solution during 20 seconds. Such regime provides the overhang in area of maximum constriction. Nanogap fabrication problem was solved by electromigration technique. This method is described in [1]. In present work the electromigration process was carried out for the first time in the absence of a heat removal from the gap formation region to substrate. It was shown that the heat removal into the substrate does not play a significant role, all the heat was going away from a broken place through the gold nanowires. A typical size of received nanogaps amounts to 1 - 4 nm.

A method for incorporation of complex compounds of rhodium (Rh (III)) and terpyridine molecules in nanogaps to form the single-electron transistor was first developed. It was shown that the incorporation of the molecules into the gap occurs. It is shown that the incorporation of the molecules into the gap occurs more effectively when they are deposited on the nanowire before gap formation. Measured current-voltage characteristics of fabricated transistors confirm the presence of molecules in nanogap. These I-V curves measured at 77 K show that electron transport through the molecule provided by intramolecular charge center - a single rhodium atom – has a character of correlated electron tunneling.

Thus, in this work single-electron transistors based on complex compounds of rhodium and terpyridine molecules are fabricated by new technique of electrodes creation and technique of molecules incorporation into the gap between electrodes. Measured characteristics of fabricated transistors show correlated electron tunneling through the intramolecular charge center - a single rhodium atom.

1. Dagesyan S.A., Soldatov E.S., Stepanov A.S. "Forming extremely small gaps in metal nanowires and studying their properties". Bulletin of the Russian Academy of Sciences: Physics, **78** (2), pp. 139-143, 2014.

Dielectrophoresis method for single electron transistors creation

A.G. Galstyan*, S.A. Dagesyan, E.S. Soldatov, O.V. Snigirev
Lomonosov Moscow State University, Faculty of Physics, Moscow, Russia
* Presenting Author, E-mail: ag.galstjan@physics.msu.ru

In this contribution we present a way of creation of the planar high-temperature single-electron transistors using the dielectrophoresis method [1] to embed single 2-4 nm gold nanoparticles into the gap between the electrodes. The nanogaps were produced using electromigration technique [2]. Then they were placed to the nanoparticles solution, and the electric voltage was applied. Thus the nanoparticles were drawn to the gap, and this process was controlled by specially designed control system. The change of the electrical resistance of the gap was used to define the presence of the particle in the gap.

The optimal solvent for the nanoparticles solution was defined. Also it is shown that the applied potential in the range 1.8-3 V is optimal for the protraction and fixation of a single particle. This has allowed to produce single-electron transistors based on gold nanoparticles.

The properties of the electron transport through the obtained transistors were investigated in the wide range of temperatures (77 – 300 K). These devices have a typical Coulomb blockade region of 200-300 mV. Moreover, for the resulting device we have measured the 2D stability diagrams. These diagrams show the dependence of the current through the system on two parameters: on the voltage on the gate and on the drain-source voltage. The typical obtained diagram is given in Figure 1. It looks like recurring rhombi what is a distinctive feature of the single-electron transistors. So the electrical measurements prove the effectiveness of the suggested single-electron transistor formation method.

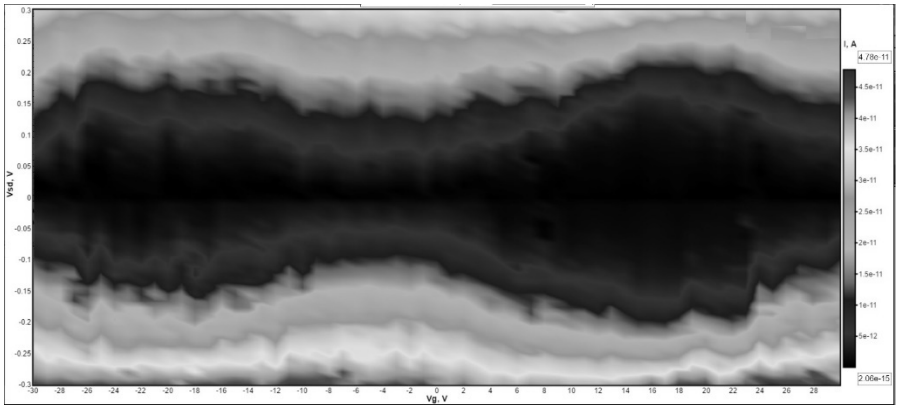

Figure 3. The resulting 2D stability diagram of the single-electron transistor at 77 K temperature.

1. N.G. Green, H. Morgan, and J.J. Milner "Manipulation and trapping of sub-micron bioparticles using dielectrophoresis". Journal of Biochemical and Biophysical Methods, **35,** pp. 89-102, 1997.
2. S.A. Dagesyan, E.S. Soldatov, and A.S. Stepanov. "Forming extremely small gaps in metal nanowires and studying their properties". Bulletin of the Russian Academy of Sciences: Physics, **78**, pp. 139-143, 2014.

Single-electron transistor based on several dopant atoms

S. Dagesyan[1], V. Shorokhov[1], D. Presnov[2], E. Soldatov[1], A. Trifonov[2], V. Krupenin[1]
1. M.V. Lomonosov Moscow State University, Moscow, Russia, dagesyan@physics.msu.ru
2. Skobeltsyn Institute of Nuclear Physics, Moscow, Russia.

The significant progress in nanofabrication can lead to the development of fabrication technologies in atomic scale range [1]. It became possible to satisfy the growing interest to studies of electron transport through single atoms. This new research field is actively developing at the moment [2-4]. Devices based on single atom structures are proposed to be a basis for the future nanoelectronics and for quantum computing systems [5]. The simplest single atom structure is a single-electron transistor based on single dopants in crystal lattice.

Most of the existing single-atom transistor fabrication techniques contain significant random factor: the position and amount of dopant atoms in the transistor structure can't be controlled precisely. The researchers often face with complex systems when the electron transport is realized through the several atoms in the transistor structure. Despite this fact there is a lack of published experimental results on electrical characteristics of such complex systems.

In this work we would like to demonstrate a single-electron transistors based on several dopant atoms in the transistor channel. Transistors were fabricated using silicon on insulator (SOI) material. Phosphorus atoms were used as dopants.

Fabricated transistors consist of the following parts: 1) a crystalline silicon solid bridge with localized impurity atoms; 2) source and drain macroscopic lead electrodes with a higher dopant concentration; 3) gate electrodes located near the bridge. The cross section of the bridges was about 50×30 nm^2.

The transistors electrical measurements were carried out at 4.2 K. The current through transistors channel were measured both as a function of the source-drain voltage and the gate voltage. Stability diagrams of transistors were built using this data. They electrical properties were compared with the simple theoretical model.

This work was supported by "Russian science foundation" (grant № 16-12-00072)

1. Manfrinato V.R., et al. "Resolution limits of electron-beam lithography toward the atomic scale." Nano letters **13** (4), pp. 1555-1558, 2013.
2. Presnov D.E., et al. "Arsenic dopant single-atom single-electron transistor." Book of Abstracts of Intenational Conference "Micro- and Nanoelectronics - 2014", ICMNE 2014, Zvenigorod, Russia, (October 6-10, 2014), P2–02.
3. Moraru D., et al. "Atom devices based on single dopants in silicon nanostructures." Nanoscale Research Letters **6** (1), pp. 1-9, 2011.
4. Fuechsle M., et al. "A single-atom transistor." Nature Nanotechnology **7** (4), pp. 242-246, 2012.
5. Hollenberg L.C.L., et al. "Charge-based quantum computing using single donors in semiconductors." Physical Review B **69** (11), p. 113301, 2004.

Formation of metal electrodes with a nanoscale separation using an evaporated resist

G. Zharik, S. Dagesyan, E. Soldatov
M.V. Lomonosov Moscow State University, faculty of Physics, dagesyan@physics.msu.ru

Creation of electronic devices based on single molecules is a promising challenge. There are many experimental works devoted to specific features of the electron transport through different types of molecules [1-3]. The intensive work in this field became possible since several techniques of nanometer scale gaps obtaining were proposed [4-5]. A nanometer scale gap between metal electrodes is an interface that can provide the electrical contact to a single molecule. But the most popular methods of a nanogap creation are difficult to use for some practical applications. They contain a technological steps such as electromigration process or electroplating that make the production process not scalable because requires a special chip design.

In this work we would like to demonstrate a simple technique that allows to produce nanogaps (<5 nm) between gold electrodes using nothing else standard nanolithography procedures. The method is based on ion etching of gold film through a polymer mask formed by the electron-beam lithography. An argon plasma was used for the ion etching. A low molecular weight polystyrene was used as a negative tone resist. The substrate with 20 nm gold film was coated by 25 nm polystyrene using vacuum thermal sputtering as described in [6]. This deposition method allows making thin resist layer and varying a resist thickness by a very simple way to fine tune the process.

The electron-beam lithography patterns contained 20 nm wide lines with 30 – 10 nm separation between them. After the ion etching through the resist mask the size of the obtained gaps between metal electrodes can be even smaller due to isotropic component of etching and proximity effect during patterning. We demonstrate that small nanogaps (<5 nm) can be obtained by such simple method with a relatively high yield. Also it was shown that this method is good for making many-electrode systems with a nanometer scale separation leading contact to a small area on the surface of a substrate. The main advantages and limitations of the method are discussed.

1. Liang, Wenjie, et al. "Kondo resonance in a single-molecule transistor." *Nature* **417**(6890), pp. 725-729, 2002.
2. Park, Jiwoong, et al. "Coulomb blockade and the Kondo effect in single-atom transistors." *Nature* **417**(6890), pp. 722-725, 2002.
3. Bogani, Lapo, and Wolfgang Wernsdorfer. "Molecular spintronics using single-molecule magnets." Nature materials **7**(3), pp. 179-186, 2008.
4. Park, Hongkun, et al. "Fabrication of metallic electrodes with nanometer separation by electromigration." Applied Physics Letters **75**(2), pp. 301-303, 1999.
5. Yasutake, Yuhsuke, et al. "Simultaneous fabrication of nanogap gold electrodes by electroless gold plating using a common medical liquid." Applied Physics Letters **91**(20), p. 203107, 2002.
6. Zhang, Jian, Celal Con, and Bo Cui. "Electron beam lithography on irregular surfaces using an evaporated resist." ACS nano **8**(4), pp. 3483-3489, 2014.

Double-“striping” transistor test-structures with carbon nanotubes channels

V.M. Efimov, D.G. Esaev
Institute of Semiconductor Physics, Novosibirsk, Russia, E-mail address efimov@isp.nsc.ru, esaev@isp.nsc.ru

The real progress in single-walled carbon nanotubes (SWCNT) nanoelectronic fails by the absence of high purity semiconducting material. The remaining challenge is to obtain the 99.99% purity level for s-SWCNT [1]. Two sides of the problem are to synthesis the tubes and to control the semiconducting versus metallic purity. The recent progress in receiving pure s-SWCNT is gradually observed [2]. The control of the CNT-networks by optical tools finishes at the level of 99%. For further control of the CNT-purity the most effective devices for test measurements are the field effect transistors (FET), and their most reliable parameter - ON/OFF ratio of the source-drain current. Here we propose two main ideas for such testing. First the use of “striping” CNT-networks for elimination of percolation currents through the CNT-FET channel not only by direct (here - “vertical”) “striping” (see Fig. 1A) [3], but the same time horizontal zigzag “striping” (Fig. 1B).

Both of these methods yield the result depending on such parameters as concentration of nanotubes in network layer and width/length (*W*/*L*) relation of the channel. But in first case we have something as parallel connection and in the second consecutive connection of “elements”. In each of situations it is possible the emergence (with some probability) of the percolation channels.

The second simple method, which we used is the visualization of electrically contacting elements (souce, drain, and tubes) by modern methods of processing raster images. As an example you can see the areas of nanotubes network after “striping” procedure, which are contacting or with the source or with the drain. At the beginning the casual network of 625 twisting "nanotubes" was generated and scattered on square area. Such quantity corresponds to 5% of metal nanotubes in comparison with the 95% concentration of semiconductor CNT (in a figure aren't shown). At the edges of a square (above and below) some of nanotubes electrically contacts with drain and sourse contacts, what has been established just by allocation of the contacting pixels of black color. Of cause the areas size depend on all above-mentioned parameters as *W*/*L* and nanotubes concentration. In such a way you can modeling the different percolation situations varying not only concentration, but also length and a form of incidentally scattered nanotubes, forming CNT network layer.

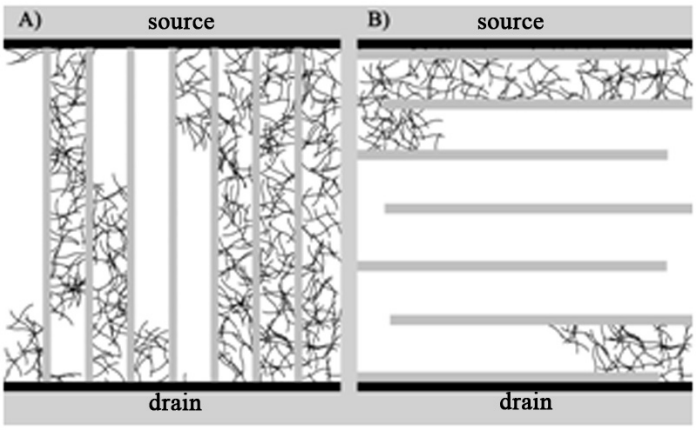

Fig.1 The areas of CNT networks contacting with source and drain of bottom-gated transistor after vertical (A) and horizontal (B) zigzag-“striping” channel layer.

1. G.S. Tulevski, A.D. Franklin, D. Frank et all. “Toward High-Performance Digital Logic Technology with Carbon Nanotubes”. ACSNANO, **8** (9), pp. 8730–8745, 2014.
2. A.E. Islam, J.A. Rogers, and M.A. Alam. “Recent Progress in Obtaining Semiconducting Single Walled Carbon Nanotubes for Transistor”. Adv. Mater., **27**, pp. 79-79-7937, 2015.
3. N. Pimparkar, Q. Cao, J.A. Rogers, and M.A. Alam. “Theory and Practice of “Striping” for Improved ON/OFF Ratio in Carbon Nanonet Thin Film Transistors”. Nano Res., **175**, pp. 167-175, 2009.

Silicon nanowire based local field probe

I. Bozhev[1], A. Trifonov[1,2], D. Presnov[1,2], V. Krupenin[1]
1. M.V. Lomonosow Moscow State University, Moscow, Russia, bozhjev.ivan@physics.msu.ru
2. Skobeltsyn Institute of Nuclear Physics, Moscow, Russia.

Recently, a lot of efforts have been focused on studies of various micro- and nano-objects and systems. Of particular interest to scientists is the study of their electrical properties. However, high-sensitivity, high-resolution and high-local tools are required for this kind of experiments.

Scanning or local high-sensitive field/charge probe with nanometer scale resolution will be a candidate to investigate a big amount of nano-objects and systems like a quantum dots, solid state qubits, nanoelectronic devices, nanoscale biological objects, which are very important in modern science.

One of the main methods for investigating of a surface potential distribution is the electric force scanning probe microscopy (SPM). But it is very difficult to achieve high sensitivity for the electric field imaging required for studying nano-objects using this instrument.

We propose a new method of electric field imaging - active sensor with a nanowire channel field-effect transistor (NW FET). NW FET is known as a device having high field/charge sensitivity with a potential of high space resolution [1].

The probe consists of a silicon chip with a NW FET positioned at a distance of several nanometers from the chip corner. This chip is attached at a certain angle to the holder for tuning fork mode of SPM to bring the probe to the tested surface. We have developed a new technique of the active probes fabricating. It begins with the silicon on insulator (SOI) wafer that consists of three layers: a thin 100 nm silicon layer on top of a 200 nm silicon dioxide film which, in turn, is positioned over a much thicker silicon base.

The first step is producing of the trenches, which direct the cleavage. To produce the trenches SOI wafer was covered by thin masking layer of silicon nitride in which the etching mask was formed using lithography and reactive-ion etching (RIE). Silicon wet etching in potassium hydroxide is known to be crystal orientation-dependent. After etching the wafer through a rectangular mask, we obtain a triangular trench in it. Etching stops at {111} planes. The intersection of these planes selects one direction in the crystal, and when we break the plate, the cleavage will occur along this line. After etching in potassium hydroxide solution, silicon nitride mask was removed by hydrofluoric acid solution.

At the second step NW FET structure was formed with e-beam lithography, metal mask sputtering and RIE at the intersection of the axes of the trenches. Then the sample was split into four pieces. NW FET channels with the angle shape were formed at a distance of several nanometers from the chip corner. Finally, the probe is attached to a tuning fork and bonded with thin wires to the sample holder.

Possibility of electric field imaging and sensitivity to electric field was demonstrated.

The work was supported by Russian Foundation for Basic Research projects No. 14-07-00828 and 16-29-03266.

1. J. Salfi, I. Savelyev, M. Blumin, S. Nair, and H. Ruda. "Direct observation of single-charge-detection capability of nanowire field-effect transistors". Nature nanotechnology, **5**(10), pp. 737-741, 2010.

Design and modeling of GAA FET with a monocrystalline silicon channel

S.N. Orlov[1], E.S. Gornev[1], A.S. Klyuchnikov[1], V.P. Timoshenkov[2], O.P. Gutshin[1], P.G. Bobovnikov[1]

1. Molecular Electronics Research Institute, Zelenograd, Moscow, Russia, sorlov@mikron.ru

2. National Research University of Electronic Technology (MIET), Zelenograd, Moscow, Russia, valeri04@hotmail.com

The decrease of VLSI topological norms is connected with the solution of many problems that require significant material costs [1]. The aim of this work is to develop the design of GAA FET (Gate All Around) with monocrystalline silicon channels formed in several levels one above the other within the grooves in a silicon wafer (fig. 1). Technology of such GAA FET structures will provide a significant increase in the integration degree of VLSI compared to conventional planar transistors due to the formation of multilevel 3D structures using the same topological norms.

It is proposed the technology of forming transistor structures in the process of multilevel processing of silicon side surface. Processing is carried out using lithography in conditions of fixing process levels by stopper layers. The main stopper layer is SOG (spin-on glass) - glass that can be applied by spin coating. SOG layer covers the grooves in the silicon wafer. Further SOG is etched in the top of the groove. The second thin stopper layer covers the groove wall and further removed from the groove bottom. If necessary, the photoresist mask is formed on the wafer surface. SOG is etched up to the next level. Local processing carried on the side silicon surface not covered by the stopper layers, including etching, chemical deposition and other processing. The above operations are repeated again to form the second and subsequent levels of the structures on the side of the silicon surface. GAA FET construction is designed taking into account for using of technology with minimal topological norms of 180 nm.

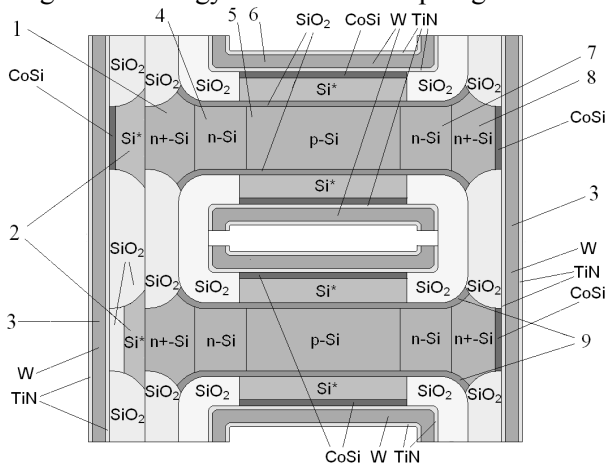

1 – source;
2 – horizontal polysilicon lines;
3 – vertical tungsten lines;
4 – lightly doped source region;
5 – horizontal channel (monocrystalline silicon microgirder);
6 – polysilicon gate;
7 – lightly doped drain region (LDD – Light Doped Drain);
8 – drain;
9 – gate dielectric.

Figure 1. Vertical section GAA FET structure

Simulation of electrical characteristics in TCAD environment was conducted for the n-channel MOSFET for different parameters: diameter round monocrystalline silicon microgirder, sizes of LDD-region, impurity concentrations. The impurity concentration in the LDD-restricted area limited below the impurity concentration in the substrate from above the breakdown voltage. With the channel diameter decreasing to substrate thickness of 100 nm, the threshold voltage is almost not changed, further it drops sharply, the breakdown voltage decreases. For transistors with a microgirder diameter of 150 nm LDD-domain parameters for the specified electric parameters were chosen. For the length of the LDD region, 200 nm when the impurity concentration in it $1.4 \cdot 10^{18}$ cm^{-3}, a threshold voltage is 0.412 V and the breakdown voltage is 5.32 V. As a result of the simulation was shown the ability to work of GAA FET at the supply voltage 1.8 V. It has been shown that output current-voltage characteristic becomes stable to kink and avalanche carrier generation with a decreasing the monocrystalline silicon microgirder diameter.

1. G.Ya. Krasnikov and O.M. Orlov. “Distinctive features and problems of CMOS technology for decrease in the node size to 0.18 μm or less”. Nanotechnologies in Russia, **3**(7), pp. 502-506, 2008.

Nanowire based Field Effect Transistor for the detection of different biological objects

D. Presnov[1,2], G. Presnova[3], I. Bozhjev[2], M. Rubtsova[3], A. Trifonov[1,2], V. Krupenin[2]
1. Nuclear Physics Institute, Moscow State University, 119991 Moscow, Russia,
2. Laboratory of Cryoelectronics, Moscow State University, 119991 Moscow, Russia, denis.presnov@phys.msu.ru
3. Faculty of Chemistry, Moscow State University, 119991 Moscow, Russia.

Resent time the nanowire based field-effect transistors (NW FETs) was attracted a particular attention for the researchers in the field of detection of different biological objects. Due to its unique sensitivity, high surface-to-volume ratio, mechanical stability and relatively simple fabrication technology the NW FET becomes the main base element for biosensor applications [1, 2].

In this work, we report on Si NW FET with Schottky contacts (Si-Ti) fabricated [3] by traditional methods (e-beam lithography and reactive ion etching) from silicon-on-insulator (SOI) without complicated processes of doping and thermal annealing. The surface of the nanowire was functionalized by a new method using GOPS-SH and 5 nm gold nanoparticles (GNP) which provides the high density of antibody active sites and improved surface-to-volume ratio enhancing electrical performance of the transistor [4]. The pH sensitivity of our Si NW FET with GNPs was reached the value of 70 mV per unit pH. Our transistors were used for detection of prostate specific antigen (PSA), which is a molecular marker of prostate cancer, in buffer and human serum.

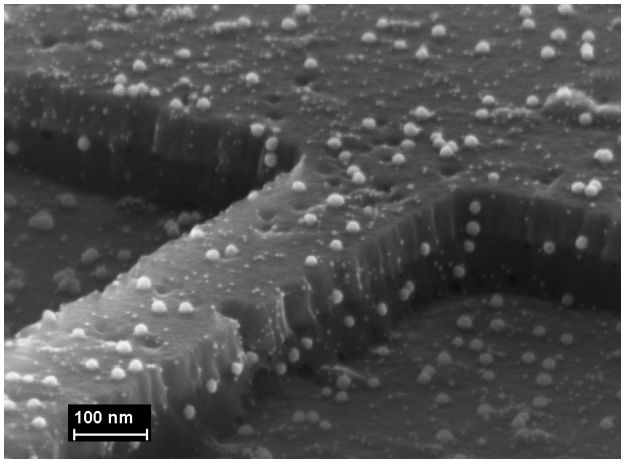

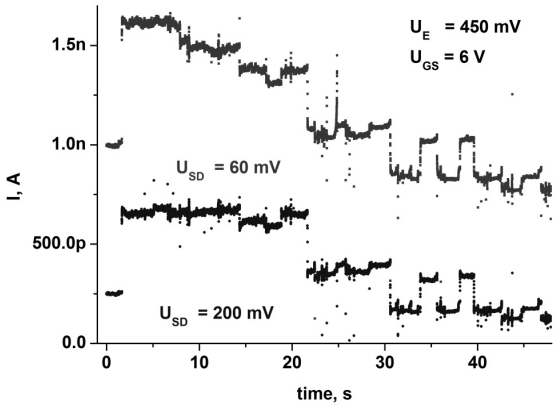

There were several transistors fabricated on the same chip with a distance about 50 μm from each other. The right figure shows the real time response signals of the transport current *I* for two closely positioned transistors. The conductivity of NW was modulated by the voltage at the main gate - silicon substrate of SOI wafer. AgCl reference electrode served as an additional gate for the transistor was immersed in the solution drop for adjusting its operating point. Preliminary measurements showed the synchronicity of changes in the responses of the sensors to external stimuli. We suggest the future development of our biosensor in a multichip configuration from several NWs, each of which will be modified by antibodies of various specificity for simultaneous definition of various compounds in one test. The work was supported by the Russian Foundation for Basic Research (grants 16-29-03266 and 14-07-00828).

1. A. Zhang and C.M. Lieber, "Nano-Bioelectronics", Chem. Rev.**116**, pp. 215-257, 2016.
2. M.A.M. Azmi, Z. Tehrani, R.P. Lewis, K.-A.D. Walker, D.R. Jones, D.R. Daniels, S.H. Doak, O.J. Guy, "Highly sensitive covalently functionalised integrated silicon nanowire biosensor devices for detection of cancer risk biomarker", Biosensors and Bioelectronics **52**, pp. 216-224 (2014).
3. D.E. Presnov, S.V. Amitonov, P.A. Krutitskii, V.V. Kolybasova, I.A. Devyatov, V.A. Krupenin, and I.I. Soloviev. "A highly ph-sensitive nanowire field-effect transistor based on silicon on insulator". Beilstein journal of nanotechnology, **4**, pp. 330–335, 2013.
4. M.Yu. Rubtsova, G.V. Presnova, V.A. Krupenin, D.E. Presnov, V.G. Grigorenko, and A.M. Egorov, "Biosensor based on a nanowire field-effect transistor for the determination of prostate specific antigen", In Biosensors 2016. Elsevier Procedia Technology, 2016, in press.

Characteristics simulation of single-electron transistor based on the molecule with accentuated single-atom Rh detached charge center

A.A. Parshintsev, V.V. Shorokhov, E.S. Soldatov
M.V. Lomonosov Moscow State University, Faculty of Physics, Moscow, Russia, parshincev@physics.msu.ru

Solid state single-electronics based on the transistors with a single-atom charge center is a new promising direction of nanoelectronics [1]. Investigation realisation of single-atom single-electron devices is possible using molecules with accentuated single-atom detached charge center. One of the basic elements for such investigation is a single-electron monomolecular transistor (SET). The scheme of SET is provided on Fig. 1. In this work transport characteristics of SET based on the molecule $Rh(tpy\text{-}C_4H_4\text{-}O\text{-}C(O)\text{-}(CH_2)_4\text{-}C_3H_5S_2)_2$ were investigated by computer simulation.

Unrestricted Hartree - Fock method in Firefly QC [2] with various basis sets including ADZP, aug-cc-pVTZ-DK Diffuse [3] was used to calculate electron energy spectra of the molecule in different charge states. Analytical parametric model for obtaining the molecule energy spectra was proposed.

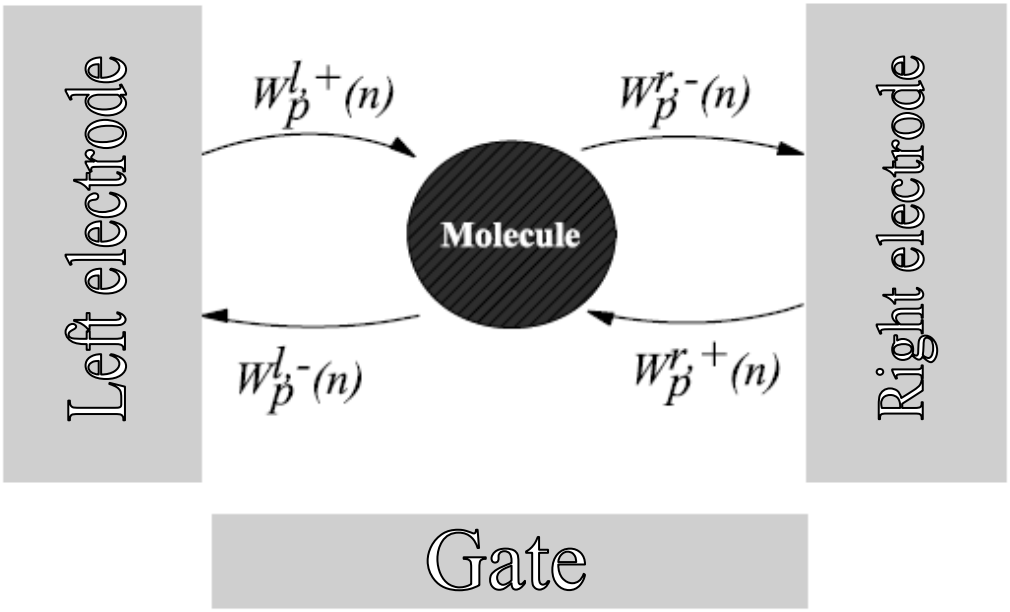

Fig. 1. The scheme of SET and possible events between electrodes and a molecule. Here $W_p^{(l,r),+}(n)$, $W_p^{(l,r),-}(n)$ are rates of electron tunneling from the left (right) electrode to the molecule and vice versa.

I-V curves at different temperatures and stability diagrams of the SET were calculated using Monte-Carlo simulation.

This work is supported by Russian Science Foundation, grant №16-12-00072.

1. Fuechsle M. et al. Nat. Nanotechnol. **7**, pp. 242–246, 2012.
2. A.A. Granovsky. Firefly version 8, http://classic.chem.msu.su/gran/firefly/index.html.
3. EMSL Basis Set Exchange Library, https://bse.pnl.gov/bse/portal.

Model of Nanodiode Conductivity as Description of I-V Features of ReRAM in Conductive State

A.A. Popov, A.E. Berdnikov, A.A. Mironenko, V.N. Gusev
Yaroslavl Branch of Institute of Physics & Technology of Russian Academy of Sciences, 150007, Yaroslavl, Russia;
e-mail: imiraslab4@yandex.ru

We investigated effect of conductive switching in metal – insulator– semiconductor structures (MIS) for ReRAM applications [1, 2]. Nanodiode approximation was used for the description of ReRAM I-V features in conductive state. We assumed that nanodiode consists of semi-infinite semiconductor and nanosize diameter filament with high conductivity. Such structures appear during ReRAM switching on.
Model based on spreading resistance depended on filament diameter. In semi-spherical approach spreading resistance defined by equation (1).

$$R = \rho/(2\pi d) \quad (1)$$

where ρ is the silicon resistivity, d is the diameter of the filament. The region near the filament during positive direct current flow takes additional concentration of charge carriers. Dependence of the current on voltage may be expressed by equation (2).

$$I = fU^{3/2} \quad (2)$$

where f is a coefficient.
Experimental ReRAM sample has been fabricated on the wafer of p-type monocrystalline silicon. Dielectric layer has been produced as 40 nm thick non-stoichiometric silicon oxide deposited by low frequency PECVD. Aluminum used for metallization. Effect of conductive switching was registered on this structure. In Fig.1 we present experimental data in conductive state and voltage applied in positive direction. Current is shown in horizontal axis and corresponding value of the voltage to the power 3/2 shown in vertical axis. Straight line is the interpolation of experimental data. It's obvious, that deviation of experimental data from straight line insignificant. It confirms the validity of the equation (2).

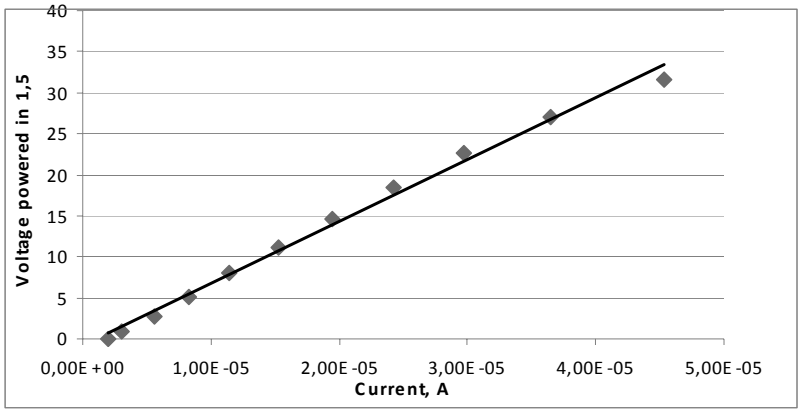

Fig.1. Experimental I-V data: current on horizontal axis and voltage to the power 3/2 on vertical axis. Solid line is linear trend.

If semiconductor and filament form Schottky diode and appropriated voltage applied in negative direction, then in semiconductor near filament appears region of the field generating pairs of the charge carriers. It means that the negative part of I-V curve shifted on same voltage, which greater than band gap. Below this voltage current provided only thermal generation, and it's negligible.

1. A.E. Berdnikov, V.N. Gusev, et al. Semiconductors, **47** (5), p. 641, 2013.
2. Mehonic A., Cueff S., et al. Journal of Applied Physics **111**, 074507, 2012.

The study of crystallization kinetics of phase transformations in thin films $Ge_2Sb_2Te_5$ by electrical measurements

P. Lazarenko[1], A. Yakubov[1], A. Babich[1], A. Sherchenkov[1], S. Kozyukhin[2], A. Shuliatyev[1]
1. National Research University of Electronic Technology, Zelenograd, Russia, aka.jum@gmail.com
2. Kurnakov Institute of General and Inorganic Chemistry, RAS, Moscow, Russia, sergkoz@igic.ras.ru

Currently electric phase change memory (PCM) is one of the candidates for the replacement of flash memory. The advantages of PCM in comparison with flash memory is low power consumption, high reading and writing rates, a large number of write cycles, high radiation resistance. For PCM cells the most widely used materials are from ternary system Ge-Sb-Te, in particular $Ge_2Sb_2Te_5$ (GST225). However, many fundamental and important practical issues related to the phase transformations and electro-physical properties of thin films are not fully understood. So, the aim of this work is to study the crystallization kinetics of phase transformations in $Ge_2Sb_2Te_5$ thin films by electrical measurements.

The initial chalcogenide semiconductor GST225 was synthesized with using of the mixture of elements with 99.99 % purity. Thin films in amorphous state were prepared by thermal evaporation of material in vacuum chamber. The thicknesses of the films were determined by atomic force microscopy (NT-MDT SolverPro) and were in the range from 80 to 100 nm. Rutherford backscattering spectroscopy (RBS) and Energy Dispersive X-Ray Analysis (EDX) were used to study the compositions of thin films, which were close to those of the synthesized materials. The structures of the synthesized alloys and as-deposited films were checked by X-Ray diffraction (XRD). Differential scanning calorimetry (DSC-50, Shimadzu) at different heating rate flow was used to examine the thermal properties of investigated materials and kinetics of crystallization. Electrophysical characteristics of thin film were investigated on a special stand, containing heating stage HFS600E-PB4 Linkam and picoammeter Keithley 6485. Temperature dependences of the resistivity of GST225 thin films were measured at different heating rate (1, 5, 10, 20 °C/min).

The temperature dependencies of resistivity of GST225 thin film for different heating rates (dT/dt) is shown in Figure 1. Exponential temperature dependence of resistivity of amorphous thin films in the range from room temperature to 120 °C was observed for all curves. The activation energies of conductivities were estimated with using of the Arrhenius plots σ vs $1/kT$ and a least square method (E_a = ~0.29 eV for all films).

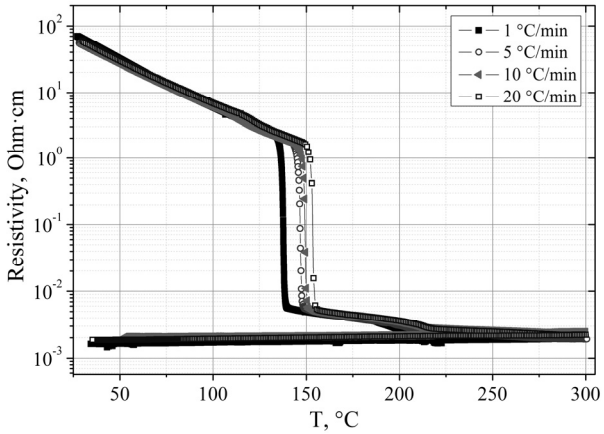

Figure 1 - Temperature dependences of resistivities for GST225 thin films

Sharp drops in resistivity for GST225 were observed in the ranges from 120 to 170 °C and from 180 to 220 °C. Data of XRD and DSC showed that first and second sharp drops of resistivity are caused by phase transformations from amorphous state to metastable rock salt and then to stable hexagonal structures, respectively. The shift of the sharp drops in the resistivity and therefore the shift of the phase transition to higher temperatures with increasing heating rate is clearly visible and correlates with the DSC data. Both structural changes are thermally activated processes. Energies of activation of phase transformations were estimated by Kissinger's method and were compared with the DSC data.

This work was supported by the Russian Federation President's grant (MK-8105.2016.8).

Thermoelectric and electro-physical properties of the phase change memory materials on the quasi-binary line $GeTe\text{-}Sb_2Te_3$

A. Sherchenkov[1], P. Lazarenko[1], D. Terekhov[1], V. Kalugin[2], S. Kozyukhin[3], A. Yakubov[1], A. Babich[1]

1. National Research University of Electronic Technology, aa sherchenkov@rambler.ru
2. Zelenograd Nanotechnology Center, viktor118@mail.ru
3. Kurnakov Institute of General and Inorganic Chemistry, RAS sergkoz@igic.ras.ru

Last decade non-volatile phase change memory (PCM) devices are actively developed. The most promising programming materials are considered to be chalcogenide semiconductors on the quasi-binary line $GeTe\text{-}Sb_2Te_3$. These tellurium-based semiconductors have extremely low thermal conductivities, high Seebeck coefficient, electrical conductivity, and so high thermoelectric properties. PCM cells experience multiple cycling with large current and temperature variations. In these conditions PCM materials can provide high thermoelectric effects, which can significantly influence the performance of the cell including programming current and reliability. However, the knowledge of thermoelectric and electro-physical properties of chalcogenide semiconductors on the quasi-binary line $GeTe\text{-}Sb_2Te_3$ is insufficient. So, the aim of this work was investigation of the thermoelectric and electro-physical properties for thin films of the chalcogenide semiconductors on the quasi-binary line $GeTe\text{-}Sb_2Te_3$.

Thin films of chalcogenide compounds $Ge_2Sb_2Te_5$ (GST225), $GeSb_2Te_4$ (GST124), and $GeSb_4Te_7$ (GST147) on the quasi-binary line $GeTe\text{-}Sb_2Te_3$ were deposited by thermal evaporation of the synthesized material in vacuum, with the substrate temperature during evaporation did not exceeding 50°C. According to the Rutherford Backscattering Spectroscopy (RBS) and Energy Dispersive X-Ray Analysis (EDXRA) compositions of the synthesized material and thin films were close to GST225, GST124, and GST147. XRD study (D8 ADVANCE Bruker and Rigaku Smart Lab.) showed that the synthesized materials had polycrystalline structure, while as-deposited thin films were amorphous.

The set-up on the basis of multimeter HP 34401A-01 and power supply Agilent E3674 was used for the investigation of Seebeck coefficients and determination of the type of conductivity for investigated films. Samples containing Al electrodes and deposited upon them investigated thin films were fabricated on pyroceramics substrates. The distances between electrodes were 5 mm, and temperature gradient was 5 °C.

Influence of the composition variation along the quasi-binary line $GeTe\text{-}Sb_2Te_3$ on the thermoelectric and electro-physical properties of thin films was investigated. GST amorphous thin films have high Seebeck coefficients (in the range from -600 to -1000 μV/°C), which drops nearly on the order of magnitude after the crystallization. Negative values of Seebeck coefficients, indicating on the dominating p-type conductivity for GST thin films.

Temperature dependences of the resistivities showed that crystallization was accompanied by the drastic decrease of resistivity. This sharp drop correlated with results of XRD and AFM investigations and data of optical measurements obtained earlier by ellipsometery. It was found that crystallization temperature increases with moving along the quasi-binary line $GeTe\text{-}Sb_2Te_3$ from $GeSb_4Te_7$ to $GeSb_2Te_4$, and then to $Ge_2Sb_2Te_5$, while the phase transition temperature range decreases. Current-voltage characteristics of amorphous thin films have three voltage ranges with different dependencies due to the different mechanisms of charge carrier transport. Ohmic dependencies and space charge limited current determines current-voltage characteristics in the low ($E < 10^3$ V/cm) and middle ($10^3 < E < 10^4$ V/cm) electric field intensity ranges, respectively.

So, influence of the composition variation along the quasi-binary line $GeTe\text{-}Sb_2Te_3$ on the thermoelectric and electro-physical properties of thin films was investigated.

This work was supported by the Ministry of Education and Science of Russian Federation (project ID: RFMEFI57514X0096).

Investigation of memristor effect on the titanium nanowires fabricated by focused ion beam

O. Ageev, A. Kolomiytsev, V. Smirnov, I. Jityaev
Southern Federal University, Institute of Nanotechnologies, Electronics and Electronic Equipment Engineering, Taganrog, Russia, askolomiytsev@sfedu.ru

The development of new types of electronic components and computing systems for the processing and storage of information is a priority for the development of modern science, where the use of the basic principles of nanotechnology plays a key role. One of the main objectives of the modern nanoelectronics is to provide promising non-volatile memory elements having a high speed, combined with the small size recording information cells [1].

Recently memristors widely used when designing the resistive memory cells based on metal-insulator-metal structures, showing the recording time of about 10-30 nanoseconds. In the memristor technology commonly used metal oxides, but it is also known that planar structures based on carbon nanotubes, ZnO nanowires, graphene, as well as metal nanowires have demonstrated the memristor effect. However, the mechanism of occurrence of memristor effect of such materials is poorly understood and requires further research. The main problem in metal nanowire memristor technology is the production of experimental samples of nanoscale conductance channel width of less than 10 nm. This type of structures can be manufactured using Focused Ion Beam (FIB) technology. FIB enables reproducible and precise material processing with high accuracy. Material removal by ion beam milling and FIB-induced chemical vapor material deposition can be used for the fabrication of structures with micro- and nanoscale dimensions. The key feature of FIB is the high spatial resolution which is provided by the application of a gallium ion beam 7 nm in diameter, as well as by the possibility of varying the impact of the parameters over wide limits.

The purpose of this study is to investigate the memristor effect of nanoscale titanium wires fabricated using focused ion beam.

In this study, the nanowire memristor structure was fabricated by FIB local milling with a FEI Company DualBeam system Nova NanoLab 600, combining a Ga^+ FIB and a field emission scanning electron microscope. The following FIB parameters were used: the accelerating voltage of the ion beam – 30 keV; the ion beam current – 10 pA; and the dwell time of the ion beam - 1.0 μs. As a result, the memristor structures were formed with different widths of 280 nm, 13.5 nm and 7.8 nm (Fig. 1a). We tested electrical properties of the FIB-fabricated memristors using AFM Ntegra Vita (NT-MDT Co.). The current–voltage (I–V) characteristic of the planar structure was obtained by applying a voltage up to 5 V (Figs. 1b, 1c).

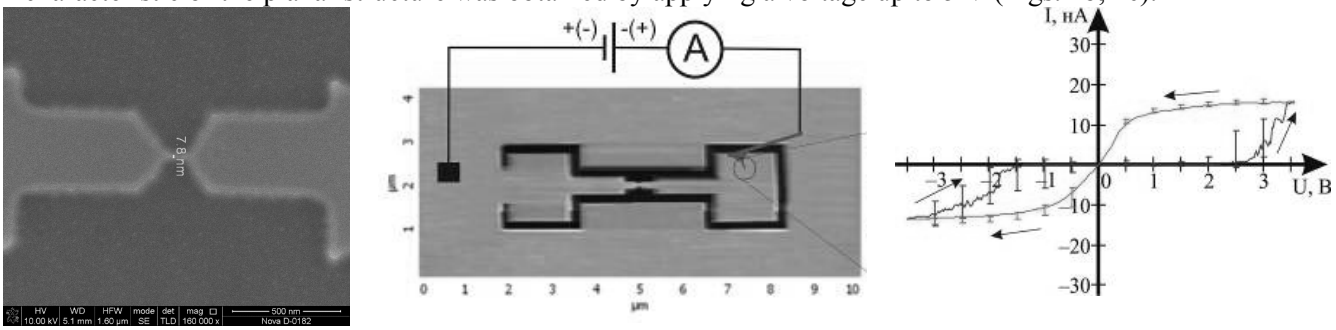

a) b) c)

Fig. 1. Investigation of 7.8 nm Ti nanowire memristor: a – SEM-image, b – AFM measurement scheme, c – CVC in the high-resistance state.

It is shown that the use of FIB technology allows forming planar Ti memristor structures with different parameters. The analysis of the CVC measuring shows that the resistivity ratio in the high- and low-resistance states is higher than 10^2. The obtained results can be used for the design and fabrication of resistive energy-efficient memory elements with a high density of storage cells on the basis of Ti nanowires.

This work was supported The President of the Russian Federation Grants Council (Grant no. MK-6163.2016.8).

1. S.L. Johnson, A. Sundararajan, D.P. Hunley, and D.R. Strachan. “Memristive switching of single-component metallic nanowires”, Nanotechnology, **21**, pp. 125204, 2010.

Modeling of resistive switching mechanism in HfO_2 ReRAM

S. Ivanov[1,2], D. Voronov[1,2], O. Orlov[2]
1. Moscow Institute of Physics and Technology, Dolgoprudny, Russia, sergei.v.ivanov@phystech.edu
2. Research Institute of Molecular Electronics, Zelenograd, Russia, oorlov@mikron.ru

This work is devoted to modeling of resistive switching mechanism in bipolar HfO_2 ReRAM. Due to the fact that ReRAM is one of the main candidates for the role of universal memory, the claimed topic has considerable relevance. Despite the existence of functional prototypes, the world scientific community has not accepted unified model describing resistive switching mechanism. Existing models have a lot of contradictions and disadvantages.

This paper presents a model of ReRAM element, which allows to describe the processes of programming and erasing of the memory element and obtain the current-voltage characteristic. The model is developed for ReRAM element based on MIM-structure with HfO_2 active layer and TiN electrodes.

The model suggests that the conductance of active layer depends on concentration of oxygen ions. High concentration of ions corresponds to low-conductive hafnium oxide and area with low concentration of oxygen corresponds to high-conductive filament. Application of an electric field and subsequent heating causes oxygen ions to migrate across the structure, which causes a switching between high and low resistance states. The model based on equations, describing the processes of heating, thermal activation and diffusion:

$$\begin{cases} \nabla\left(\sigma(\vec{r},n_D)\cdot\vec{\nabla}\varphi(\vec{r})\right)=0 & (1)\\ C_{th}(\vec{r},T)\dfrac{\partial T(\vec{r},t)}{\partial t}=\nabla\left(K_{th}(\vec{r},T,n_D)\cdot\vec{\nabla}T(\vec{r},t)\right)+\sigma(\vec{r},n_D)\cdot\left|\vec{\nabla}\varphi(\vec{r})\right|^2 & (2)\\ \dfrac{\partial n_D(\vec{r},t)}{dt}=\nabla\left(D(\vec{r},T)\cdot\vec{\nabla}n_D(\vec{r},t)+\mu(\vec{r},T)\cdot n_D(\vec{r},t)\cdot\vec{\nabla}\varphi(\vec{r})\right) & (3)\\ D(T)=D_0\exp\left(-\dfrac{E_A}{k_B\cdot T}\right) & (4)\\ D(T)=\dfrac{\mu(T)\cdot k_B\cdot T}{q} & (5)\\ \sigma^{met}=\dfrac{\sigma_0}{1+\alpha(T-T_0)} & (6)\\ \sigma^{ins}=\sigma_0 e^{-\frac{E_{AC}}{k_B T}} & (7) \end{cases}$$

1 – Continuity equation for electric current, 2 – Heat equation, 3 – Fick's second law of diffusion for oxygen vacancies, 4 – Arrhenius equation for diffusivity, 5 – Einstein–Smoluchowski relation for mobility, 6 – Temperature dependence of metal conductivity, 7 – Temperature dependence of dielectric conductivity.

Special methods of numerical analysis were used to solve this system. The model also considers the heating of the electrodes and changing of heat capacity and thermal conductivity.

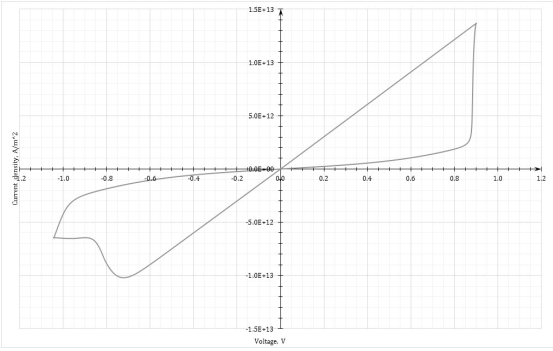

Fig 1. Calculated IV-characteristic of HfO_2 ReRAM element

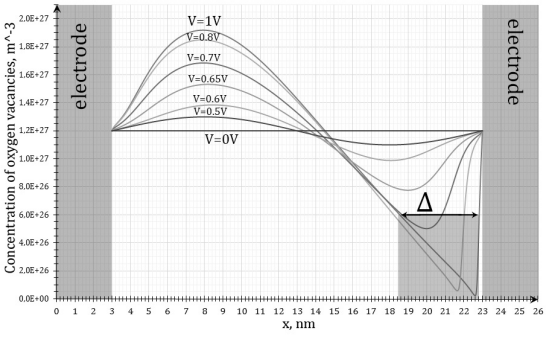

Fig 2. Concentration of oxygen vacancies across the structure

Calculation allowed us to obtain the distributions of electric potential, temperature and concentration of oxygen ions across the structure in processes of rewriting. It allows to obtain electrophysical characteristics of memory element. Obtained results showed good agreement with the experimental.

The resistive switching of vertically aligned carbon nanotubes by the action of electric field

O. Ageev, Yu. Blinov, M. Ilina, O. Ilin, V. Smirnov
Southern Federal University, Institute of Nanotechnologies, Electronics and Electronic Equipment Engineering, Department of Nanotechnologies and Microsystems, Taganrog, Russia, E-mail address ageev@sfedu.ru

An urgent task of contemporary micro- and nanoelectronics is the development of memory type combining non-volatility, high performance, low power consumption and the possibility of reducing the size of the cell. One of the promising trends in this area is the development of resistive random-access memory (ReRAM) based on vertically aligned carbon nanotubes (VA CNTs) because the vertical orientation of nanotubes provides a significant decrease in the cell area as compared to the traditional memory, and the technology of preparing VA CNTs based on plasma-enhanced chemical vapor deposition (PECVD) makes it possible to locally grow nanotubes during a process compatible with the silicon technology [1, 2].

The aim is to make and study the resistive switching parameters the experimental model the memory cell based on individual vertically aligned carbon nanotube.

Experimental model of memory cell was made on the basis of the atomic force microscope (AFM) probe with deposited on its tip a nanotube with a diameter of 92 nm and a length of 2.12 μm. Deposition of nanotube on the probe was carried out from an array VA CNTs grown by PECVD by the action of a local external electric field at a voltage of 30 V. As the lower electrode was used pyrolytic graphite. As the top electrode was used probe with a platinum coating (brand NSG10/Pt). Contact the deposited on probe nanotube with the lower electrode was carried out using a feedback system of the AFM. Schematics of the experimental model is shown in Fig. 1a. Study of the resistive switching parameters the memory cell was carried out by the AFM in spectroscopy mode using probe nanolaboratory Ntegra ("NT-MDT", Russia). The obtained current voltage characteristics (CVCs) of the memory cell are shown in Fig. 1b.

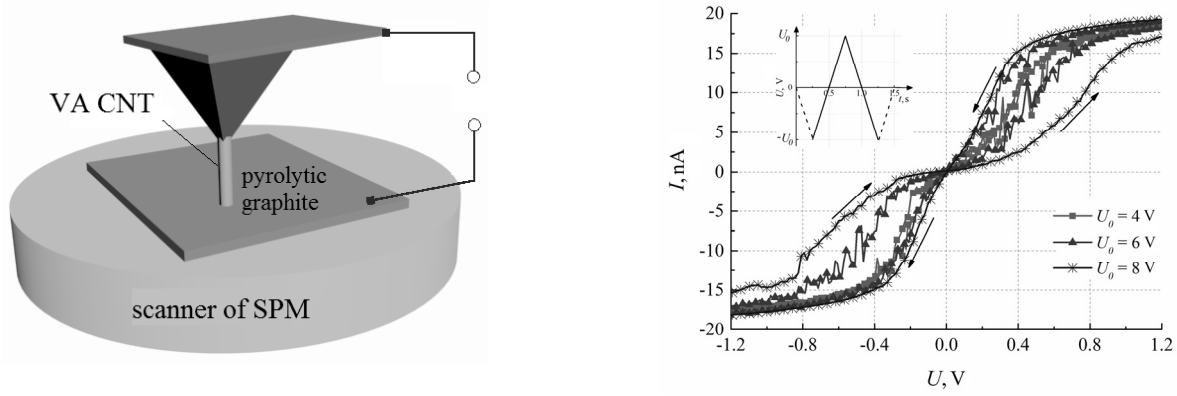

a) b)

Fig. 1. Schematics of memory cell based on VA CNT (a) and CVCs of memory cell (b). In inset (b) is voltage pulse.

The studies of the memory cell have shown that the resistive switching of the VA CNT is observed at 6 V and more (Fig. 1b). The resistance ratio of the cell in the high- to a low -resistance states (R_{HR}/R_{LR}) amounts 7 at recording voltage of 8 V and reading voltage of 0.2. The mechanism of resistive switching of VA CNT is based on a deformation and polarization of the nanotube by the action of electric field [2].

The results can be used in the development nanoelectronics devices based on VA CNTs, including the ReRAM. The results were obtained using the equipment of the Research and Education Center and Center of Common Using “Nanotechnologies” of Southern Federal University.

The reported study was funded by RFBR according to the research projects No. 16-29-14023 ofi_m and No. 16-37-00101 mol_a.

1. O.A. Ageev, Yu.F. Blinov, O.I. Il’in, A.S. Kolomiitsev, B.G. Konoplev, M.V. Rubashkina, V.A. Smirnov, and A.A. Fedotov. “Memristor Effect on Bundles of Vertically Aligned Carbon Nanotubes Tested by Scanning Tunnel Microscopy”. Tech. Phys., **58** (12), pp. 1831-1836, 2013.

2. O.A. Ageev, Yu.F. Blinov, O.I. Il’in, B.G. Konoplev, M.V. Rubashkina, V.A. Smirnov, A.A. Fedotov. "Study of the Resistive Switching of Vertically Aligned Carbon Nanotubes by Scanning Tunneling Microscopy". Phys. Solid State, **57** (4), pp. 825–831, 2015.

Exploring energy landscape of magnetic nanostructures with Nudged Elastic Band Micromagnetics

O.S. Trushin[1], N. Barabanova[1], E. Granato[2], S.C. Ying[3]
1. Yaroslavl Branch of the Institute of Physics and Technology of RAS, Yaroslavl, Russia, otrushin@gmail.com.
2. LAS, National Institute for Space Research, São José dos Campos, Brazil
3. Department of Physics, Brown University, P.O. Box 1843, Providence, Rhode Island, 02912, USA

Magnetic nanostructures have attracted new interest in recent years [1] due to its potential for application in new generations of computer memory. Micromagnetic model is an important tool for theoretical studies of magnetic nanostructures. It assumes a phenomenological description of the magnetic system where the total energy of the system is a functional of a continuous magnetization function. Numerical implementation of the model assumes spatial discretization of the system using fine grid. We focus here on the numerical study of the thermal stability of the magnetic state which is an important issue concerning the reliability of nanomagnets as memory elements. This is related to magnitude of energy barriers separating different magnetic states corresponding to local minima of the energy functional. Theoretical estimates of energy barriers can be done using Nudged Elastic Band method within the micromagnetic model [2]. We have developed our own code implementing NEB within micromagnetics [3]. In this work we have studied the energy landscapes of ring shaped magnetic nanostructure. These structures are particularly interesting for magnetic memory, since the shape provides conditions for magnetic flux closure that helps prevent mutual interference of neighboring memory cells.

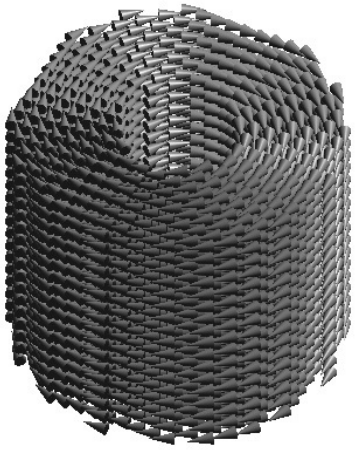

Fig. 1. Side view on the model. Cones show local magnetization vectors at grid points.

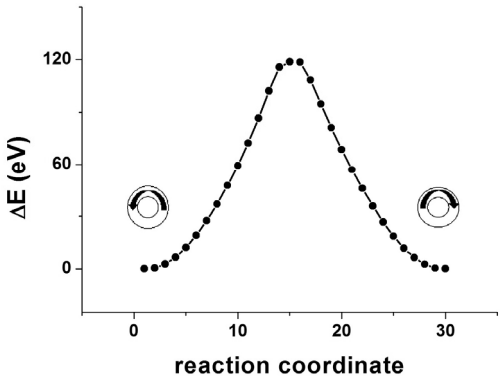

Fig. 2. Energy profile along the transition path between two states of magnetization of the nanoring.

Single layer permalloy nanoring with thickness 50 nm, internal radius 10 nm and external radius 30 nm has been considered (fig. 1). As the result of simulation we were able to identify several local minima corresponding to different magnetic states of the ring. The lowest energy minimum corresponds to a vortex state. Energy barriers separating local minima were determined that vary from dozens up to hundreds eV (fig. 2). This is much higher than thermal energy at room temperature and implies thermal stability of the magnetic structure. Our finding shows potential reliability of the magnetic nanoring as an element of magnetic memory.

1. M. Klaui and C. Vaz "Magnetization configurations and reversal in small magnetic elements", *in Handbook of magnetism and advanced magnetic materials*, ed. by H. Kronmuller and S. Parkin, Vol. 2, John Willey & Sons, Ltd., 2007.
2. D. Suess et al. "Reliability of Sharrocks equation for exchange spring bilayers", Phys. Rev. B, **75**, 174430, 2007.
3. O. Trushin, N. Barabanova "Micromagnetic software package MICROMAG and its applications to study elements of spintronic", Russian Microelectronics, **42,** pp. 176–183, 2013.

Some features of magnetotransport properties of Ni/NiO thin film structures

V.A. Berezin, I.V. Malikov, G.M. Mikhailov
Institute of Microelectronic Technology and High Purity Materials, Russian Academy of Sciences, 142432, Chernogolovka, Russia, berezin@iptm.ru

Nickel oxide (NiO) with NaCl-type structure is an antiferromagnetic (T_N = 523 K) and wide band-gap (E_{gap} = 3.8 eV) semiconductor with p-type conductivity caused by Ni deficiencies. It possesses an excellent stability in air, good crystallinity and transparency. So far, NiO thin films have been widely studied as a promising material for potential applications to electrochromic display devices, gas-sensors, UV-light-emitting diodes, ultraviolet-detectors and a resistive random-access memory (ReRAM) using the resistive switching characteristics of NiO and many others.

Relatively new requests of NiO films include its application in metal-insulator electronics and as exchange bias material. Its potential barrier height decreases down to 0.2 eV in thin NiO films and this property makes NiO promising in antenna-coupled tunnel junctions as a fast detector in terahertz and infrared radiation frequency ranges.

Sapphire substrates of R- and C- orientations were used for film growth in our experiments. The simplest method to produce NiO thin film is the oxidation of Ni film on air or in oxygen. However, oxidation on air experiments revealed the disadvantages of this method: it is difficult to grow a relatively thick and at the same time uniform films; magnetotransport properties of Ni films with oxidized surface become deteriorated with increasing magnetic reversal fields and widening magnetoresistance peaks when oxidation time of nickel film is long enough; epitaxial Ni films of different crystalline orientations with thicker oxide on its surface do not demonstrate the exchange bias after annealing in magnetic field. Deterioration of magnetortansport properties obviously connected with increasing nonuniformity of the interface between Ni and Ni-oxide originated during Ni-oxidation.

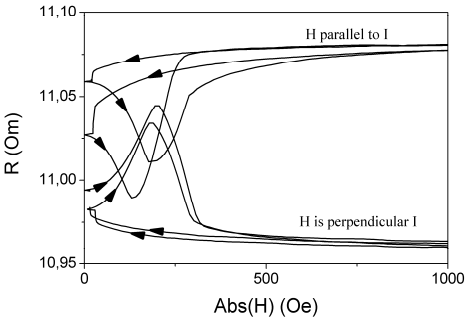

Fig.1 Magnetoresistance of double NiO/Ni films

In contrast neither annealing of pure Ni films nor reactive deposition of NiO on the top of Ni film does not lead to deterioration of magnetotransport properties. Another approach to grow NiO films that used in our experiments is reactive evaporation of Ni target by pulse laser deposition at the presence of molecular oxygen. Oxygen pressure in the growth chamber was maintained at $1.5 \cdot 10^{-4}$ Tor. Deposited NiO films were found to be smooth and transparent. Moreover, NiO films on C-sapphire plane are epitaxial. Grown (111) plane of antiferromagnetic NiO is the spin uncompensated. As the result, after annealing above T_N = 252 ^oC in magnetic field, magnetoresistance of bi-layered NiO/Ni films with equal layer thicknesses exhibits strong exchange bias as shown on fig 1. In turn, NiO films grown on R-sapphire plane do not possess any exchange bias, because of their spin compensated surface. However, these films after annealing above T_N in magnetic field show small exchange bias in magnetoresistance, indicated on modification of magnetic structure at Ni-NiO interface during magnetic annealing. All this confirm quality of sintered NiO films. Using sintered NiO films tunnel structures of Ni/NiO/Fe their current-voltage characteristics were measured and the results are presented in fig.2. These structures demonstrate quite strong nonlinearity which is useful for detection and mixing of radiation. Important characteristic of such structures - responsivity $R = (r_j/4)\times(d^2I/d^2U)$ was found about 2.5. Provided investigation gives base for nanotechnology developing of perfect monocrystalline Ni-NiO tunnel junction.

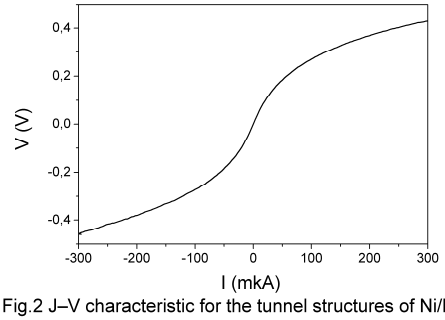

Fig.2 J–V characteristic for the tunnel structures of Ni/NiO/Fe

Geometric effects in current-voltage characteristics of a cross-shaped MDM structure Ni/NiO/Fe

I.V. Malikov, L.A. Fomin, G.M. Mikhailov
Institute of Microelectronic Technology and High Purity Materials, Russian Academy of Sciences, 142432 Chernogolovka, Russia, e-mail address: malikov@iptm.ru

The interest to metal-dielectric-metal (MDM) structures is connected with their potentialities as detectors and mixers of electromagnetic waves of IR (infrared) and THz (terahertz) frequency ranges. The application of MDM structures in these devices requires a dielectric layer to be of the tunnel thickness, the material for which is typically metal oxides. Among them nickel oxide is of particular interest due to its low barrier height of 0.2 eV at the layer thickness of several nanometers, although for the bulk compound it has about 3 eV band gap and is considered as a wide-band semiconductor with antiferromagnetic order. Cross-shaped MDM structures are commonly used for four-point probe measurements of vertical transport assuming that these measurements enable the determination of the tunnel barrier height by eliminating the influence of the resistance of supplying conductors. In our experiments a "crisscross" of two metallic stripes separated by a tunnel dielectric is used, which is a simplest device that can easily be prepared without applying the lithographic method.

A Ni layer as a stripe 100 μm wide was deposed onto the surface of a sapphire substrate through a mask by pulse laser deposition. The resulting film was then oxidized in a muffle furnace. The NiO film thickness was found to be 8-10 nm for the structures used. After that a stripe of Fe 200 μm wide was sputtered onto it lateral and normal to the Ni stripe by electron-beam evaporation through the mask. The thickness of each metal layer was 60 nm.

A typical I-V dependence of the sample measured by the four-point probe method is shown in fig. 1. It is seen that a negative slope of the I-V curve occurs at relatively small values of the current. As the current increases either in the positive or negative direction, the curve slope gradually changes by shifting towards the I-V branch of the curve positive slope. As a result, the I-V curve takes the N-like shape. It follows that the differential bending resistance of such a structure has negative values at small currents.

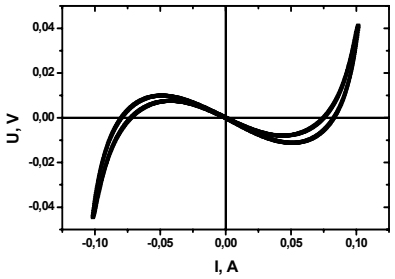

Fig.1. Current-voltage characteristics of the crisscross Ni/NiO/Fe structure.

To verify the possibility of sign changing of the measured voltage, we calculated the potential distribution for a simplified model structure. It is seen that at large R_{NiO} resistance, the resistance of the cross-shaped structure is negative. When the NiO interlayer resistance decreases, the normalized structure resistance increases, reaches a zero value and moves towards positive values.

The measured I-V dependence can be easily explained if account is taken of the measurement geometry, possible changes in the oxide resistance due to temperature increase caused by the structure heating or by the voltage effect in the tunnel layer during the current passing.

Thus the calculations of the potential distribution for a simplified model structure confirm the possibility of sign changing in the structure used in the experiment. This can be explained by the fact that at high resistance of the oxide interlayer, the potential difference at the ends of a separate stripe is small as compared to the potential drop on the interlayer. Therefore, the voltage measured in the bending geometry used is negative. As the interlayer resistance decreases, the lateral electron transport becomes dominating. This results in that the current tends to flow to the far end of the lower stripe where the voltage increases and the potential there becomes higher than at the far end of the upper stripe. Thereby, the measured voltage becomes positive. At further decrease of the interlayer resistance, the voltage measured in the positive area tends to reach a plateau. Thus, the calculations showed that, irrespective of numerical values, bending differential resistance of the structure can change its sign depending on the ratio of the metallic electrode resistance to that of the metal oxide and, together with experiments, reveal the geometric effect in current-voltage characteristics of a cross-shaped MDM structure Ni/NiO/Fe.

Basic cells for energy efficient superconducting neural networks

A. Schegolev[1,2], N. Klenov[1-6], I. Soloviev[3-5], M. Tereshonok[2]
1. Physics Department, Moscow State University, 119991, Moscow, Russia
2. Moscow Technical University of Communications and Informatics (MTUCI), Moscow, 111024, Russia
3. Lomonosov Moscow State University Skobeltsyn Institute of Nuclear Physics, 119991, Moscow, Russia
4. Lukin Scientific Research Institute of Physical Problems, Zelenograd, 124460, Moscow, Russia
5. Moscow Institute of Physics and Technology, State University, Dolgoprudniy, Moscow region, Russia
6. N. L. Dukhov All-Russia Research Institute of Automatics, 127055, Moscow, Russia

Problems like image or pattern recognition, or identification of radio signal sources are of great importance nowadays. Effective solution of these problems can be found with neural networks. However, implementation of neuron algorithms require special shapes of a neuron activation function. In the frame of conventional CMOS (Complementary Metal-Oxide-Semiconductor) technology activation functions are commonly simulated by means of FPGA (Field Programmable Gate Array) which is quite hardware and power consuming. We propose a new physical basis for energy efficient simulation of activation function be means of a single adiabatic superconducting interferometer containing just a few Josephson junctions. These are two neuron cells: Sigma-cell and Gauss-cell with sigmoid- and Gaussian-like activation functions respectively (see Fig. 1). Sigmoid function is most suitable for learning algorithms like perceptron used for image or pattern recognition problems. At the same time, multi-layer perceptron should have complex and bulky topology, and also requires rather lengthy training for identification of radio signal sources [1]. Solution of this task can be found using radial-basis functions (RBF) networks. These networks make decision based on probabilistic approach where each unit of a sample area has its own probabilistic (Gaussian) distribution [2, 3]. Designs of our neurons are developed using the adiabatic superconductor logic cell library [4] elements. Both cells have simple topology and low energy consumption, working in superconducting regime. Utilization of standard cell library allows easy development of interface circuits. We consider further optimization of their energy efficiency with introduction of Josephson junction with a complex weak link including ferromagnetic material.

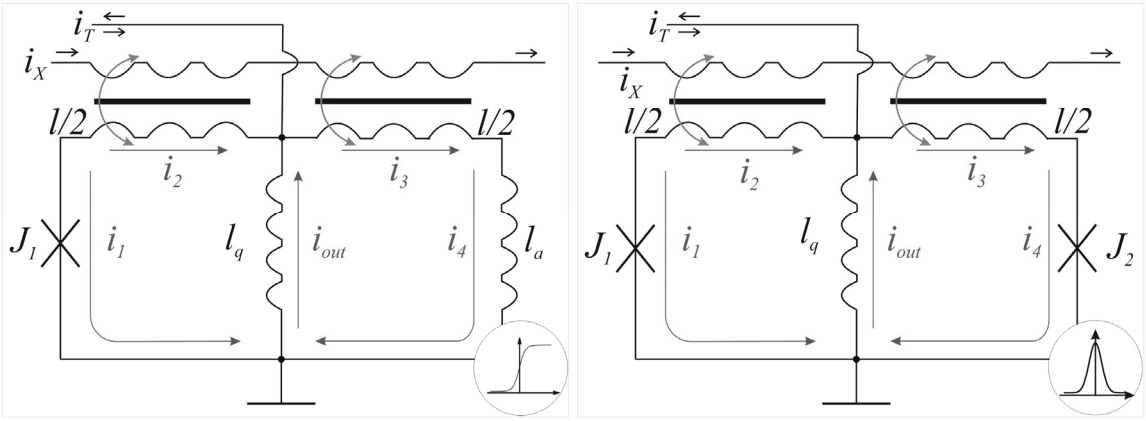

Fig. 1. Principle schemes of Sigma-cell (leftward) and Gauss-cell (rightward).

The work was supported by the Ministry of Education and Science, grant number, 14.Y26.31.0007, President of Russian Federation grant МК-5813.2016.2 and RFBR grant 16-29-09515-ofi_m.

1. F.X. Rosenblatt. *Principles of Neurodynamics: Perceptrons and the Theory of Brain Mechanisms*. Spartan Books, Washington DC, 1961.
2. S.S. Adjemov, N.V. Klenov, M.V. Tereshonok, D.S. Chirov. Moscow University Phys. Bull. **70**(6), pp. 448–456, 2015.
3. S.S. Adjemov, N.V. Klenov, M.V. Tereshonok, D.S. Chirov. Programming and Computer Soft. **42**(3), pp. 121–128, 2016.
4. N. Takeuchi, Y. Yamanashi, N. Yoshikawa. “Adiabatic quantum-flux-parametron cell library adopting minimalist design”. J. Appl. Phys., **117**, 173913, 2015.

Capture into resonance a quantum particle moving in a double-well potential

C.S. Kim[1], D.S. Pashin[2], A.M. Satanin[2]
1. Department of Physics, Chonnam National University, S. Korea, E-mail: cskim@jnu.ac.kr
2. Lobachevsky State University of Nizhny Novgorod, Nizhny Novgorod, Russia, E-mail: sarkady@mail.ru

It is well know that broad range of problems in low dimensional devices can be considered in framework of an archetypical model of a particle with an effective mass moving in a double-well potential. For instance, the electron motion in the field of two quantum dots or quantum coherent phenomena in SQUIDs can be formulated as the problem of quantum dynamics in this kind of potential well, which is shown schematically in Fig. 1(a). The Hamiltonian near the two minima for such kind of systems reads

$$\hat{H} = \frac{\hat{p}^2}{2m^*} - \frac{1}{2}m^*\omega^2 x^2 + \frac{\mu x^4}{4} + Fx\,, \qquad (1)$$

where m^* is the particle effective mass, ω and μ are parameters of the potential well, and F is the external force.

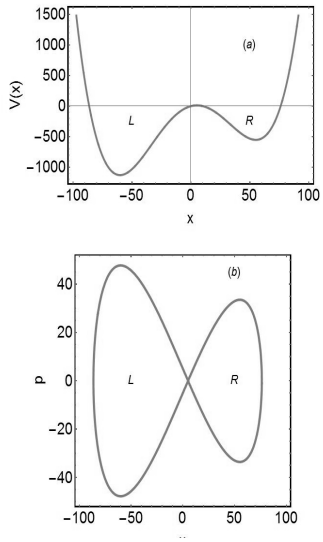

Fig. 1. Double-well potential (a) and the classical contour of the

Let us consider a case when the particle at the initial moment has been exited by an electromagnetic or external current pulse such a way that the absorbed energy may be great than the top of the barrier between the wells. It is supposed that for chosen parameters of the wells the states of particle with confined energy may be separated by a low penetrated barrier. In addition to (1) we take in account the coupling of the particle to its environment which gives the decay of energy. It is known that in the classical regime the probability to capture the particle into the left or right well is proportional the phase space area covered by separatix [1, 2].

In the present work we investigate a question: In which well (the left or the right) the dissipative quantum particle, having at the first energy great than the barrier maximum, may be found with high probability after some time when the energy particle cross the classical energy of motion around of the separatrix? We report here on analytical and numerical investigations of quantum dissipative dynamics a particle moving in a potential with two equilibrium states. The density matrix approach is used to treat the formulated problem.

A new scenario of particle penetration into the wells arises for energy region near the separatrix (Fig. 1 (b)). First of all, we are applying the quasiclassical approach to analyze this problem. If we neglect for a moment the asymmetry parameter, we have found that the turning points for the energy near the separatrix are located approximately on the distance $a \approx \sqrt{2m\omega^2/\mu}$ from the barrier maxima, and the orbit period behaves as $T(E) \approx 2\omega^{-1}\ln\left(2a\sqrt{m\omega^2/2E}\right)$. It shows that the typical spacing of the energy eigenvalues near the separatrix is going to the zero. We have found that in opposite to this conclusion the quasiclassical consideration gives the finite distance between levels that is $\Delta E \approx \pi\hbar\omega/\ln a$. This result is in accordance with numerical calculation of Hamiltonian spectrum. Secondly, we have used the Pauly master equation to calculate the probability to capture particle into the wells (or into the resonances). The qualitative result of our investigations states that the probability of capture the particle into the well proportional the number of levels which find room in the well. Finally, we have investigated the dependence of the probability to find the system in one of states of equilibrium for the quantum and the quasiclassical case, depending on initial conditions and noise.

1. I.M. Lifshitz, A.A. Slutskin, V.M. Nabutovskii, “Motion of charged particles in a varying inhomogeneous electromagnetic field”, Soviet Physics JETP, **14**, p. 669, 1962.
2. V.I. Arnold, “Small denominators and problem of stability of motion in classical and celestial mechanics”, Russian Mathematical Surveys, **18**(6), p. 85, 1963.

Efficiency of the detection signal by means of GaAs tunnel diodes in MHz and quasi THz ranges

M.A. Dresvyannikov[1], A.L. Karuzskii[1], A.V. Perestoronin[1], V.V. Priimochenko[2], A.M. Tskhovrebov[2], L.N. Zherikhina[2]

1. P. N. Lebedev Physical Institute RAS, Moscow, Russia

2. National Research Nuclear University, Moscow, Russia

Originally we planned to conduct research on the effectiveness of detection of tunnel diodes mainly in terms of pure applications like in close paper [1]. However, faced with the effect of increasing the curvature autodyne TD CVC (see item 4), which led to abnormally high detection efficiency in the 10 GHz microwave range, we have seen that these studies are interesting from the theoretical point. Guided by the fact that the effectiveness of the detector is characterized by its Ampere-on-watt characteristic that is estimated from the current-voltage characteristics according to the formula $K_{A/W} = \frac{d^2I}{dV^2} \Big/ \frac{dI}{dV}$ initially we just expected to obtain high value of efficiency at the CVC extremum point that for RTD, which has been more less observed in the above-mentioned work.

1. With replacing conventional germanium diode tunnel in the MHz-Ohm range and applying to the TD voltage, which biases its operating point to the peak or trough, there is increasing in detection efficiency of 20 ÷ 25 dB, which is a significant result in the context of optimization of electronics of the new generation RF-SQUIDs.

2. Studies of the effectiveness of the tunnel diode' functionality as a passive detector showed that in the range of 3 cm at the room temperature and near the tunnel current peak TD has several times higher Amperes / per / Watt performance than the best commercially available microwave detector diodes.

3. Under $T \approx 77$ K (nitrogen temperatures) in the range of 3 cm tunnel diode as a passive detector showed that near the peak of the tunneling current Ampere / per / Watt characteristic of TD increases in 1.5 ÷ 2 times that in the case of unsaturated temperature factor gives a hope that at the temperature $T = 4.2$ K it is possible to achieve the level of efficiency comparable to SIS Josephson elements.

4. It is observed that the effect of the formation autodyne CVC section with abnormally high curvature (in CVC trough area of reversible disruption of internal generation in the frequency f_{int} is much higher than the frequency of the signal detected $f \approx 10$ GHz), and Ampere / on / Watt feature increases to a value of 100 ÷ 200 A/W. At the same time at a frequency $f = 110$ GHz detection efficiency in this anomalous area is completely reset, which gives an upper bound for f_{int}. Thus, 10 GHz << f_{int} << 110 GHz.

5. According to measurements in non-waveguided quasi-optical circuit at the frequency of 110 GHz at the beginning of the recession of the tunneling current (right CVC section with abnormally high curvature) tunnel diode provides effective detection of 10 ÷ 40 mA/W and in conditions close to self-arousal of "low-frequency" (tens of MHz) generation sensitivity in the range of 3mm reached values of more than 1 A/W.

1. G.N. Izmaylov, Yu.A. Mityagin, V.N. Murzin, S.A. Savinov, S.S. Shmelev, E.M. Apostolova. Measuring equipment, No. 8, 2013 (in Russian).

Electrically stimulated high-frequency replicas of a resonant current in GaAs/AlAs resonant-tunneling double-barrier THz nanostructures

A.A. Aleksanyan, A.L. Karuzskii, I.P. Kazakov, Yu.A. Mityagin, V.N. Murzin, A.V. Perestoronin, S.S. Shmelev, A.M. Tshovrebov

P. N. Lebedev Physical Institute of Russian Academy of Sciences, Moscow, Russia, karuz@sci.lebedev.ru

Quantum effects, harmonics generation and high-frequency rectification mechanisms in high-speed resonant tunneling diodes (RTDs) are rather promising to promote semiconductor nanoelectronic devices up to the THz and sub-THz range. A rigorous tunneling theory is crucial to optimize the fabricated RTD and to analyse its interaction with an ac field [1]. To elaborate an RTD with advanced frequency properties it is necessary to compare the computed current-voltage characteristics with the measured *I-V* curves, as usual distorted externally. There are several reasons of the distortions, causing the measured *I-V* curves to have the hysteresis, bistability, discontinuities, humps, plane and stepped sections in the negative differential conduction (NDC) region. The most basic are the excessive series resistance ($R\mathrm{B}_{\mathrm{sB}}$), parasitic oscillation, charge build-up and LO-phonon replicas of a tunneling peak [2-4]. There have been several means to extract the parameters of a test RTD accurately: to monitor the oscillation status by measuring the second derivative of *I-V* curve, to place a resistor ($R\mathrm{B}_{\mathrm{pB}}$) in parallel with the RTD, which could stabilize most of test circuits, etc. [4]. These means are used here to extract the reasons of experimentally found periodical features [5] of the NDC exhibited by the *I-V* characteristics of a high-quality THz RTD [6]. The NDC oscillations (Fig. 1) are considered taking account of the high-frequency (36 meV) LO-phonon-replicas. Under topological variations of the measurement circuit (shunt $R\mathrm{B}_{\mathrm{pB}}$ or serial load $R\mathrm{B}_{\mathrm{sB}}$) striking changes in the *I-V* curves have been found (Fig. 2) and analysed schematically using Kirchhoff's voltage law. The tunneling current flows from an emitter to a collector via a quantum well, the conduction-band profiles of which are disposed in the inversion-like nonequilibrium cascade manner. That supplies the revealed electromotive force in the *I-V* characteristics of an RTD (Fig. 2). The observed low average NDC ~1/300 $\Omega\mathrm{P}^{-1\mathrm{P}}$, period of NDC oscillations ~72 meV in conditions of a slight asymmetry of barriers, number of these periods (7 or 4) depending on the barrier width (20 or 14 Å), and cascade excessive energy provide together an evidence in support of the resonant tunneling assisted by a stimulated excitation of LO-phonon-branch polariton replicas.

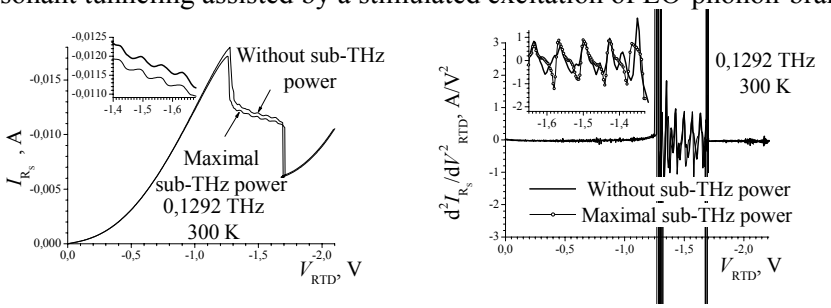

Fig. 1. Second derivatives (right) of *I-V* curves (left) for a double-barrier RTD with and without incident sub-THz power. *T*=300 K, active layers of AlAs/GaAs barriers/well 23/45/20 Å. Inserts show more details.

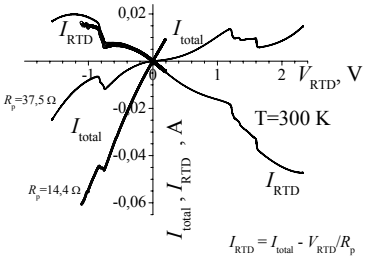

Fig. 2. *I-V* curves for total and RTD currents for the measurement circuit with a shunt R_p.

This research was supported by RFBR (14-02-00658, 15-02-09055), by RAS Grants (24, IV.12 and III.7).

1. V.V. Kapaev. "Nonlinear theory of the narrow-band generation and detection of terahertz radiation in resonant tunneling heterostructures". JETP, **121,** pp. 303-320, (ZhETF, **148**, pp. 349-368), 2015.

2. C.J. Goodings, H. Mizuta, J.R.A. Cleaver. "Electrical studies of charge build-up and phonon-assisted tunneling in double-barrier materials with very thick spacer layers". J. Appl. Phys., **75**, pp. 2291-2293, 1994.

3. V.J. Goldman, D.C. Tsui, J.E. Cunningham. "Evidence for LO-phonon-emission-assisted tunneling in double-barrier heterostructures". Phys. Rev. B, **36**, pp. 7635-7637, 1987.

4. M. Bao, K.L. Wang. "Accurately measuring current-voltage characteristics of tunnel diodes". IEEE Transactions on Electron Devices, **53**, pp. 2564-2568, 2006.

5. A.A. Aleksanyan et al. "Features of the effect of the parameters of resonance systems with different configurations on the current-voltage characteristics of resonant-tunneling nanostructures in a subterahertz frequency range". Vestnik NIYaU "MIFI", **3**, pp. 671-679, 2014 (in Russian).

6. S. Suzuki et al. "Fundamental oscillation of resonant tunneling diodes above 1 THz at room temperature" Appl. Phys. Lett., **97**, 242102, pp. 1-3, 2010.

The spatially dispersive eigenvalues of permittivity operator and frequency-dependent surface impedance for conductors without the dc dissipation

M.A. Dresvyannikov[1], A.P. Chernyaev[2], A.L. Karuzskii[1], Yu.A. Mityagin[1], A.V. Perestoronin[1], N.A. Volchkov[1]

1. P. N. Lebedev Physical Institute of Russian Academy of Sciences, Moscow, Russia, karuz@sci.lebedev.ru

2. Moscow Institute of Physics and Technology (State University), Dolgoprudny, Moscow District, Russia

An operator of the permittivity can completely describe alone a microwave response of conductors with the spatial dispersion. It was found recently [1] in the surface impedance (Z) approximation that the square of its complex number is reciprocally proportional to an eigenvalue (ε_a) of the absolute permittivity operator ($\boldsymbol{\varepsilon}_a$). An eigenvalue problem for the nonself-adjoint permittivity operator $\boldsymbol{\varepsilon}_a$ was considered generally [2, 3] to search the wave solutions for conductors and superconductors. An appearance of additional solutions (additional waves) due to the spatial dispersion can strongly influence the properties of nanoelectronic devices or novel superconducting materials in the form of anomalous losses [4], for example, and should be accounted in simulation and modeling of micro- and nanoelectronic devices. The solutions found correspond to the spatially dispersive eigenvalues ε_a. The mathematical component of the presented formalism was discussed clearly in previous papers [1-3]. A significant role of the spatial-type force resonances was revealed and resonance conditions were derived. These conditions concern the arguments and do not relate to the moduli of complex ε_a and Z in the first approximation. It was concluded [3] that the modulus $|Z|$ is proportional to $\omega^{2/3}$ for all normal conductor solutions except that for the superconductor. In this connection there was some criticism related to the idea that the electrodynamics of superconductors should be in principle reduced to those for conductors as the temperature approaches and beyond the critical temperature. However, the reduction of the superconductor's electrodynamics to those for conductors is not rather straightaway. Early the problem resulted in a supplement of the Maxwell equations by postulating an additional London equation for an explanation of the Meissner effect [5]. It discriminates between the superconductor and the conductor without the dc dissipation, i.e. the perfect conductor, in their non-zero-field cooling behavior. The formalism incorporating spatial dispersion effects [2, 3] is applied here to derive the general frequency dependences of moduli $|\varepsilon_a|$ and $|Z|$ for superconductors or perfect conductors. Again [3] only the spatial field inhomogeneity in the form of a wave number is considered at first, assuming the problem is stationary. Taking into account an absence of the dc dissipation the dependencies $Z \sim \omega$ and $\varepsilon_a \sim 1/\omega^2$ are found for both superconductors and perfect conductors. That follows from the behaviour of the ponderomotive interaction. An Abraham force achieves the highest magnitude when the spatial inhomogeneity gets the largest value corresponding to the London penetration depth. The zero spatial inhomogeneity corresponds to the zero Abraham force and absolutely unstable spatially homogeneous configuration. So the conclusions obtained here in the surface impedance approximation show that the spatial dispersion results in an appearance of the Meissner effect in perfect conductors in the same manner as in superconductors contrary to the previous considerations [5], which do not incorporate the spatial dispersion effects. A driving force of its appearance is the Abraham force.

This research was supported by RFBR (14-02-00658, 15-02-09055), by RAS Grants (24, IV.12 and III.7).

[1] N.A. Volchkov et al., "Additional microwave modes in systems with conductivity of metals and superconductors". JETP, **111,** pp. 292-297, 2010; J. Phys.: Conf. Ser., **400,** pp. 022048-1-022048-5, 2012.

[2] M.A. Dresvyannikov et al., "Conducting media with spatial dispersion in a microwave field: eigenvalue problem for permittivity operator", Proc. SPIE **9440**, ICMNE-2014, 944016, pp. 944016-1 – 944016-9.

[3] M.A. Dresvyannikov et al., "Spatial-dispersion eigenvalues for permittivity operator of conductors and superconductors in a microwave field", J. Low Temp. Phys., pp. 1-7, 2016, DOI 10.1007/s10909-016-1546-4 (online first).

[4] A.S. Shcherbakov et al., "Giant absorption of high-frequency electromagnetic field power in high-temperature superconductors", Fiz. Met. Met., **64**, pp. 742-746, 1987 (in Russian).

[5] F. London, *Superfluids, Vol. I: "Macroscopic Theory of Superconductivity"*, Dover Publications, New York, 1961.

Diamond photocell for vacuum-ultra-violet matrix detector

E. Il'ichev, A. Kuleshov, R. Nabiev, G. Petrukhin, E. Teverovskaya, G. Rychkov
National Research University of Electronic Technology, Zelenograd, Russia
E-mail: mstlena2@mail.ru

Vacuum-ultra-violet matrix detector (VUVMD) has many important applications, including satellite-based missile plume detection, air quality monitoring, space research, high temperature flame detection and astronomical investigations.

Among suitable materials able to be photon sensitive in special range 50 - 230 nm, polycrystalline diamond has the peculiar property of efficient operation as photoelectron emitter. Diamond film can be operated as converted into electron emitted in the vacuum. Different from photoconductive detectors in the same spectral range the photoelectron yield increases continuously with photon energy.

We describe the design and technology of manufacturing a diamond photocell (DPC) for vacuum-ultra-violet matrix detector (see Fig. 1). DPC represents a through divergent channel in a conducting plate. The channel walls are covered with a conducting polycrystalline diamond film. VUV photons entering the channel from the wide side strike the walls and generate photo-electrons in the diamond film. Owing to a low work function of the diamond surface, a fraction of these electrons leave the film and form electron gas in the channel. Due to diffusion and an applied electric field, these electrons are extracted from the narrow side of the channel. DPC simulate electron multiplier concentrator [1]. The sensitivity of the DPC was found to be better in range of 185 - 205 nm than the sensitivity reported in article [2, 3].

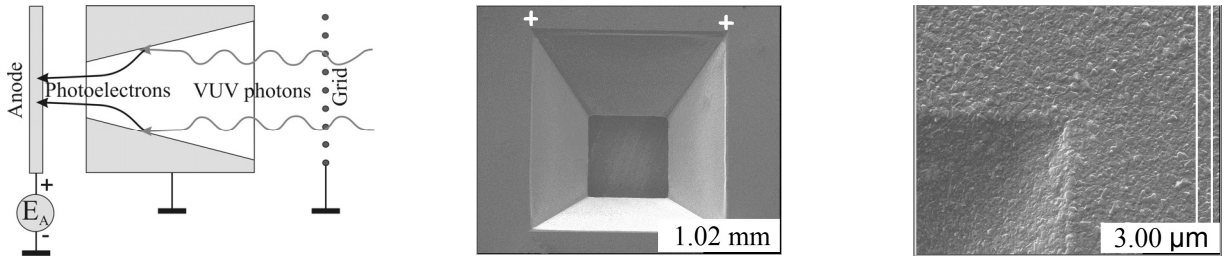

(a) (b) (c)

Figure 1. Diamond photocell: (a) operation concept of diamond photocell; (b), (c) SEM image of the DPC.

Quantum efficiency as a function of the anode potential measured in the near-ultraviolet spectral region (185-205 nm) is shown in Fig. 2.

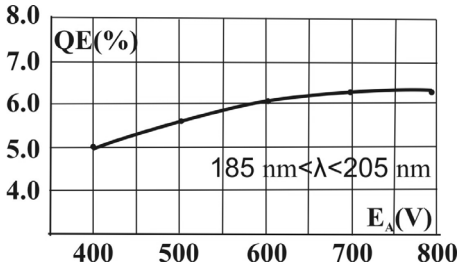

Figure 2. Quantum efficiency as a function of the anode potential.

1. E.A. Il'ichev, A.E. Kuleshov, E.A. Poltoratskii, and G.S. Rychkov. "Electron multiplier concentrator on the base of polycrystalline diamond film". Diamond and Related Materials, **20**, pp. 23-25, 2011.
2. A.S. Tremsin and O.H.W. Siegmund. "UV photoemission efficiency of polycrystalline CVD diamond films". Diamond and Related Materials, **14**, pp. 48-53, 2005.
3. G. Cicala, M.A. Nitti, A. Tinti et. al. "Effect of properties of MWPECVD polycrystalline diamond films on photoemissive response". Diamond and Related Materials, **20**, pp. 1199-1203, 2011.

3D-simulation of silicon micro-ring resonator with Comsol

S.A. Degtyarev[1], S.N. Khonina[1,2], V.S. Solovyev[2]
1. Samara National Research University, Samara, Russia, sealek@gmai.com
2. Image Processing Systems Institute of RAS, – Branch of the FSRC "Crystallography and Photonics" RAS, Samara, Russia, khonina@smr.ru

Ring microresonators are used as photonics devices as transmission and suppression spectrum filters [1], signal delayers [2], as resonators for microlasers [3]. But full vector 3d simulation of this device is not commonly met in recent publications. In this work we simulate silicon ring resonator with Comsol Multiphysics software. Scheme of a simple ring resonator is shown on figure 1a.

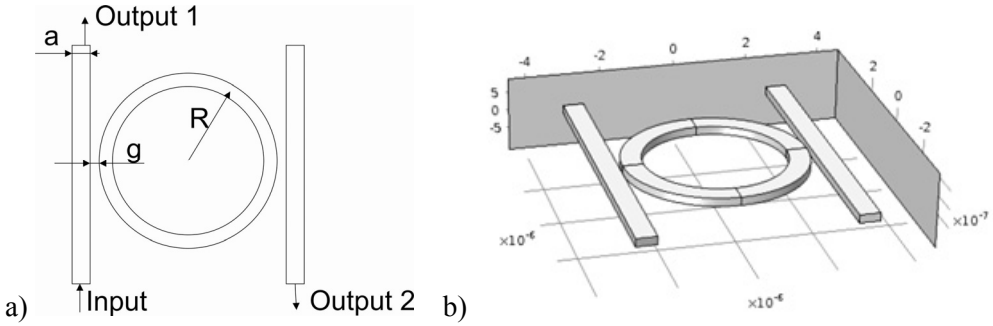

Figure 1. (a) scheme of a ring resonator; (b) 3d view of the scheme

Simulated resonator has the following parameters: gap g = 100 nm, wavelength λ = 1556.9 nm, height of structure h = 220 nm, width of the waveguide a = 540 nm. For simplification the structure is hung on vacuum. For chosen wavelength refractive index of silicon n = 3.48. Radius of the ring should be chosen that optical path in the ring includes only integer number of wavelengths. That is $R = q\lambda/2\pi n$, here q = 30 is the number of wavelengths which are packed in the ring. Thus, R = 2136.1 nm.

This formula for the radius of resonator is approximate because the ring has a non-zero width. In this work the radius is counted from the center to the middle of ring waveguide as it shown on figure 1a. Notice that the mode of the ring waveguide can be slightly decentered relative to the center of the waveguide. Thus, resonance radius can differ from the meaning which is calculated with mentioned formula.

It has been observed during simulation of resonance with Comsol. We create a scheme from figure 1b. And we reveal that there is no resonance if the radius of ring resonator is calculated with approximate formula. To find the resonance radius we vary theoretically calculated meaning. Thus, we find out that the resonance is achieved if the radius is 2146.1 nm. It is 10 nm greater than theoretically meaning.

Also we calculate transmission and suppression spectrums which are depend on the radius of the ring and the wavelength obviously.

In addition, in this work we provide numerical investigation of resonance radius dependence on the waveguide width a. As an example we receive that if a = 540 nm, R = 2146.1 nm; if a = 560 nm, R = 2119.4 nm; if a = 400 nm, R = 1926.4 nm.

In this stage of our work we can make few conclusions which can help us for the following manufacturing of the silicon ring resonator on substrate. For the total pumping of energy from the first output to the second we need one-mode waveguides as an entrance and output silicon trap and a ring resonator too. Thus, width a can vary from $\lambda/2n$ to λ/n. In our case width a is from 223.7 to 447.4. Manufacturing tolerance can be simulated as introducing simple deviations of geometry, sinusoidal relief function, minor ellipticity and so on.

1. A. Biberman, M.J. Shaw, E. Timurdogan, J.B. Wright, M.R. Watts. "Ultralow-loss silicon ring resonator". Optics Letters, **31**(20), pp. 4236-4238, 2012.
2. K.J. Vahala. "Optical microcavities". Nature **424**, pp. 839-846, 2003.
3. W.R. McKinnon, D.-X. Xu, C. Storey, E. Post, A. Densmore, A. Delage, P. Waldron, J.H. Schmid, and S. Janz. "Extracting coupling and loss coefficients from a ring resonator". Optics Express, **17**(21), pp. 18971-18982 2009.

Zero bias THz detection using GaAs/AlAs double-quantum-well resonant tunneling diodes

S. Savinov[1], V. Egorkin[2], V. Kapaev[1,2], I. Kazakov[1], N. Maleev[3], V. Murzin[1]
1. P.N. Lebedev Physical Institute of the Russian Academy of Sciences, Moscow, Russia, s.a.savinov@gmail.com
2. National Research University of Electronic Technology, Moscow, Zelenograd, Russia
3. Ioffe Institute of the Russian Academy of Sciences, St. Petersburg, Russia

The development of compact high-sensitivity room-temperature THz detectors is still actual problem. One of solutions is application of diode nonlinear elements with a strongly asymmetric current-voltage characteristic for rectification of the THz waves at zero bias what allows to simplify circuit layouts and reduce the shot noise. Such an asymmetry can be easily enough obtained in resonant tunneling diode (RTD) heterostructures with two quantum wells of differing width [1]. As shown in [2] by numerical simulation of resonant tunneling transport under external AC field, the optimal RTD parameters should be corresponded to the certain arrangement of the lowest energy states in quantum wells and Fermi level in fore-barrier regions.

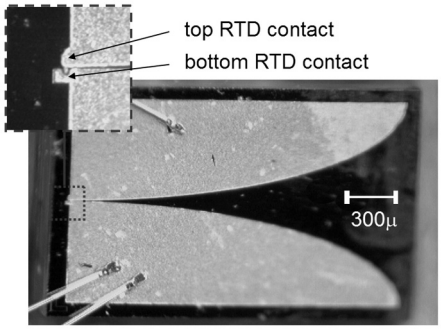

Figure 1. The photo of RTD based THz detector element with Vivaldi antenna.

The present work is devoted to experimental investigation of THz detector elements fabricated on the basis of GaAs/AlAs double-quantum-well RTD with near optimal parameters. Two type samples were grown by MBE with the nominal thicknesses of active region layers 12/**100**/20/**90**/12 Å and 20/**100**/20/**90**/20 Å. The mesa structure of RTD (∅ ≈ 2 μm) was located in usual feed point of Vivaldi antenna (Fig. 1). The IMPATT diode was used as a microwave source (f = 0.111 THz, P ≈ 50 mW). After passing through a calibrated waveguide attenuator the THz waves were radiated to the free space via horn antenna and then focused to the sample using a teflon lense. The measured current-voltage curves $I_0(V_{dc})$ showed a noticeably nonlinear behavior (Fig. 2a) – value of the ultimate sensitivity $\beta = (d^2I_0/dV_{dc}^2)/(2 \cdot dI_0/dV_{dc})$ at zero bias voltage reached of 20 A/W. The experiments on detection revealed a power function dependence of rectification current ΔI_0 on THz intensity in the available attenuation range 0÷50 dB and the figure-of-eight polar pattern of antenna with relation $\Delta I_0^{max}/\Delta I_0^{min} \approx 100$ (Fig. 2b). The calculated ampere-watt sensitivity of detector elements subject to electromagnetic simulation data is about 0.1–1 A/W.

a)

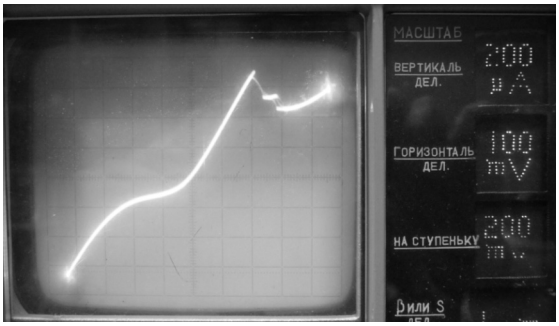

b)

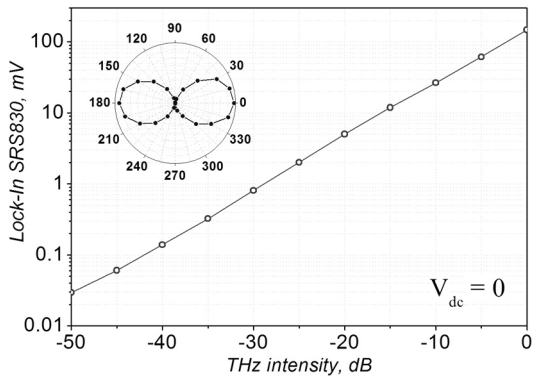

Figure 2. a) A typical room temperature current-voltage characteristic of fabricated RTD based detector element; b) The sensitivity curve and polarization dependence of RTD based detector element measured at zero bias voltage.

The research was supported by RFBR (grant № 14-02-00658) and MES of Russia (ass. № 2014/101).

1. S. Takahagi, H. Shin-ya, K. Asakawa, et al. "Equivalent Circuit Model of Triple-Barrier Resonant Tunneling Diodes Monolithically Integrated with Bow-Tie Antennas and Analysis of Rectification Properties towards Ultra Wideband Terahertz Detections", Jpn. J. Appl. Phys., **50**, pp. 01BG01-1–01BG01-5, 2011.
2. V.I. Egorkin, V.V. Kapaev, "Detection of Terahertz Radiation by Resonant Tunneling Nanoheterostructures", Russian Microelectronics, **45**, pp. 205-210, 2016.

A low actuation voltage bistable MEMS switch: Design, fabrication and preliminary testing

I.V. Uvarov, V.V. Naumov, O.M. Koroleva, E.I. Vaganova, I.I. Amirov
Yaroslavl Branch of the Institute of Physics and Technology RAS, Yaroslavl, Russia, i.v.uvarov@bk.ru

Electrostatically actuated MEMS switches are widely used in various radio frequency and microwave systems [1]. In comparison with RF switches based on pin-diodes and field-effect transistors, MEMS switches have advantages of low power consumption, small insertion loss in the closed state, high isolation in the opened state, low harmonic distortion and high radiation resistance. One of the main disadvantages of MEMS switches is the high actuation voltage, which is typically around a few tens of volts [2]. The most effective way to make the actuation voltage lower is to reduce the stiffness of the movable electrode. However, in the vast majority of conventional switches the breaking of a contact between the movable and signal electrodes is carried out by the force of elasticity (passive opening). Reducing the stiffness makes the breaking force lower and leads to the stiction of the electrodes. Here we propose the design of the switch, which allows, if necessary, to overcome stiction and break the contact (active opening mechanism).

The switch is shown in Fig. 1. The movable electrode is a metallic beam, attached in the middle of its length to the torsion springs. Driving and signal electrodes (also metallic) are situated under the each arm of the beam symmetrically with respect to the clamping points. Beam has the contact bumps on its bottom side above the signal electrodes. Bumps localize the area of contact of the beam with the signal electrode and prevent the contact of the beam with the gate electrode when triggered.

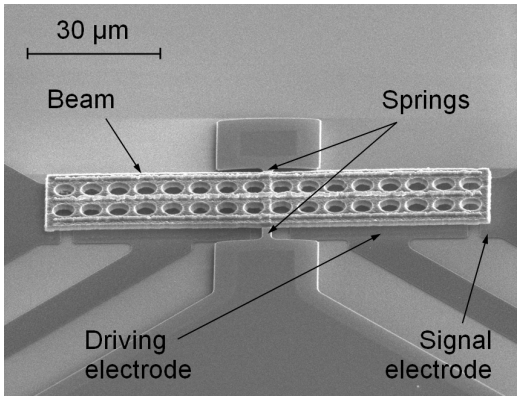

Fig. 1. SEM image of the switch.

Initially the beam is in a horizontal position. When the voltage is applied to the one of driving electrodes, beam bends towards the electrode under the electrostatic force and comes in contact with the signal electrode. When the driving voltage is removed, switch retains its state, because the elastic force generated in the torsion springs is insufficient to overcome the stiction between the beam and the signal electrode. To break the contact, another driving electrode is used. When the voltage is applied to it, the beam is tilted to the opposite direction and comes in contact with another signal electrode. Thus, after the first actuation two states of the switch are possible, and both of them are stable in the absence of driving signals.

MEMS switch was fabricated by surface micromachining on thermally oxidized silicon wafers. Driving and signal electrodes were made of Cr and had a thickness of 50 nm. The beam and the springs were formed on the sacrificial layer of amorphous Si with the thickness of 1.5 μm. Springs were made of Cr and had a thickness of 0.3 μm. Estimated stiffness of springs was $3.9 \cdot 10^{-9}$ N·m. Beam was made of Al and had a length of 100 μm, a width of 8 to 32 μm (depending on the design) and a thickness of 2 μm. Deposition of materials was performed by magnetron sputtering, the sacrificial layer was removed by SF_6 plasma etching.

Testing of switches was performed in air under normal conditions. The beam was grounded, DC voltage was applied to the driving electrode to actuate the switch. The actuation was registered by a change of the resistance between the beam and the signal electrode. The voltage of the first actuation was in the range of 6.5 ÷ 13.0 V. A good agreement between the experimental data and the results of FEM simulation was observed. Recovery voltage exceeded the first actuation voltage at 3-4 times and was in the range of 26.6 ÷ 32.0 V. In the future we plan to reach the 5 V level for the recovery voltage by reducing the gap between the beam and the electrodes and, possibly, by modifying the beam design. The active contact breaking mechanism allows to do it without the risk of stiction failure.

This work was supported by RFBR research project No. 16-37-60065 mol_a_dk and performed using the equipment of Facilities Sharing Centre “Diagnostics of Micro- and Nanostructures”.

1. G.M. Rebeiz. *RF MEMS: Theory, Design, and Technology.* John Wiley & Sons, New Jersey, 2003.
2. A.K. Sharma, A.K. Gautam, P. Farinelli, A. Dutta, and S.G. Singh. "A Ku band 5 bit MEMS phase shifter for active electronically steerable phased array applications". J. Micromech. Microeng., **25**, p. 035014, 2015.

Anchored multi-DOF MEMS gyroscope having robust drive mode

P. Verma, S.N. Khonina, V.S. Pavelyev
Samara National Research University, 34, Moskovskoye Shosse, Samara, 443086, Russia;
Email: payalsedha@gmail.com, khonina@smr.ru, pavelyev10@mail.ru

Abstract: This paper presents the new architecture of 2-DOF (degree-of-freedom) drive mode and 1-DOF sense mode gyroscope with the concept of additional anchoring that retains all the advantages of the Dynamic Vibration Absorber (DVA) concept while being operated at high frequencies. These concepts allow reduction of the bandwidth by varying the coupling parameter during the design, thereby increasing the mechanical sensitivity. In the present design, the anchoring concept has been implemented by adding a central anchor for the sense mass.

Introduction: DVA type system [1-3] is used for increasing robustness of vibratory gyroscopes. This design is aimed at operating the device in robust mode and also achieving high sensitivity by utilizing single resonance of the sense mode. No doubt, this concept reduces the complexity of the drive electronics, but its application is limited to low frequencies. When such devices are designed for high operating frequency the bandwidth becomes considerably high whereby amplitude decreases significantly, which is undesired. By reducing the bandwidth, the sensitivity of the devices can be further improved. In order to narrow down the bandwidth, the sense-to-drive mass ratio of the device has to be reduced considerably that leads to large drive mass or very small sense mass. Since the mass of drive oscillator does not contribute to the sensitivity, increasing its size does not benefit the design. On the other hand, smaller size of sense mass results in a very low sense capacitance value due to limited number of sense comb fingers.

2-DOF drive DVA system: Figure 1(a) shows the schematic view of the DVA system [2, 3]. The DVA system has 2-DOF drive mode characterized by active mass, m_1 and passive mass system $(m_2 + m_f)$, with only two suspension elements, k_{1x} and k_{2x}. The structural frequencies for this system can be formulated as,

$$\omega_{1x}^2 = (k_{1x} + k_{2x})/m_1;\ \omega_{2x}^2 = k_{2x}/(m_2 + m_f);\ \omega_c^2 = k_{2x}/\sqrt{m_1(m_2 + m_f)}, \quad (1)$$

where ω_{1x} and ω_{2x} are the structural frequencies of active mass m_1 and the passive mass system $(m_2 + m_f)$, while ω_c is a term that expresses the strength of coupling between two masses.

It is evident from Eq. (1) that the terms ω_{2x} and ω_c are inter-dependent, that is, $\omega_c^2 = \mu^2\omega_{2x}^2$, where, the proportionality constant, μ^2, is sense-to-drive mass ratio of the system, defined as $\mu^2 = (m_2 + m_f)/m_1$. From this, it can be inferred that the structural frequency of passive mass system $(m_2 + m_f)$ and the amount of coupling between the masses cannot be defined independently.

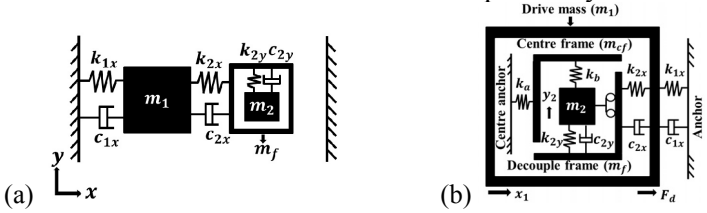

Figure 1: (a) Schematic view of DVA-type 2-DOF drive dynamic system; (b) centre anchoring structure.

2-DOF drive with centre anchoring structure: The structural frequencies of the centre anchored 2-DOF drive [Fig. 1(b)] dynamic system can be formulated as,

$$\omega_{1x}^2 = (k_{1x} + k_{2x})/m_1;\ \omega_{2x}^2 = (k_{2x} + k_a)/(m_2 + m_f + m_{cf});\ \omega_c^2 = k_{2x}/\sqrt{m_1(m_2 + m_f + m_{cf})}, \quad (2)$$

It can be observed in Eq. (2) that, unlike the DVA type system, there is no dependence of coupling between ω_{2x} and ω_c through mass ratio, μ^2. This proves the concept of centre anchoring for reduction of drive bandwidth while improving mechanical sensitivity without reducing the mass ratio.

1. C. Acar, *Robust micromachined vibratory gyroscopes*, Ph.D. dissertation, University of California, Irvine, 2004.
2. P. Verma, R. Gopal, S.K. Arya, "Analytical modeling and simulation of a 2-DOF drive and 1-DOF sense gyro-accelerometer", Microsystem Technologies, **19**, pp. 1238-1249, 2013.
3. P. Verma, K.Z. Khan, S.N. Khonina, N.L. Kazanskiy, R. Gopal, "Ultraviolet-LIGA based fabrication and characterization of a non-resonant drive mode vibratory gyro/accelerometer", J. Micro/Nanolith. MEMS MOEMS, **15**(3), pp. 035001-(1-9), 2016.

Design and technological features of creating and successfully tested linear acceleration

N. Parfenov[1], S.Timochenkov[2], A. Timochenkov[2]
1. MAI (National Research University), Moscow, Russia, sedennik@mail.ru.
2. MIET (National Research University), Moscow, Russia, spt@miee

Modern aerospace and high-tech equipment in terms of exposure to shock and vibration loads, high moisture, and wide temperature range make high demands on the parameters of physical quantity sensors and other MEMS devices.Currently these demanding requirements at this stage can satisfy the developed and manufactured and successfully tested, the parameters which determine in the inertial navigation systems the location and orientation of moving objects no external sources of information.
In this work, we have designed and manufactured capacitive microaccelerometer comb type. The structure is based on the sensitive element (SE), the inertial mass which is suspended on the torsion bars. The design of the comb probe was performed using the finite element method in the ANSYS program based on the results of modal analysis.
Static analysis for the model *f* was conducted under the condition of linearity of the deformation of the suspension. The calculation showed that the relative displacement of the pendulum from the influence of gravity along the axis of sensitivity is 0.06 μm/g.
Inertia mass mounted on the torsion under the influence of acceleration is moved, which alters the distance between the moving and fixed combs, and, consequently, the value of the capacitor formed by the capacitors. By measuring capacitance it is possible to estimate the magnitude of the applied acceleration. Along with this to assess the error characteristics of the sensor was used to control the chasers that need the voltage (selected experimentally), and in the event the electric field was the movement of the inertial mass. Due to the change of the containers, which were assessed using measuring combs, was possible to judge the presence of error.
Developed accelerometer had a differential structure intended to compensate for the drift parameters and suppression of various interference. For this, an additional capacitor was used with the capacity about the one of the main capacitor. The voltage is applied to the capacitors with a phase displacement of 180°. Structurally, microaccelerometer consists of 30 pairs of differential electrodes.
The starting material for the manufacture of the accelerometer were used the silicon and silicon dioxide coated with a layer of glass, which was afterwards vented. To provide clearance between the inertial mass and the stator, on top of the glass is placed a layer of low resistance single crystal silicon of orientation (100) which is then etched rotor [1].
Thus, a pilot sample of a modern comb type microaccelerometer was developed and produced. The calculated structure is able to withstand a linear acceleration up to 500*g*.

1. Parfenov N.M., Timoshenkov S.P., Timoshenkov S.A. Research and development of integrated MEMS-transducers of mechanical quantities. Nano-and Microsystem technology, 2015, No. 5, pp. 49-52 (in Russian).

Biosensor platform based on carbon nanotubes covalently modified with aptamers

I.A. Komarov[1], E.I. Rubtsova[1], A.V. Golovin[2], T. Kholina[2], I.I. Bobrinetskiy[1]
1. National Research University of Electronic Technology, Moscow, Russia, master_kom@mail.ru.
2. Lomonosov Moscow State University, Moscow, Russia, golovin@gmail.com.

Small portable flexible sensors for health parameter detection are one of a great area of today scientists and engineers development. There are several promising detection methods with high sensitivity and selectivity: shortDNA [1] structures for example aptamers [2] or antibodies [3]. Among these types of affinity agents the most promising is aptamers due to its technology can be incorporated to the standard organic electronics processes. Aptamers are short oligonucleotides that have high specificity to the target along with stability and possibility high yield chemical synthesis for mass production. At the same time biosensor substrate can be flexible and reliable for integration into personal healthcare systems.

We developed new biosensor design based on flexible polymer substrate with conductive thin film of carbon nanotubes (CNTs) chemically modified with aptamer and covered by flexible passivation layer with a window for analyte exposition (fig. 1). After computer simulation we choose "RA-36" aptamer for thrombin - main enzyme of blood coagulation cascade. One of our goals was to create stable sensor suitable for repetitive measurements. To achieve this we covalently immobilized aminomodified aptamer on carboxylized CNTs transferred to a flexible polymer substrate.

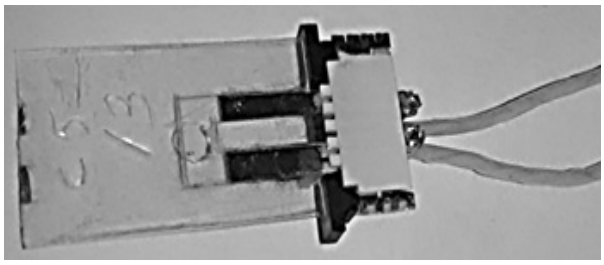

Fig. 1. Photography of biosensor in use.

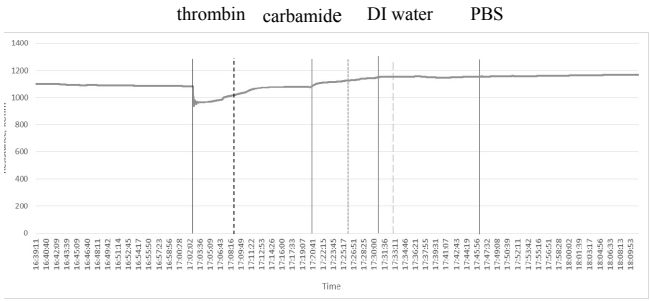

Fig. 2. Sensor response to PBS.

Binding results we controlled with high performance liquid chromatography (HPLC) and Raman spectroscopy. HPLC revealed high yield of covalent binding reaction. Presence of nucleotides on CNTs was also confirmed with Raman spectroscopy. The stability of sensor was demonstrated by repetitive applying of buffer to sensor.

Sensor response on thrombin was measured with 2 μM human thrombin solution in PBS buffer (fig. 2). Resistance of aptasensor decreased after thrombin exposition with response time about 30 seconds. We suppose relatively low response reflects that density of aptamers is so high they hinder one with another.

In this work we have shown that it is possible to covalently bind aptamer to carboxyl modified CNTs with high yield. The stability of sensor increased while decreasing of sensor response because of high aptamer density.

1. C. Hu, Y. Zhang, G. Bao, Y. Zhang, M. Liu, Z.L. Wang, "DNA Functionalized Single-Walled Carbon Nanotubes for Electrochemical Detection", J. Phys. Chem. B, **109** (43), pp. 20072-20076, 2005.
2. A.-E. Radi, "Electrochemical Aptamer-Based Biosensors: Recent Advances and Perspectives", International Journal of Electrochemistry **2011**, pp. 1-17, 2011.
3. B. Byrne, E. Stack, N. Gilmartin, R. O'Kennedy, "Antibody-Based Sensors: Principles, Problems and Potential for Detection of Pathogens and Associated Toxins", Sensors, **9**, pp. 4407-4445, 2009.

A wireless micromechanical gauge for remote measurement of pressure in vacuum range

A. Boyko, P. Kovyrkin, A. Shalimov, S. Timoshenkov
National Research University of Electronic Technology, Moscow, Zelenograd, Russia, ant_nico@mail.ru

A lot of micromechanical vacuum gauges based on membranes, Pirani sensors and oscillators were developed during the last years, some of them are already commercially available. Benefits of the use of MEMS-based vacuum gauges are small-size and low power consumption, low cost at mass production. Such gauges are applicable in electronics, MEMS, vacuum technique and allow measuring a pressure in a wide vacuum range up to 10^{-6} mbar [1]. Many of MEMS contain vibrating three-dimensional structures like beams, cantilevers, membranes, etc., energy loss owing to gas damping can be utilized for determining pressure. Friction vacuum gauges are sensible to damping of moving plate in the surrounding gas [2].

This work describes wireless micromechanical friction vacuum gauge aimed for remote control of pressure. Micromechanical resonator sensible to gas damping is a "core" of the gauge and includes silicon proof mass and static glass substrate. Silicon mass is made by bulk micromachining and is joined to static glass substrate by anodic bonding. Control electrodes are formed onto silicon and glass components using physical vapor deposition. The gap between moving mass and static substrate is about of 5-10 μm. Gas located between moving plate and static substrate makes a main contribution to energy loss of vibrating system. Electrostatic capacitive driving was implemented, moving of silicon mass is detected using capacitance-to-voltage converter transducing the change of electric capacity between electrodes to voltage signal. Time-domain method was used to measure damping characteristics that are proportional to the surrounding pressure. In accordance to time-domain procedure an excitation of proof mass has to be done to stimulate free oscillations. A saw-tooth signal provides eligible repeatability of this procedure; proof mass is displaced from the equilibrium position by smooth rising of voltage amplitude and than released.

Developed vacuum gauge consists of above-mentioned resonator, interfacing circuit and computing device. Interfacing circuit generates saw-tooth driving pulse, reads analogous signal and converts it to digital data array. Electronic circuit comprises driving pulse microcontroller, high-voltage amplifier, capacity-voltage transducer and radio transceiver. Transmission of converted digital signal from interface unit towards computer and contrariwise was carried out by Bluetooth 4.0 technology, which ensures simple interaction between components, an ability of connecting additional devices and constructing of wireless sensor and actuator network (WSAN) [3]. The use of wireless technology allows overcoming a critical loss of week signal in electric wiring as well as to place sensor in locations difficult to reach with a wire. Developed electronic circuit is compatible with the most of common data interface units and could be incorporated into plant automation systems.

To value a pressure several steps have been carried out in series: excitation of moving mass; an output data reading and recording; the pressure computation using specialized program. Many of conventional personal computer or even smartphones can be adopted for data processing storage and visualization. The program developed using integrated development environment (IDE) Borland C++. An algorithm of pressure calculation based on time-domain method according to that various characteristics of free oscillations are obtained and analyzed [4]. As a sort of parameter under investigation could be decay time of damping oscillation, decaying of amplitude or number of peaks of decaying sine curve. To increase noise stability and accuracy of time-domain measurements we have applied an estimation of full length of sine curve. This approach is notably effective at a short decay time. The results of the work are promising for applying in automatic test equipment, Internet of things (IoT) and MEMS industry.

1. Gorecka-Drzazga A. "Miniature and MEMS-type vacuum sensors and pumps", Vacuum **83,** pp. 1419-1426, 2009.
2. Volklein F., Meier A. "Microstructured vacuum gauges and their future perspectives", Vacuum **82,** pp. 420-430, 2008.
3. Zhang Sh., Zhang H. "A Review of Wireless Sensor Networks and Its Applications", Proc. of the IEEE Int. Conf. on Automation and Logistics, Zhengzhou, China, 2012, pp. 386-389.
4. Zhang M., Llaser N., and Rodes F. "High-precision time-domain measurement of quality factor", IEEE Trans. Instrumentation and Measurement, **61**(3), pp. 842-844, 2012.

Angular electrochemical sensor for precise azimuth determination

D.L. Zaitsev[1], A.N. Antonov[1], V.G. Krishtop[2]

1. Moscow Institute of Physics and Technology (State University), Moscow, Russia, Dmitry_Zaytsev@mail.ru

2. Institute of Microelectronics Technology and High Purity Materials, Chernogolovka, Russia.

This paper describes using a low-noise angular motion sensor to precisely determine azimuth direction in a dynamic-scheme method of measuring Earth's rotation velocity vector [1]. The scheme includes installing a sensor on a rotating platform so that it could scan a space and seek for the position of highest Earth's rotation vector projection on its axis. We take a precision angular sensor based on ECT (electrochemical transduction) technology. ECT-based angular sensors far superior to angular MEMS-sensors, and it is very promising to use microelectronic technology for their manufacture [2].

Spatial orientation of an object is commonly described in terms of the two local axes: the local vertical and the local meridian. Vertical orientation could be precisely determined by measuring the g-force by the accelerometer. However, the accurate measuring of azimuth direction is a difficult task. Magnetic compassing cannot provide good accuracy and gyro compassing requires expensive IMU systems or mechanical gyroscopes. The world level of precise measurements is typically 1 mil (mill radian) for civilian-class systems. Still there exists a solution to achieve this level of precision using a relatively low-cost sensor. The solution is based on a dynamic-scheme signal modulation method. The angular accelerometer or gyroscope is placed on a platform which rotates about a vertical axis and the sensor's sensitivity axis is directed horizontally. In this case, the projection of the Earth's rotation angular velocity to the sensor's axis, and hence its output signal, changes periodically during the rotation of the platform (Fig. 1). The phase of this periodic signal allows for determining the azimuth. Dynamic analysis method and its comparison with the static approaches are presented in many works [3,4].The main advantage of the dynamic scheme is to transfer the signal associated with the Earth's rotation from 0 Hz to the frequency of platform rotation, which eliminates errors associated with sensor's zero-frequency bias drift.

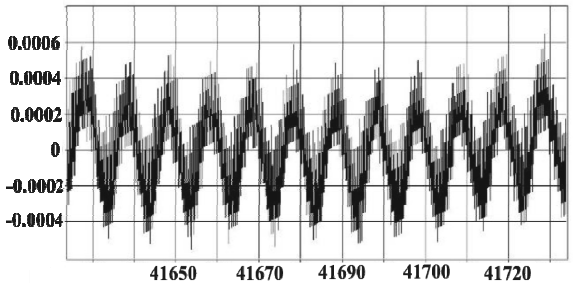

Fig. 1a. Angular motion sensor signal during the platform rotation. On the x-axis - the recording time in seconds, on the y-axis - ADC counts.

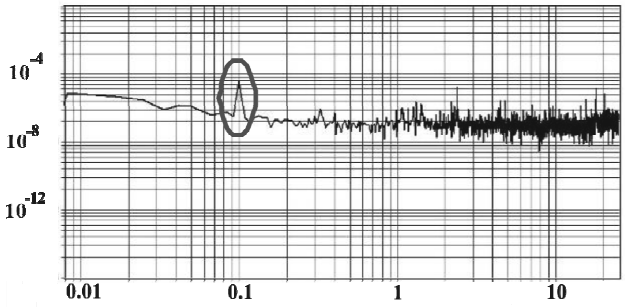

Fig. 1b. The spectrum of the sensor signal during the platform rotation. On the x-axis - the frequency in Hz and on the y-axis - the angular velocity in radians / sec.

Low noise angular sensor provides a qualitatively better precision parameters, for azimuth determination, than the same for MEMS and fiber-optics gyros [5]. Confirmed in experiments measuring accuracy is 0.07º for a measurement time of 200 seconds. This value exceeds the previously obtained the global level using low-cost sensors of angular motion. Thus, with respect to the achieved world-class novelty of this paper is to implement a high-precision device using a new element base — highly sensitive ECT sensor of angular motion with low noise flour.

1. D.L. Zaitsev, V.M. Agafonov, E.V. Egorov, A.N. Antonov, V.G. Krishtop, «Precession Azimuth Sensing with Low-Noise Molecular Electronics Angular Sensors», Journal of Sensors, Vol. 2016, Article ID 6148019.

2. V.G. Krishtop, V.M. Agafonov, A.S. Bugaev, "Technological principles of motion parameter transducers based on mass and charge transport in electrochemical microsystems", Russ. J. of Electrochemistry, 2012, **48** (7), pp. 746–755.

3. G. Eduardo Sandoval-Romero, Victor Argueta-Diaz, "A simple Theoretical Comparison Between Two Basic Schemes in Function of the Earth's North Pole Detection: The Static Method," Journal of Sensors, Vol 2010, Article ID 253642.

4. Concerning Gyrocompasses: *R.B. Dyott*, "Method for finding true North using a fibre-optic gyroscope", Electronics Letters, 1994, **30** (13).

5. Iozan L. I.; Kirkko-Jaakkola M.; Collin J.; Takala J.; Rusu C. "North Finding System Using a MEMS Gyroscope" Measurement Science & Technology, 2012, 23 02500

The simulation model of planar electrochemical transducer

D.A. Zhevnenko[1,2], S.S. Vergeles[3,2], T.V. Krishtop[4,5], D.V. Tereshonok[6], V.G. Krishtop[1,7,*)]

1. Institute of Microelectronics Technology and High Purity Materials, Chernogolovka, Russia.
2. Moscow Institute of Physics and Technology (State University), Dolgoprudny, Russia.
3. Landau Institute for Theoretical Physics, Chernogolovka, Russia.
4. Kotel'nikov Institute of Radio-Engineering and Electronics, Russian Academy of Sciences, Moscow.
5. Amadeus IT Group, Sophia Antipolis, France.
6. Joint Institute for High Temperatures of the RAS, Moscow, Russia.
7. Seysmotronika LLC, Moscow, Russia.
*) vgkvgk@mail.ru

Planar electrochemical systems are very perspective to built modern motion and pressure sensors. Planar microelectronic technology was successfully used for electrochemical transducer (ECT) [1, 2] of motion parameters. The most important advantage of electrochemical transducers of motion parameters is the high steepness of conversion of the mechanical signal to electric current.

In this work, we have developed a mathematical model of a planar electrochemical system which detects the mechanical signals. Standard approach to solving this problem has been used [1]. Navier–Stokes and the convective-diffusion equations were solved numerically using a Butler-Volmer boundary condition and a continuity condition. The advantage of our work is the calculating for absolute values of physical parameters, while most previous articles simulating the ECT with three components of electrolyte are provide the only quantitative or comparative results, for example [3-5].

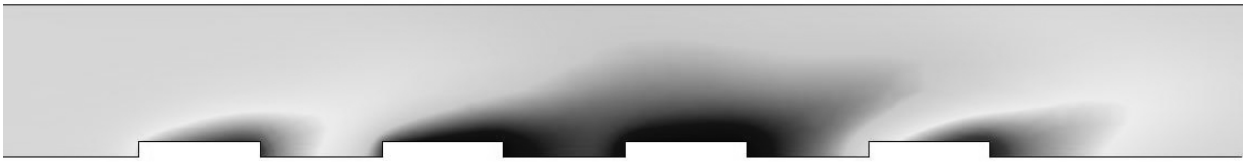

Figure 1. The calculated concentration gradient in the planar electrochemical four-electrode transducer under the condition of the high electrolyte flow.

We have calculated the true values of the fluid streams, concentrations and currents in our planar transducer. For the case of system parameters corresponding to the experimental samples, calculated values were close to the experimental data. Thus, we developed the realistic mathematical model which is able to provide the correct results. It planned to use this model for studying of properties of various electrochemical systems and optimizing of characteristics.

1. V.G. Krishtop, V.M. Agafonov, and A.S. Bugaev, «Technological Principles of Motion Parameter Transducers Based on Mass and Charge Transport in Electrochemical Microsystems», Russian Journal of Electrochemistry, **48** (7), pp. 746–755, 2012.
2. V.M. Agafonov, V.G. Krishtop, M.V. Safonov. "Measuring Means Based on Molecular-Electron Transfer in Micro- and Nanostructures". Nano- i mikrosistemnaya tekhnika, **6**, pp.47-53, 2010 (in Russian).
3. Z. Sun, V.M. Agafonov. "Numerical modeling of a four-electrode electrochemical accelerometer based on natural convection: the boussinesq flow model vs. the compressible flow model". Russian Journal of Electrochemistry, **48** (8), pp. 835-842, 2012.
4. I.P. Kasperovich, V.G. Krishtop, "Modelling of the processes of convection-diffusion in the solid-liquid planar type nanostructures with various geometries". Proceedings of the 1st Russian-Belarusian Scientific-Technical Conference «Element base for national radio electronics», **1**, pp. 28-29, 2013 (in Russian).
5. V.M. Agafonov, A.A. Orel. "Simulation of Physical Processes Occurred in Molecular-Electronic Transducer Based on Planar Technology". Nano- i mikrosistemnaya tekhnika, No. 5. pp. 50-57, 2008 (in Russian).

The planar silicon-based microelectronic technology for electrochemical transducers

A.V. Novikov[4], A.E. Egorchikov[4], A.N. Dolgov[4], E.S. Gornev[4], V.G. Popov[1,2], I.V. Egorov[1,3], V.G. Krishtop[1,3,*)]

1. Institute of Microelectronics Technology and High Purity Materials, Chernogolovka, Russia.
2. Moscow Institute of Physics and Technology (State University) Dolgoprudny, Moscow region.
3. "Seismotroniks" LLC, Moscow
4. JSC Mikron, Zelenograd, Russia
**) krishtop@iptm.ru*

The traditional technology for fabricating the electrochemical sensors is well known and based on wire mesh packaging for sensing element in electrolytic liquid [1, review]. The most important advantage of motion parameter transducers based on mass and charge transport in electrochemical systems is exceptionally high rate of mechanical signal conversion to electric current. Devices of this class are based on the principle of diffusion charge transport under the conditions of forced convection appearing as a result of external acceleration.

In this report, we describe the new modern microelectronic technology for fabrication of electrochemical transducers (ECT). The modern microelectronic technological opportunities are allow to improve the operating characteristics of electrochemical registrars [2, 3]. Actually, ECT-based devices are able to make a concurrence with the best MEMS systems.

We combine the advantages of up–to–date microelectronic technologies and devices based on an electrochemical transducer. In this report, we developed the new technology for the sensitive element of electrochemical microsensors, produced the pilot samples and discussed the preliminary testing results. This technological route is suitable for the mass production.

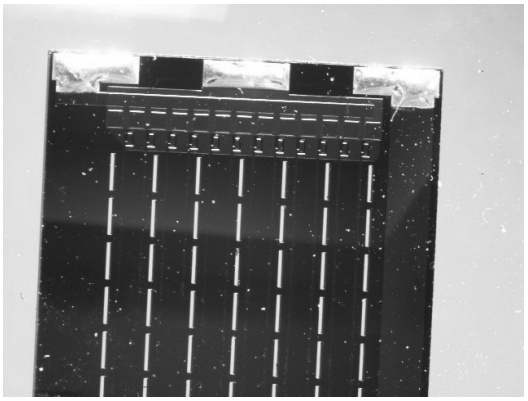

Figure 1. The sample of the electrochemical motion sensor.

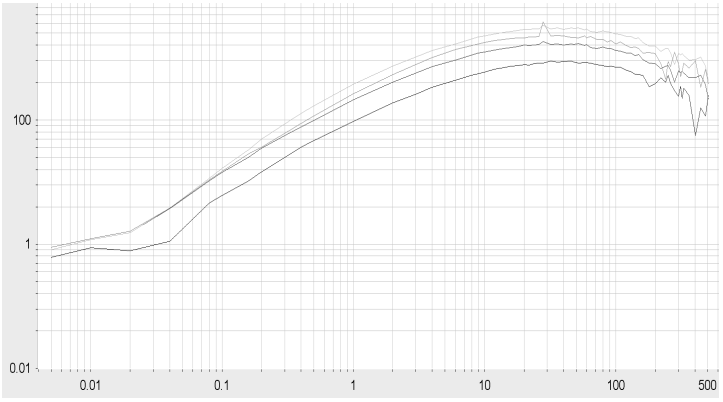

Figure 2. Transfer function of the planar sample of motion sensor (blue) in comparison with classic mesh sensors (other).

1. A.S. Shabalina, D.L. Zaytsev, E.V. Egorov, I.V. Egorov, A.N. Antonov, A.S. Bugaev, V.M. Agafonov, V.G. Krishtop. "Modern measuring instruments based on molecular electronic transducers", Uspekhi sovremennoi radioelektroniki (Achievements of Modern Radioelectronics), №9, pp. 33-42, 2014 (in Russian).
2. V.G. Krishtop, V.M. Agafonov, and A.S. Bugaev, "Technological Principles of Motion Parameter Transducers Based on Mass and Charge Transport in Electrochemical Microsystems", Russian Journal of Electrochemistry, **48** (7), pp. 746–755, 2012.
3. V.M. Agafonov, V.G. Krishtop, M.V. Safonov, "Measuring Means Based on Molecular-Electron Transfer in Micro-and Nanostructures", Journal of Nano and Microsystem Technique, №6, pp. 47-53, 2010 (in Russian).

The precision seismometer based on planar electrochemical transducer

A.S.Shabalina[1], V.G. Krishtop[2]
1. Moscow Institute of Physics and Technology (State University), Moscow, Russia.
2. Institute of Microelectronics Technology and High Purity Materials, Chernogolovka, Russia.

Precision seismometer based on simplest planar electrochemical transducer (ECT) was manufactured and tested. We investigated the amplitude-frequency and volt-ampere characteristics, self-noise level and the transducer's impedance frequency dependence.

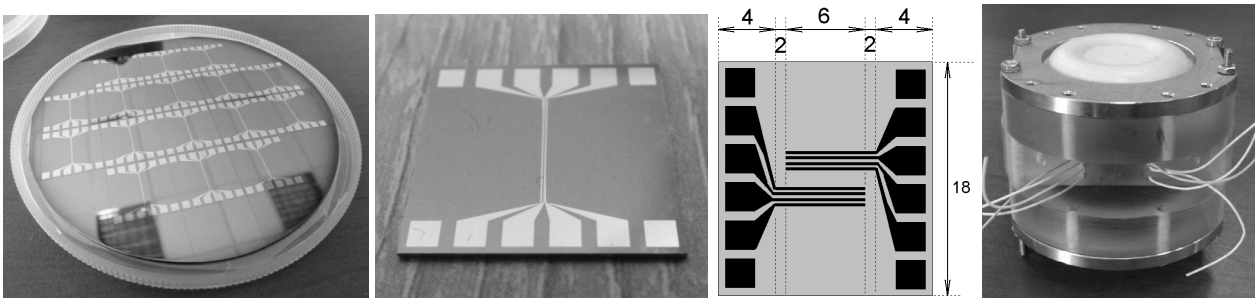

Figure 1. The planar ECT transducer. a) Structure on wafer, b) Single sample, c) Scheme. d) Sensor.

Seismic electrochemical sensors, based on idea of molecular-electronic transfer (MET) are successfully used in seismology and geophysical studies. The main concept of the molecular electronic transfer lies in diffusion charge transfer principal under the condition of forced convection generated by an outer acceleration. MET sensor cells used nowadays are manufactured from two pairs of plane-parallel mesh electrodes separated by porous dielectric spacers. The present technology has certain restriction of such sensor parameters as self-noise level, high frequency range and fabrication cost [1]. However, the appliance of new planar transducer may overcome all mentioned drawbacks [2].
The planar transducer cell is made of silicon substrate with four evaporated platinum electrodes (Fig.1, a-c). The precision seismometer based on ECT was assembled (Fig. 1, d) and main sensor characteristics were drawn (Fig. 2, a-d).

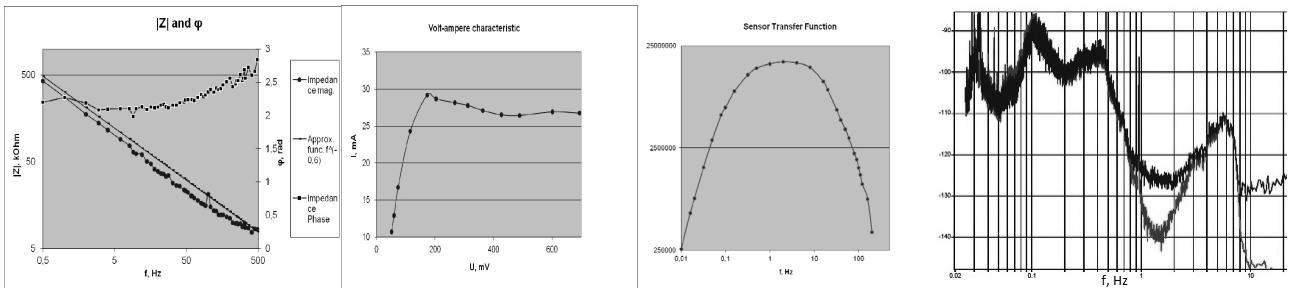

Figure 2. The planar ECT transducer characteristics. a) The impedance magnitude and phase. b) Volt-ampere characteristic. c) Sensor transfer function. d) Signal power spectral density of ECT transducer (blue) and reference low-noise seismometer CME 6011 (red).

The experimental data show that the seismometer based on planar electrochemical transducer provides a respectable self-nose and gain level in comparison with the traditional molecular-electronic sensor. Given experimental data analysis gives rise to predicate that new planar transducer application for precision seismometers allows to improve frequency and self-noise sensor characteristics in high frequency domain.

1. V.M. Agafonov, D.L. Zaitsev, A.S Shabalina, "Noise characteristics of miniature molecular electronic measurers of angular motion parameters", Izvestiya vuzov. Instrum. Technol., **52** (7), pp. 55-59, 2009 (in Russian).
2. V.G. Krishtop, V.M. Agafonov, and A.S. Bugaev. "Technological Principles of Motion Parameter Transducers Based on Mass and Charge Transport in Electrochemical Microsystems". Russian Journal of Electrochemistry, **48** (7), pp. 746-755, 2012.

Integral planar supercapacitor with CNT-based composite electrodes for heat-sensitive MEMS and NEMS

E.A. Lebedev[1], A.V. Alekseyev[1], I.M. Gavrilin[1], A.V. Sysa[1], E.P. Kitsyuk[2], R.M. Ryazanov[2], D.G. Gromov[1]

1. National Research University of Electronic Technology, Shokin sq., bld. 1, Zelenograd, Moscow, Russia.
2. Scientific Manufacturing Complex "Technological Centre", 5 pas. 4806, Zelenograd, Moscow, Russia.
E-mail: dr.beefheart@gmail.com

With the extensive development of autonomous MEMS, NEMS, systems-on-crystal and implantable electronics, the demand for new types of miniature electrical energy accumulation and storage devices has been aroused. Planar micro-sized devices compatible with the integral technology are the most promising candidates, because they can be placed on the same wafer with the powered device and be manufactured in the same technological cycle [1-3]. As high power density and long-term stability energy storage devices the exceptional position occupied by the supercapacitors with electrodes based on carbon nanotubes (CNT) having outstanding electrical and mechanical characteristics. However, the high thermal budget of the conventional CNT's synthesis processes creates a significant limitation for their use in conjunction with heat-sensitive components. This paper presents a method for the planar supercapacitor with a composite CNT-based electrodes formation at room temperature.

The proposed devices have a comb-like structure nested into each other, which are formed on the wafer surface using conventional microelectronic techniques: magnetron sputtering, photolithography and wet etching. The composite electrodes formation realized using electrophoresis of carbon nanotubes from alcohol suspension at room temperature. A preliminary synthesis of CNTs beyond the technological route avoids the high-temperature stage and allows to reduce the thermal budget of the process and to protect heat-sensitive components. The suspension was a result of ultrasonic dispersion of pre-synthesized by CVD method and functionalized CNTs, nickel nitrite (II) which acted as a charger, as well as sodium lauryl sulfate and hydroxypropyl cellulose (for suspension stabilization), in ethyl alcohol. Study of the effect of the electric field strength (from 5 to 100 V/cm) and distance between the electrodes (from 2 to 20 mm) of the deposition rate and sediment structure was conducted. The composition and morphology of deposited layers were monitored using SEM and EDX.

It was experimentally found that to obtain a dense sediment with good adhesion it's necessary to produce a cyclical deposition, wherein the short stages of deposition (up to 120 seconds) alternating with phase of drying; thickness of a deposited layer is determined by the number of deposition cycles (for example, at a field strength of 80 V/cm after one 60-seconds deposition cycle the thickness of sediment was about 1 micron). Also, the optimal mode for the local deposition of the composite material directly on the narrow line of current collectors was determined. For the capacitive characteristics study manufactured planar supercapacitors were covered by solid-state electrolyte based on polyvinyl alcohol and H_3PO_4, and charge-discharge characteristics and cyclic voltammetry scans with different scanning rates (from 10 to 100 mV/s) were carried out.

1. B. Xie, Y. Wang, W. Lai, W. Lin, Z. Lin, Z. Zhang. "Laser-processed graphene based micro-supercapacitors for ultrathin, rollable, compact and designable energy storage components". Nano energy, **26**, pp. 276-285, 2016.
2. C. Zhang, J. Xiao, L. Qian, S. Yuan, S. Wang, P. Lei. "Planar integration of flexible micro-supercapacitors with ultrafast charge and discharge based on interdigital nanoporous gold electrodes on a chip". Journal of Materials Chemistry A, **4**, pp. 9502-9510, 2016.
3. X. Long, Z. Zeng, E. Guo, X. Shi, H. Zhou, X. Wang. "Facile fabrication of all-solid-state flexible interdigitated MnO2 supercapacitor via in-situ catalytic solution route". Journal of power sources, **325**, pp. 264-272, 2016.

Monte Carlo simulation of electron transport in GaAs/AlAs quantum wire transistor structure under the effect of terahertz electric field

A.V. Borzdov[1], V.M. Borzdov[1], V.V. V'yurkov[2]
1. Belarusian State University, Minsk, Belarus, borzdov@bsu.by
2. Institute of physics and technology, Russian Academy of Sciences, Moscow, Russia, vvyurkov@gmail.com

Semiconductor structures with one-dimensional electron gas (or quantum wire structures) have been attracting much research attention for decades. A^3B^5 quantum wires have been considered as the basis of novel high electron mobility transistors [1, 2]. Quantum wire transistors could be promising candidates for ultra-high frequency operation modes. At that not only stationary, but also transient and periodic processes occurring in the structures with one-dimensional electron gas are of great interest [3, 4]. Also the possibility of an ultra high frequency generator based on the quantum wire structure has been proposed [5].
In current study electron transport in gate-all-around GaAs quantum wire transistor structure is simulated by means of ensemble Monte Carlo method. The structure consists of a thin rectangular 10×10 nm^2 GaAs channel surrounded by 5 nm thick AlAs barrier layer with aluminum gate. To calculate electron states in the quantum wire the Monte Carlo procedure is coupled with self-consistent numerical solution of corresponding two-dimensional Schrodinger and Poisson equations. Electron transport is simulated under the effect of longitudinal external electric field varying harmonically in time.
The transistor structure is supposed to be long enough. At that electron transport is defined by scattering processes in the structure. Electron scattering rates are calculated with account of collisional broadening. The calculation procedure includes electron scattering by confined modes of acoustic and polar optical phonons [6, 7], and GaAs/AlAs interface roughness scattering [8].
The response of electron drift velocity on the action of harmonic longitudinal electric field is calculated for several values of electric field strength amplitude and gate bias. The periodical electric field has a 1 THz frequency. The simulation temperature is 300 K. The nonlinear behaviour of electron drift velocity due to scattering processes is observed. It is proposed that the transistor structure could be used as multiple harmonic oscillations generator.

1. S.K. Islam, F.C. Jain. “Analysis of quantum wire high electron mobility transistor“. Solid-State Electron., **39**, pp. 615-620, 1996.
2. S. Sasaki, K. Tateno, G. Zhang, H. Suominen, Y. Harada, S. Saito, A. Fujiwara, T. Sogawa, and K. Muraki. “Encapsulated gate-all-around InAs nanowire field-effect transistors”. Appl. Phys. Lett., **103**, pp. 213502-1-213502-5, 2013.
3. D. Pozdnyakov, A. Borzdov, V. Borzdov, and F. Komarov. “Modelling of non-stationary electron transport in semiconductor nanowires and carbon nanotubes”. Proc. SPIE, **7025**, pp. 70251S-1-70251S-9, 2008.
4. D. Pozdnyakov, A. Borzdov, V. Borzdov, and V. Labunov. “Calculation of electrophysical parameters of thin undoped GaAs-in-Al_2O_3 quantum nanowires and single-wall armchair carbon nanotubes”. Proc SPIE, **7521**, pp. 75210S-1-75210S-9, 2010.
5. L. Fedichkin, V. V’yurkov. “Quantum ballistic channel as an ultrahigh frequency generator”. Appl. Phys. Lett., **64**, pp. 2535-2536, 1994.
6. A.V. Borzdov, D.V. Pozdnyakov, V.O. Galenchik, V.M. Borzdov, and F.F. Komarov. “Self-consistent calculations of phonon scattering rates in the GaAs transistor structure with one-dimensional electron gas”. phys. stat. sol. (b), **242**, pp. R134-R136, 2005.
7. A.V. Borzdov, D.V. Pozdnyakov. “Scattering of electrons in the GaAs/AlAs transistor structure”. Phys. Solid State, **49**, pp. 963-967, 2007.
8. D. Pozdnyakov. “Influence of surface roughness scattering on electron low-field mobility in thin undoped GaAs-in-Al_2O_3 nanowires with rectangular cross-section”. phys. stat. sol. (b), **247**, pp. 134-139, 2010.

TCAD model of tunnel field effect transistor, integrated in basic SOI CMOS technology

Y. Chaplygin, A. Krasukov, T. Krupkina, A. Mukhammedov, D. Rodionov
National Research University of Electronic Technology, Moscow, Russia, ieem@miee.ru

The problem of energy consumption is one of the limiting factors in the development and high-performance microprocessor-based systems, and mobile electronics devices. Possible applications of traditional CMOS elements to create low-power devices is limited due to the inability to reduce sufficiently the slope characteristics in the subthreshold region. In this regard, IC designers are considering the possibility of using tunnel field effect transistor (TFET) to reduce power consumption

The principle of TFET operation is based on the band-to-band tunneling effect. The device has several advantages: low leakage current, low slope in the subthreshold region, decreasing of short-channel effects. The main disadvantage is the low on-state current of the device. To overcome this limitation, a large number of transistor structures are investigated, including the structures with high-K dielectrics, mechanical stresses, as well as hetero- and non-planar structures [1-3]. The functional layers used in the composition of SOI CMOS technology also allow the creation of transistor structures working on the band-to-band tunneling effect. To study the characteristics of the possible TFET structures based on the SOI CMOS process flow, the process-device model was developed in Synopsys TCAD [4]. The model includes the use of conventional masks set, however, it is possible to eliminate some process steps, depending on the formed TFET structure.

As an example, the conventional layers formed in the SOI CMOS ICs process with design rules of 0.5 μm were used. Initial calibration of the model parameters carried out on the electrical characteristics of n- and p-channel MOS transistors produced by this technology.

The basic variant of the TFET was formed as a structure of MOS transistor with p+ - source and n+ - drain. To use the advantage of the tunneling probability increasing for the abrupt p-n junctions, the structure with the replacement of traditionally used LDD layers by the p+/n+ regions was also investigated.

To simulate the effect of phonon-assisted band-to-band tunneling in the case of heavily doped regions equations of Schenk model were included in the device modeling. The preliminary analysis showed that the internal electric field may exceed 3.0e+05 V/cm for a typical TFET structures in on-state, which leads to a decrease of the carrier lifetime and requires for the inclusion of strong field effect in the SRH recombination model. Simulation results are presented on Figure 1 including the dopant distribution in 2D TFET structure, the device region near p+ source and gate with maximum band-to-band tunneling and the contribution of various mechanisms to the on-state device current (band-to-band tunneling and impact ionization).

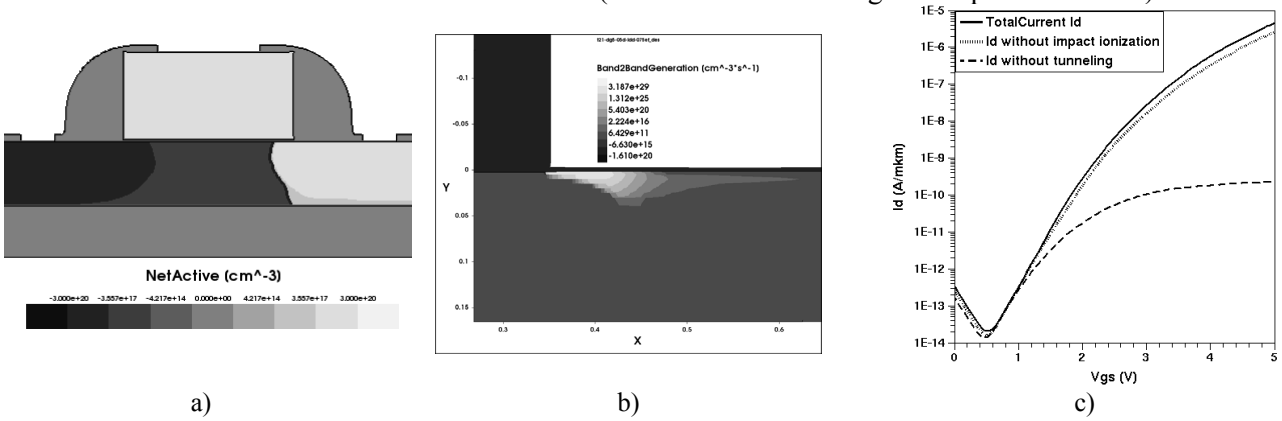

a) b) c)

Fig. 1. Simulation of TFET integrated in basic SOI CMOS technology: a – 2D TFET process model; b – region of band-to-band tunneling; c –simulated $I_d(V_{gs})$ characteristics (total, without impact ionization, without tunneling).

1. H. Ilatikhameneh, T.A. Ameen, G. Klimeck et al. “Dielectric Engineered Tunnel Field-Effect Transistor”. IEEE Electron Dev. Lett., **36**, pp. 1097-1100, 2015.
2. A. Rajoriya, M. Shrivastava, H. Gossner et al. “Sub 0.5 V Operation of Performance Driven Mobile Systems Based on Area Scaled Tunnel FET Devices”. IEEE Trans. El. Dev., **60**, pp. 2626-2633, 2013.
3. Z. Yang “Tunnel Field-Effect Transistor With an L-Shaped Gate”IEEE Electron Dev. Lett., **37**, pp. 839-842, 2016.
4. Synopsys TCAD. http://www.synopsys.com/tools/tcad

Compact Modeling of Radiation-Induced Drain Leakage Current

M.G. Drosdetsky, V.V. Orlov, G.I. Zebrev
National Research Nuclear University MEPHI, Moscow, Russia, e-mail: m.drosdetsky@gmail.com

Electrical level simulation of digital circuits is essentially based on compact models of MOSFETs. Characterization and modeling of ionizing radiation effects in MOSFETs, simplicity, and accuracy of the model make the compact modeling the challenging research area jointly in device physics, electronic engineering and applied mathematics [1].

One of the important problems for modern integrated circuits, exposed to ionizing irradiation, are increasing leakage drain currents, irradiation impacts mainly through the buildup of the oxide traps and rechargeable interface traps, which influence on the threshold voltage V_T, subthreshold slope *SS*, low-field mobility μ_0, etc. The objective of this report is to provide a compact MOSFET model, which allows us to simulate the dose dependencies of the drain leakage currents in a wide temperature range for a single transistor and integrated circuits. The validity of the proposed model has been verified by comparison with the I-V in a range of measurement temperatures before and after irradiation and annealing [2].

The subthreshold leakage current of MOSFETs is a parameter which is very sensitive to the fine temporal kinetics of buildup and annealing of the oxide-trapped charge. One of the annealing mechanisms in MOSFETs is the tunnel relaxation of non-equilibrium charged oxide traps located near the Si-SiO_2 interface [3]. The rate of this annealing mechanism is approximately independent of temperature and linear with logarithmic time. To improve the accuracy of the leakage current simulation we propose threshold the voltage shift model that includes the impact of simultaneous buildup and anneal of the positively charged defects in the oxide near or at the Si-SiO_2 interface. It was shown that the model is suitable for accurate simulation of the integrated circuit supply current dose dependencies at different temperatures and dose rates.

1. I. Esqueda, H. Barnaby, M. King. “Compact Modeling of Total Ionizing Dose and Aging Effects in MOS Technologies. IEEE Trans. on Nucl. Sci., **62**, No.4, pp. 1501-1515, 2015.
2. V.V. Orlov, V. Felitsyn, G.I. Zebrev. “Compact Modeling of I-V Characteristics in Irradiated MOSFETs: Impact of Operation Temperature and Interface Traps,” a report, accepted to 16th European Conference on Radiation and its Effects on Components and Systems (RADECS), Bremen, pp. 1-4, 2016.
3. G.I. Zebrev, M.G. Drosdetsky, “Temporal and Dose Kinetics of Tunnel Relaxation of Non-Equilibrium Near-Interfacial Charged Defects in Insulator,” a paper, accepted for publication to IEEE Trans. Nucl. Sci., 2016.

Total Ionizing Dose Effects Modeling in Common-Gate Tri-Gate FinFETs Using Verilog-A

M. Gorbunov[1,2], G. Zebrev[2,1]
1. Scientific Research Institute of System Analysis, Russian Academy of Sciences, Moscow, Russia, gorbunov@niisi.msk
2. National Research Nuclear Institute MEPhI, Moscow, Russia, gizebrev@mephi.ru

Continuous scaling after ~20 nm technology node leads to the necessity of developing new (non-planar) transistors using novel materials. In CMOS technology, two base concepts are present: multi-gate 3D structures (known as FinFETs) and quasi-planar Ultra Thin Body and BOX (UTBB). The former structures can have 2-4 independent gates or to be "gate all around" FET based on bulk Si or using Silicon-on-Insulator (SOI) substrate. The latter structure has the architecture similar to planar one, but provides the advantages of extremely thin and electrically controllable active region.

A number of radiation effects studies were provided for modern "decanano" structures [1-3]. The experimental results were analyzed by means of TCAD simulations using the detailed technology information about the features of such structures. Unfortunately, very often the integrated circuits (IC) designers do not have such details. Industry-oriented transistor model developers, e.g. the University of California, Berkeley, willfully designed universal models, whose parameters extraction process do not depends on (unknown) structure details. This is the reason why TCAD simulation results practically cannot be directly implemented to SPICE models that must take into account the radiation effects. One of the possible solution is implementing the physical radiation models to transistor (SPICE-level) models using Verilog-A hardware description language (HDL), e.g. as the authors showed in [4].

The UC Berkeley had developed two BSIM SPICE compact models by 2015: BSIM-CMG and BSIM-IMG for common and independent gates correspondingly. Unlike older models written in C, BSIM-CMG and BSIM-IMG had been developed in Verilog-A from the very beginning [5]. We consider only BSIM-CMG model in this paper as it describes the common gate connection often considered for radiation tests. It models the electrical characteristics of SOI or bulk based common multi-gate (CMG) structures: double, triple, quadruple and even cylindrical gate (e.g., nanowire FETs) [6]. It is important to note that both CMG and IMG models do not take into account the influence of substrate potential on the threshold voltage of main transistor [7].

As shown in [3], the total ionizing dose (TID) induced degradation depends on channel length and width, electrical bias and device geometry. BSIM-CMG provides gate, buried and field isolation oxide thickness as the standard SPICE parameters. Although it also has fin height parameter, it does not have parameters describing fin's imperfections (e.g., fin shape complexity). The mean sources of TID degradation in bulk and SOI FinFETs are the leakage current and charge trapping in BOX correspondingly [3]. The radiation-induced charge trapping strongly depends on the electric field magnitude and distribution. Verilog-A radiation effects model can use the simplified semi-empirical equations with experimental results calibration. The influence of substrate potential on main transistor's threshold voltage V_{THFG} can be calculated by means of coupling coefficient $K = \Delta V_{THFG}/\Delta V_{THBG}$.

1. B.L. Bhuva, N. Tam, L.W. Massengill, D. Ball, I. Chatterjee, M. McCurdy, and M.L. Alles, "Multi-Cell Soft Errors at Advanced Technology Nodes," IEEE Trans. Nucl. Sci., **62** (6), pp. 2585-2591, 2015.
2. N. Seifert, S. Jahinuzzaman, J. Velamala, R. Ascazubi, N. Patel, et al., "Soft Error Rate Improvements in 14-nm Technology Featuring Second-Generation 3D Tri-Gate Transistors," IEEE Trans. Nucl. Sci., **62** (6), pp. 2570-2577, 2015.
3. H. Hughes, P. McMarr, M. Alles, et al., "Total Ionizing Dose Radiation Effects on 14 nm FinFET and SOI UTBB Technologies," 2015 IEEE Radiation Effects Data Workshop (REDW).
4. M.S. Gorbunov, I.A. Danilov, G.I. Zebrev, P.N. Osipenko, "Verilog-A Modeling of Radiation-Induced Mismatch Enhancement," IEEE Trans. Nucl. Sci., **58** (3), pp. 785–792, 2011.
5. BSIM-CMG 110.0.0. Multi-Gate MOSFET Compact Model Technical Manual, 2015.
6. Y.S. Chauhan, D.D. Lu, S. Vanugopalan, et al. FinFET Modeling for IC Simulation and Design Using the BSIM-CMG Standard. Elsevier, 2015.
7. http://www-device.eecs.berkeley.edu/bsim/?page=BSIMCMG_FAQ

I-V Characteristics simulation of silicon carbide Ti/4H-SiC Schottky diode

P. Panchenko, S. Rybalka, A. Malakhanov, E. Krayushkina, A. Radkov
Bryansk State Technical University, Bryansk, Russia, E-mail: freonko@gmail.com

Silicon carbide of 4H-SiC type represents an excellent candidate for high-temperature power electronic device applications because of its high breakdown voltage, low series resistance, and stability under harsh chemical and high temperature conditions [1]. In particular, 4H-SiC Schottky diodes for power electronics in future must be produced by domestic company the «GROUP KREMNY L» (Bryansk). It is obviously that for development of component base on the base of SiC studying and optimisation of such important device as Schottky diode it is necessary. Therefore in this work simulation of current-voltage (*I-V*) characteristics in 4H-SiC Schottky diode with Ti Schottky contact with used of TCAD program has been carried out. The parameters for simulation were following: the concentration of donors (nitrogen) in the substrate equals 10^{18}, in the epitaxial layer equals 8×10^{15}, anode material is Ti (titanium), thickness of the epitaxial layer (4H-SiC) is 15 μm, radius of the structure is 200 μm. For simulation model of current-voltage characteristics has been solved electrostatic Poisson's equation in cylindrical coordinates together with continuity equations for electrons and holes. Forward (a) and reverse (b) current-voltage characteristics of Ti/4H-SiC Schottky diode are presented in Fig. 1. On the base of thermionic emission theory it is established that forward current-voltage characteristics (Fig. 1a) in terms of the proposed the simulation model of Schottky diode corresponds to the almost "ideal" diode with effective Schottky barrier height $\varphi_B = 1.17$ eV with average ideality factor of Schottky diode $n = 1.09$. Above-mentioned parameters are very good agreements with experimental data for such type of silicon carbide Schottky diode [1, 2]. From reverse current voltage simulation follows that the breakdown voltage for Ti/4H-SiC Schottky diode equals ~2 kV (see Fig. 1b).

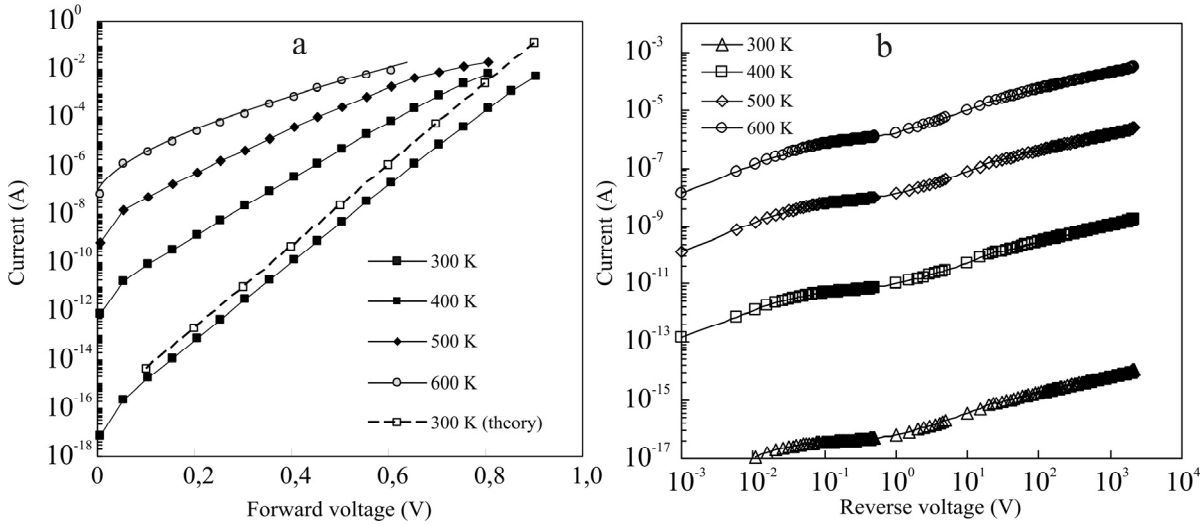

Fig. 1. Ti/4H-SiC Schottky diode forward (a) and reverse (b) *I-V* characteristics.

Theoretical value of breakdown voltage calculated for Ti/4H-SiC Schottky diode is 1.875 kV that is in close agreement with simulation reverse current-voltage data (~2 kV). Finally, forward and reverse current-voltage characteristics of 4H-SiC Schottky diode with Ti Schottky contact have been obtained on the base of simulation model in TCAD in framework of the physical analytical models based on Poisson's equation, drift–diffusion and continuity equations. In addition, on the base of thermionic emission theory have been calculated important parameters (ideality coefficient, effective Schottky barrier height, breakdown voltage) for Ti/4H-SiC Schottky diode. Authors would like to thank Dr. Surin B.P. for help in carrying out of TCAD simulation. This work was supported by the Russian Ministry of Education (Grant No. 02.G25.31.0201).

1. T. Kimoto, J.A. Cooper. *Fundamentals of Silicon Carbide Technology. Growth, Characteriztion, Devices, and Applications*. Wiley-IEEE Press, New York, 2014.
2. D. Perrone, M. Naretto, S. Ferrero, L. Scaltrito, C.F. Pirri. "4H-SiC Schottky Barrier Diodes Using Mo-, Ti- and Ni-Based Contacts". Materials Science Forum, **615-617**, pp. 647-650, 2009.

Layout-aware simulation of soft errors in sub-100 nm integrated circuits

A. Balbekov[1], M. Gorbunov[2], S. Bobkov[3]

1. SRISA, Moscow, Russia, balbekov@cs.niisi.ras.ru. 2. SRISA, MEPhI, Moscow, Russia, gorbunov@cs.niisi.ras.ru. 3. SRISA, MEPhI, Moscow, Russia, bobkov@cs.niisi.ras.ru.

In space environment electronic hardware is subjected to ionizing radiation of different origin. At a modern point of a technical progress the ability to resist the radiation defines active shelf time of a spacecraft. Ionizing radiation is a flow of charged particles: electrons, protons, heavy ions, which are the source of Single Event Effects (SEE) in the integrated circuits. Traveling through a volume of an integrated circuit charged particle interacts with matter, losing energy and generating charge. When generated charge is collected by electric circuit it transforms into parasitic current and voltage pulses – Single Event Transients (SET). With the coincidence of distinct conditions, circuit can treat SET as a valid signal and be subjected to a Soft Error (SE). If the charge has been collected by more than one electric node, it produces multiple SET, this lead to Multiple Errors (ME). Volume of the generated chard stays the same, while devices dimensions and density scales down. There are reports about 10 upsets in 65nm memory unit [1], further scaling of the technology dimensions make it worse.

There are different approaches to model ME. The most precise one is to use T-CAD software, but it is not compatible with large circuits, composed of hundreds of devices. Less accurate, but more scalable approach is to use Monte-Carlo algorithms for particle interaction with matter, combined with simplified device structure. This approach was realized in MUSCA SEP [2] and MRED [3] software. This software need appropriate competence from designer and additional data from T-CAD or physical measurements of device. The third approach is to use SPICE simulators with simplified models. This is a fast and accessible approach, but not accurate, appropriate only for the estimations. This work presents a development of the third approach.

The developed technique involves several steps: to connect the Verilog-A SET model to the affected device, to simulate circuit, to detect upset, to save data, to repeat until sufficient data is collected, and to present the data in an illustrative form. To consider ME it is essential to take in account circuit physical layout. For aromatization reasons a layout-aware tool was developed. Tool takes layout as GDSII file, extracts circuit from it, compares it with source SPICE circuit. The result is a mapping list of the devices from layout and source; this is a general Layout-vs-Schematic (LVS) process. SEE impact area is an area that placed on the layout; additional model parameters for each impact area are passed to the tool. Tool defines which devices were affected and produces file with SPICE definition of the Verilog-A model with passed parameters. This file connects to the SPICE simulation configuration file and, then SPICE simulation can be performed. The main model parameters are deposited charge and activation delay. If circuit detects upset, than charge, position and time are saved; this detected charge is now a critical charge. After many repetitions with changes of charge and position tool gathers 2D spatial critical charge distribution; that then is transformed to the sensitivity map. Sensitivity map reflects the layout areas with different critical charges. Knowing critical charge tool can provide information about fault tolerance of the circuit with respect of the layout and accounting ME.

Developed technique and tool providing it are designed for sub-100 nm circuits, they provides possibility to simulate multiple SET; that are the main source of upsets in the space environment. Provided technique is technology independent and compatible with widespread circuit designer tools. Technique provides only estimation possibilities, but it can be used by circuit developers without incorporating T-CAD or physical measurements.

1. Gorbunov M.S., et al. "Design of 65 nm CMOS SRAM for space applications: A comparative study". IEEE Transactions on Nuclear Science **61** (4), pp. 1575-1582, 2014.

2. Artola L. and Hubert G. "Modeling of elevated temperatures impact on single event transient in advanced CMOS logics beyond the 65-nm technological node". IEEE Transactions on Nuclear Science **61** (4), pp. 1611-1617, 2014.

3. Warren K.M., et al. "Monte-Carlo based on-orbit single event upset rate prediction for a radiation hardened by design latch". IEEE Transactions on Nuclear Science 54 (6), pp. 2419-2425, 2007.

Spatial distribution of gate tunnel current in flash-memory cells: Monte Carlo simulation

O.G. Zhevnyak
Belarus State University, Minsk, Belarus, Zhevnyakol@tut.by

In present paper the spatial distributions of gate tunnel current in flash-memory cells are calculated. The effects of drain and gate voltages on these distributions are studied. Main problem is connected with the non-uniformity and complexity gate tunnel current distributions along the transistor's channel [1]. Our investigation is performed by using of simulation of electron transport at gate oxide in short-channel MOSFETs which are the basic elements of flash-memory cells. Used simulation transport models, algorithms and procedures are described in our book with co-authors [2]. The model of electron tunneling through tunnel oxide is based on direct solution of Schrödinger equation.

For example on figure obtained simulation dependencies of spatial distribution of relation of gate tunnel current to drift one in studied flash-memory cells at various drain voltages are presented. Considered MOSFETs have the following parameters: gate oxide thickness is equal 5.6 nm, transistor's channel length is equal to 0.5 μm, acceptor substrate concentration is equal 10^{24} м$^{-3}$.

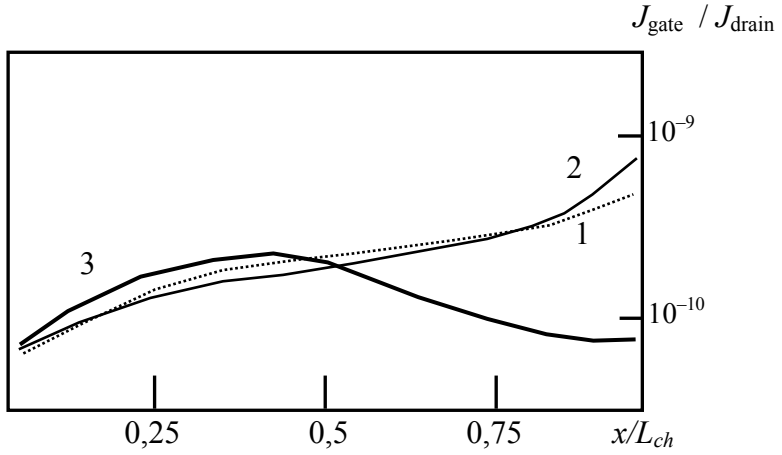

Figure. Relation of gate tunnel current to drift one in MOSFET's channel along its length at various drain voltages: 1 – V_{drain} = 1 V; 2 – V_{drain} = 2 V; 3 – V_{drain} = 3 V; V_{gate} = 2 V, d_{tun} = 2 nm.

Obtained results show that definite relations between gate and drain voltages effect specifically on behavior of dependencies of relation of gate tunnel current to drift one. At $V_{drain} > V_{gate}$ the peak of these dependencies is dislocated from drain point into channel. The spatial dependencies of numerical values of gate current in flash-memory cells are also non-uniform. It may be explained by peculiarities of electron scattering in channel at tunnel oxide.

1. G.Ya. Krasnikov, N.A. Zaitsev, I.V. Matyushkin. "Tunneling in MOS systems: The dependence of the effective barrier height on the structure of the transition layer at the Si/SiO_2 interface in the presence of impurities". Russian Microelectronics, **30**, pp. 317-323, 2001.
2. V. Borzdov, O. Zhevnyak, F. Komarov, V. Galenchick, *Monte Carlo simulation of device structures of integral electronics*, BSU, Minsk. 2007 (in Russian).

Synthesis of the quasi-static current-voltage characteristics of the multi-barrier heterostructures for generation of terahertz electromagnetic radiation

V.A. Gergel, A.V. Verhovtseva, N.M. Gorshkova, V.S. Minkin, V.V. Pavlovskij
Kotelnikov Institute of Radio Engineering and Electronics of RAS, Moscow, Russia,
E-mail address: vgergel@mail.ru.

Quasi-hydrodynamic model of electron drift in multi-barrier heterostructures [1] is generalized to the situation with a nonuniform distribution of the height of the individual energy barriers. Calculate the spatial distribution of the electron temperature and the electrical potential as the electron beam density function for this type of generalized heterostructures. It turned out that at the same altitude region of negative differential resistance occurs when unacceptable for such structures voltages. Potential distribution they obtained highly heterogeneous. This leads to a lack of differential resistance region within reasonable limits the supply voltage of 5-10 V. It turns out that the situation can be partially corrected by using contact sublayer bordering the half-height barrier. At the same time, using the methodology of the band Engineering, consistently calculated potential distribution at each of the barriers, starting with the first of them bordering on highly doped contact sublayer narrow bandgap material. The calculations make it possible to design appropriate test multi-barrier structure so that each of the barriers falling voltage does not exceed the value of the order of one volt. To obtain the negative differential resistance it is necessary to distribute uniformly the potential, which can vary corresponding to height of first three barriers. Since excess of this value over one critical barrier affects the possibility of a region of negative differential resistance necessary for the excitation of electromagnetic oscillations in subteraherz frequencies corresponding resonance microelectronic devices. The latter determines the practical significance of the unit.

This work was partially supported by Russian Foundation for Basic Research (research projects No. 15-07-05912a and No. 15-07-06032a).

1. V.A. Gergel, A.V. Verhovtseva, N.M. Gorshkova, V.S. Minkin, M.N. Yakupov. “The mechanism of electrical instability in multibarrier heterostructures. Features of high frequency impedance”. Journal of Communications Technology and Electronics, **57**, pp. 481-484, 2012.

Terahertz pulse generator on the basis of a heterostructure $Al_xGa_{1-x}As/GaAs$

S.A. Nikitov[1], P.P. Maltsev[2], V.A. Gergel[1], A.V. Verhovtseva[1], N.M. Gorshkova[1], V.V. Pavlovskij[1], V.S. Minkin[1], R.A. Khabibullin[2]

1. Kotelnikov Institute of Radio Engineering and Electronics of RAS, Moscow, Russia, E-mail address: vgergel@mail.ru.

2. Institute of UHF semiconductor electronics of RAS, Moscow, Russia

Designed and manufactured semiconductor device that generates microsecond pulses of electromagnetic radiation in the terahertz frequency range. Its main element has a seven or nine barriers of heterostructure $Al_xGa_{1-x}As/GaAs$, grown by molecular beam epitaxy on a plate highly conductive GaAs. It contains a relatively thick (1 μm) highly alloyed layer of GaAs ($N = 1\times10^{17}$ cm^{-3}), acting as the rear electrical contact. Then, on the contact layer were deposited successively alternating layers of non-alloyed and high-$Al_xGa_{1-x}As/GaAs$ ($N_d = 1\times10^{18}$ cm^{-3}) GaAs of the same thickness (40 nm). The Al content in the main central barrier layers (x = 0.25), while the two outermost (upper and lower) 2 times smaller value (x = 0.125). The thickness of the final top layer of doped GaAs has been selected equal 0.3 μm for safe subsequent metal deposition. After epitaxy on a plate by liquid etching formed rectangular elements of meso-wide 20 μm, the length of which is chosen approximately equal to a quarter wavelength of the expected radiation. Depth corresponding etching reaches the lower contact layer of GaAs. Further, in the center of meso-pillar formed resistive pad 10 μm in diameter and, at the same time the same ohmic circular area 10 mm in width, standing away from the edge of the mesa-pillar on 5 μm. Thereafter, the structure was deposited on the first metallization layer, which is then covered with an insulating layer SiO_2 of 0.5 μm thick. After opening the corresponding window in the dielectric it all covered with a top layer of metallization, in which the respective photolithography formed a resonant antenna structure, which topology consisted of two halfwavelength strip lines of the same width, are connected with each other and with the active mesa-pillar narrower quarterloops width 20 μm. Note that these elements are resonant at the same time and bypass the high frequency power supply high output impedance “exposing” the desired operating point on the negative resistance section S-shaped characteristics of the active mesa-heterostructure. The observed S-shaped current-voltage characteristics of samples are due to thermoinjective instability when Joule heating of the electrons stimulates thermoinjection through energy barriers. In consideration electron drift in heterostructures occurs in the non-local energy balance mode, when the electrons are heated in the undoped barrier layers in which the high electric field is concentrated and cooled to heavily doped GaAs layers, in which the electric field is relatively small. At the same time a certain portion of the electron heat flux reaches the next barrier and stimulates thermoinjection of electrons through the barrier into the next GaAs potential well. It is for this compensation effect electric field in the barriers is reduced in a certain increase of the current range. Despite the marked non-locality, the average Joule energy is transformed into a crystal cell, resulting in a corresponding heating of the entire sample. The electrical device is powered by microsecond current pulses with a repetition frequency of about 1 kHz.

The research is executed under financial support of Ministry of education and science of Russia, Agreement No. 14.607.21.0141 from 27 October 2015.

Stark-shift based quantum dot-cavity electrometer

A.V. Tsukanov[1,2], V.G. Chekmachev[1,2]

1. Institute of Physics and Technology, Russian Academy of Science, Moscow, Russia
2. Moscow Institute of Physics and Technology, Dolgoprudny, Russia, vgchekmachev@mail.ru

In this paper we propose the scheme (fig. 1a) of an optical quantum sensor of external electric field which design based on a double quantum dot (DQD) placed in a high quality optical semiconductor microcavity (MC). The characteristic DQD frequencies of the observed nontrivial single-electron dynamics are determined using spectroscopic simulation in the steady-state regime (fig. 1b). Due to Stark shifts of excited energy levels of DQD located at the edge of microdisk the hybrid electron-photon spectrum changes depending on the strength and direction of electric field. Probe laser with tunable wavelength excites the structure in single-photon regime and photon spectrum from MC is detected. We analyze the system's behavior with the use of a standard technique based on solving the Lindblad equation for the density matrix of an electron-phonon system with regard to the escape of photons from the cavity to the continuum and the relaxation of an excited electron with the emission of a photon or phonon. It will be shown that due to the design features, such a device has several advantages: high sensitivity, availability of different channels for excitation and measuring, the ability to accurately detect the spatial distribution of the field.

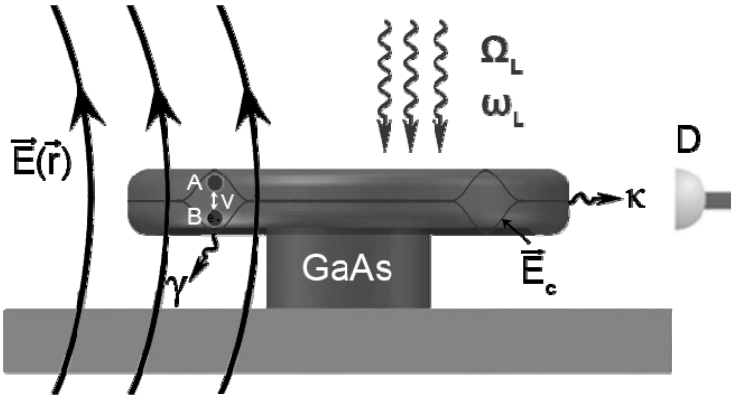

Figure 1a. Scheme of the sensor based on DQD and MC.

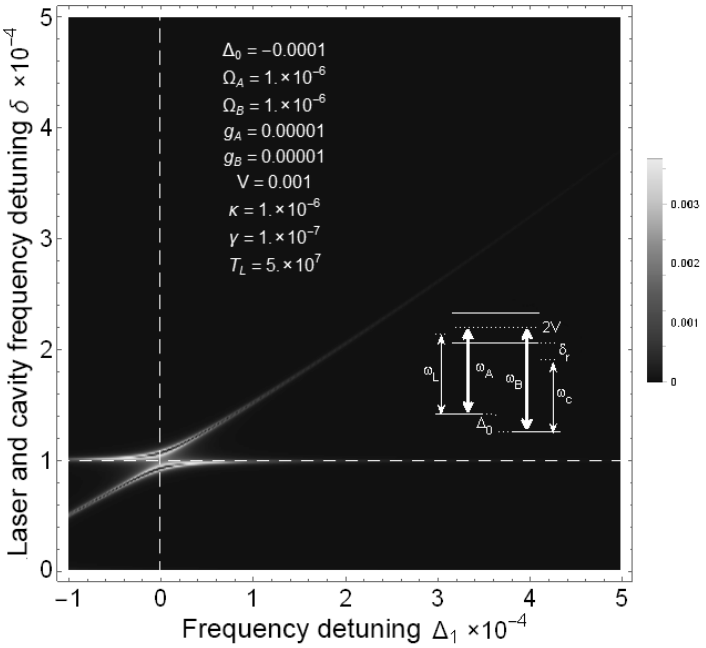

Figure 1b. Typical spectroscopic response of the hybrid system.

Single-photon transmission and spectroscopy of diamond microring isomers

A.V. Tsukanov[1,2], I.Yu. Kateev[1,2], M.S. Rogachev[1,2]
1. Institute of Physics and Technology, Russian Academy of Science, Moscow, Russia
2. Moscow Institute of Physics and Technology, Dolgoprudny, Russia, ikateyev@mail.ru

Recently solid-state optical structures, such as microresonators, waveguides, photonic isomers etc, attract great interest because the can be used as elements of an optical quantum network. Interaction between sites of the network, for example, is supplied by photonic isomers. Here we study theoretically spectroscopy of a diamond three-microring isomer and optimize its design to provide good transport and dissipative properties.
In a framework of tight-binding model spectrum and electromagnetic field distribution of the isomer were calculated with account of photon energy dissipation. We employ a weak laser as a probe for the isomer spectrum. The probability of one-photon excitation due to laser photon injection is calculated in the steady-state regime. The spectroscopic response is represented by three clearly distinguishable peaks corresponding to isomer whispering-gallery eigen-modes and the electromagnetic field of each mode has antinodes near ring edge. Fine tuning of the microring spectrum can be provided by additional layers deposition on an isomer surface. We obtain dependence of the eigen-mode wavelength on thickness and refractive index of additional layers.
NV-center placed at the electromagnetic antinode in one of the microrings interacts with the isomer mode. This leads to anticrossing in spectroscopic response of isomer (fig. 1). This effect can be used in designing of magnetic or electric field sensor.

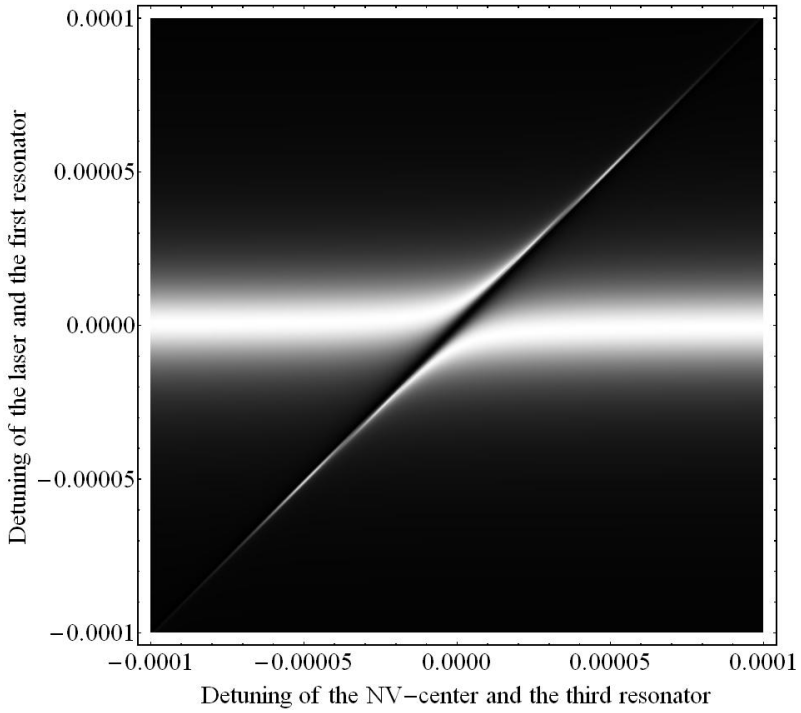

Figure 1. A dependence of isomer exiting probability on laser and NV-center zero-phonon transition frequencies (spectroscopic response).

Hamiltonian matrix elements for Josephson silent qubits

A.V. Kuznetsov[1], N.V. Klenov[1-4], S.V. Bakurskiy[3]

1. Lomonosov Moscow State University, Physics Faculty, Moscow, 119991, Russia, nvklenov@gmail.com;
2. Moscow Technical University of Communications and Informatics (MTUCI), Moscow, 111024, Russia;
3. Lukin Scientific Research Institute of Physical Problems, Zelenograd, Moscow, 124460, Russia;
4. Lomonosov Moscow State University Skobeltsyn Institute of Nuclear Physics, Moscow, 119991, Russia

The goal of the work is to describe the method to determine an orthonormalized basis of Josephson flux quantum bit (qubit) states under two-level approximation for systems with double-well potential. This basis was used to calculate qubit`s Hamiltonian matrix, thus allowing to verify all calculation procedures correctness by comparison of our results with other works.

The calculations were carried out both for well-known three-junction and four-junction flux qubits and for perspective silent qubits (see insets of the Figures for the principle scheme and potential energy of the mentioned device). The obtained dependences are presented in Figures 1 and 2 for silent qubit eigen-energies versus:

(Fig. 1) the significance of the second harmonic in current-phase relation of the junctions;

(Fig. 2) normalized external flux.

Here $E_A=E_{A1}+E_{A2}$, $E_B=E_{B1}+E_{B2}$, and E_{A1}, E_{A2}, E_{B1}, E_{B2} are Josephson energies that correspond to the first and the second harmonic amplitudes in the mentioned current-phase relations.

Out results for Hamiltonian matrix allow to explore qubit dynamics during logic operations, including the case of the so-called remagnetization (NOT-gate), on the picosecond timescale.

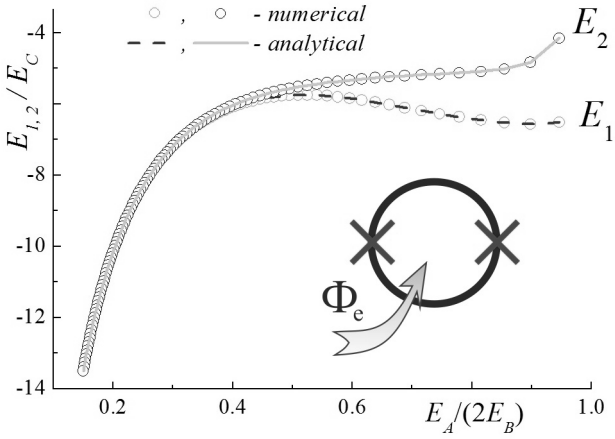

Fig. 1

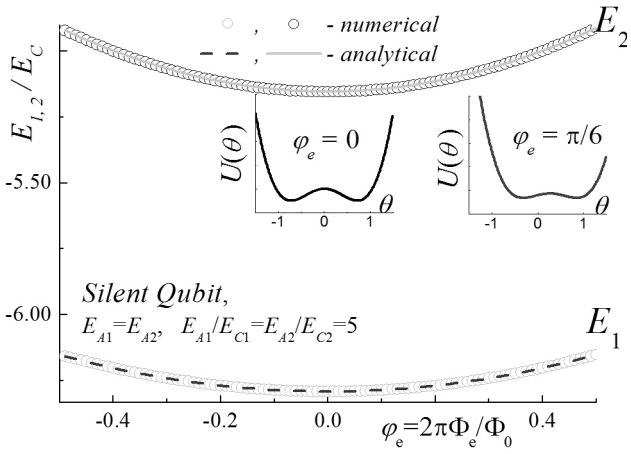

Fig. 2

The work was supported by the Ministry of Education and Science, grant number MK-5813.2016.2 and RFBR grants 16-29-09515-ofi_m and No. 15-32-20362-mol_a_ved.

Selective measurement of qubit states by using of Josephson bifurcation oscillator

M.V. Denisenko*, A.M. Satanin
Lobachevsky State University of Nizhni Novgorod (National research university)
**mar.denisenko@gmail.com*

Recently different methods of non-demolition measurement of superconducting qubits, which realize as projective [1, 2] as well as continuous single-shot measurement [3], have been developed. The idea of using bifurcation oscillator for measurements was proposed in the work [4]. This idea received further elaboration in latest publications [1, 2], where the protocol of nondestructive measurement of qubit states was developed. It is important to note, that the basic assumption of the mentioned publications is that the measuring device (bifurcation oscillator) is working in a purely classical regime. Meanwhile, during the states initialization the qubit and the oscillator interact, leading to "entanglement" of their systems, therefore, it is important to understand how the quantum system (the qubit) is sensitive to the back-action effect in different modes of operation of the measuring device (oscillator).

In the present work, we study the detector (or "pointer") – nonlinear oscillator – which is working in mesoscopic regime, when the average number of quanta on the oscillator during of the measuring process varies from a few dozen to a few hundred. To do this, we based on the methodology described in works [1, 2], which we generalized to the scenario of the interim monitoring of states both in single realization (similar to single-shot measurements [3]), and in the average in the ensemble (similar to projective measurements [3]).

We report here the results of studying the influence of duration of recording information impulse on the qubit and parameters of the oscillator control signal in system interaction with a bosonic bath on the basis of the quantum trajectories method [5].

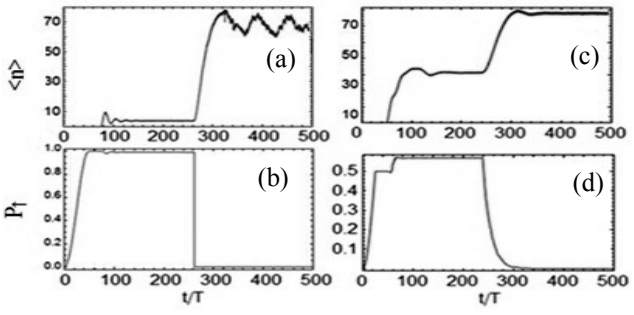

Fig. 1. One realization of the interim monitoring of average energy of a nonlinear oscillator <n> (a) and the probability of finding the qubit in the upper level $P_\uparrow$ (b) for a π-pulse pumping of a qubit. Average over 10000 realizations of the dynamics of the superposition π/2 Rabi pulse pumping of a qubit $P_\uparrow$ (d) and the average number of photons in the oscillator (c).

We develop the protocol for the detection of the quantum system states (the probability of population levels) for the "recording" of indications of the number of photons (proportional to average energy <n>) weakly nonlinear oscillator in mesoscopic mode of operation.

It is shown that for a given recording pulse duration we can determine the relative magnitude of the measuring device influence on the state of a quantum system, that is, the back-action effect. For recording impulse π-type (see Fig. (a, b)), it is possible to conduct single-shot measurement, where individual quantum jumps can be seen in Fig. (b). For the average system dynamics on the base of statistical data we studied the evolution of the density distribution of the average energy of the oscillator (see Fig. (c, d) as the example of the π/2 recording impulse), which shows the percentage of qubit status in a particular basis state.

Thus, the conducted in the present work simulation demonstrates the possibility of selective measurement or separation superposition states of qubit by using the bifurcation oscillator, which is operated similarly to Stern-Gerlach beam splitting experiment.

1. I. Siddiqi *et al*., Dispersive measurements of superconducting qubit coherence with a fast latching readout, Phys. Rev. B. **73**, 054510 (2006).
2. T. Picot *et al*., Role of relaxation in the quantum measurement of a superconducting qubit using a nonlinear oscillator, Phys. Rev. B. **78**, 132508 (2008).
3. D.H. Vijay *et al*., Observation of quantum jumps in a superconducting artificial atom**,** Phys. Rev. Lett. **106**, 110502 (2011).
4. I. Siddiqi *et al*., RF-Driven Josephson bifurcation amplifier for quantum measurement, Phys. Rev. Lett. **93**, 207002 (2004).
5. K. Molmer *et al*., Wave-function approach to dissipative processes in quantum optics, Phys. Rev. Lett. **68**, 580 (1992).

Quantum approach to the simulation of logistics model and nonlinear oscillations

Yu.I. Bogdanov[1,2,3], N.A. Bogdanova[1,2], D.Yu. Kulko[1,3], V.F. Lukichev[1]
1. Institute of Physics and Technology, Russian Academy of Sciences
2. National Research University of Electronic Technology MIET
3. National Research Nuclear University 'MEPHI'

The idea of quantum computers and quantum simulators was proposed by Feynman in 1982 to deal with exponential complexity of simulation of quantum systems by a classical computer. At the core of these devices is new quantum hardware that allows one to simulate desired quantum systems by other quantum systems. To date, the technology does not allow us yet to create a universal quantum computer and to perform operations with required accuracy. A more realistic solution is to create quantum simulators for solving various problems of modeling quantum and classical dynamical systems. On the basis of generalization of Prigogine works on statistical mechanics and the theory of Koopman - von Neumann we have developed a new approach to description of any classical dynamical system by the notions of quantum theory. The proposed theory is applicable to any systems, including non-Hamiltonian and dissipative dynamical systems. We consider the procedure for transition from classical dynamical systems to quantum systems and use the logistics model and the van der Pol oscillator as examples. In terms of the formalism of quantum field theory and quantum optics, the systems under consideration reduce to the evolution of a quantized electromagnetic field in a nonlinear medium. Thus it is possible to study classical dynamical systems with the use of highly specialized quantum simulators.
This work was supported by the Program of the Russian Academy of Sciences in fundamental research.

Analysis of triphoton polarization state tomography accuracy

Yu.I. Bogdanov[1,2,3], G.V. Avosopyants[1,3], K.G. Katamadze[1,4], L.V. Belinsky[1,3], Yu.A. Kuznetsov[3]
1. Institute of Physics and Technology, Russian Academy of Sciences, 117218, Moscow, Russia.
2. National Research Nuclear University "MEPHI", 115409, Moscow, Russia.
3. National Research University of Electronic Technology MIET, 124498, Moscow, Russia.
4. M. V. Lomonosov Moscow State University, 119991, Moscow, Russia.

Reliable generation and measurement of triphoton states has yet to be achieved in laboratory. We give an overview of the problems in generating and measuring triphoton quantum states and analyze several protocols of quantum measurements, which allow for high precision of reconstruction when sizes of available statistical data samples are limited. The tomography procedure under investigation is based on root approach to state estimation. In particular, we use the generalized Fisher information matrix to assess the accuracy of the quantum state parameters measurement. We use tomographic protocols, based on the symmetry of the Platonic solids. We demonstrate the capability to reconstruct triphoton quantum states with precision close to the maximum achievable value allowed by quantum mechanics.
The work was supported by the Russian Science Foundation, grant no 14-12-01338.

Quadrature state tomography adjustment by means of coherent states reconstruction

Yu.I. Bogdanov[1,2,3], K.G. Katamadze[1,4] , G.V. Avosopyants[1,3], S.P. Kulik[4]
1. Institute of Physics and Technology, Russian Academy of Sciences, 117218, Moscow, Russia.
2. National Research Nuclear University "MEPHI", 115409, Moscow, Russia.
3. National Research University of Electronic Technology MIET, 124498, Moscow, Russia.
4. M. V. Lomonosov Moscow State University, 119991, Moscow, Russia.

Quantum state tomography is one of key problems of quantum optical technology and quantum information. This problem is especially difficult in the continuous variable case, for example for quadrature state reconstruction. In this case, fine adjustment of experimental setup is of utmost importance. Typically this problem is reduced to the approximation problem: we need to fit experimental data with some function, which corresponds to the quantum state. The model of the quantum state plays here a significant role and the general model is a fully mixed state in the Fock basis. For most experimentally available quantum states it contains a huge number of parameters to be reconstructed. It makes fitting procedure very slow and low-precise. Here we introduce a model of a partially mixed state in the basis of squeezed displaced Fock states, which allows to significantly decrease the number of estimated parameters and increase the precision of tomography. This model was experimentally tested for the tomography of coherent states. We show that this model allows us to rich the fidelity up to 99.98% while being in good agreement with experimental data.
This work was supported by Russian Foundation for Basic Research (project 14-02-00749 A) and by the Grant of President of Russian Federation № MK-5860.2016.2.

Fast polarization QKD scheme based on $LiNbO_3$ phase modulators

A. Duplinskiy[1,2], V. Ustimchik[1,2], A. Kanapin[1,3], and Y. Kurochkin[1]
1. Russian Quantum Center (RQC), Business Center «Ural», 100, Novaya st., Skolkovo, Moscow reg., 143025, Russia
E-mail: a.duplinsky@rqc.ru
2. Moscow Institute of Physics and Technology, 9 Institutskiy per., Dolgoprudny, Moscow Region, 141700, Russian Federation
3. Lomonosov Moscow State University, GSP-1, Leninskie Gory, Moscow, 119991, Russian Federation

Quantum key distribution (QKD) is an actively developing technology, with many different protocols and methods of encoding information. BB84 is the first and still the most widely used and robust QKD protocol which security has been fully proven [1]. Nowadays optical schemes implementing BB84 using polarization encoding have some drawbacks – to reach high frequencies, different laser sources are used for different states of polarization, which leads to a problem of proving the indistinguishability of pulses. Another downside is the passive choice of basis on the Bob's device. It means that we need four single-photon detectors for BB84 protocol implementation.

Usage of low voltage electro-optical phase modulators based on $LiNbO_3$ Pockels cell to implement fast polarization tracking source has been proposed [2], which allows one to use single laser source for polarization encoding implementation, solving the problem of indistinguishability. However authors observed that source output signals significantly disturbed by polarization mode dispersion in lithium niobate.

We present a polarization encoding QKD system where both Alice and Bob use phase electro-optical $LiNbO_3$ modulators for polarization tracking. Alice creates one of four polarization states – two diagonal and two circular. Bob uses his modulator to active choose of basis in which he measures the state – diagonal or circular. This allows Bob to use only two detectors except of four for BB84 protocol with Bob's passive choice. Also a proper calibration of polarization controller between Alice and Bob allows two phase modulators to compensate each others polarization mode dispersion.

The presented system allows high frequency (up to GHz) polarization encoding using only two single photon detectors and a single laser source.

This work is supported by the Federal Program «Research and development in priority areas of Russian scientific and technological complex for 2014-2020» (Agreement 14.582.21.0009).

1. P. Shor and J. Preskill. "Simple Proof of Security of the BB84 Quantum Key Distribution Protocol". Phys. Rev. Lett., **85**, pp. 441-444, 2000.
2. M. Jofre, A. Gardelein, G. Anzolin, G. Molina-Terriza, J.P. Torres, M.W. Mitchell, and V. Pruneri. "100 MHz amplitude and polarization modulated optical source for free-space quantum key distribution at 850 nm". J. Lightw. Technol., **28**, pp. 2572–2578, 2010.

1D models in analysis of solid state NMR absorption lines

M.M. Kucherov[1], O.V. Falaleev[2]
1. Siberian Federal University, Institute of Space and Information Technology, Krasnoyarsk, Russia, Mkucherov@sfu-kras.ru.
2. Siberian Division of the Russian Academy of Sciences, Krasnoyarsk Research Center, Krasnoyarsk, Russia, Falaleev_ov@mail.ru

Modern applications of nuclear magnetic resonance and electron spin resonance, and especially quantum computing problems call for more effective formalism to describe relaxation and evolution of various orders of coherence in the presence of various control effects.

Our work is devoted to the possibilities of one-dimensional models in the statistical theory of shape of the NMR absorption line. In the absence of isolated groups of magnetic nuclei the problem of calculating the shape of the NMR absorption line is still one of the most difficult problems of solid state radiospectroscopy. The difficulties of the theory are compounded by the clear lack of experimental data: for strict verification of theoretical conclusions, essentially NMR absorption spectra are used that represent single lines with flat tops, manifested to a greater or lesser extent. The absence of fine structure of the spectra makes them insufficiently critical in comparing theory and experiment. The same circumstance has given rise to the widely held view that fine structure of shapes of the NMR absorption lines occurs only in the presence of isolated groups of magnetic nuclei in crystals. Therefore, considerable interest relates with the experimental data obtained on the crystals, in which the magnetic nuclei form a one-dimensional lattice.

It is motivated by the fact that in isolated quantum system in $d = 1$ spatial dimension, breakdown of equilibration is captured by the phenomenon known as many-body localization (MBL). Recent experimental advances make it possible to produce isolated, strongly interacting ensembles of disordered particles. In the MBL case, injections of energy propagate at most a finite distance even after a long time. This length is about a few lattice parameters for the limiting case. It allows us to solve the problem by considering a group of spins in the open translational-invariant lattice.

On this basis, we have developed an approach following the method of direct-product formalism which was formalized by A.A. Nevzorov and J.H. Freed [1]. In the high-temperature approximation, as a testing the detailed comparison of the known theoretical and experimental data on the shape of the absorption lines for the equidistant linear chain of spins has been carried. The region of existence of so-called cross-singular dips [2] in the absorption spectra of polycrystalline two-spin systems is found unexpectedly extensive in one-dimensional case. In particular, a qualitative explanation is achieved to some of the experimental data on ^{13}C NMR in a completely substituted diamond [3]. Here we suggest a formulation for the description of many-body dynamics based on structures that take into account the permutation symmetries and quantum coherences of a multispin system.

The line shape expression in the thermodynamic limit is obtained. Computational experiment has been also used with a direct diagonalization of the spin Hamiltonian along with theoretical calculations. In general, we demonstrate wider applicability of one-dimensional models than they are considered presently. Finally the quantitative analysis of the dipole-dipole NMR experimental spectra with cross-singular dips has been made for the particular compound: the polycrystalline trichloroacetic acid.

1. A.A. Nevzorov and J.H. Freed. J. Chem. Phys., **112**, pp. 1413-1424, 2000.
2. O.V. Falaleev, L.G. Falaleeva. JETP Letters, **68**, pp. 93-97, 1998.
3. K. Schaumburg, T. Shabanova, J.P.F. Sellschop. J. Magn. Res., **A112**, pp. 176-187, 1995.

Author Index

Author Index

Author Index

Author Index

Author Index

Author Index

Author Index

Author Index

Author Index

Author Index

Научное издание

Труды международной конференции МИКРО- И НАНОЭЛЕКТРОНИКА – 2016

Сборник тезисов

3–7 октября, 2016, г. Звенигород, РФ

Под редакцией:
чл.-корр. РАН В.Ф. Лукичева;
д.ф.-м.н. *К.В. Руденко*

Составитель к.ф.-м.н. *В.П. Кудря*

Издание доступно на электронном ресурсе e-library и www.icmne.ftian.ru

Напечатано с готового оригинал-макета

Подписано в печать 15.09.2016 г.
Формат 60x90 1/8. Усл.печ.л. 29,25. Тираж 240 экз. Изд. № 247.

Издательство ООО “МАКС Пресс”
Лицензия ИД N 00510 от 01.12.99 г.

119992, ГСП-2, Москва, Ленинские горы,
МГУ им. М.В. Ломоносова, 2-й учебный корпус, 527 к.
Тел. 8(495)939-3890/91. Тел./Факс 8(495)939-3891.

Отпечатано в ППП «Типография «Наука»
121099, Москва, Шубинский пер., 6
Заказ №